Universitat Autònoma de Barcelona

Electrochemical and optical nanoparticle-based biosensors for point-of-care applications

Lourdes Rivas Torcates

Thesis dissertation to apply for the

PhD in Chemistry

Department of Chemistry - Faculty of Science

Universitat Autònoma de Barcelona

PhD directors

Prof. Arben Merkoçi
ICREA & Nanobioelectronics and Biosensors Group
Institut Català de Nanociència i Nanotecnologia (ICN2)

Dr. Alfredo de la Escosura Muñiz
Nanobioelectronics and Biosensors Group
Institut Català de Nanociència i Nanotecnologia (ICN2)

Prof. Josefina Pons Picart
Department of Chemistry
Universitat Autònoma de Barcelona
Bellaterra (Barcelona), Spain

2014

The present thesis titled "*Electrochemical and optical nanoparticle-based biosensors for point-of-care applications*" presented by Lourdes Rivas Torcates to obtain the degree of Doctor, has been performed at the laboratories of the Nanobioelectronics and Biosensors Group at the Institut Català de Nanociència i Nanotecnologia (ICN2), under the supervision of Prof. Arben Merkoçi, Dr.Alfredo de la Escosura Muñiz and Prof. Josefina Pons Picart.

Bellaterra, 25th September 2014

Directors

Prof. Arben Merkoçi	Prof. Josefina Pons Picart
ICREA Professor	Department of Chemistry
Nanobioelectronics & Biosensors Group	Faculty of Science
Institut Català de Nanociència i Nanotecnologia	Universitat Autònoma de Barcelona

Dr. Alfredo de la Escosura Muñiz
Senior Researcher
Nanobioelectronics & Biosensors Group
Institut Català de Nanociència i Nanotecnologia

Lourdes Rivas Torcates
Nanobioelectronics & Biosensors Group
Department of Chemistry (UAB)
Institut Català de Nanociència i Nanotecnologia (ICN2)

Acknowledgment for the financial and logistical support

Universitat Autònoma de Barcelona for the given grant in the framework of the "Programa de beques per a personal Investigador en Formació (PIF) per a departaments de la Universitat Autònoma de Barcelona" and Nanobioelectronics and Biosensors Group of the Institut Català de Nanociència i Nanotecnologia (ICN2) for the financial support to carry out all the research work here presented.

Acknowledgments are also given for the financial supports from several institutions / programs: MEC (Madrid) for the projects MAT2011-25870 and IT2009-0092; NATO Science for Peace and Security Programme for the project SfP98380; EU for the FP7 contracts number 246513 ''NADINE" and 315653 "POC4PETS".

Acknowledgments / Agradecimientos

Finalmente, llegó la hora de agradecer a quienes han hecho posible la realización de esta tesis y hacer de mi estancia en Barcelona, una de las etapas más provechosas a nivel académico y sobre todo, a nivel personal.

A la **Prof. Fina Pons**, quien me recibió con entusiasmo en su grupo en la Unidad de Química Inorgánica para continuar con mi aprendizaje en el mundo de la síntesis y química de coordinación. Un día, la crisis tocó a nuestra puerta y a pesar de esta indeseable visitante, con el mismo entusiasmo y apoyo moral me condujo hasta el grupo de Nanobioelectronics and Biosensors, en aquel entonces ubicado en la ETSE. El cambio a una nueva línea de investigación supuso para mí muchas interrogantes, pero que fueron disueltas rápidamente por el apoyo y confianza ofrecidos por el **Prof. Arben Merkoçi**, quien siempre ha estado dispuesto a tender una mano amiga (y académica) cuando se necesita. Sin duda alguna, el ritmo frenético de información que recibía a diario y en cada seminario, debía ser dosificada y detallada por el **Dr. Alfredo de la Escosura**, que con su paciencia infinita, conocimiento y experiencia, ha aclarado muchas de mis inquietudes (y que aún continúa en ello). A mis tres Directores, gracias su apoyo, motivación y paciencia durante todo este tiempo, dentro y fuera del laboratorio.

A mis compañeros de camino del Nanobioelectronics and Biosensors Group, por compartir los buenos momentos y los no tan buenos, por las discusiones científicas, por las tardes (casi noches) de café en la que podíamos liberar las presiones académicas y reírnos de nuestros asuntos más "mundanos". A **Anna**, el pulpo de nuestro laboratorio, que con mil cosas en la cabeza y tres mil por hacer, siempre atiende nuestras peticiones, definitivamente sin ella, el grupo no sería lo que es. A **Gemma**, quien fue el puente de conexión entre el grupo de Inorgánica y el NBS & B Group, gracias por ser mi mentora en el tema de síntesis y por introducirme en el nuevo grupo. A mis tres postdocs favoritas: **Carmen**, **Sandrine** y **Briza**, por su ayuda no sólo en la parte académica, sino también por los buenos momentos compartidos, las tardes artesanales de "chic@s", por las comidas deliciosas del país que cada una representaba y por muchas cosas más. Ahora mis compañeros de despacho. A las tres Mar…**María**, **Marisol** y **Mariana**, las otras participantes de las tardes de "chic@s", a las dos primeras por su energía contagiosa y sus escandalosas risas en el laboratorio que me hicieron desconcentrar unas

cuantas veces, pero a las que sucumbí segundos más tarde. Y a la última, a quien admiro profundamente por su metódica forma de trabajar y concentración máxima en el despacho del "Cotillas group", por sus valiosísimos aportes científicos y por su incondicional apoyo en todo momento. A **Miquel Cadevaaaaaal**, por nuestras discusiones científicas, por siempre comentarme curiosidades y también un poco de la historia de Catalunya. A **Flavio**, porque aunque siempre peleábamos por (literalmente) cualquier cosa, creo que por problemas de comunicación entre flaviano y español, aprendí a ser más tolerante y ya después me reía de tus cosas. Ahora, en el despacho más silencioso, agradezco a **Claudio**, mi gurú del Lateral Flow, por iniciarme a distancia en este mundillo que sin duda, ha sido la conexión perfecta entre el papel y la Ciencia. También por su disposición a responder cuanta cosa se me ocurriera, por confiar en mi gusto artesanal para llevar consigo su diario de viajes y por traerme de sus viajes a Italia, lo que alegraba mis tardes, mi debilidad achocolatada: Pan di Stella. A **Helena**, siempre discreta y enérgica, por nuestras conversaciones sobre el futuro de nuestros trabajos y por no abandonar nunca las ganas de ordenar el laboratorio de tal manera, que ni daban ganas de tocarlo. A **Alex Chamorro** el próximo Alcalde de Cerdanyola, por su empatía, por su manera *naif* de ver el acontecer político de mi país y por su pesimismo ocasional, que me permitió explotar en algunos momentos, mis dotes de coach motivacional. A **Luisinho**, el portugués más internacional que conozco, por su energía explosiva, por su manera relajada de ver la vida, por hacerme reír con sus ocurrencias y por permitirme enseñarle en sus inicios qué no debía hacer para explotar el laboratorio…ahh…y por dejar un agujereado recuerdo en mi bata de laboratorio. A **Adaris**, la reina del Caribe, y a **Edén**, por sus terapias alternativas, a ambos, gracias por los momentos compartidos en ambos grupos. Ahora, un merecido agradecimiento a "mis niños", los "lourdinhos" y calificativos varios: **Alex Zamora** y **Daniel Quesada**. Recuerdo la época en la que Dani, muy temeroso, hacía sus primeros experimentos y no tenía ni idea de todo lo que le explicaba. Claro!... él estaba exactamente como yo cuando llegué al grupo unos años atrás. Pero pronto aprendió y altamente motivado, pudo "captar" a su amigo de carrera, Alex, para iniciarlo en el mundo de la nanotecnología. Mis alumnos con el pasar del tiempo, se convirtieron en mi mano derecha, en quien confiaba mis experimentos (las primeras veces con recelo maniático) y con quienes pasé meses, cortando y ensamblando tiras de lateral flow….ya hemos perdido la cuenta de cuantas hemos hecho hasta la fecha, pero estábamos a punto de convertirnos en una ensambladora. De mi experiencia docente tanto en mi país como en

la UAB, esta es la más enriquecedora que he tenido hasta la fecha, porque la enseñanza fue directa y exclusiva y el hecho de verlos ahora discutiendo con bases los problemas científicos de su propia investigación y enseñando lo que aprendieron conmigo a otros nuevos investigadores, me hace entender que enseñando también se aprende y que he hecho un buen trabajo. Estoy infinitamente orgullosa de "mis niños" y estoy segura que llegarán lejos por su determinación y ganas de seguir aprendiendo.

A **Lorena Serrano**, de Vetgenomics por preparar las infinitas muestras de ADN y por "rezar" conmigo a través de Whatsapp para que todo saliese bien en los análisis. Después de muchos intentos, valió la pena!

A las personas que hicieron posible mi breve estancia en el **Laboratori de Sensori e Biosensori** en la Università degli Studi di Firenze, en especial a la **Prof. Giovanna Marraza**, por permitirme aprender nuevas técnicas en su laboratorio. A mis compañeros **Andrea**, **Diego**, **Anca** y **Vasi**, quienes hicieron de los calurosos días de laboratorio, una amena experiencia.

A todos aquellos que han pasado por el grupo y que tuve el placer de haber aprendido de sus trabajos y de su cultura: **Marisa**, **Sergi**, mi querida **Tiziana**, **André**, **Irene**, **Lenka 1**, **Lenka 2**, **Serdar**, **Erika**, **Laura**, **Deniz**, **Hassan**, **Abdelmoneim**, **Amal**, la dulce **Jihane**, **Yuki**, **Sevinç**, **Thiago**, **Anna F**., **Natalia**, **Andrezj** y en especial, **Gisele**, mi compañera del Lateral Flow, por sus nuestras charlas vespertinas y por su apoyo.

A los técnicos del ICN2 responsables de la caracterización de materiales: **Belén** y **Marcos**, por su experticia en el manejo de muestras y por responder cada pregunta que hacía en las sesiones de TEM/SEM. A **Guillaume** y **Pablo** por atender diligentemente mis inquietudes en el XPS y rayos X.

A mi **familia**, por su apoyo durante todo este tiempo, por escuchar mis lamentos científicos, por respetar mi tiempo de escritura y animarme en esos días grises. Por último, pero no menos importante, a la persona quien me ha acompañado enteramente en esta aventura: **Ian**. Por hacerme reaccionar y hacerme ver lo maravillosa que es la Ciencia, por creer en mí y por motivarme para que siga haciendo lo que me gusta: *aprender*. Gracias por vivir esta experiencia conmigo. TQF!

Thesis Overview

This Thesis describes the study and development of different strategies based on novel properties of nanoparticles and other micromaterials for the improvement of the performance of two biosensing platforms with interest for analytical applications.
The first one consists in screen printed carbon electrodes (SPCEs) used in combination with iridium oxide nanoparticles (IrO_2 NPs). These nanoparticles are employed both as novel electrocatalytic labels for biomarkers detection, and also as electrode surface modifiers for impedimetric detection of small molecules such as toxins. The second platform consists in lateral flow assay (LFA) strips used in combination with gold nanoparticle (AuNP) labels, where different amplification strategies are developed for the improvement of the assay sensitivity, applied for protein and DNA detection.

In **Chapter 1**, a general overview about the use of nanoparticles in electrochemical and paper-based platforms is presented. The first part gives a general overview on electrochemical biosensors and the different related applications of nanoparticles either as labels or modifiers of the surface of the working electrode of screen-printed carbon electrodes (SPCE) used as electrotransducer. The second part is focused on the use of nanoparticles in paper-based sensors, including basic concepts and the state-of-the-art of their application in this type of sensors.

In **Chapter 2** the objectives of this Thesis are presented.

The third chapter (**Chapter 3**) presents the evaluation of the electrocatalytic activity of citrate-capped IrO_2 NPs toward the water oxidation reaction and their use as novel electrochemical labels in protein diagnostics. Magnetic beads modified with antibodies are used as platform for the immunoassay which is applied for the detection of Apolipoprotein E (ApoE), a biomarker of Alzheimer disease. The main feature of the developed device is the signal generation in the same medium where the immunoassay takes place avoiding the use of additional reagents, which is expected to allow a simpler and user-friendlier methodology for protein detection.

In **Chapter 4**, a novel aptasensor based on SPCEs modified with conductive films of thionine and adsorption of citrate-capped IrO_2 NPs is presented. This system is explored for label-free impedimetric detection of ochratoxin A (OTA), a highly toxic compound which represents a public health problem due to its presence in foods above the limit established by worldwide organizations. Each fabrication step has been characterized by electrochemical impedance spectroscopy (EIS) in the presence of a redox probe. The developed device is able to detect low concentrations of OTA showing also good specificity and reproducibility.

A new strategy for improving the sensitivity of AuNPs-based LFAs by using printed barriers deposited onto the nitrocellulose membrane by wax printing technique is presented in **Chapter 5**. Pillars of different designs and distributions were printed, in order to create hydrophobic barriers that can cause flow delay. The controlled delays in microfluidics increase the binding time between the immunocomplex and the detection antibody, in addition to the generation of pseudo turbulences in the pillars zone that improves mixing between the analyte and the labeled antibody. This microfluidics delay in certain zones (incubation areas) combined with the generation of the pseudo turbulences directly affects the analytical performance of the LFA being transduced to a better sensitivity and detection limit.

In **Chapter 6**, a novel LFA design with enhanced sensitivity able to detect very low quantities of isothermal amplified Leishmania DNA sequences with interest for animals diagnostics is presented. The enhanced methodology takes advantage of the use of AuNPs tags connected with polyclonal secondary antibodies which recognize primary ones. The polyclonal nature of the secondary antibodies allowed their multiple connections with primary ones, giving rise to the enhancement of the AuNP signal. Furthermore, an endogenous control was introduced so as to avoid false negatives and the analysis accordingly performed.

Finally, general conclusions and the future perspectives are discussed in **Chapter 7**.

Additionally, **Annex A** describes preliminary studies related to the size- and shape-effect on the electrochemical response of AuNPs (including nanospheres and concave nanocubes) using differential pulse voltammetry (DPV) on SPCEs. The **Annex B** lists the publications, book chapter and manuscript submitted that resulted from this thesis.

Resumen

Esta Tesis describe el uso y desarrollo de diferentes estrategias basadas en propiedades novedosas de nanopartículas y otros micromateriales para la mejora en la sensibilidad de dos plataformas biosensoras para aplicaciones analíticas.

La primera consiste en electrodos serigrafiados de carbón en combinación con nanopartículas de óxido de iridio (IrO_2 NP_S). Estas nanopartículas son empleadas tanto como novedosas etiquetas electrocatalíticas en la detección de biomarcadores, así como también en la modificación de la superficie de los mencionados electrodos para la detección impedimétrica de pequeñas moléculas tales como las toxinas. La segunda plataforma consiste en tiras de flujo lateral en combinación con nanopartículas de oro (AuNP) como etiquetas ópticas, en la cual diferentes estrategias de amplificación son desarrolladas para mejorar la sensibilidad de estos ensayos y su aplicación para la detección de proteínas y ADN.

En el **Capítulo 1**, se presenta una introducción general acerca del uso de nanopartículas en plataformas electroquímicas y las basadas en papel. La primera parte contempla los conceptos generales de biosensores electroquímicos y las diferentes aplicaciones de nanopartículas ya sea como etiquetas o como modificadores de superficies electrotransductoras. La segunda parte está enfocada en el uso de nanopartículas en sensores basados en papel, incluyendo conceptos básicos y el estado del arte de sus aplicaciones en este tipo de sensores.

En el **Capítulo 2** se presentan los objetivos de esta Tesis.

El tercer capítulo (**Capítulo 3**) presenta la evaluación de la actividad electrocatalítica de IrO_2 NPs estabilizadas por iones citrato, hacia la reacción de oxidación de agua y su uso como nueva etiqueta electroquímica en el diagnóstico de proteínas. Esferas magnéticas modificadas con anticuerpos son usadas como plataformas para immunoensayos la cuales son aplicadas en la detección de Apolipoproteina E (ApoE), un biomarcador asociado a la enfermedad de Alzheimer. La principal característica del dispositivo desarrollado es la generación de señal en el mismo medio donde toma lugar

el immunoensayo evitando así el uso de reactivos adicionales, ofreciendo una metodología más simple y amigable para la detección de proteínas.

En el **Capítulo 4**, se describe un nuevo aptasensor basado en la modificación de electrodos serigrafiados de carbón modificados con películas conductoras de tionina y la adsorción de IrO_2 NPs estabilizadas en citrato. Este sistema libre de etiquetas (*label-free*) es empleado en la detección impedimétrica de ocratoxina A (OTA), un compuesto altamente tóxico que representa un problema de salud pública debido a su presencia en alimentos por encima de los límites establecidos por organizaciones alrededor del mundo. Cada paso de fabricación es caracterizado por espectroscopía de impedancia electroquímica en la presencia de un mediador redox. El dispositivo desarrollado es capaz de detectar bajas concentraciones de OTA mostrando también buena reproducibilidad y especificidad.

Una nueva estrategia para mejorar la sensibilidad de ensayos de flujo lateral basados en AuNPs mediante barreras depositadas sobre la superficie de nitrocelulosa empleando la técnica de impresión de cera, es reportada en el **Capítulo 5**. Diferentes diseños de pilares fueron impresos para crear barreras hidrofóbicas que puedan causar retrasos en el flujo de la muestra. Los retrasos controlados en la microfluídica, incrementan el tiempo de reconocimiento entre el inmunocomplejo y el anticuerpo de detección, además de la generación de pseudo-turbulencias en la zona de los pilares mejoran el reconocimiento entre el analito y el anticuerpo etiquetado. Estos retrasos microfluídicos en las áreas de incubación combinados con la generación de pseudo-turbulencias afectan el rendimiento analítico de los ensayos de flujo lateral siendo traducidos en mejor sensibilidad y límite de detección.

En el **Capítulo 6**, se describe un nuevo diseño de ensayo de flujo lateral con sensibilidad mejorada capaz de detectar muy bajas cantidades de secuencias de ADN de Leishmania isotérmicamente amplificadas. Esta metodología toma ventaja del uso de AuNPs como etiquetas ópticas conectadas con anticuerpos secundarios (de tipo policlonal) los cuales reconocen anticuerpos primarios. La naturaleza policlonal de los anticuerpos secundarios permite múltiples conexiones con los primarios, dando lugar a una mejora en la señal producidas por las AuNPs. Además de la introducción de control endógeno para evitar falsos negativos.

Finalmente, las conclusiones generales y las perspectivas futuras son discutidas en el **Capítulo 7**.

Adicionalmente, en el **Anexo A**, se describen estudios preliminares relacionados con el efecto producido en la señal electroquímica por el cambio del tamaño y forma de AuNPs (incluyendo nanoesferas y nanocubos cóncavos) analizadas usando voltametría de pulso diferencial y electrodos serigrafiados de carbón. En el **Anexo B** se incluyen las publicaciones, un capítulo de libro y manuscritos enviados que resultaron de esta tesis.

List of acronyms

Acronyms	*Definition*
Ab	Antibody
AChE	Acetylcholinesterase
AD	Alzheimer Disease
AFB_1	Aflatoxin B_1
AMI	Acute Myocardial Infarction
ApoE	Apolipoprotein E
ASSURED	*A*ffordable, *S*ensitive, *S*pecific, *U*ser-friendly, *R*apid and robust, *E*quipment-free and *D*eliverable to end-users
AuNPs	Gold Nanoparticles
BSA	Bovine Serum Albumin
CanL	Canine Leishmaniasis
CCD	Charged Couple Devices
CEA	Carcinoembryonic Antigen
CFU	Colony-Forming Units
CL	Control Line
CRP	C-reactive protein
CV	Cyclic Voltammetry
DNA	Deoxyribonucleic acid
DON	deoxynivalenol
DPV	Differential Pulse Voltammetry
e.g.	*Exempli gratia* (for example)
EA	Ethanolamine
EDC	1-Ethyl-3-(3-dimethylaminopropyl)carbodiimide
EDTA	Ethylenediaminetetraacetic Acid
EIA	Enzymatic Immunoassay
EIS	Electrochemical Impedance Spectroscopy
ELISA	*Enzyme-Linked ImmunoSorbent Assay*
et al.	*Et alii* (and collaborators)
FAM	Fluorescein Amidite
FITC	Fluorescein Isothiocyanate
f-PSA	Free Prostate Specific Antigen
hCG	Human Chorionic Gonadotrophin
HER	Hydrogen Evolution Reaction
HIgG	*Human Immunoglobulin* G
HIgM	Human Immunoglobulin M
HIV	Human Immunodeficiency Virus
HPLC	High Performance Liquid Chromatography

Acronyms	*Definition*
HRP	Horseradish Peroxidase
ICAT	Immunochromatographic Assay on Thread
ICP-OES	Inductively Coupled Plasma-Optical Emission Spectrometry
IgG	Immunoglobulin G
IgG	Immunoglobulin G
IGSS	Immunogold Silver-Staining
IrO_2 NPs	Iridium Oxide Nanoparticles
ISDPR	Isothermal Strand-Displacement Polymerase Reaction
ITO	Indium Tin Oxide
IUPAC	International Union of Pure and Applied Chemistry
LED	Ligh-Emitting Diode
LF	Lateral Flow
LFA	Lateral Flow Assay
LFIA	Lateral Flow Immunoassay
LoD	Limit of Detection
MAR™	Magnetic Assay Reader
MB	Magnetic Beads
miRNA	Micro-ribonucleic acid
NADH	Dihydronicotinamide Adenine Dinucleotide
NALF	Nucleic Acid Lateral Flow
NALFIA	Nucleic Acid Lateral Flow Immunoassay
NASBA	Nucleic Acid Sequence Based Amplification
NC	Nitrocellulose
NPs	Nanoparticles
OC	Oligochromatography
OTA	Ochratoxin A
OVA	Ovalbumin
PAP	Prostatic Acid Phosphatase
PBS	Phosphate Buffer Saline
PCR	Polymerase Chain Reaction
pKi	Isoelectric Point
POC	Point-of-care
POCT	Point-of-care testing
PSA	Prostate Specific Antigen
QDs	Quantum Dots
***R*ct**	Charge-transfer Resistance
RIA	Radioimmunossay
RIgG	Rabbit Immunoglobulin G
RNA	Ribonucleic acid

Acronyms	*Definition*
RPA	Recombinase Polymerase Amplification
rRNA	Ribosomal Ribonucleic Acid
RSD	Relative Standard Deviation
SEM	Scanning Electron Image
SPCE	Screen-Printed Carbon Electrodes
SPIA	Sol Particle Immunoassay
SPMNP	Superparamagnetic Nanoparticles
ssDNA	Single-stranded Deoxyribonucleic acid
Sulpho-NHS	N-hydroxysulfosuccinimide
TCP	Trichloropyridinol
TEM	Transmission Electronic Microscopy
TiO_2	Titanium oxide
TL	Test line
TL1	Test line 1
TL2	Test line 2
TMB	Tetramethylbenzidine
t-PSA	Total Prostate Specific Antigen
UV-Vis	Ultraviolet-Visible
WHO	World Health Organization
WOR	Water Oxidation Reaction
XPS	X-ray Photoelectron Spectrometry

Index

Chapter 1

Introduction

Related publication

Chapter 14 in press at "Gold Nanoparticles in Analytical Science and Technology" (Comprehensive Analytical Chemistry Series – Elsevier), Eds M. Valcárcel, A.I. López-Lorente)

Lateral flow biosensors based on gold nanoparticles

Lourdes Rivas[1,2], Alfredo de la Escosura-Muñiz[1], Josefina Pons[2], and Arben Merkoçi[1,3]

[1]ICN2-Nanobioelectronics & Biosensors Group,Institut Català de Nanociència i Nanotecnologia, Campus UAB, 08193 Bellaterra (Barcelona), Spain

[2]Department of Chemistry, Universitat Autónoma de Barcelona, 08193, Bellaterra, Barcelona, Spain

[3]ICREA - Institució Catalana de Recerca i Estudis Avançats, 08010 Barcelona, Spain

1.1. Point-of care biosensors

During the last years, the development of analytical devices for detecting and quantifying a wide range of analytes with interest in food quality control, bio-security and especially, clinical diagnostics is continuously increasing. For example, monitoring of food and environment contaminants can lead to proper solutions that would avoid the effects produced in human health.[1,2] In particular, biomarkers detection at low concentrations is extremely important in clinical diagnostics, even before any symptom of disease appears, since an early diagnosis is crucial for increasing medical treatment success and patient survival rates.[3,4] In this regard, the development of the point-of-care (POC) testing devices, which can be used near to the patient or in resource-limited settings, has been growing in last years.[5] The World Health Organization (WHO) has established the ASSURED criteria which have been widely applied in POC devices for their application in disease controls. The conditions POCs must fulfill are Affordable, Sensitive, Specific, User-friendly, Rapid and robust, Equipment-free and Deliverable to end-users.[6]

Biosensors represent interesting POC devices which fulfill the mentioned ASSURED criteria. According to the International Union of Pure and Applied Chemistry (IUPAC), a biosensor is an analytical device in which the recognition system is based on biochemical or biological mechanisms.[7] A biosensor consists in mainly two integrated components: i) a biological element (such as enzymes, antibodies, ssDNA, tissues, microorganisms, etc.) or a synthetic receptor that recognizes and selectively binds to the target of interest and ii) the transducer or detector element that converts the binding reaction in a measurable quantity (see Fig. 1) which is displayed by a signal processor or reader device in a user-friendly way. Usually, biosensors can be divided according to the biological signaling mechanism or the signal transduction mode. Additionally, these transduction methods can be classified in two main groups: chemical or physical, in relation to the changes measured from the recognition event. In general, this classification leads to optical (surface plasmon resonance, chemiluminescence, fluorescence), electromechanical/mass (quartz crystal microbalance, surface acoustic wave), electrochemical (amperometry, potentiometry, conductimetry and voltammetry) beside other (ex. thermal change-based) biosensors.

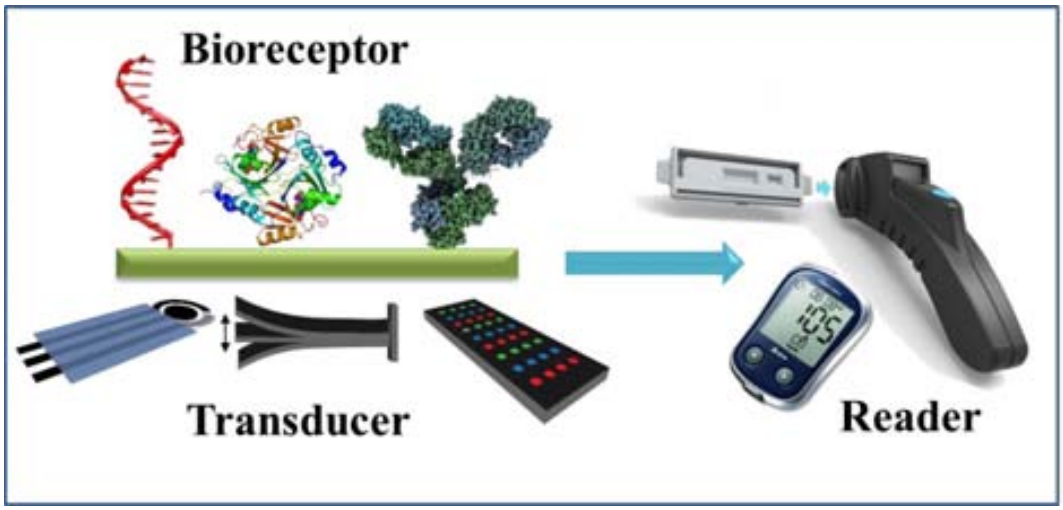

Figure 1.1. Schematic representation of main components of a biosensor (different possible bioreceptors and transducers) that result in an integrated biosensing system.

Commonly biosensors can be referred as *label-based* and *label-free* according to the transduction method. A label-based biosensor needs a *signaling label* (*e.g.* enzymes, nanoparticles, quantum dots) for monitoring the events produced on the transducer surface, since the recognition event doesn't give rise to changes in any (physic)chemical property that can be detected by the transducer. On the other hand, in a label-free biosensor the interaction between the target and the recognition element on the transducer surface can be detected directly without the use of a tag/label.

An important part of the work presented in this thesis was devoted to the development of nanomaterials-based electrochemical biosensors. Due to the fact that several comprehensive reviews have been addressing nanomaterials-based electrochemical biosensors,[8–12] the following section 1.2 is briefly describing this topic followed by section 1.3 related to the state-of-the-art of the use of nanoparticles in paper-based sensors, a growing research area which represents the second main topic of this PhD thesis.

1.2. Nanomaterials-based electrochemical biosensors

Electrochemical biosensors are very interesting for POC devices, since they allow the analysis of different species with high specificity and sensitivity, besides of their quickness, ease of use and the possibility of conducting the analysis "on-site". A typical example of these electrochemical biosensors is the glucose sensor,[13] which has been

widely studied and improved through three generation of biosensors and also been commercialized since decades.In recent decades, nanomaterials have gained much interest due to their novel and unique properties which makes them useful for different fields. The term nanomaterial is referred to any material with size dimensions in nanoscale (1-100nm). Their physical and chemical properties depend on the size, as well as the percentage of atoms at the surface of the material that becomes significant as the size become smaller, making them more chemically reactive.[14] In particular, nanomaterials such as nanoparticles, carbon-based nanomaterials and nanocomposites, have been used for the development of new and highly sensitive biosensors or for improving the performance of the existing ones, offering new methodologies for electrochemical signal transduction.[15–18]

Application of nanomaterials in electrochemical biosensing can be classified according to their two main functions either as labels or as modifiers of electrotransducing surfaces. Both strategies take advantage of the outstanding properties of nanomaterials (especially, nanoparticles) in order to enhance the electrochemical signal when used as label, or to improve the electron transfer rate when used as modifiers of electrochemical transducers.

1.2.1. Nanomaterials as labels

The analytical performance of electrochemical assays has been improved thanks to the excellent catalytic activity, conductivity and biocompatibility of nanomaterials used as labels, that allows to obtain lower limits of detection (LoD) to in electrochemical bioassays.[19]

Different strategies for labelling biomolecules with nanomaterials have been reported. Briefly, these approaches include: i) covalent interactions, performed by direct chemical reaction, linker chemical reaction and click chemistry, forming stables bioconjugates; ii) non-covalent strategy make use of the electrostatic interactions, π-π stacking or Wan der Waals forces between the biomolecule and nanoparticle; and iii) affinity interactions such avidin/biotin which enable the effective conjugation of biomolecules to nanomaterials. A comprehensive review was assembled by Lei, where all these methods and their application for signal enhancement are explained.[20]

Detection of nanoparticles (NPs) as labels can be conducted directly by generation of electrochemical signals due to their own redox properties, or indirectly because of their electrocatalytic properties towards to other species.

1.2.1.1. Direct electrochemical detection

In despite of the high sensitivity that offers the well-established stripping voltammetry, in which dissolution of metal NPs and subsequent voltammetric detection of metal ions in solution is achieved, this technique requires an extra analytical step and the use of toxic reagents. On the other hand, it is possible the metal detection without the dissolution of NPs, but it is necessary a direct contact between the electrode surface and superficial atoms of NPs. Thus, this strategy could result in a loss of sensitivity compared with stripping voltammetry. However, this type of detection offers advantages for sensing applications due to their fast response, procedure simplification and the reduced cost of analysis.

The use of gold nanoparticles (AuNPs) as label on the direct electrochemical detection of anti-Human IgG was described for first time by Costa García *et al*. obtaining a LoD of 1.38 x 10^{-8} M.[21] After this pioneer work, other important contributions emerged to the direct electrochemical detection. Pumera and co-workers described a new method for direct detection of AuNPs absorbed on the surface of graphite-epoxy composite electrode followed by their electrochemical oxidation in acidic media at fixed potential. The resulting tetrachloroaurate ions generated near the electrode surface were detected by differential pulse voltammetry (DPV), obtaining a LoD of 1.8 x 10^{8} AuNPs/cm^3.[22] Analysis of cadmium-sulfide quantum dots (CdS QDs) has been also reported, but in this case the Cd (II) ions present on the CdS QDs crystalline structure are electrochemical reduced to Cd (0) and immediately reoxidized to Cd (II), registering the oxidation peak.[23] A double-codified nanolabel based on AuNPs modified with anti-human IgG horseradish peroxidase (HRP), has been reported for detection of human IgG.[24] Thanks to the properties of this nanolabel, it was possible to measure the analyte concentration which was directly related to the AuNPs labels by using stripping voltammetry (Fig. 1.2A). The LoD for this electrochemical assay was significantly lower (260 pg/mL HIgG) than typical ELISA tests, showing to be a sensitive and rapid method. CdS QDs have been used as labels for the detection of carcinoembryonic antigen (CEA) in a disposable screen-printed graphite electrode by using square wave

anodic stripping voltammetry to amplify the signal current response obtained from the dissolved anti-CEA-CdS QDs (Fig. 1.2B).[25] The reported sensitive device showed a LoD of 32 pg/mL of CEA, comparable to other electrochemical assays and showed potential uses for POC diagnostics.

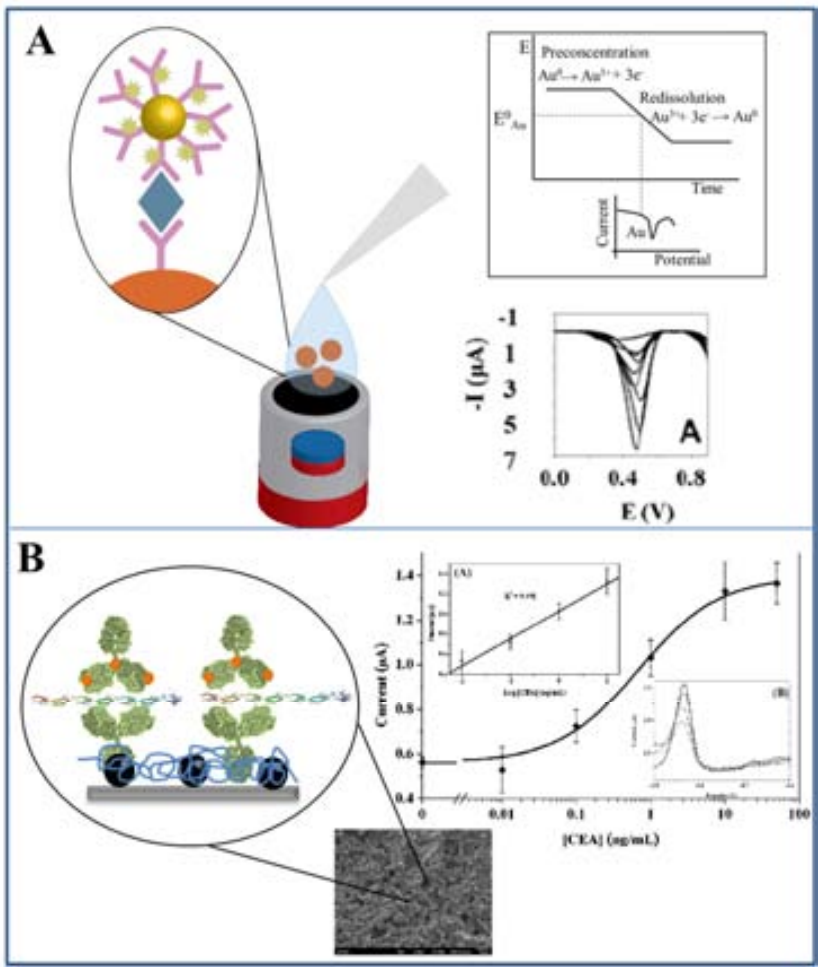

Figure 1.2. Direct electrochemical detection of nanoparticles. (A) Direct detection of HIgG based on a pre-oxidation of AuNPs as labels and later reduction of generated Au(III) ions. (B) Detection of QDs as labels in acidic solution by using square wave anodic stripping voltammetry. Adapted with permission from references [24] and [25].

1.2.1.2. Indirect electrochemical detection: electrocatalytic determination

Alternatively to the direct electrochemical detection, electrocatalytic properties of NPs have been exploited to achieve high sensitive detection. By definition an electrocatalyst is a catalyst that participates in an electrochemical reaction and contributes to the electron transfer between the electrode and the reactants facilitating an intermediate reaction. AuNPs are known also for their electrocatalytic properties, being their effect

towards the silver deposition and the hydrogen ions reduction the most exploited in biosensing applications. In this regard, silver deposition on AuNPs has been reported for detection of DNA hybridization on magnetic beads used as immobilization platforms.[26] This assay involves the hybridization of a target oligonucleotide to probe-coated magnetic beads, followed by binding of the streptavidin-coated AuNPs to the captured target. Then, the DNA-linked aggregate is covered with silver, following the catalytic precipitation of silver on gold; these assemblies are magnetically collected on the electrode, leading a direct contact of the silver tag allowing the solid-state stripping detection. More recently, a novel magnetoimmunoassay with enhanced sensitivity due to the catalytic effect of AuNPs on the electroreduction of silver ions has been reported by our group.[27] By choosing a suitable deposition potential, the direct electrocatalytic reduction of silver ions occurs onto the AuNPs surface and once a silver layer is already formed more silver ions are going to be reduced due to a self-enhancement deposition (Fig. 1.3A). Using this strategy, it was possible to obtain a low protein detection limit (23 fg/mL) which resulted to be 1000 times lower compared with direct electrochemical detection of AuNPs.

On the other hand, electrochemical reduction of hydrogen ions by AuNPs was described for the first time by our group.[28] Hydrogen ions present on the acidic medium are catalytically reduced to molecular hydrogen by the AuNPs on the surface electrode, generating a catalytic current which is related to the concentration of AuNP and enables their highly sensitive quantification (Fig. 1.3B). This method has been reported for the anti-hepatitis B virus antibodies detection[29] and tumor cells detection.[30]

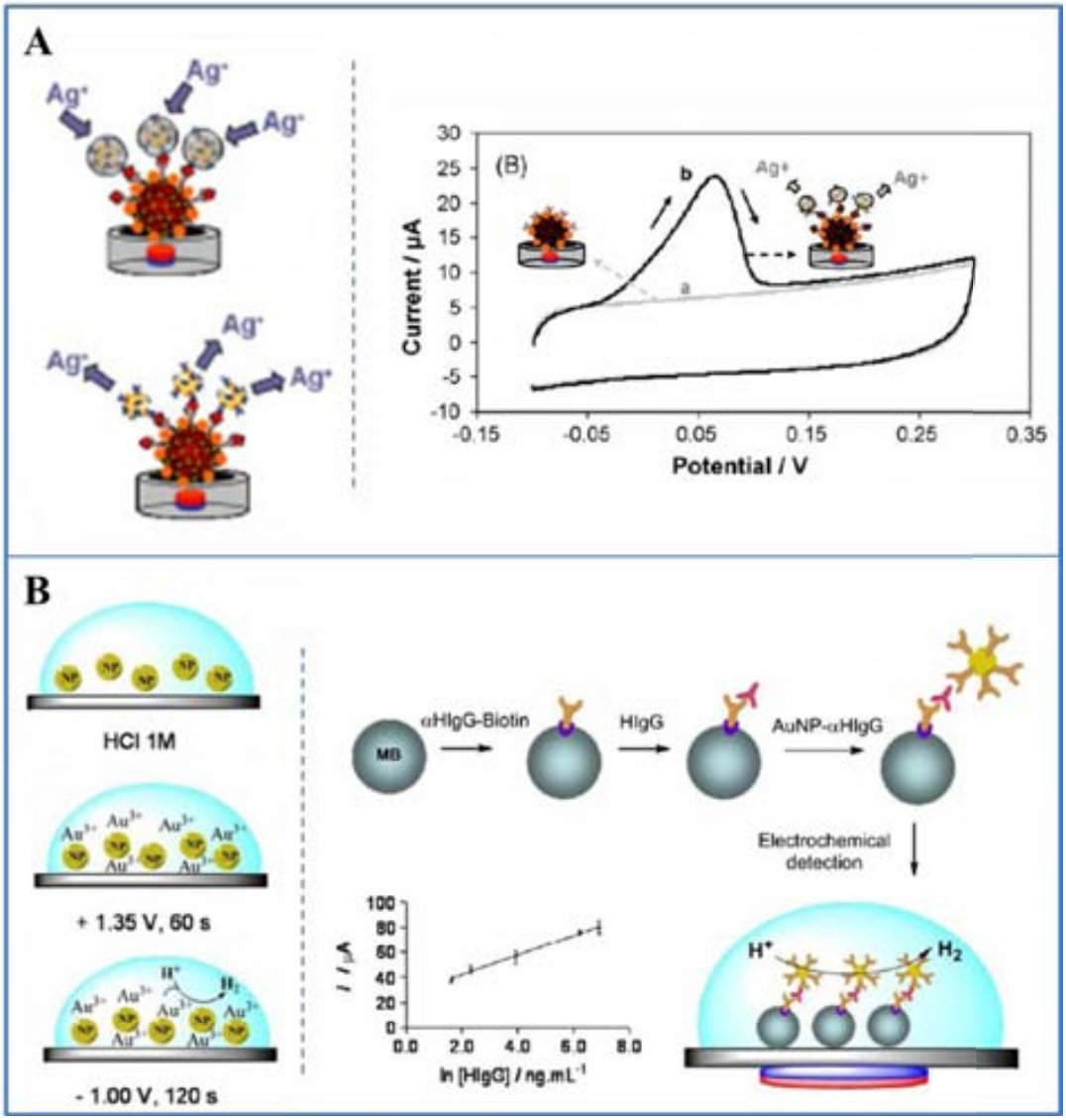

Figure 1.3. Indirect electrochemical detection based on electrocatalytic properties of nanoparticles. (A) Left. Detection based on the catalytic properties of AuNPs on the silver electroreduction in a magnetosandwich immunoassay and the further silver reoxidation. Right. Peak current obtained by the re-oxidation of silver ions that can be related with the protein concentration. (B) Left. Hydrogen Evolution Reaction induced by AuNPs: In acid media, AuNPs are superficially oxidized at +1.35 V generating Au (III) ions, followed by catalytic reduction of hydrogen ions at -1.0 V promoted by the released gold ions and AuNPs. Right: Detection of HIgG by indirect electrochemical method. Adapted with permission from references [27] and [28].

Catalytic activity of platinum nanoparticles toward oxygen reduction reaction has been reported by Polsky *et al*.[31] In this work, the antibodies were previously immobilized onto AuNPs and then Pd was deposited onto the AuNPs surface, forming core-shell Au@Pd NPs. Detection of antibodies is achieved indirectly by measuring the catalytic current generated from this electrocatalytic reduction in glassy carbon electrodes.

1.2.2. Nanomaterials as modifiers of electrotransducing surfaces

Electrochemical performance of an electrode is strongly influenced by its size and composition that can be tailored in order to enhance the analytical output. Modification of electrotransducer surfaces can be achieved with NPs, promoting the electron transfer and improving the electrochemical response.

AuNPs were the first example of nanoparticle-modified electrodes because of their electrocatalytic and conductive properties, and also their ease of synthesis. In addition, AuNPs offer stable immobilization platforms without degrading the activity of the biomolecules which is a major advantage in the design of biosensors.[10,32]

Different methods for incorporating NPs to conventional surface electrodes are described in literature such as: i) adsorption of nanoparticles to the bulk electrode surface; ii) addition of NPs in a composite; and iii) layer-by-layer.[32] Ding *et al.* reported the electrodeposition of AuNPs to an ionic liquid carbon paste electrode for determination of α-fetoprotein at clinical relevant levels.[33] Determination of human chorionic gonadotrophin (hCG) with high sensitivity was reported by Chen and co-workers by using a highly hydrophilic, non-toxic and conductive colloidal AuNPs/titania sol–gel composite membrane prepared on a glassy carbon electrode.[34] An ultrasensitive immunosensor for detecting prostate specific antigen was conducted in a pyrolytic graphite electrode modified with glutathione-decorated AuNPs assembled layer-by-layer, showing a LoD 8-fold better than other reported methods (Fig. 1.4A).[35]

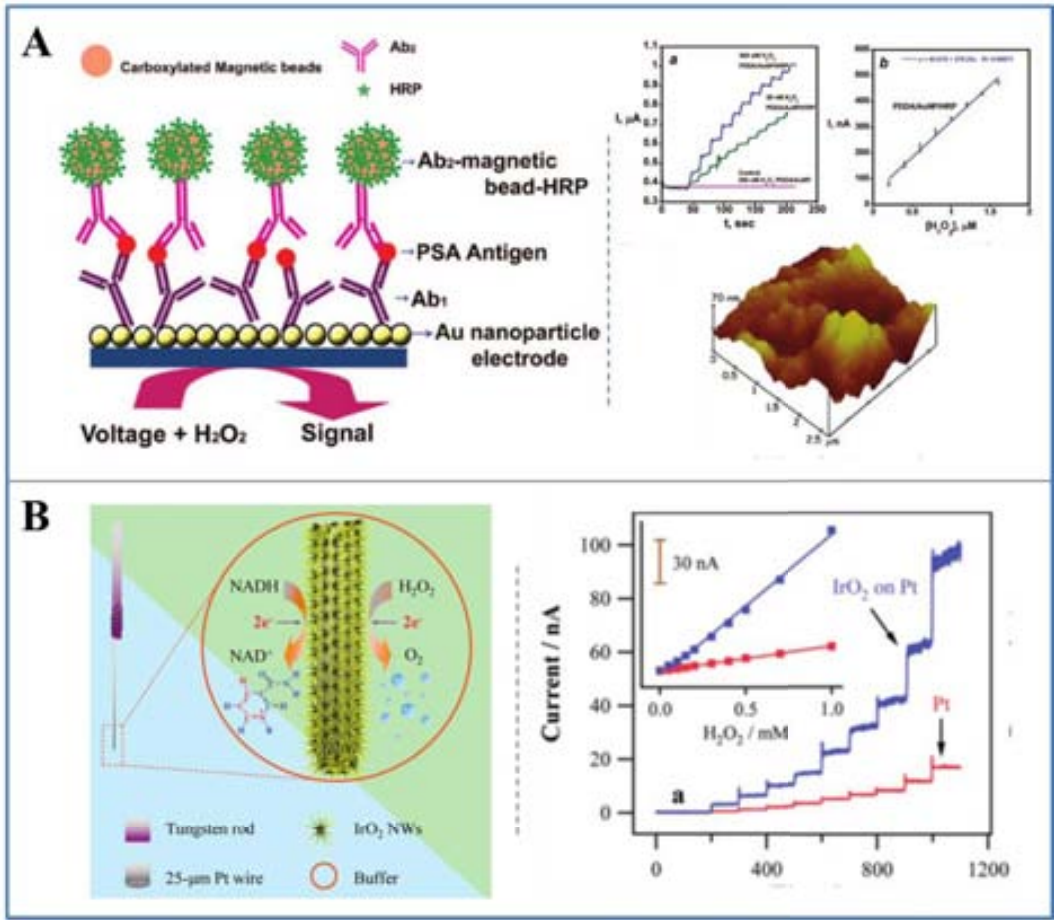

Figure 1.4. Nanomaterials as modifiers of electrotransducing surfaces. (A) Left: Scheme of detection of prostate specific antigen using a modified pyrolitic graphite electrode with glutathione-decorated AuNPs assembled layer by layer. Left: catalytic electrochemical reduction of hydrogen peroxide on HRP/AuNP electrodes from rotating disk amperometry and atomic force microscope images of AuNP platform after covalent linkage of anti-PSA antibodies onto the glutathione carboxylate groups of AuNPs. (B) Left: hierarchically driven single crystalline IrO_2 on a platinum microwire, which is directly used as an electric signal transducer for highly effective sensing of biologically relevant molecules such as H_2O_2 and NADH. Right: amperometric responses of the bare Pt microwire and IrO_2-platinum microwire electrodes to successive additions of H_2O_2 aliquots into a stirred PBS solution at neutral pH. Adapted with permission from references [35] and [36].

Metal oxides often exhibit semiconductor properties that may be modified by decreasing the size up to the nanoparticulate state. Nanostructurated metal oxides constitute exceptional immobilization platforms and/or mediators thanks to inherent properties of nanoparticles, besides to chemical stability, nontoxicity also exhibit enhanced electron-transfer kinetics and biocompatibility, providing suitable

microenvironments for the immobilization of biomolecules.[37] In this regard, nanostructurated metal oxides are used in a wide range of analytical applications.

Wen *et al.* reported a sensitive sensor for hydrogen peroxide (H_2O_2) detection by using Au/Pt hybrid nanoparticles self-assembled onto amino-functionalized titanium oxide (TiO_2) colloid spheres obtaining a LoD at nanomolar levels.[38] Moreover, the TiO_2-Au/Pt was employed on the photoelectrochemical catalysis of glucose, demonstrating the excellent performance-enhancing of this hybrid material. Recently, Shim and co-workers, reported the analytical application of hierarchically driven IrO_2 nanowires on the surface of platinum microwires for the electrochemical detection of H_2O_2 and dihydronicotinamide adenine dinucleotide (NADH) without the aid of enzymes, achieving a LoD of 5 μM and a very short response time of 10 s (Fig. 1.4B).[36] Detection of *Mycobacterium tuberculosis* has been reported by using a gold electrode modified with nanostructurated zirconium oxide film in which a ssDNA specific to the bacteria is immobilized, achieving a LoD of 0.065 ng/μL in less than 60 s.[39]

Electrochemical biosensors are significant tools for a wide range of analytical applications, especially in diagnostics, because of their good performance and sensitivity. New trends on POCT are leading to simple, portable and easy-to-measurements biosensing devices, taking advantages of the nanotechnology and material science in order to develop a new generation of biosensors that satisfies the requirements of an ASSURED device.

1.3. Lateral flow technology

1.3.1. General introduction: Historical perspective

The concept of rapid body fluid tests is documented in the history since thousand years ago. In ancient China, a saliva-based diagnostic called "the rice test" determined the guilt of an accused person.[40] The earliest urine-based tests for determining the pregnancy was documented on Egyptian papyrus of 1350-1200 BC [41,42]: if the urine of the woman was able to provoke (or not) the growth of wheat, then it was possible to give a pregnancy diagnosis. In the Middle Age and Renaissance, pregnancy and some diseases could be diagnosed by the color of the urine. In nineteen century, physicians still practiced the examination of urine in a more rational way including scientific approaches but it was not until early 1900 that the term "hormones" was introduced by Ernest Starling.[43] After this study, scientists began to explore in detail a particular hormone that can be found only in pregnant woman called human chorionic gonadotropin (hCG). [44,45] In this context, many advances have been achieved until the development of devices for rapid diagnostic methods being lateral flow (LF) devices one of the most important.

The basic principles of the LF dated back middle 1950 starting with the work of Plotz and Singer using the latex agglutination test.[46] At the same time, other applications in immunoassays with special importance for LF were developed. The radioimmunossay (RIA) by Berson and Yalow[47] based on the detection of radioactive compounds, although being a very sensitive and specific technique due to the special equipment and precautions required, was replaced by a safer and nonhazardous-based technique such as the enzymatic immunoassay (EIA).[48,49] In 1980 Leuvering *et al*.[50] reported the sol particle immunoassay (SPIA) in which silver and gold colloids was used as labels for sandwich immunoassays obtaining limits of detection comparable to RIA and superior in comparison to EIA. This work became pioneer in the use of nanoparticles as labels in immunoassays.

The main application for LF technology is the human pregnancy test developed in mid-1970's. The "early pregnancy test" (e.p.t.^{TM}) developed by Warner-Chilcott was a complex system that involved the use of different tubes and reagents and the result was obtained about two hours making difficult and ambiguous the determination of the end point. Since the launching of this home-diagnostic method, lateral flow assay (LFA) gained more importance in the biosensors field and continued progressing becoming

completely established in the late '80s by the introduction of several patents related to LF devices for pregnancy test.[51–53] In 1988, Unipath Ltd, launched the first one-step rapid LF assay for home pregnancy test known as Clearblue brand. This test was specifically qualitative: if two blue lines are developed means that woman is pregnant being the result visualized in few minutes. In a pregnant woman, levels of hCG rapidly rise and can be detected in urine from 9 -10 days after conception[54] and Clearblue™ is able to detect hCG protein in urine. Although pregnancy tests have been conceived for providing qualitative visual results (yes/no response), it is possible to obtain semi-quantitative results in order to estimate the pregnancy stage. Pregnancy test market has also evolved for generating new and more accurate devices and nowadays it is possible to find digital pregnancy test which give semi-quantitative results. This is a new generation of devices where LF technology is integrated with electronics in the same platform.

1.3.2. Lateral Flow technology and its format assays

1.3.2.1. Operation Principles

The LFAs are based on chromatographic principle in which test sample flows through a solid substrate via capillary action. Each strip is composed by dry pre-stored reagents and different porous membranes that have specific functions.

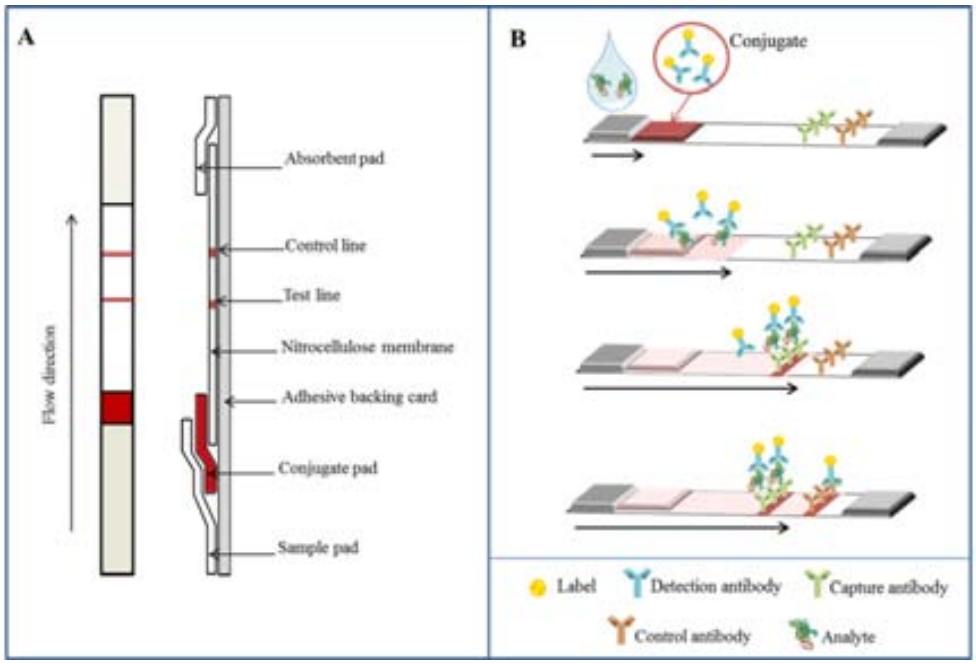

Figure 1.5. (A) Components of a lateral flow strip. (B) Scheme of a typical lateral flow assay (LFA).

Figure 1.5 shows a typical scheme of LF strip. As pre-requisite for the proper functioning of LFA, all the components of the strips must be previously treated for making them hydrophilic and overlapped between them over an adhesive backing card to guarantee the continuous flow of the sample. The fluid sample applied at the end of the strip (at the sample pad) migrates through the next region, the conjugate pad, where nano/microparticles conjugates are immobilized. This conjugate is composed by the biological components of the assay, *e.g.* antibodies, which are attached to the particles and previously have been deposited in the conjugated pad. In this step, the analyte interacts with the biological component of the conjugated particle forming a complex. There is a wide variety of particles used as labels (see Section 1.3.2.2.2), but the most commonly used are latex microparticles and AuNPs. The sample continues migrating by capillary forces through the detection pad, composed by a porous membrane in which the biological complementary part of the assay has been previously deposited. The capture lines, test and control line, are constituted by antibodies, antigens or proteins and their function is to capture the analyte and the excess of conjugated particle, respectively. The excess of reagents is absorbed by the wicking or absorbent pad located at the end of the LF strip. Visual results can be interpreted as the presence or absence of analyte in sample and can be detected by naked-eye or using a strip reader.

According to the type of format used, the results can be interpreted in opposite way. In figure 1.6 details of two main LFA formats such as the sandwich (direct) and competitive assay are shown. For the detection of molecules with a high molecular weight, with two or more antigenic sites *e.g.* big proteins, the sandwich assay is used (figure 1.6A). In this case, the presence of analyte shows two colored zones: test and control lines. On the other hand, if the analyte is a low molecular weight molecule with one antigenic site (hapten) for binding with antibody, *e.g.* pesticides or toxins, the competitive assay is employed. In this type of assay, the analyte and the analyte immobilized at the membrane compete for binding with the detector antibody. The presence of analyte is indicated by the absence of test line, therefore, only one line at the control zone is observed (see figure 1.6B).

In both cases, the control line is always visible and independent of the format used allowing to control the adequate migration of the sample through the strip.

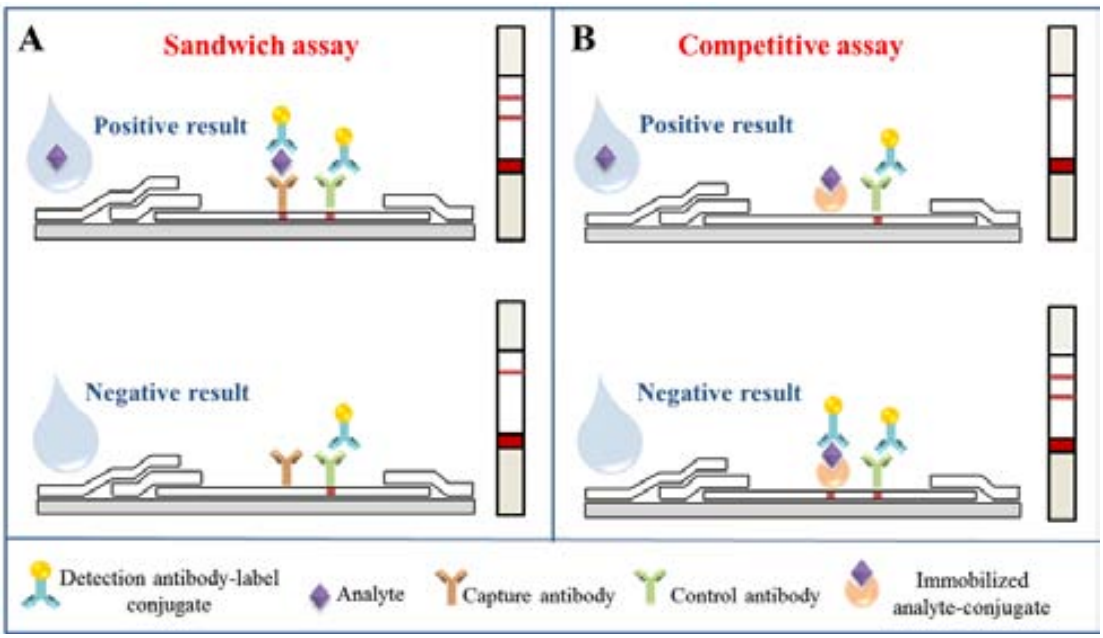

Figure 1.6. Typical formats of LFAs: (A) direct and (B) competitive assays.

1.3.2.2. Components

1.3.2.2.1. Assay membranes

The function as well the materials that constitute the different components of LFA are summarized in Table 1.1 and discussed in the following part.

a) Sample pad

Its purpose is to receive and then distribute the sample in a controlled and uniform way, releasing the analyte with high efficiency.[55] Additionally, it controls the rate flow that enters to the conjugation pad preventing flooding of device. The most commonly used sample pads are porous materials such as cellulose. Cellulose has large bed volumes (> 25 µL/cm^2) and are extensively used for testing various kinds of liquid samples (ex. urine). Due to adsorption capability loading of blocking agents, pH and ionic strength modifiers and viscosity enhancers is easy to be performed.

When pre-treated by impregnation with proteins, buffers and detergents, the sample pad can modulate the flow properties increasing the sample viscosity, preventing non-specific adsorptions of both the conjugate and analyte, increasing the reaction time in the conjugate pad modulating in this way the interaction with the sample.

b) Conjugate pad

The function of this pad is to keep the dried conjugated particles and hold them stable in the pad until the test is run and to uniformly transfer the signaling reagent (ex. gold nanoparticles conjugates) and sample onto the membrane.[55] When the sample flows through the conjugate pad, the signaling reagent solubilizes, recognizes the analyte and the formed conjugate moves through the membrane. Assay sensitivity can be severely affected by the conjugate deposition, drying, inadequate conjugate mixing and releasing from the pad. Ideally, the conjugate pad must have low non-specific binding of signaling reagent or analyte to the pad, allow a suitable formation of the immunocomplex at the test line. In addition must ensure a constant flow and bed volume so as to avoid problems of uneven signals that can alter the sensitivity of assay. Glass fibers, cellulose filters, surface-treated (hydrophilic) polyester or polypropylene filters and rayon are the most used materials for conjugate pad.

To ensure an optimal release of the sample, the pad must be pre-treated with a pH adjusted buffer containing proteins and surfactants, followed by a suitable drying.

The deposition of conjugated particles can be achieved manually (batch mode) or by using a dispensing machine that delivers in a continuous mode solutions of reagents including suspension of nanoparticles modified with antibodies.

c) Detection pad

Its main purpose is to bind irreversibly the capture reagents at the test and control lines and facilitate the visualization of colored bands indicating the presence or absence of analyte in the sample.[55]

Nitrocellulose (NC) is the most widely used material for detection membranes in LF technology and other point-of-care (POC) devices. Depending on the application, other materials, *e.g.* nylon and polyethersulfone can be used as detection membrane.

NC is a versatile polymer that has been used for years due to its unique as biomolecules adsorbing properties. For this reason, the use of NC has been extended to powerful blotting techniques for identifying the presence of biomolecules such as proteins (Western blot), DNA (Southern blot) and RNA (Northern blot).[56–58] Based on these applications, over the past 25 years, NC has gained importance as a suitable porous support on LF technology.

Detection membrane is the most important part of a lateral flow assay because the binding and detection occurs within it. Therefore, the adsorption of biomolecules is an essential aspect for a good performance of LFAs. Even though the binding protein to NC has been reported and used for powerful and existing techniques, the binding mechanism is still not clear enough.[57] Different mechanisms have been proposed for explaining the binding mechanism. According to one of the theories proteins are thermodynamically driven to adsorb to nitrocellulose by non-covalent interactions.[56] Others claim that an initial attraction of protein to NC involves the interaction between the dipoles of the nitro groups on the NC and the carbonyl groups in peptide bonds of protein.[59] Either way, different forces (hydrogen bonding, hydrophobic and electrostatic interactions) are involved in the adsorption process of protein to NC; as recommended LF manufacturers must consider all these interactions, materials and assay reagents for optimizing the binding of the proteins to NC.[60]

Membranes made of nitrocellulose are hydrophobic by nature. However, membranes can easily be wet due to the presence of surfactants added during membrane production[55]. Selection of type and amount of surfactant use to be recommended by the manufacturer but also adapted according to the application. Once the membrane is processed and ready to be used, depositing of the capture reagents at test and control lines, can be carried out using either contact or non-contact dispensing system. The best option is non-contact dispenser, typically inkjet system, because the membrane does not suffer damages that can impede a normal flow of the sample. Nevertheless, low-contact dispenser systems can be found in the market.[61] In this case, the nozzles can dispense the sample with a minimal contact pressure avoiding any mechanical stress on the membrane.

Flow rate is difficult to be measured since decays exponentially while the fluid front moves through the membrane.[55] A common parameter to evaluate the NC membranes is the capillary flow time which is the time required for a liquid to move along and fill completely 4-cm long of membrane. The capillary flow time and the sensitivity of the assay increase when the pore size decreases, since the reagents spend more time on the membrane and the formation of immunocomplex between the analyte and the label is more effective at the test line.

Another parameter is the thickness of the membrane since it has a direct influence on bed volume and signal visibility. Bed volume is the volume of liquid required to saturate a given area of membrane and is related to the porosity and the thickness. As the thickness increases, the bed volume also increases. However, this consideration may be not important when an absorbent pad is used because the total volume of the sample is governed mainly by the bed volume of the absorbent pad.[55] When capture reagents are dispensed onto the membrane the liquid penetrates downward into it and moves laterally. In a thin membrane, spreading of the reagents will be occurring since its insufficient depth provokes the diffusion of the liquid (including nanoparticles used as labels) through the whole membrane causing difficult to be visualized signals (diffused / undefined detection and control lines).

d) Absorbent pad

Located at the end of the strip, its main function is to drain off the fluid from the membrane. Using an absorbent pad, the volume of the sample can be increased, being the background signal reduced and the sensitivity of the assay improved.

Most of absorbent pad are made of high-density cellulose and no treatments are required. However, once the experiment is achieved and a visual record is needed, it is recommendable to remove the absorbent pad because it can act as reservoir once the liquid has evaporated and it might release the excess of label reagent causing false positives.[62]

Table 1.1. Components of LFA and their functions.

Components	*Material*	*Function*
Sample pad	Cellulose	Distributes the sample in a controlled way for releasing the analyte with high efficiency
Conjugation pad	Glass fiber	Retains the conjugate between its fibers until the test is running. Coupling of analyte and conjugate takes place in this pad
Detection pad	Nitrocellulose	Binds irreversibly the capture reagents and facilitates the visualization of test and control lines
Absorbent pad	Cellulose	Drains off the excess of fluid of the detection pad

1.3.2.2.2. Labels

Immunoassay conjugate consists of an antibody with an appropriate label which function is to generate a signal that correlates with the immunocomplex formed and its antigen, allowing the detection by using techniques such as colorimetry, fluorescence and luminescence.[63]

Most of the commercial LFAs use colored latex beads, carbon nanoparticles and gold nanoparticles which allow visual detection without the use of readers if the test provides a qualitative response. On the other hand, if LFA is intended to be quantitative, the use of a reading system is required depending on the type of label used, for example: charged couple devices (CCD) cameras for AuNPs or colored beads; readers based on ligh-emitting diode (LED) technology for fluorescent labels, and magnetic readers such as Magnetic Assay Reader (MAR™) for superparamagnetic labels.

Applications of traditional labels will be briefly summarized in this section, while gold nanoparticles, will be discussed in detail in section 1.3.4.

a) Latex beads

Latex beads are spherical microparticles composed of an amorphous polymer (usually polystyrene). These beads have been used as the first labels in LF technology due to their high binding protein capacity.[63] Latex beads with various sizes and with controlled surface chemistries and able to incorporate colored dyes, fluorescent dyes and also magnetic or paramagnetic components have been already developed and are available in the market. Sensitivity of LFA that employs colored latex beads is in principle lower compared with the achieved with gold nanoparticle labels since their smaller sizes (typically 20-40nm) and consequently their higher surface area to volume ratio allow them to bind more antibodies onto their surface.

b) Liposomes

Liposomes are colloidal vesicles formed by a lipid bilayer membrane capable to encapsulate part of the aqueous media in which they are dispersed.[64] They can encapsulate *i.e.* visual and fluorescent dyes or enzymes inside their cores, improving the sensitivity of LFA. It is possible to add different functional groups to the lipid surface for coupling with biomolecules or chemicals. Different studies with interest for example for DNA[65], allergenic agents[66] and other analytes have been reported. However, liposomes have some disadvantages related to their high production cost, short shelf-life and propensity to leakage and fusion of encapsulated molecules.

c) Carbon nanoparticles

Carbon nanoparticles are the most inexpensive label for LFA and provide an excellent color contrast to the white NC membrane. These amorphous labels are suitable for physical adsorption because of their hydrophobic features and have been used for DNA[67,68] and small molecules *e.g.* chemical contaminants[69,70] detection. The main limitations of carbon nanoparticles are related to their low density, which difficult their visualization by electron microscopy (TEM or SEM), their irregular sizes and shapes and the requirement of surfactants addition to stabilize the carbon dispersions.[71]

d) Fluorescent labels

Organic and inorganic fluorophores can also be used as labels. A typical organic fluorophore for labeling antibodies is fluorescein isothiocyanate (FITC) which is

reactive to the primary amines of antibodies producing a fluorescent conjugate.[72] LFA using fluorescent labels to detect for example influenza virus has been shown to be more sensitive that colorimetric assays.[73]

Organic fluorescent dyes (*e.g.* $Ru(bipy)_3^{2+}$) have been used for coating of silica nanoparticles and their subsequent use in LFA demonstrating to be remarkably more sensitive than gold nanoparticles for nucleic acid detection.[74]

Inorganic fluorophores such as QDs and lanthanides also have been reported for LF applications. QDs are semiconductor nanoparticles in size range of 1-10 nm composed of GaN, GaP, ZnO, ZnS, CdS or CdSe[75]. As a consequence of their small sizes, they have unique properties such as the high quantum yield and molar extinction coefficients, broad absorption spectra and resistance to photobleaching and chemical degradation.[76] Uses of QDs in biosensors have grown in last years because of their advantages over common fluorophores. QDs can be conjugated to different biomolecules, especially antibodies. However, the main limitation of QDs is related to their low colloidal stability in biological media.[75]

QDs have been used as labels in LFA in competitive assays for detection of a primary metabolite biomarker for pesticides[77] toxins detection[78] and also, in sandwich formats for cancer biomarkers.[79]

Lanthanides (*e.g.* Eu(III)) also have unique fluorescent properties that can be applied for their use as sensitive labels for prostate-specific antigen (PSA) detection in LFA, increasing 300-fold the sensitivity of assay.[80]

1.3.3. Lateral Flow Assays advantages and limitations

LF is a well-established technology that has many advantages such as a) rapid qualitative or semi-quantitative tests; b) easy to use (results can be interpreted by untrained personnel); c) utility for in-field applications in remote areas where high-tech equipment is not available; d) prolonged shelf-life (about a year) and often without refrigeration; e) small volumes required; f) relatively low-cost production; g) good sensitivity and specificity and h) possibility of integration with electronics and electrochemical systems.

Despite of the mentioned advantages, LF technology has also limitations, especially related to reproducibility and sensitivity issues such as a) restricted volume around microliter level; b) higher volumes could deteriorate the strip and delay the assay time; c) pre-treatment is required for non-liquid samples and a filter must be added to the strip; d) integration with electronic/electrochemical systems is still a challenge; e) less sensitive than other immunoassay techniques, *e.g.* ELISA; f) multiple detection is challenging due to some cross-reactivity issues and the fact that the setup for dispensing on membrane requires spatial differentiation.
Nevertheless, LF technology has a wide range of applications in different fields and it is the most used POC test because fulfills the requirements for this class of device. Many efforts are currently being conducted in order to improve, either the used materials or the assay platforms with the purpose of solving sensitivity issues beside others. In this context, new strategies to enhance the sensitivity of LFA will be discussed in section 1.3.5.

1.3.4. Gold nanoparticles based LF biosensors

AuNPs have been used for many years in biomedical applications and their unique chemical and physical properties make them attractive for areas such as: diagnostic, therapy and immunology.[81–85]

In 1971, Faulk and Taylor[86] published the first report about the use of AuNPs as labels for immunoelectron microscopy. Nine years later, Leuvering *et al.* [50] presented the "sol particle immunoassay" (SPIA), the first colorimetric report using AuNPs as labels for hCG detection. Nowadays, AuNPs are the most used labels for LFA due to their signaling properties combined with their biocompatibility and low or missing toxicity overall for in-vitro applications.

There are a wide range of synthetic methods for obtaining AuNPs most of them based on chemical reduction of chloroauric acid, $HAuCl_4$.[82,87] Reduction of Au(III) to Au(0) in aqueous media in presence of citrate as mild reducing agent and stabilizer is the most used method for synthesizing AuNPs, as pioneered by Turkevich and co-workers.[88] Well dispersed and size-controlled AuNPs are obtained by controlling the ratio

citrate:Au.[89] Non-controlled sizes and uneven shapes of AuNPs can affect the performance of LFA.

AuNPs surface can be functionalized by biomolecules (*e.g.* antibodies and nucleic acids) due to their affinity for thiol-containing ligands. Antibodies can be attached (conjugated) to the AuNPs surface through hydrophobic and ionic interactions, or through chemisorption of thiol groups present in their structure.[90]

Three are the most reported methods for binding proteins to AuNPs:[91] i) gold nanoparticles surrounded by a layer of negative charges can be conjugated firmly to any protein positively charged due to the ionic binding; ii) aminoacids-containing proteins bind to the AuNPs through hydrophobic binding; iii) gold and sulphur bonding. AuNPs can be conjugated to antibodies by the cysteine residues in the protein.

Control of pH and a suitable concentration of antibody must be determined for avoiding flocculation of AuNPs.[92] The pH of a AuNPs dispersion must be adjusted before the conjugation at slightly above the isoelectric point (pKi) of the antibody. Aggregation of AuNPs conjugated will occur if the pH is below the pKi. By contrary, if the pH is above the pKi of the antibody, a limited adsorption will occur because of the charge repulsion between the AuNPs and the antibody.[93]

The optimum size of AuNPs for using as labels in LFA is around 20-40nm: below 10nm AuNPs have not bright and intense color and above 40nm AuNPs, they are prone to flocculation.

Lou *et al*.[94] studied the influence of the nanoparticle size for lateral flow applications. They prepared conjugates with four different AuNPs sizes (14nm, 16nm, 35nm and 38nm) and they found that different sized AuNPs had different conjugation efficiencies under different pH values and concentrations of antibody. Moreover, they proved that 16nm AuNPs remained stable at the lowest concentration of antibody but they observed less sensitivity than with 38nm AuNPs in real samples.

In the following part some of the most important applications of AuNP-based LF for different analytes such as protein, DNA, etc. are described and accordingly discussed.

Table 1.2 gives and overview of the applications for different fields of AuNPs-based lateral flow technology.

1.3.4.1. Protein detection

LF technology is well diversified in several sectors, being the pregnancy self-testing the largest segment on the LF market where a great number of companies commercialize these tests.[93] In addition, a high number of approaches for the detection of proteins of interest in different fields have been reported in the last years.

A study related with detection of thrombin (a serine protease related to the coagulation system) and aptamer-based LFA have been reported by Xu *et al.*[95] Aptamers are synthetic nucleic acids able to recognize a wide range of analytes with the same or even higher specificity than antibodies do. The strategy developed by Xu and co-workers for detection of thrombin introduced the use of aptamers instead of antibodies in a LFA achieving a limit of detection (LoD) of 2.5 nM of thrombin. Comparing the aptamer-based LFA with the traditional antibody-based LFA, the authors found more sensitive assay using the synthetic nucleic acids.

Cancer biomarkers detection using LFA also have been reported. One of the examples includes CEA which acts as biomarker for several cancer including colon, breast, ovarian and lung cancer. Zeng and co-workers[96] developed a LFA for detecting CEA in human serum. They could detect CEA in a 10-min assay with a LoD of 5 ng/mL. Although this value was higher than the LoD provided by a commercial ELISA kit for CEA detection, the assay time was considerably shorter (around 90 min) and simpler, opening the way to rapid and simple diagnostic kits. .

Prostate specific antigen (PSA) is a glycoprotein synthetized in the prostate gland and their presence in high concentrations in male serum is related with prostate cancer u other prostate disorders. Fernández-Sánchez *et al.*[97] reported the sensitive detection of free and total PSA (f-PSA and t-PSA, respectively). They developed an integrated AuNPs based-LF strip with an electrochemical system by using impedimetric detection, achieving a LoD of 3 ng/mL of PSA. One year later, the same group[98] reported a sensitive detection of f-PSA and t-PSA in one-step LFA. The authors achieved a series

of optimizations including a careful selection of materials and experimental conditions, for achieving a visual LoD of 1 ng/mL for both biomarkers.

Another prostatic cancer biomarker is the prostatic acid phosphatase (PAP) which is combined with PSA test that leads to a more accurate cancer diagnostics. For this reason Fang and co-workers[99] developed a semi-quantitative barcode LFA for PAP detection in human serum samples. Based on the stepwise capture of analyte, they achieved a LoD of 0.25 ng/mL in 30 min.

Choi and co-workers[100] reported an enhanced LFA for the detection of troponin I, a biomarker related to the acute myocardial infarction (AMI). They detected up to 0.01 ng/mL of troponin I in serum, which is lower than the cutoff value of 0.1 ng/mL for diagnosis of myocardial infarction. Following a similar strategy, Zhu *et al.*[101] reported the simultaneous detection of two biomarkers (troponin I and myoglobin) related to the AMI. They used an AuNPs doubly labeled complex, in which biotinylated ssDNA was used as a linkage to integrate two AuNPs of different sizes (13nm and 41 nm). With this enhanced strategy, very low LoD of 1 ng/mL and 1 μg/mL, were reached for troponin I and myoglobin, respectively.

1.3.4.2. Nucleic acids

Nucleic acid detection is of outstanding importance in molecular diagnosis due to the interest in human and veterinary research beside others.[102,103] When a small amount of DNA is available, it is required a previous amplification that can be achieved by using the polymerase chain reaction (PCR) or isothermal amplification techniques. Over the last years, a new generation of integrated and sophisticated miniaturized POC nucleic acid devices is emerging.[104] An easy and low-cost alternative approach is the use of nucleic acid lateral flow (NALF) assay, which uses nucleic acids hybridization event to capture and detect synthetic DNA sequences or amplified nucleic acid products.[105] Usually, the capture of nucleic acids can be performed in two main formats: i) in an antibody-dependent or ii) antibody-independent manner (see figure 1.7). The former one, named nucleic acid lateral flow immunoassay (NALFIA), uses an antibody which is located at the test line and a labeled amplicon or a complementary sequence to the amplicon. When an antibody-independent format is used, the attachment of the

oligonucleotide probe can be carried out through biotin-streptavidin linkage or by using UV irradiation for covalently binding it to the NC surface.

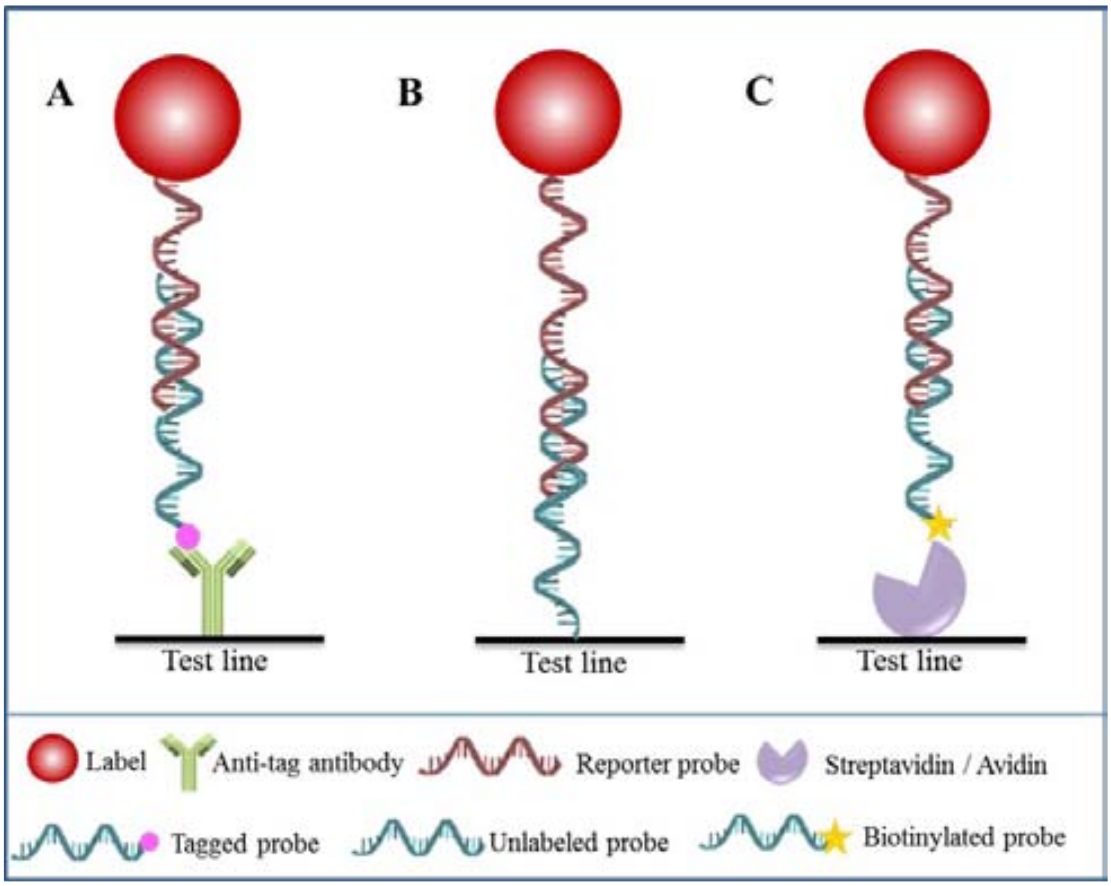

Figure 1.7. General strategies for the capture probe immobilization in nucleic acid lateral flow (NALF) assays. (A) Anti body-dependent format. An anti-tag antibody is attached at test line and recognizes a tagged probe which hybridizes with a reporter labeled probe. (B) Anti body-independent format without molecular receptor. An unlabeled probe is directly attached at test line. Detection is produced when a reporter labeled probe hybridize to the other probe. (C) Antibody-independent format using a molecular receptor. The most common strategy takes advantage of the biotin/streptavidin linkage for attaching the biotinylated probe on the test line.

Piepenburg *et al*.[106] developed an isothermal amplification method (recombinase polymerase amplification, RPA) which allow them to detect few copies of pathogen genomic DNA, using NALFIA format (see figure 1.7A). In this work, a double labeled (biotin/carboxyfluorescein-FAM) RPA amplicon was captured by an anti-biotin antibody immobilized at test line. When the flow is passing through the membrane, the visualization of the lines is produced by the binding between an anti-FAM-AuNPs conjugate and the amplicon tail labeled with FAM.

A similar approach was reported by He and co-workers[107] who developed a NALFIA for detection of the mutation in the R156H gene of keratin. The gene was amplified by

isothermal strand-displacement polymerase reaction (ISDPR) technique using primers labelled with digoxin and biotin and finally detected using streptavidin receptors and anti-digoxigenin-AuNPs labels, obtaining LoD of 1 fM of R156H-mutant DNA.

Detection and quantification of microRNA (miRNA) can be achieved in NALFIA devices as reported by Hou and co-workers[108]. AuNPs were conjugated to a thiol-DNA that acts as detection probe whereas a biotin ssDNA serves as the capture probe. Detection is produced when the anti-avidin antibody immobilized at test line recognizes the avidin–biotin–AuNPs-sample complex. The authors reported a perfect match between the capture probe with tested miRNA and detection probe, instead of the common sandwich in which the tested probe hybridizes with the capture and detection probes. Finally, they used the silver enhancement method to catalytically growth silver on the AuNPs and in this way increase the sensitivity of the assay, reaching a LoD of 5 amol opening the way to further application of this method for the detection of other short oligonucleotides.

Detection of single DNA mutations, also known as single oligonucleotide polymorphism (SNP), can be achieved with high sensitivity and specificity by using NALFIA devices as reported by Xiao *et al*.[109] They used AuNPs as label, the circular strand displacement reaction for amplifying the target and the ligation reaction performed by T4 DNA ligase (a type of enzyme from bacteriophage T4 that enables of DNA strands) which provides high specificity recognizing single-base mismatches. With this strategy, the authors reported a LoD of 0.01 fM for wild-type target DNA with high specificity and also, the performance of the device using human genomic DNA clinical samples showed to be excellent.

On the other hand, in the antibody-independent NALF, the capture reagent is an oligonucleotide probe that can be labeled (*e.g.* biotin) or not, which is located at test line instead of antibody (see figure 1.7B-C). An unlabeled oligonucleotide probe can be covalently attached to nylon and nitrocellulose membranes by cross-linking using UV irradiation. In 2007, Aveyard and co-workers[110] reported the first NALF device with these features for the detection of amplified PCR products. They reported a sandwich assay between the target probe which was complementary to the AuNPs-labeled probe and the capture probe attached to the NC. Also, they studied the effect of different AuNPs sizes in the performance of the assay and they found that sensitivities of devices

with AuNPs of 80 nm were higher than AuNPs of 40 nm which are the most common size used for LF purposes and showed the possibility to detect unpurified PCR products using an antibody-independent format.

The most common format in NALF devices uses biotin labeled oligonucleotide probes attached to the NC surface via biotin-streptavidin linkage (see figure 1.7C). Following this format, Mao and co-workers[111] developed a sensitive and rapid NALF for DNA detection with a LoD of 50 pM of target. They used an enzymatic-signal enhancement and applied the device for detection of human genomic DNA obtaining a LoD of 1.25 fM, value considerably low compared with the obtained with alternative techniques such as microarray or surface plasmon resonance based analysis.

Lie and co-workers[112] developed a NALF for detection of amplified DNA sequences by ISDPR. The sensitivity of this device based on this isothermal amplification is comparable or even better than the obtained with colorimetric or fluorescence-based analysis. Following this approach, they were able to detected human genome at levels of 25 ng/mL in clinical samples.

1.3.4.2.1. Infectious agents detection

LFA of nucleic acids with interest for POC infectious diseases diagnostics also have been reported. Infectious diseases cause millions of death every year and most of them are caused by late detection and lack of suitable treatment overall in countries with less resources for which the application of LFA should be of great interest so as to detect an infectious disease in early stages.[113–116]

Although there are five mayor types of infectious agents such as bacteria, viruses, fungi, protozoa and helminthes[117] in this section the described examples will include bacteria and viruses detection based on the use of NALF and NALFIA devices.

Horng *et al.*[118] developed a NALFIA device for detection of *Legionella* bacteria from environmental cooling tower samples using multiplex-nested PCR as amplification method of 16S rDNA and *dnaJ* DNA fragments. In multidetection and specific AuNPs-based NALFIA they could identify the presence of *Legionella* species and more specifically, *Legionella pneumophila* if one or two test lines were colored, respectively. The authors reported a LoD of 0.5 colony-forming-units (CFU)/mL and also, 100%

sensitivity and specificity for *L. pneumophila* compared with traditional detection methods.

For *Vibrio Cholerae* detection, a foodborne pathogen, Chua and co-workers[119] developed a NALFIA which consisted in an antibody-dependent format by using PCR technique and double labeled primers (biotin/fluorescein and digoxigenin/fluorescein). Microspheres coated with streptavidin, anti-digoxin and anti-mouse IgG antibody were deposited on the strip which acts as test, internal control of PCR amplification and migration control lines, respectively. The DNA target, biotin labeled DNA, was captured by the streptavidin located at test line. The internal control, digoxigenin labeled DNA, was captured by the anti-digoxigenin antibody and the migration control line was visualized through the binding between AuNPs–mouse anti-fluorescein antibody conjugate and an anti-mouse antibody. Using this strategy they could verify the efficiency of the DNA amplification and they could detect up to 5 ng of target DNA (see figure 1.8A).

Recently, Liu *et al.*[120] developed an ultrasensitive NALFIA for *Salmonella* detection, a common foodborne pathogen; it was based on the hybridization between AuNPs-DNA probes complementary to the 16S ribosomal RNA and DNA of the bacteria. A LoD of 5 fmol was found for the synthetic ssDNA. For the *Salmonella* cultured samples, nucleic acids from 10^7 cells were detected in 30 min by naked-eye. Using silver enhancement of AuNPs, the LoD was improved up to 10^4 cells in other additional 10 minutes.

The catalytic deposition of gold (III) on AuNPs is an amplification strategy used for the enhancement of the NALF signal. Two representative works have applied this strategy for infectious agents enhanced detection. In the first one, a semi-quantitative detection of amplified HIV-1 RNA using a NALF device using was developed by Rohrman *et al.*[121] Two complementary probes were covalently attached to the NC surface by UV irradiation and the RNA target sequence was isothermally amplified by nucleic acid sequence based amplification (NASBA) technique (see figure 1.8B). The authors reported a LoD of 10^{11} copies/mL of amplified HIV RNA using gold enhancement which match with the clinical range for viral HIV-1 loads. In the second one, detection of *Escherichia coli* 157:H7 in a NALF device using locked nucleic acids (LNA)-AuNPs conjugates was reported by Rastogy and co-workers.[122] With the enhancement protocol

the sensitivity of the assay was improved by 3-fold when LNA-AuNPs conjugates were used in NALF device instead of DNA-AuNPs conjugate.

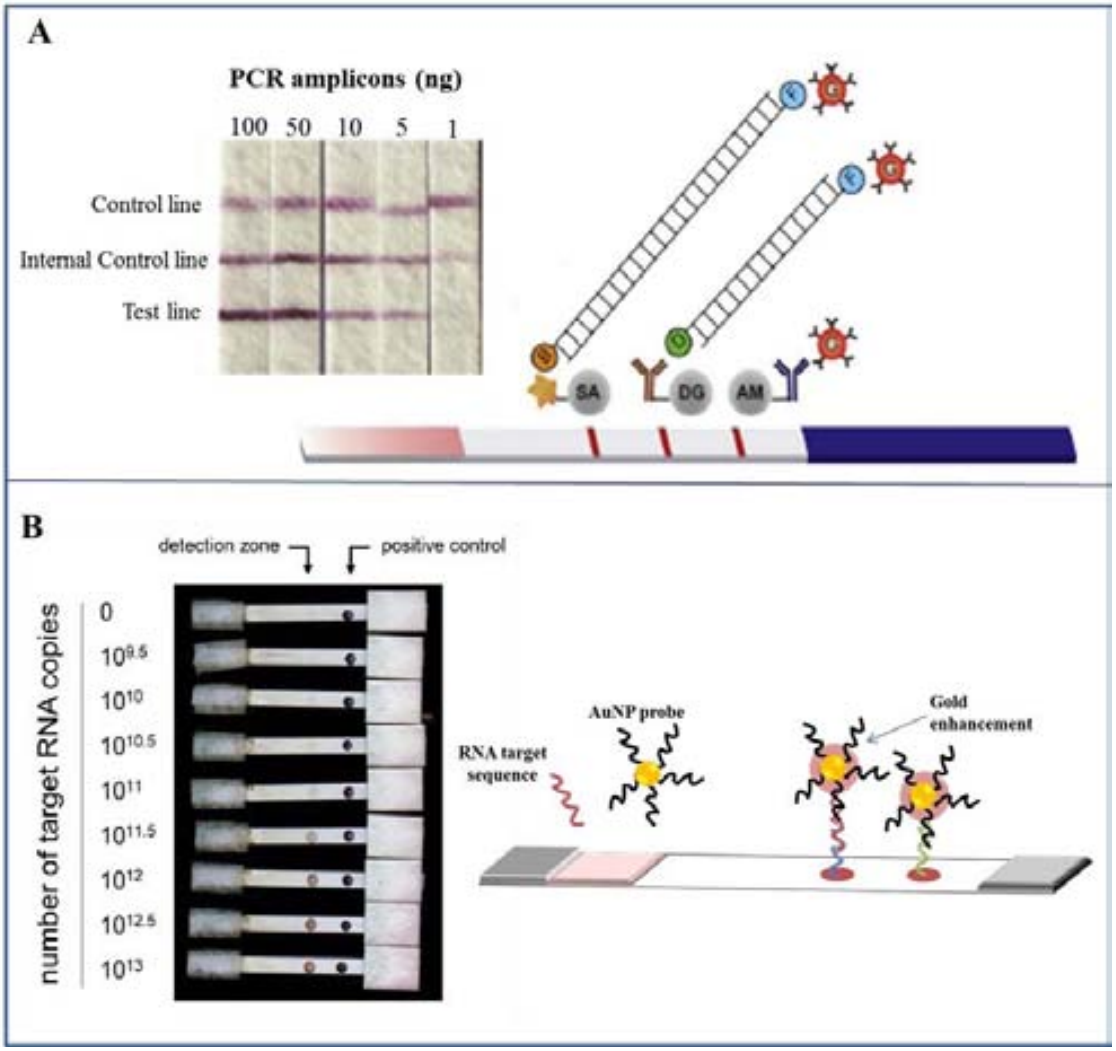

Figure 1.8. NALFIA and NALF assays for Infectious agents detection. (A) Scheme of NALFIA for visualization of PCR amplicons by using capture reagents coated onto carrier beads and immobilized onto a glass fibre membrane and picture of strips for a PCR amplicon range of 1-100 ng. (B) Left: Image of NALF devices for a serie of in vitro transcribed RNA from 9.5 to 13 log10 copies. Right: NALF design for HIV-1 detection. Adapted from [119] and [121] with permission.

1.3.4.3. Mycotoxins

A toxin is a poisonous substance produced by living cells and organisms. Among the different classes of toxins, mycotoxins are natural secondary metabolites produced by different species of fungi that mainly belong to *Aspergillus*, *Penicillium* and *Fusarium* genera.[123] Mycotoxins represent a health risk problem for human and animals because

they are capable to cause diseases. First-screening methods for mycotoxins detection as LFA have been commercially developed and reviewed in last few years.[124–126]

Since mycotoxins are very small compounds, a suitable LFA for their detection is the competitive format as stated in Section 1.3.2.1. Therefore, some works related to the detection of mycotoxins using AuNPs as labels in a competitive LFA format will be discussed in this section.

Aflatoxins are carcinogen mycotoxins which are produced by *Aspergillus flavus, Aspergillus nomius*, and *Aspergillus parasiticus*, species of fungi. Delmulle *et al*.[127] developed a qualitative LFA for detection of aflatoxin B_1 (AFB_1) in pig feed. Rabbit anti-mouse antibodies and AFB_1-bovine serum albumin conjugate were immobilized at control line and test line, respectively. When the liquid sample passes through the membrane, AuNPs labeled-monoclonal anti-AFB_1 antibodies are saturated by the presence of the toxin resulting in a non-visible test line and visible control line which indicates the proper performance of the LFA. Using this LFA format, they obtained a visual LoD of 5 μg/kg of AFB_1, in a simple and rapid test.

A modified competitive format assay was proposed by Moon and co-workers [128] for detection of aflatoxin B_1. The authors reported the immobilization of polyclonal anti-AFB_1 on the NC membrane and AuNPs-AFB_1-BSA conjugate as detection reagent. In the absence of AFB_1, the conjugate can bind to the anti-AFB_1 located at detection zone, giving rise to the visible line. On the contrary, if the AFB_1 is present in the sample, it inhibits the binding of the conjugate with antibodies avoiding the visualization of test zone. With this modified competitive LFA format, the authors reported a visual LoD of 10 μg/mL of AFB_1 and also, they examined the cross-reactivity to similar compounds such as ochratoxin-A (OTA) finding that the device was only specific to AFB_1. One year later, Moon *et al*.[129] improved the modified competitive format and semi-quantification was possible using a Smartphone for acquisition and processing of the image. With this technology it is possible to discriminate between the blank from contaminated samples on the base of peak and area values, provided by and Android application, being able to quantify up to 5 μg/kg of AFB_1.

Zearalenone (ZEA) and deoxynivalenol (DON) are secondary metabolites produced by fungi *Fusarium* species, which can be found in grains. Simultaneous detection of these mycotoxins was first reported by Kolosova and co-workers.[130] They developed a LFA

in a traditional competitive format and results were visually evaluated by using AuNP of 40 nm. In absence of toxins in sample, three lines were observed (migration control and test lines). For positive samples, only the control line is visualized due to the presence of both mycotoxins. Finally, if two lines appeared (control and one of the test line) the sample was positive for ZEA or DON. Cut-off levels observed for both mycotoxins were of 1500 and 100 μg/kg for DON and ZEA, respectively. In addition, spiked wheat samples were analyzed with the LF strips resulting in good agreement with the amount spiked, proving the reliability of the assay.

Detection of DON using AuNPs as labels was also reported by Kolosova *et al.*[131] According to experimental results, they could detect DON at low and high concentration levels between 250-500 and 1000-2000 μg/kg, respectively. Spiked wheat and pig feed samples demonstrated accurate and reproducible results. Moreover, LFA were tested in real field conditions proving the applicability of the devices.

Fumonisins belongs to the same family of ZEA and DON mycotoxins. They occur mainly in maize, wheat and cereals. From the group B fumonisins, fumonisin B1 (FB1) is considered as a possible carcinogen to humans by the International Agency for Research on Cancer.[132] A semi-quantitative LFA was developed for detection of total type B fumonisins in maize by Molinelli *et al*.[133] They reported a LoD of 199 μg/kg in a test range up to 4000 μg/kg, with no cross-reactivity toward other mycotoxins and the applicability of the device was proved by the screening of 23 naturally contaminated maize samples.

Ochratoxins are produced by fungi species such as *Aspergillus ochraceus, Aspergillus carbonarius, Aspergillus niger* and *Penicillium verrucosum.* The most relevant toxin of this group is OTA, one of the most abundant food-contaminating mycotoxins. A semi-quantative LFA was developed by Anfossi and *et al.*[134] for detection of OTA in cereals. They reported the use of ovalbumin as AuNPs stabilizer and as membrane blocker so as to reduce non-specific adsorptions. Additionally, the use of polyethylene glycol instead or organic solvents for OTA extraction, allowed to avoid the matrix effects caused for the cereals used. Under these conditions, they reported a LoD of 1.5 μg/kg of OTA in samples.

Recently, semi-quantative detection of OTA in wine and grape must, which represent a major source of OTA dietary intake, was described by Anfossi and co-workers.[135] The reported LFA allowed OTA detection in wine in 5 min with a LoD of 1 μg/L with a simple sample pre-treatment which only implied its dilution with sodium bicarbonate, polyethylene glycol and ethanol.

Another interesting strategy for OTA detection based on aptamer based-LFA was developed by Wang and co-workers.[136] The principle of the assay consisted on the competition for the aptamer (labeled with AuNPs) between OTA and complementary DNA probes located at the test line. The results indicated that the developed aptamer-based LFA was more sensitive than those conventional immunoassays due to their high specificity to a wide range of targets including small compounds. Visual LoD was 1 ng/mL and semi-quantitative LoD 0.18 ng/mL obtained with a strip reader (see figure 1.9)

1.3.4.1. Pesticides

The term pesticide is referred to substances used for controlling or destroying plant or animal pest, that also includes herbicides, fungicides and insecticides.[137] The health and environmental risk that represent these substances makes necessary the control of their use by setting the amount of pesticide in agricultural products. Nowadays, nanomaterials are bringing new opportunities for pesticides detection because the analysis can be achieved *in situ* by using electrochemical and optical techniques.[138,139]

For screening and rapid detection of pesticides, different LFA in a competitive format due to the low molecular weight of these substances have been developed.

Wang *et al.*[140] developed a semi-quantitative LFA for detection of carbaryl which belongs to the class of carbamates and it is used as insecticide. They could obtain a LoD of 100 μg/L, higher than conventional methods as membrane-based ELISA, but the LFA provided in an one-step the semi-quantative carbaryl detection avoiding the use of carcinogenic and mutagenic substrates.

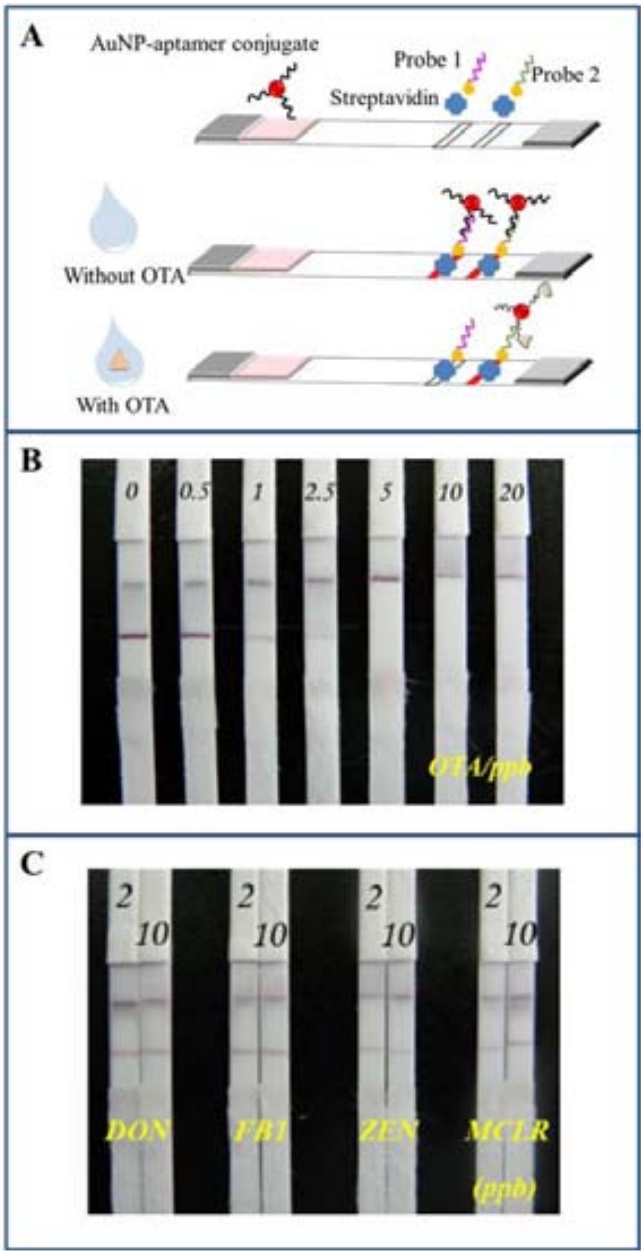

Figure 1.9. Detection of ochratoxin-A in an aptamer-based LFA. (A) Scheme of competitive aptamer-based LFA. (B) Picture of the strips for different OTA concentrations. (C) Specificity test towards several mycotoxins. Adapted from [136] with permission.

Atrazine is an organic compound used as herbicide which has been detected in water by Shim and co-workers[141] using AuNP-based LFA in a competitive format The authors reported a visual limit of detection of 3 ng/mL and specificity tests showed a high selectivity to atrazine without cross-reactivity with other pesticides. Additionally, the results for the spiked water samples were in good agreement with the obtained by direct competitive ELISA and high performance liquid chromatography (HPLC). An improved detection of atrazine by employing AuNP-based LFA in a competitive format was presented by Kaur *et al*.[142] In this work, they prepared a novel and very stable tracer

by synthetizing derivatives of atrazine which served as hapten molecules, that were first conjugated to a carrier protein (*e.g.* BSA) and finally to AuNPs, forming the hapten-protein-AuNPs conjugate. As the typical competitive assays, the atrazine and the conjugate compete with the available sites in the anti-atrazine antibody. The authors reported limits of detection below 0.1 ng/mL of atrazine in water samples.

Triazophos belongs to the class of organophosphates pesticides and it is widely used as insecticide and acaricide. Gui and co-workers[143] developed a competitive AuNP-based LFA for detecting residues of this compound in a short time, obtaining a LoD of 5 ng/mL in water and soil.

1.3.4.2. Heavy metals

Detection of metal ions is of vital importance in environmental monitoring due to the potential hazardous effects that can affect the human health. Heavy metals such as mercury, cadmium and lead are released to the environment due to industrial activities, causing contamination to water and soil. Biological uptake of heavy metal ions through the food chain can cause chronic poisoning. Other heavy metal ions such as chromium, zinc or copper are necessary for metabolic functions, but their presence at high levels can cause damage to liver, pancreas and stomach affecting seriously the human health.[144]

Traditional analytical techniques for metal detection such as inductively coupled plasma mass spectroscopy (IP-OES) or atomic absorption spectroscopy (AAS) are used for metal detection due to their reliable results but these analyses are not compatible with the field applications due to the use of complex instrumentation. In recent years, the use of biosensors for metal ion detection has been growing because of their remarkably selectivity through different metals which makes them sensitive and easy-to-use devices. In this context, Mazumdar *et al.*[145] described a LFA for lead detection in paints using AuNPs-DNAzyme conjugates. A deoxyribozyme or DNAzyme is a DNA molecule that is able to catalyze a reaction in the presence of a particular metal ion. In this approach, the authors prepared an enzyme-substrate-AuNPs complex composed by a modified 8-17 DNAzyme with biotin at one tail and thiol group in the other one, in order to be conjugated to the AuNPs and then, spotted at the conjugation pad. In the

absence of Pb^{2+}, the substrate remains uncleaved and a red line at the control zone is observed due to the binding with the biotin modified tail of the complex. On the other hand, if Pb^{2+} is present on the sample the cleavage of the substrate is produced and can migrate and be captured by a complementary DNA sequence located at the test line. With this strategy, the authors reported a LF device with useful industrial applications and with LoD of 0.5 μM of Pb^{2+}.

Following a similar approach, Fang and co-workers[146] reported the detection of Cu^{2+} with high sensitivity and selectivity. In a sample containing Cu^{2+} the cleavage of the substrate is produced and then, the cleaved product is analyzed in the NALF device. Two complementary DNA sequences are deposited on the strip to form the test and control lines. AuNPs are modified with a first probe which is complementary to the cleaved piece at 5'end, forming a DNA-AuNPs conjugate that migrates through the membrane. The test line is visualized when the second DNA probe located in this zone hybridizes with the cleaved piece at the 3' end. Finally, the excess of DNA-AuNPs conjugate migrates until the control zone and the hybridization between the third DNA probe and the conjugate is produced. The intensity of color of the test line is proportionally related to the concentration of Cu^{2+} in the sample, obtaining a limit of detection of 10 nM. In the absence of copper ion, the cleavage in the substrate is not produced and only the control line is visualized, indicating that the biosensor works properly. In addition, the authors used sample solutions containing different metal ions and the results showed high specificity towards Cu^{2+}.

He *et al*.[147] reported the detection of Hg^{2+} in aqueous solutions based in the thymine-Hg^{2+}-thymine coordination chemistry by using thymine-rich hairpin DNA probes. Briefly, in the presence of Hg^{2+} and the thymine-rich DNA probe, the thiolated hairpin DNA probe immobilized on the surface of AuNPs opens to form DNA duplexes (thymine-Hg^{2+}-thymine). While these DNA duplex moves through the membrane, the test line is visualized due to the recognition between the anti-digoxin and the digoxin labels on the duplexes. Finally, the control line is visualized through the hybridization between the thiolated hairpin DNA and a biotinylated control probe. Using this strategy, the authors reported a limit of detection of 0.1 nM and showed that the presence of other metal ions in samples do not affect the detection of Hg^{2+}. In a similar and less sensitive approach, Yang and co-workers[148] described the detection of Hg^{2+} using a thiolated DNA probe conjugated to AuNPs which hybridizes with a second biotinylated probe

forming a DNA duplex due to the strong thymine-Hg^{2+}-thymine coordination. This complex is visualized because of the binding between the streptavidin located at test line and the biotinylated DNA duplex. A third DNA probe, complementary to the thiolated one, produced the visualization of control line. In the absence of mercury ion, only the control line is observed. By using this strategy, the authors reported a LoD of 6 nM for Hg^{2+} and a high selectivity towards this metal ion.

Detection of Cr^{3+} ion in water and serum samples by using a gold-based LFA was reported by Liu *et al*.[149] The principle of the assay consisted in a competitive format, where the AuNPs were conjugated to antibodies against isothiocyanobenzyl-EDTA (iEDTA)-chelated Cr^{3+}. In the absence of Cr^{3+}, the conjugated-nanoparticle can be captured by the coating antigen and the goat anti-EDTA deposited at the test and control line, respectively. Therefore, two lines can be observed on the strip. In contrast, in presence of Cr^{3+}, the nanoparticle-conjugated reacts first with the Cr^{3+} in the sample and in consequence just the control line is observed. The authors reported a LoD of 4.8 ng/mL and also tested samples with different metal ions showing a high specificity towards Cr^{3+} ion.

Determination of Cd^{2+} in drinking and tap water using a competitive LFA was recently introduced by López-Marzo and co-workers.[150,151] The detection principle of Cd^{2+} ion is based on the competition between the Cd-EDTA complexes with the Cd-EDTA-BSA-AuNPs conjugate for the same binding site of a purified monoclonal antibody, which specifically recognizes Cd-EDTA complexes but no free Cd^{2+} ions. This affinity is associated with certain residues such as histidine-H96 and tryptophan, on the heavy chain variable regions of the antibody which are important as antigen recognition sites. A very low limit of detection of 0.1 nM was found which constitutes the lowest value reported for paper-based biosensors (see figure 1.10). The authors also tested the specificity of the assay using different metal ions with Cd^{2+} ion and the results showed several degrees of interference that can be reduced optimizing the concentration of reagents such as EDTA and OVA or BSA.

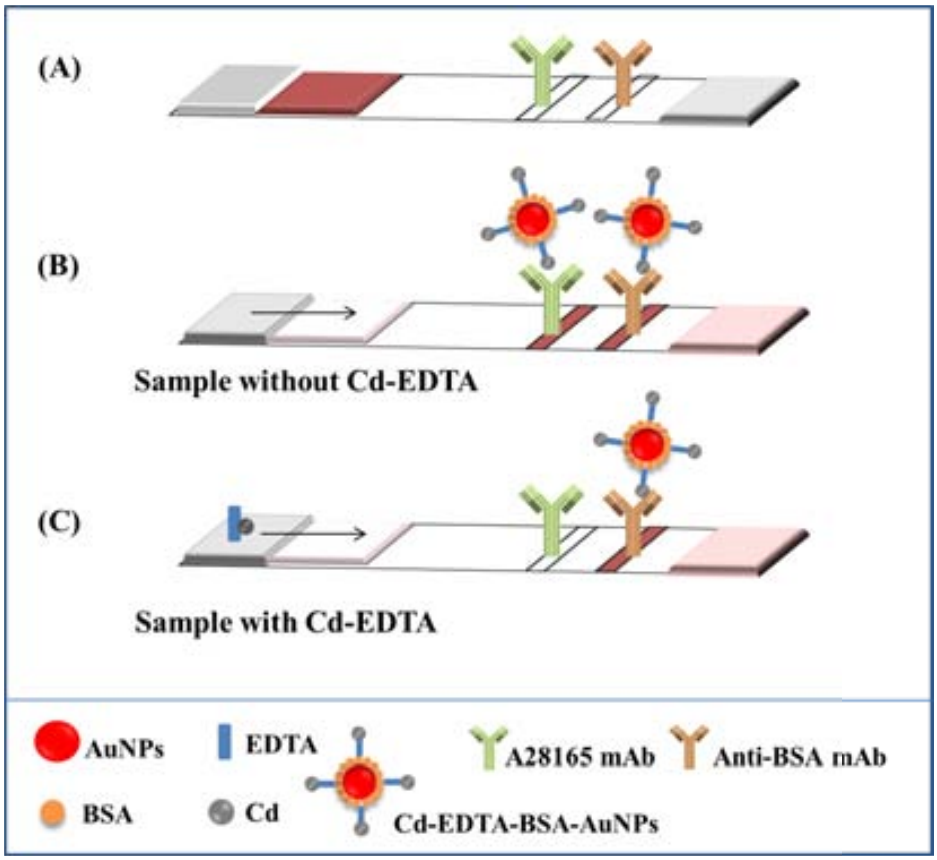

Figure 1.10. Cadmium analysis in waters through LFA-based immunodetection of Cd-EDTA. (A) Configuration of the LF strip and its state after adding the sample without (B) and with (C) Cd-EDTA. Adapted from [150] with permission.

1.3.5. New trends on lateral flow technology

1.3.5.1. Amplification strategies

In last years, many efforts have been focused in order to improve the sensitivity of LFAs, being of special interest those which exploit the benefits offered by the nanotechnology.

Most of the different strategies used for developing more sensitive devices require additional assay steps. The immunogold silver-staining (IGSS) is a technique used for enhancing the signal which is based on the reduction of silver ions over the surface of AuNPs increasing their size and therefore, improving the sensitivity of the assay. Shyu *et al*.[152] described a AuNP-based LFA for determining ricin, reporting a limit of detection of 50 ng/mL in a standard assay but when they used the silver-enhancement as signal amplifier method, the LoD decreased considerably to 100 pg/mL. Cho and co-

workers,[153] reported the detection of cardiac troponin I in a cross-flow chromatographic assay using the IGGS as signal amplifier and this method increased the sensitivity by 51-fold compared with the conventional gold-based LFA.

Other method for enhancing the sensitivity of LFA by *in situ* increasing the size of AuNP is the gold-mediated amplification. Rastogi and co-workers[122] developed a device for detection of DNA specific to *Escherichia Coli* O157:H7 by using locked nucleic acids (LNA) and this amplification method. To achieve autocatalytic deposition of gold over the AuNP surface and subsequent growth of AuNP, an aliquot of amplifier solution composed by $HAuCl_4$ and formaldehyde in a suitable ratio was dropped directly over the membrane once the conventional assay was developed. Using this strategy, the authors reported 0.4 nM as LoD.

Signal amplification in a LFA for human IgG detection using gold nanoparticles as carriers of enzymatic labels has been very recently reported by Parolo *et al*.[154] In this work they described the use of AuNP as direct labels giving a less sensitive detection range, but when the nanoparticles were coupled with an antibody modified by HRP, they could act also as carriers labels. Three different HRP substrates were tested and added to the strips after the direct detection with AuNP. The 3,3,5,5-Tetramethylbenzidine (TMB) gave the best result for LFA applications (see figure 1.11), enhancing the LoD up to one order of magnitude (200 pg/mL) compared with the traditional assay (5 ng/mL).

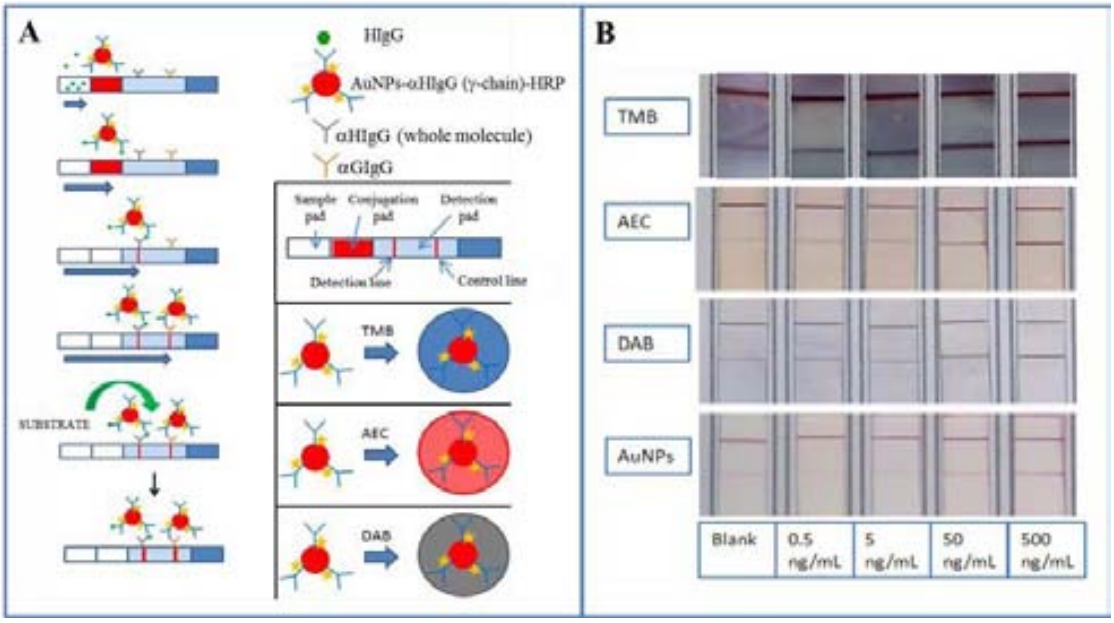

Figure 1.11. LFA signal amplification using AuNPs as carriers of enzymes. (A) Principle of the enhanced assay using HRP enzyme and three different substrates: TMB, AEC and DAB. (B) Pictures of LFA strips for different HIgG concentrations using the three different substrates. Adapted from [154] with permission.

Although the mentioned methods greatly increase the sensitivity of LFA, they required two steps: detection and signal amplification, which implies more reagents, additional procedures and longer detection times.

Another interesting method for intensifying the signal involves the use of gold-nanoparticles of different sizes in the same lateral flow strip. Choi *et al*.[100] studied the effect produced in the LFA sensitivity using gold nanoparticles of different sizes for troponin I detection. The assay consisted in the recognition between 40mn AuNP nanoparticles and 10nm AuNP primarily accumulated at the test line. Briefly, smaller AuNP were conjugated to anti-troponin I antibody and blocked by BSA, bigger AuNP were conjugated to anti-BSA antibody and both groups were retained in different conjugate pads. When the sample flows through the membrane, the smaller nanoparticles recognize the analyte and flow fast arriving first to the test zone. In contrast, bigger nanoparticles flow slower due to their size, they recognize the conjugated of 10nm AuNP and an increase in sensitivity of around 100-fold is consequently achieved (see figure 1.12)

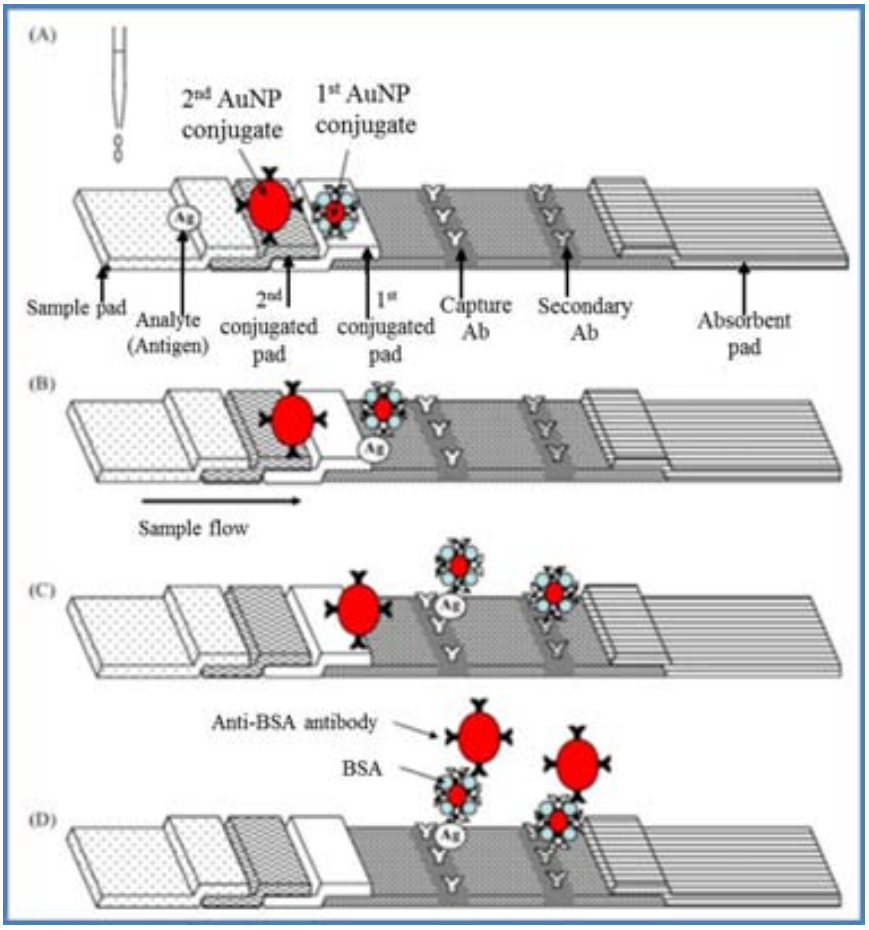

Figure 1.12. LFA signal amplification using dual AuNP conjugates. Adapted from [100] with permission.

Other methods for signal amplification using a composite formed by the immobilization of AuNP over a Fe_2O_3 nanoparticles core was reported by Tang and co-workers [155]. They applied this strategy for fast screening of aflatoxin B2 in a competitive LFA and found a LoD of 0.9 ng/mL which was 3-fold lower than the value found for conventional LFA using AuNP as label.

Inspired by this work, Liu and co-workers[156] reported the use of Fe_3O_4 nanoparticles aggregates as labels for detection of pesticide residues. The authors achieved a controlled aggregation of magnetic nanoparticles by cross-linking the polyethylene glycol-coated Fe_3O_4 NP bearing surface carbonyl groups with poly-L-lysine, followed by the conjugation with anti-pesticide antibodies. Employing this approach, they reported a LoD of 1.7 ng/mL which was 40-fold lower that the assay with Fe_3O_4 NPs.

An interesting and simple strategy based on changes of architecture of gold-based LFA was also very recently presented by Parolo *et al*.[157] The authors studied the effect on the sensitivity of the assay by simply changing the dimensions of the conjugate and sample pad. Increasing the size of sample pad and keeping constant the conjugate pad size, no clear positive effect on sensitivity was observed. However, by increasing the size of both the conjugate and sample pad an 8-fold improvement in the limit of quantification was achieved (see figure 1.13).

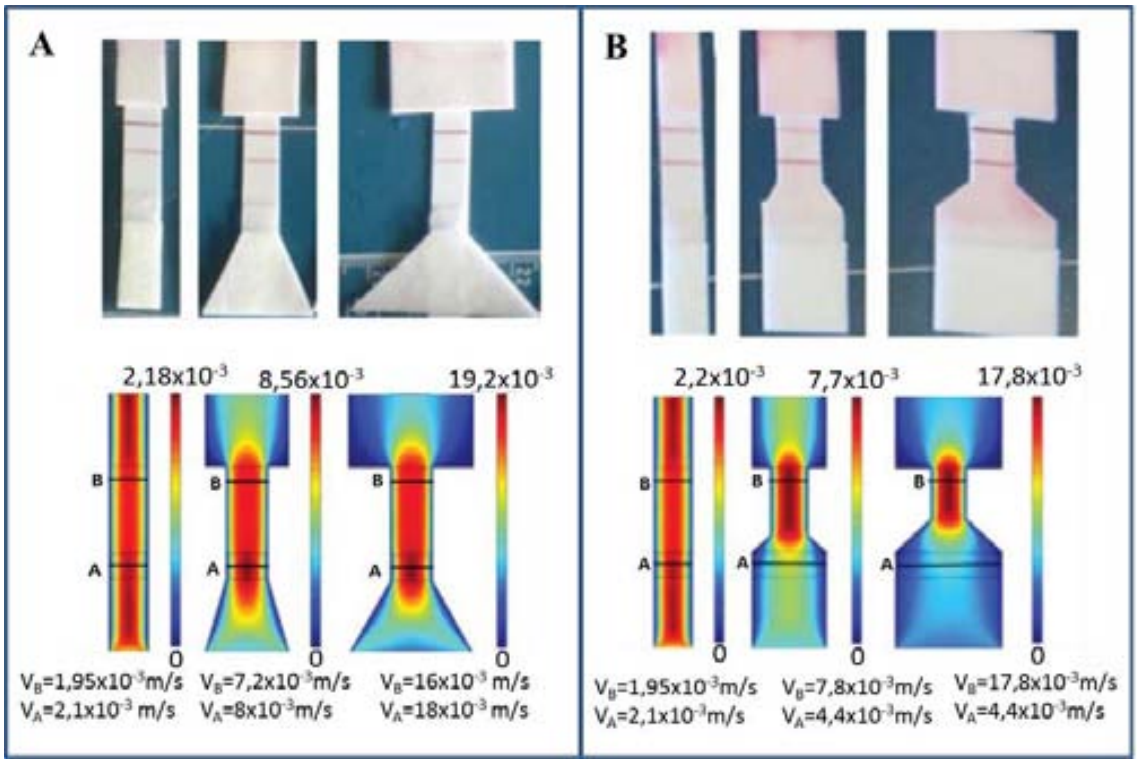

Figure 1.13. LFA signal amplification by changing the standard LF strip geometries. (A) Above: Pictures of LFA with different sample pad architectures for 60 ng/mL of human IgG (HIgG). Bottom: Flow speed simulations for sample pads with different sizes. (B) Above: Pictures of LFA with different sample and conjugation pads designs for 60 ng/mL HIgG. Bottom: Flow speed simulations for sample and conjugation pads with different designs. Adapted from [157] by permission of The Royal Society of Chemistry.

1.3.5.2. Multianalyte detection

In most of diseases, the detection of more than one biomarker is usually required for offering an accurate diagnostic. In consequence, the need to detect multiple analytes in a single device is becoming a growing topic in paper-based biosensors field. Multianalyte LF assays are important because they allow the simultaneous detection of different analytes in a single assay with short detection times and low cost.

Nevertheless beside advantages the possible cross-reactivities between antigens and antibodies in the sample that could affect the results of the LF assay should be carefully considered.

Commercial multianalyte LFA for different applications such as, (i) the triple line QuickVue® developed by Quidel Corporation for detection of Influenza A or B virus[158]; (ii) a multiplexed LFA for HIV/syphilis by CTK Biotech[159] (iii) the dual detection of *Cryptosporidium parvum* and/or *Giardia duodenalis* (pathogens related to animal diseases) developed by Megacor Diagnostik[160] and (iv) the sensitive detection of *E. coli* Shiga toxin 1 and 2 commercialized by Meridian Bioscience have been reported.[161]

Recently, Yonekita *et al.,* [162] described a novel method by using AuNP-labelled antimicrobial peptides (AMP) as recognition molecules for bacteria in LFA. In addition, the authors developed a multianalyte LFA for detection of *E. coli* strains O157, O26 and O111 up to 10^4 CFU/mL in beef.

Even though the detection of toxins is vital for avoiding the effects produced to the human health, few works have been reported for their multidetection. Unisensor[163] developed the first multiplex dipstick for detection of four main classes of mycotoxins: zearalenone (ZEN), T-2 and HT-2 toxins, deoxynivalenol (DON) and fumonisins (FB_1/FB_2). This device allows the detection in just less than 30 min with high specificity and sensitivity.

1.3.5.3. Integration of novel materials

Magnetic particles have been used for years as well-established labels in bioassays because they are not affected by reagents, are stable over time and can be manipulated by applying a magnetic field. In recent years, the use of superparamagnetic nanoparticles (SPMNP) has become an attractive alternative to the traditional labels for LFA, because of their quantitative measurement that can be achieved over the entire thickness of nitrocellulose membrane, instead of the eye-naked detection which employs color intensity as signal only if the labels are located 10μm coming from the top layer of membrane.[55] With the use of these new labels, it is consequently possible to obtain better sensitivities in LFA.

In this context, Wang *et al*.[164] presented a study about the size and magnetite content of SPMNP and their use as label in LFA using hCG as model protein. The authors found that smaller sizes of SPMNP between 111-133 nm are related to shorter times of detection. In addition, while higher was the content of magnetite higher was the signal intensity, which was stable over the time allowing to recheck the results.

An application of magnetic LFA was developed by Xu and co-workers for detection of cardiac troponin I.[165] They could detect up to 0.01 ng/mL of analyte (1000-fold lower than ELISA test) in a wide range of 5 orders of magnitude, just in 15 min.

A recent study of magnetic LFA was described by Zheng *et al*.[166] for rapid detection of parvalbumin (Pa). The authors reported limit of detection of 5 μg/mL and 0.046 μg/mL of Pa for visual and quantitative detection. The results were obtained in less than 20 minutes and were in agreement with Western Blot assay (93% of accuracy).

Other materials to replace the traditional supports, such as nitrocellulose in LFA have been also studied. In this sense, cotton threads have been used for Zhou *et al*.[167] as support for transporting and mixing liquids, applied to the detection of C-reactive protein (CRP) and demonstrating the possibility of a quantitative and multiplex assay. The authors reported the AuNP-based immunochromatographic assay on thread (ICAT), using cotton threads and nylon fibers bundles as membrane and pads, respectively. Briefly, the assay consisted in placing the sample onto the nylon fiber bundle where detection antibody-AuNP conjugate, as well the capture and control antibodies located in the cotton thread at test and control zone, respectively were vacuum dried. Immediately after this step, a buffer solution for allowing the flow of the sample and the conjugate through the cotton threads and subsequent detection was added (see Figure 1.14). With this strategy, it was possible to detect up to 377 pM of CRP, value comparable to other reported LFA for CRP but with the advantage of the possible simultaneous detection of several analytes (CRP, leptin and osteopontin) in a reduced space and the possibility to customize ICAT *à la carte* thanks to the modularity of this assay. Currently, studies related to long-term stability and the type of sample are being investigated by this group.

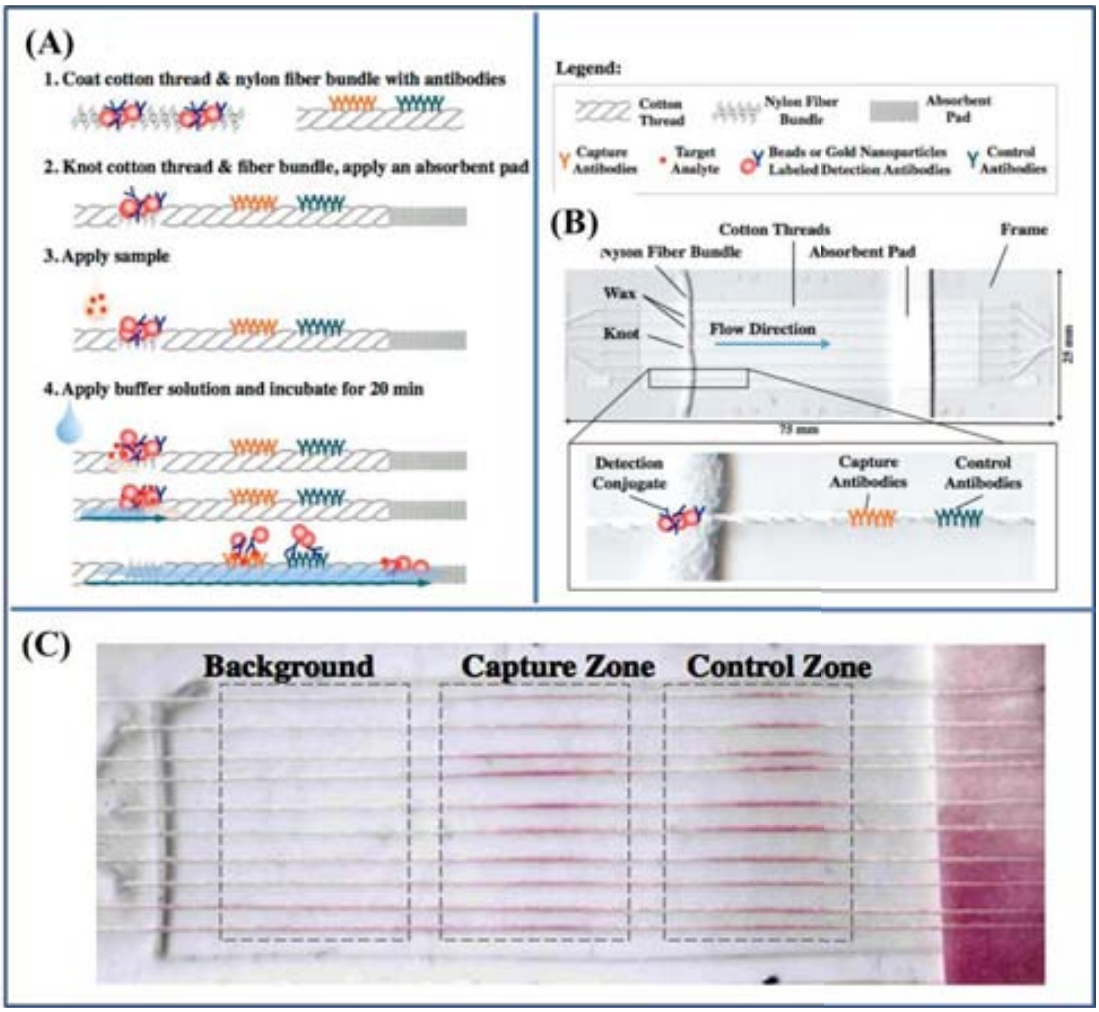

Figure 1.14. Immunochromatographic assay thread (ICAT). (A) Schematic representation of the ICAT and steps for detection. (B) Picture of an ICAT cartridge with six threads and configuration of ICAT. (C) Picture of a completed ICAT after detection. Red color is due to AuNPs located at the capture and control zone. Unbound AuNPs are absorbed by the wicking pad, on the right. Adapted from [167] with permission.

Even though the nitrocellulose is the most common material for immobilizing antibodies in LFA, the research about the use of cellulose substrates for developing bioactive paper biosensors has highly increased in the last years. Usually the functionalization of cellulose is achieved under harsh conditions, but Credou and co-workers[168] recently developed a method for functionalizing cellulose based in the aryldiazonium chemistry. All the functionalization procedures were done in mild conditions: in water, in a single step and at room temperature. The authors applied the biofuncionalized cellulose as detection pad in an AuNP-based LFA which resulted to be less efficient than nitrocellulose but more than pristine cellulose. Nevertheless, the

authors developed a new method for modifying cellulose without damaging the activity of biomolecules and they successfully proved the use of biofunctionalized sheets in LF technology.

1.3.5.4. Integration with electrochemistry

Electrochemical detection in conjunction with colorimetric methods enables to quantify the results of an assay, taking advantage of the red-ox properties of some of the tags used in LFA.

Detection of PSA has been achieved in a LFA coupled to electrochemistry using core-shell quantum dots of CdSe@ZnS.[169] In this work, a sandwich LFA format was achieved and the captured labels at test zone were detected by dissolving cadmium contained in the NP which was subsequently detected by stripping voltammetry in a disposable screen-printed electrode. The authors reported a reproducible coupled assay with a low detection limit of 0.02 ng/mL PSA.

Mao *et al.*[170] developed a simultaneous visual detection of rabbit IgG (RIgG) and human IgM (HIgM) as protein models in a LFA and subsequent quantitative detection of dissolved Au(III) ions by stripping voltammetry. LoD achieved with this methodology were 1.0 ng/mL and 1.5 ng/mL of RIgG and HIgM, respectively.

Sensitive detection of trichloropyridinol (TCP), a metabolite biomarker of exposure to organophosphorus insecticides was achieved in a LFA integrated with electrochemistry.[171] The enzyme-linked immunoreaction was developed in the LF strip and all the captured HRP-labeled antibodies located at the test zone were measured in a screen-printed electrode by using square wave voltammetry, allowing detecting up to 0.1 ng/mL TCP.

Du *et al.*[172] developed a sensitive integrated LFA electrochemical detection for the determination of organophosphorus pesticides. This work is based on parallel measurements of post exposure and baseline acetylcholinesterase (AChE) enzyme activity. The proposed device was composed by the LFA and a screen-printed electrode located under the test zone and the signal was enhanced using carbon nanotubes allowing the electrochemical detection at low potentials. Authors reported a limit of detection of 0.02 nM of organophosphorus pesticide.

1.4. Conclusions and future perspectives

In past decades significant efforts for the development of reliable, easy to use, fast in response, portable and low-cost electrochemical biosensors for the detection of a wide range of analytes has been observed. Nevertheless, many of the conventional techniques that offer high analytical performances, are time consuming, slow in response and sometimes require expensive or complicated procedures. Current challenges for electrochemical biosensors are focused to their further miniaturization and reaching of simplified read-out and multiplexing capabilities. In this context, nanotechnology is offering the development of miniaturized and cost-efficient electrochemical devices that may fulfill the gap between proof of concept lab devices and real applications with interest in different fields such as medicine, environmental, food analysis and bio-defense.

Undoubtedly, the application of different nanomaterials has brought new possibilities to biosensing field, due to the well-known unique properties of nanomaterials which are strongly dependent of the size and shape. Nanomaterials can be integrated in an electrochemical biosensor playing different functions either as labels in the recognition event due to their biofunctionalization capability or as components of the sensing part because of their conductivity, that makes them very attractive for the development of new biosensors, as well for the improvement of the existing ones.

Beside electrochemical biosensors lateral flow assays (LFA) are excellent tools which fulfill the requirements of an ASSURED device. Further advances of nanoscience and incorporation of nanomaterials to these devices brings a wide number of advantages for improving their sensitivity.

LFA technology has been quickly established with a good market position due to two main reasons: i) potentiality of satisfying the necessity of rapid diagnostic devices with moderate sensitivity for being used outside of lab settings; ii) low cost analysis and easy production. Even though the cost LFA equipment fabrication, it is considerably reasonable compared with other immunoassay technologies and the final costs of mass producing lateral flow strips are significantly low. In fact, LF technology is still improving with regard to the recent market needs for more quantitative and rapid

diagnostic devices making possible the extension of LFA to other areas, *e.g.* agriculture, veterinary, bio-defense, food, environmental control and also in nucleic acid testing.

Gold nanoparticles are the most popular label for LFA, due to their biocompatibility, easy and inexpensive preparation, stability and strong red color coming from their surface plasmon absorption. A wide variety of analytes have been tested by using LF technology, including different fields for example medical diagnostics, environmental and food. Some of these devices can be found now in the market (see figure 1.15).

Although the LFA is an old technology it is under an extensive research due to the new opportunities coming from the use of nanotechnologies and nanomaterials. The main challenge in the field consists in improving the sensitivity of the assays so as to reach the requested low detection limits for real samples applications.

Gold nanoparticles based LFA can be further improved by developing of more sensitive detection systems. Beside possible improvements of current optical detectors the integration of AuNP-electrochemical detection systems may bring significant results. This can be related to the possibility of the use of electrochemical detection systems that employ electrocatalytic properties of AuNP well known for their higher sensitivity in conventional batch systems (ex. screen-printed based electrodes already reported in biosensing of DNA, proteins and cells using AuNP). This would imply careful studies and further modification of AuNP-related electrocatalytic reactions so as to adapt these to LF designs and the composition of the LF pads/platforms.

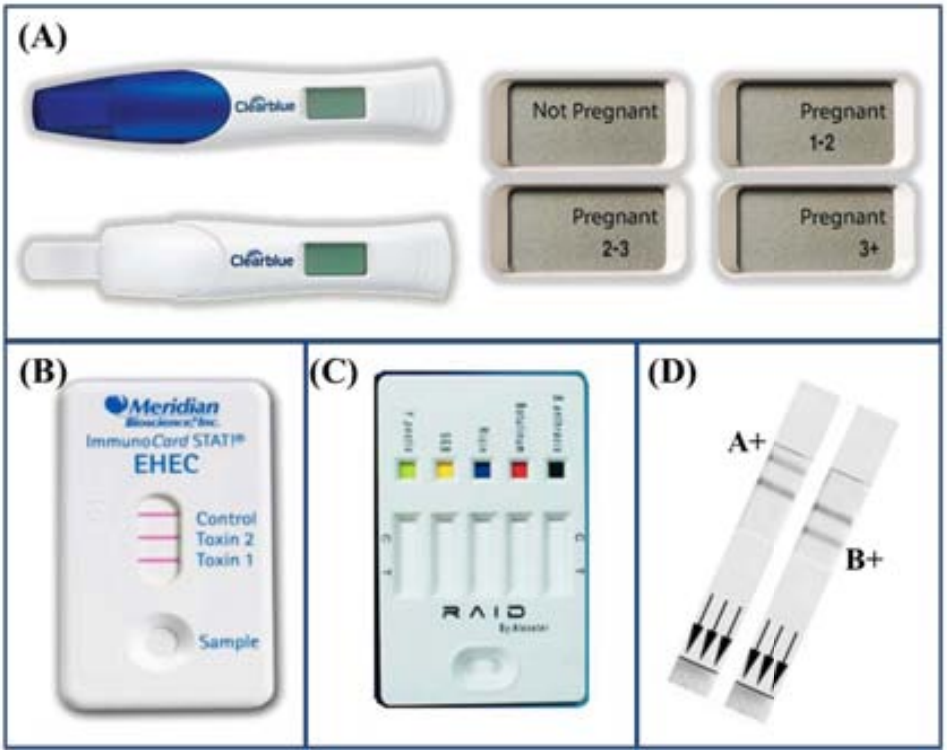

Figure 1.15. Commercial LFA devices. (A) Clearblue™ Advance Pregnancy Test with Week Estimator. Photo reproduced with kind permission from SPD Swiss Precision Diagnostics GmbH, owner of trademark ClearblueTM © 2014. All rights reserved. (B) ImmunoCard STAT! (R) for E. coli Shiga toxin 1 and 2 detection. Meridian Bioscience, Inc. All rights reserved. (C) RAID 5 for biological threat screening. Alexeter Technlogies. All rights reserved. (D) QuickVue® for Influenza A and B detection. Quidel Corporation. All rights reserved.

Future trends beside the use of gold nanoparticles seem to be focused on the development of new labels such as other catalytic nanoparticles, new nano/micromaterials for LF platform modification as well as of new architectures and strategies that would allow for faster and higher sensitive detection. Such improvements, some of which are already reported as proof of concept, are expected to bring these devices to real analytical applications in the near future for a broader range of analytes.

1.5. References

(1) Gilbert, J.; Anklam, E. *TrAC Trends Anal. Chem.* **2002**, *21*, 468–486.

(2) Mishra, R. K.; Dominguez, R. B.; Bhand, S.; Muñoz, R.; Marty, J. . *Biosens. Bioelectron.* **2012**, *32*, 56–61.

(3) De la Escosura-Muñiz, A.; Merkoçi, A. *Expert Opin. Med. Diagn.* **2010**, *4*, 21–37.

(4) Ali, M. M.; Aguirre, S. D.; Xu, Y.; Filipe, C. D. M.; Pelton, R.; Li, Y. *Chem. Commun. (Camb).* **2009**, 6640–6642.

(5) Luppa, P. B.; Müller, C.; Schlichtiger, A.; Schlebusch, H. *TrAC Trends Anal. Chem.* **2011**, *30*, 887–898.

(6) Peeling, R. W.; Holmes, K. K.; Mabey, D.; Ronald, a. *Sex. Transm. Infect.* **2006**, *82 Suppl 5*, v1–6.

(7) Thevénot, D. R.; Toth, K.; Durst, R. A.; Wilson, G. S. *Pure Appl. Chem.* **1999**, *71*, 2333–2348.

(8) Luo, X.; Morrin, A.; Killard, A. J.; Smyth, M. R. *Electroanalysis* **2006**, *18*, 319–326.

(9) De la Escosura-Muñiz, A.; Ambrosi, A.; Merkoçi, A. *TrAC Trends Anal. Chem.* **2008**, *27*, 568–584.

(10) Campbell, F. W.; Compton, R. G. *Anal. Bioanal. Chem.* **2010**, *396*, 241–259.

(11) Ronkainen, N. J.; Halsall, H. B.; Heineman, W. R. *Chem. Soc. Rev.* **2010**, *39*, 1747–1763.

(12) Turner, A. P. F. *Chem. Soc. Rev.* **2013**, *42*, 3184–3196.

(13) Yoo, E.-H.; Lee, S.-Y. *Sensors* **2010**, *10*, 4558–4576.

(14) *Nanoparticles: Building Blocks for Nanotechnology*; Rotello, V., Ed.; Springer Science: USA, 2004; p. 284.

(15) *Biosensing using nanomaterials*; Merkoçi, A., Ed.; John Wiley & Sons: NJ, USA, 2009; p. 499.

(16) De la Escosura-Muñiz, A.; Parolo, C.; Merkoçi, A. *Mater. Today* **2010**, *13*, 24–34.

(17) Yang, W.; Ratinac, K. R.; Ringer, S. P.; Thordarson, P.; Gooding, J. J.; Braet, P. *Angew. Chemie Int. Ed.* **2010**, *49*, 2114–2138.

(18) Wang, J. *Analyst* **2005**, *130*, 421–426.

(19) De la Escosura-Muñiz, A.; Ambrosi, A.; Merkoçi, A. *Trends Anal. Chem.* **2008**, *27*, 568–584.

(20) Lei, J.; Ju, H. *Chem. Soc. Rev.* **2012**, *41*, 2122–2134.

(21) González García, M. B.; Costa García, A. *Bioelectrochemistry Bioenerg.* **1995**, *38*, 389–395.

(22) Pumera, M.; Aldavert, M.; Mills, C.; Merkoçi, A.; Alegret, S. *Electrochim. Acta* **2005**, *50*, 3702–3707.

(23) Merkoçi, A.; Marín, S.; Castañeda, M. T.; Pumera, M.; Ros, J.; Alegret, S. *Nanotechnology* **2006**, *17*, 2553–2559.

(24) Ambrosi, A.; Castañeda, M. T.; Killard, A. J.; Smyth, M. R.; Alegret, S.; Merkoçi, A. *Anal. Chem.* **2007**, *79*, 5232–5240.

(25) Ho, J. A.; Lin, Y. C.; Wang, L. S.; Hwang, K. C.; Chou, P. T. *Anal. Chem.* **2009**, *81*, 1340–1346.

(26) Wang, J.; Xu, D.; Polsky, R. *J. Am. Chem. Soc.* **2002**, *124*, 4208–4209.

(27) De la Escosura-Muñiz, A.; Maltez-da Costa, M.; Merkoçi, A. *Biosens. Bioelectron.* **2009**, *24*, 2475–2482.

(28) Maltez-Da Costa, M.; de la Escosura-Muñiz, A.; Merkoçi, A. *Electrochem. commun.* **2010**, *12*, 1501–1504.

(29) De la Escosura-Muñiz, A.; Maltez-Da Costa, M.; Sánchez-Espinel, C.; Díaz-Freitas, B.; Fernández-Suarez, J.; González-Fernández, A.; Merkoçi, A. *Biosens. Bioelectron.* **2010**, *26*, 1710–1714.

(30) De la Escosura-Muñiz, A.; Sánchez-Espinel, C.; Díaz-Freitas, B.; González-Fernández, A.; Maltez-Da Costa, M.; Merkoçi, A. *Anal. Chem.* **2009**, *81*, 10268–10274.

(31) Polsky, R.; Harper, J. C.; Wheeler, D. R.; Dirk, S. M.; Rawlings, J. A.; Brozik, S. M. *Chem. Commun.* **2007**, 2741–2743.

(32) Yáñez-Sedeño, P.; Pingarrón, J. M. *Anal. Bioanal. Chem.* **2005**, *382*, 884–886.

(33) Ding, C.; Zhao, F.; Ren, R.; Lin, J.-M. *Talanta* **2009**, *78*, 1148–1154.

(34) Chen, J.; Tang, J.; Yan, F.; Ju, H. *Biomaterials* **2006**, *27*, 2313–2321.

(35) Mani, V.; Chikkaveeraiah, B. V; Patel, V.; Gutkind, J. S.; Rusling, J. F. *ACS Nano* **2009**, *3*, 585–594.

(36) Shim, J. H.; Lee, Y.; Kang, M.; Lee, J.; Baik, J. M.; Lee, Y.; Lee, C.; Kim, M. H. *Anal. Chem.* **2012**, *84*, 3827–3832.

(37) Solanki, P. R.; Kaushik, A.; Agrawal, V. V.; Malhotra, B. D. *NPG Asia Mater.* **2011**, *3*, 17–24.

(38) Wen, D.; Guo, S.; Wang, Y.; Dong, S. *Langmuir* **2010**, *26*, 11401–11406.

(39) Das, M.; Sumana, G.; Nagarajan, R.; Malhotra, B. D. *Appl. Phys. Lett.* **2010**, *96*, 133703.

(40) Mandel, I. D. *Ann. New York Acad. Sci.* **1993**, *64*, 1–10.

(41) http://history.nih.gov/exhibits/thinblueline/timeline.html.

(42) Ghalioungui, P.; Khalil, S. .; Ammar, A. R. *Med. Hist.* **1963**, *7*, 241–246.

(43) Starling, E. H. *Lancet* **1905**, *166*, 339–341.

(44) Ettinger, G. H.; Smith, G. L. M.; McHenry, E. W. *Canandian Med. Assoc. J.* **1931**, *24*, 491–495.

(45) Wide, L.; Gemzell, C. A. *Acta Endocrinol. (Copenh).* **1960**, *35*, 261–267.

(46) Plotz, C. M.; Singer, J. M. *Am. J. Med.* **1956**, *21*, 888–892.

(47) Berson, B. S. A.; Yalow, R. S. *J. Clin. Invest.* **1959**, *38*, 1996–2016.

(48) Engvall, E.; Perlman, P. *Immunochemistry* **1971**, *8*, 871–874.

(49) Van Weemen, B. K.; Schuurs, A. H. *FEBS Lett.* **1971**, *15*, 232–236.

(50) Leuvering, J. H.; Thal, P. J.; van der Waart, M.; Schuurs, A. H. *J. Immunoassay* **1980**, *1*, 77–91.

(51) May, K.; Prior, M. E.; Richards., I. Immunoassays and devices therefore. International Patent: WO 88/08534, 1988.

(52) Rosenstein, R. W. Solid phase assay. European Patent: EP 0 284 232, 1988.

(53) Campbell, R. .; Wagner, D. B.; O'Connel, J. . Solid-phase assay with visual readout. US Patent 4,855,240, 1987.

(54) Wilcox, A. . J.; Baird, D. D.; Weinberg, C. R. *N. Engl. J. Med.* **1999**, *340*, 1796–1799.

(55) Millipore Corporation. *Rapid Lateral Flow Test Strips. Considerations for product development*; 2002; p. 39.

(56) Van Oss, C. J.; Good, R. J.; Chaudhury, M. K. *J. Chromatogr.* **1987**, *391*, 53–65.

(57) Tonkinson, J. L.; Stillman, B. A. *Front. Biosci.* **2002**, *7*, c1–12.

(58) Nicholas, M. W.; Nelson, K. *J. Invest. Dermatol.* **2013**, *133*, e10.

(59) *Drugs of abuse: body fluid testing*; Wong, R. C.; Tse, H. Y., Eds.; Humana Press: New Jersey, 2005.

(60) Jones, K. D. *IVD Technol.* **1999**, *5*, 32–34.

(61) http://www.imagenetechnology.com/.

(62) Yetisen, A. K.; Akram, M. S.; Lowe, C. R. *Lab Chip* **2013**, *13*, 2210–2251.

(63) *The Immunoassay Handbook*; Wild, D. G., Ed.; 4th. ed.; Elsevier Ltd: Great Britain, 2013; p. 1036.

(64) *Medical Applications of Liposomes*; Lasic, D. D.; Papahadjopoulos, D., Eds.; Elsiever Science: Amsterdam, 1998; p. 780.

(65) Edwards, K. a; Baeumner, A. J. *Anal. Bioanal. Chem.* **2006**, *386*, 1335–1343.

(66) Wen, H.-W.; Borejsza-Wysocki, W.; DeCory, T. R.; Durst, R. A. *Anal. Bioanal. Chem.* **2005**, *382*, 1217–1226.

(67) Noguera, P.; Posthuma-Trumpie, G. a; van Tuil, M.; van der Wal, F. J.; de Boer, A.; Moers, A. P. H. A.; van Amerongen, A. *Anal. Bioanal. Chem.* **2011**, *399*, 831–838.

(68) Kalogianni, D. P.; Boutsika, L. M.; Kouremenou, P. G.; Christopoulos, T. K.; Ioannou, P. C. *Anal. Bioanal. Chem.* **2011**, *400*, 1145–1152.

(69) Vanrell, L.; Gonzalez-Techera, A.; Hammock, B. D.; Gonzalez-Sapienza, G. *Anal. Chem.* **2013**, *85*, 1177–1182.

(70) Suárez-Pantaleón, C.; Wichers, J.; Abad-Somovilla, A.; van Amerongen, A.; Abad-Fuentes, A. *Biosens. Bioelectron.* **2013**, *42*, 170–176.

(71) Posthuma-Trumpie, G. a; Wichers, J. H.; Koets, M.; Berendsen, L. B. J. M.; van Amerongen, A. *Anal. Bioanal. Chem.* **2012**, *402*, 593–600.

(72) *Principles and Techniques of Biochemistry and Molecular Biology*; Wilson, K.; Walker, J. M., Eds.; 7th. ed.; Cambridge University Press: Cambridge, 2010; p. 760.

(73) Leonardi, G. P.; Wilson, A. M.; Zuretti, A. R. *J. Virol. Methods* **2013**, *189*, 379–382.

(74) Wang, Y.; Nugen, S. R. *Biomed. Microdevices* **2013**, *15*, 751–758.

(75) Hildebrandt, N. *ACS Nano* **2011**, *5*, 5286–5290.

(76) Esteve-Turrillas, F. a; Abad-Fuentes, A. *Biosens. Bioelectron.* **2013**, *41*, 12–29.

(77) Zou, Z.; Du, D.; Wang, J.; Smith, J. N.; Timchalk, C.; Li, Y.; Lin, Y. *Anal. Chem.* **2010**, *82*, 5125–5133.

(78) Wang, L.; Chen, W.; Ma, W.; Liu, L.; Ma, W.; Zhao, Y.; Zhu, Y.; Xu, L.; Kuang, H.; Xu, C. *Chem. Commun.* **2011**, *47*, 1574–1576.

(79) Yang, Q.; Gong, X.; Song, T.; Yang, J.; Zhu, S.; Li, Y.; Cui, Y.; Li, Y.; Zhang, B.; Chang, J. *Biosens. Bioelectron.* **2011**, *30*, 145–150.

(80) Juntunen, E.; Myyryläinen, T.; Salminen, T.; Soukka, T.; Pettersson, K. *Anal. Biochem.* **2012**, *428*, 31–38.

(81) Wilson, R. *Chem. Soc. Rev.* **2008**, *37*, 2028–2045.

(82) Boisselier, E.; Astruc, D. *Chem. Soc. Rev.* **2009**, *38*, 1759–1782.

(83) Giljohann, D. A.; Seferos, D. S.; Daniel, W. L.; Massich, M. D.; Patel, P. C.; Mirkin, C. A. *Angew. Chem. Int. Ed. Engl.* **2010**, *49*, 3280–3294.

(84) Dykman, L.; Khlebtsov, N. *Chem. Soc. Rev.* **2012**, *41*, 2256–2282.

(85) Dreaden, E. C.; Alkilany, A. M.; Huang, X.; Murphy, C. J.; El-Sayed, M. A. *Chem. Soc. Rev.* **2012**, *41*, 2740–2779.

(86) Faulk, W.; Taylor, G. M. *Immunochemistry* **1971**, *8*, 1081–1083.

(87) Zhao, P.; Li, N.; Astruc, D. *Coord. Chem. Rev.* **2013**, *257*, 638–665.

(88) Turkevich, J.; Stevenson, P. C.; Hillie, J. *Discuss. Faraday Soc.* **1951**, 55–75.

(89) Frens, G. *Nat. Phys. Sci.* **1973**, *241*, 20–22.

(90) Hermanson, G. *Microparticles and Nanoparticles. Bioconjugate Techniques*; 3rd. ed.; Academic Press: San Diego, 2008; pp. 582–626.

(91) Carney, J.; Braven, H.; Seal, J.; Whitworth, E. *IVD Technol.* **2006**, *12*, 41–49.

(92) Ambrosi, A.; Castañeda, M. T.; Killard, A. J.; Smyth, M. R.; Alegret, S.; Merkoçi, A. *Anal. Chem.* **2007**, *79*, 5232–5240.

(93) Wong, R. C. *Lateral Flow Immunoassay*; Wong, R.; Tse, H., Eds.; Humana Press: Totowa, NJ, 2009; p. 236.

(94) Lou, S.; Ye, J.; Li, K.; Wu, A. *Analyst* **2012**, *137*, 1174–1181.

(95) Xu, H.; Mao, X.; Zeng, Q.; Wang, S.; Kawde, A.-N.; Liu, G. *Anal. Chem.* **2009**, *81*, 669–675.

(96) Zeng, Q.; Mao, X.; Xu, H.; Wang, S. *Am. J. Biomed. Sci.* **2009**, *1*, 70–79.

(97) Fernández-Sánchez, C.; McNeil, C. J.; Rawson, K.; Nilsson, O. *Anal. Chem.* **2004**, *76*, 5649–5656.

(98) Fernández-Sánchez, C.; McNeil, C. J.; Rawson, K.; Nilsson, O.; Leung, H. Y.; Gnanapragasam, V. *J. Immunol. Methods* **2005**, *307*, 1–12.

(99) Fang, C.; Chen, Z.; Li, L.; Xia, J. *J. Pharm. Biomed. Anal.* **2011**, *56*, 1035–1040.

(100) Choi, D. H.; Lee, S. K.; Oh, Y. K.; Bae, B. W.; Lee, S. D.; Kim, S.; Shin, Y. B.; Kim, M. G. *Biosens. Bioelectron.* **2010**, *25*, 1999–2002.

(101) Zhu, J.; Zou, N.; Zhu, D.; Wang, J.; Jin, Q.; Zhao, J.; Mao, H. *Clin. Chem.* **2011**, *57*, 1732–1738.

(102) Craw, P.; Balachandran, W. *Lab Chip* **2012**, *12*, 2469–2486.

(103) Parolo, C.; Merkoçi, A. *Chem. Soc. Rev.* **2013**, *42*, 450–457.

(104) Ahmad, F.; Hashsham, S. a. *Anal. Chim. Acta* **2012**, *733*, 1–15.

(105) Seal, J.; Braven, H.; Wallace, P. *IVD Technol.* **2006**, *12*, 41–51.

(106) Piepenburg, O.; Williams, C. H.; Stemple, D. L.; Armes, N. a. *PLoS Biol.* **2006**, *4*, 1115–1121.

(107) He, Y.; Zeng, K.; Zhang, S.; Gurung, A. S.; Baloda, M.; Zhang, X.; Liu, G. *Biosens. Bioelectron.* **2012**, *31*, 310–315.

(108) Hou, S.; Hsiao, Y.; Lin, M.; Yen, C.; Chang, C. *Talanta* **2012**, *99*, 375–379.

(109) Xiao, Z.; Lie, P.; Fang, Z.; Yu, L.; Chen, J.; Liu, J. *Chem. Commun.* **2012**, *48*, 8547–8549.

(110) Aveyard, J.; Mehrabi, M.; Cossins, A.; Braven, H.; Wilson, R. *Chem. Commun.* **2007**, 4251–4253.

(111) Mao, X.; Ma, Y.; Zhang, A.; Zhang, L.; Zeng, L.; Liu, G. *Anal. Chem.* **2009**, *81*, 1660–1668.

(112) Lie, P.; Liu, J.; Fang, Z.; Dun, B.; Zeng, L. *Chem. Commun.* **2012**, *48*, 236–238.

(113) World Health Organization. Mortality and global health estimates. Cause-specific mortality, 2000-2011 http://apps.who.int/gho/data/node.main.CODWORLD?lang=en.

(114) Rodrigues Ribeiro Teles, F. S.; Pires de Távora Tavira, L. A.; Pina da Fonseca, L. J. *Crit. Rev. Clin. Lab. Sci.* **2010**, *47*, 139–169.

(115) Lee, W. G.; Kim, Y.-G.; Chung, B. G.; Demirci, U.; Khademhosseini, A. *Adv. Drug Deliv. Rev.* **2010**, *62*, 449–457.

(116) Niemz, A.; Ferguson, T. M.; Boyle, D. S. *Trends Biotechnol.* **2011**, *29*, 240–250.

(117) Shetty, N.; Tang, J. W.; Andrews, J. *Infectious Disease: Pathogenesis, Prevention and Case Studies*; Wiley-Blackwell: Malasia, 2009; p. 664.

(118) Horng, Y.-T.; Soo, P.-C.; Shen, B.-J.; Hung, Y.-L.; Lo, K.-Y.; Su, H.-P.; Wei, J.-R.; Hsieh, S.-C.; Hsueh, P.-R.; Lai, H.-C. *Water Res.* **2006**, *40*, 2221–2229.

(119) Chua, A.; Yean, C. Y.; Ravichandran, M.; Lim, B.; Lalitha, P. *Biosens. Bioelectron.* **2011**, *26*, 3825–3831.

(120) Liu, C.; Yeung, C.; Chen, P.; Yeh, M.; Hou, S. *Food Chem.* **2013**, *141*, 2526–2532.

(121) Rohrman, B. A.; Leautaud, V.; Molyneux, E.; Richards-Kortum, R. R. *PLoS One* **2012**, *7*, 1–5.

(122) Rastogi, S. K.; Gibson, C. M.; Branen, J. R.; Aston, D. E.; Branen, a L.; Hrdlicka, P. J. *Chem. Commun. (Camb).* **2012**, *48*, 7714–7716.

(123) Bennett, J. W.; Klich, M. *Clin. Microbiol. Rev.* **2003**, *16*, 497–516.

(124) Krska, R.; Molinelli, A. *Anal. Bioanal. Chem.* **2009**, *393*, 67–71.

(125) Ngom, B.; Guo, Y.; Wang, X.; Bi, D. *Anal. Bioanal. Chem.* **2010**, *397*, 1113–1135.

(126) Anfossi, L.; Baggiani, C.; Giovannoli, C.; Arco, G. D.; Gianfranco, G. *Anal. Bioanal. Chem.* **2013**, *405*, 467–480.

(127) Delmulle, B. S.; De Saeger, S. M. D. G.; Sibanda, L.; Barna-Vetro, I.; Van Peteghem, C. H. *J. Agric. Food Chem.* **2005**, *53*, 3364–3368.

(128) Moon, J.; Kim, G.; Lee, S. *Materials (Basel).* **2012**, *5*, 634–643.

(129) Lee, S.; Kim, G.; Moon, J. *Sensors* **2013**, *13*, 5109–5116.

(130) Kolosova, A. Y.; De Saeger, S.; Sibanda, L.; Verheijen, R.; Van Petghem, C. *Anal. Bioanal. Chem.* **2007**, *389*, 2103–2107.

(131) Kolosova, A. Y.; Sibanda, L.; Dumoulin, F.; Lewis, J.; Duveiller, E.; Van Peteghem, C.; De Saeger, S. *Anal. Chim. Acta* **2008**, *616*, 235–244.

(132) International Agency for Research on Cancer. *Some Traditional Herbal Medicines , Some Mycotoxins , Naphthalene and Styrene. IARC monographs on the evaluation of carcinogenic risks to humans, vol 82.*; 2002; Vol. 82, pp. 301–366.

(133) Molinelli, A.; Grossalber, K.; Krska, R. *Anal. Bioanal. Chem.* **2009**, *395*, 1309–1316.

(134) Anfossi, L.; D'Arco, G.; Baggiani, C.; Giovannoli, C.; Giraudi, G. *Food Control* **2011**, *22*, 1965–1970.

(135) Anfossi, L.; Giovannoli, C.; Giraudi, G.; Biagioli, F.; Passini, C.; Baggiani, C. *J. Agric. Food Chem.* **2012**, *60*, 11491–11497.

(136) Wang, L.; Ma, W.; Chen, W.; Liu, L.; Ma, W.; Zhu, Y.; Xu, L.; Kuang, H.; Xu, C. *Biosens. Bioelectron.* **2011**, *26*, 3059–3062.

(137) http://www.epa.gov/pesticides/about/index.htm.

(138) Aragay, G.; Pino, F.; Merkoçi, A. *Chem. Rev.* **2012**, *112*, 5317–5338.

(139) Wang, C.; Yu, C. *Rev. Anal. Chem.* **2013**, *32*, 1–14.

(140) Wang, S.; Zhang, C.; Wang, J.; Zhang, Y. *Anal. Chim. Acta* **2005**, *546*, 161–166.

(141) Shim, W.-B.; Yang, Z.-Y.; Kim, J.-Y.; Choi, J.-G.; Je, J.-H.; Kang, S.-J.; Kolosova, A. Y.; Eremin, S. A.; Chung, D.-H. *J. Agric. Food Chem.* **2006**, *54*, 9728–9734.

(142) Kaur, J.; Singh, K. V.; Boro, R.; Thampi, K. R.; Raje, M.; Varshney, G. C.; Suri, C. R. *Environ. Sci. Technol.* **2007**, *41*, 5028–5036.

(143) Gui, W.-J.; Wang, S.-T.; Guo, Y.-R.; Zhu, G.-N. *Anal. Biochem.* **2008**, *377*, 202–208.

(144) Georgopoulos, P. G.; Roy, A.; Yonone-Lioy, M. J.; Opiekun, R. E.; Lioy, P. J. *J. Toxicol. Environ. Heal. Part B Crit. Rev.* **2001**, *4*, 341–394.

(145) Mazumdar, D.; Liu, J.; Lu, G.; Zhou, J.; Lu, Y. *Chem. Commun.* **2010**, *46*, 1416–1418.

(146) Fang, Z.; Huang, J.; Lie, P.; Xiao, Z.; Ouyang, C.; Wu, Q.; Wu, Y.; Liu, G.; Zeng, L. *Chem. Commun.* **2010**, *46*, 9043–9045.

(147) He, Y.; Zhang, X.; Zeng, K.; Zhang, S.; Baloda, M.; Gurung, A. S.; Liu, G. *Biosens. Bioelectron.* **2011**, *26*, 4464–4470.

(148) Yang, F.; Duan, J.; Li, M.; Wang, Z.; Guo, Z. *Anal. Sci.* **2012**, *28*, 333–338.

(149) Liu, X.; Xiang, J.-J.; Tang, Y.; Zhang, X.-L.; Fu, Q.-Q.; Zou, J.-H.; Lin, Y. *Anal. Chim. Acta* **2012**, *745*, 99–105.

(150) López, A. M.; Pons, J.; Blake, D. A.; Merkoçi, A. *Biosens. Bioelectron.* **2013**, *47*, 190–198.

(151) López Marzo, A. M.; Pons, J.; Blake, D. A.; Merkoçi, A. *Anal. Chem.* **2013**, *85*, 3532–3528.

(152) Shyu, R.-H.; Shyu, H.-F.; Liu, H.-W.; Tang, S.-S. *Toxicon* **2002**, *40*, 255–258.

(153) Cho, I.-H.; Seo, S.-M.; Paek, E.-H.; Paek, S.-H. *J. Chromatogr. B* **2010**, *878*, 271–217.

(154) Parolo, C.; de la Escosura-Muñiz, A.; Merkoçi, A. *Biosens. Bioelectron.* **2013**, *40*, 412–416.

(155) Tang, D.; Sauceda, J. C.; Lin, Z.; Ott, S.; Basova, E.; Goryacheva, I.; Biselli, S.; Lin, L.; Niessner, R.; Knopp, D. *Biosensors Bioelectron.* **2009**, *25*, 514–518.

(156) Liu, C.; Jia, Q.; Yang, C.; Qiao, R.; Jing, L.; Wang, L.; Xu, C.; Gao, M. *Anal. Chem.* **2011**, *83*, 6778–6784.

(157) Parolo, C.; Medina-Sánchez, M.; de la Escosura-Muñiz, A.; Merkoçi, A. *Lab Chip* **2013**, *13*, 386–390.

(158) http://www.quidel.com/.

(159) http://www.ctkbiotech.com/.

(160) http://www.megacor.at/.

(161) http://www.meridianbioscience.com/.

(162) Yonekita, T.; Ohtsuki, R.; Hojo, E.; Morishita, N.; Matsumoto, T.; Aizawa, T.; Morimatsu, F. *J. Microbiol. Methods* **2013**, *93*, 251–256.

(163) http://www.unisensor.be/.

(164) Wang, Y.; Xu, H.; Wei, M.; Gu, H.; Xu, Q.; Zhu, W. *Mater. Sci. Eng. C* **2009**, *29*, 714–718.

(165) Xu, Q.; Xu, H.; Gu, H.; Li, J.; Wang, Y.; Wei, M. *Mater. Sci. Eng. C* **2009**, *29*, 702–707.

(166) Zheng, C.; Wang, X.; Lu, Y.; Liu, Y. *Food Control* **2012**, *26*, 446–452.

(167) Zhou, G.; Mao, X.; Juncker, D. *Anal. Chem.* **2012**, *84*, 7739–7743.

(168) Credou, J.; Volland, H.; Dano, J.; Berthelot, T. *J. Mater. Chem. B* **2013**, *1*, 3277–3286.

(169) Lin, Y. Y.; Wang, J.; Liu, G.; Wu, H.; Wai, C. M.; Lin, Y. *Biosens. Bioelectron.* **2008**, *23*, 1659–1665.

(170) Mao, X.; Baloda, M.; Gurung, A. S.; Lin, Y.; Liu, G. *Electrochem. commun.* **2008**, *10*, 1636–1640.

(171) Wang, L.; Lu, D.; Wang, J.; Du, D.; Zou, Z.; Wang, H.; Smith, J. N.; Timchalk, C.; Liu, F.; Lin, Y. *Biosens. Bioelectron.* **2011**, *26*, 2835–2840.

(172) Du, D.; Wang, J.; Wang, L.; Lu, D.; Lin, Y. *Anal. Chem.* **2012**, *84*, 1380–1385.

Chapter 2

Objectives

Objectives

The main objective of this PhD thesis consists in the study and development of different strategies based on novel properties of nanoparticles and other micromaterials for the improvement of the analytical performance of electrochemical and optical biosensing systems with interest for point-of-care diagnostics.

More in detail, the specific objectives of this thesis can be summarized as follows:

- Synthesis, characterization and evaluation of electrocatalytic properties of iridium oxide nanoparticles (IrO_2 NPs) toward water oxidation reaction. Application of IrO_2 NPs as electrochemical labels for protein biomarkers (Alzheimer related) detection through proper study and optimization of all the involved physical/biochemical parameters.

- Development of a label-free impedimetric biosensor based on the application of IrO_2 NPs as modifiers of electrotransducing surfaces. Study of the impedance properties of the modified electrodes for their use in toxin detection through application of an aptamer as receptor.

- Design and study of a gold nanoparticles (AuNPs) based-lateral flow device modified with delay barriers. Study of the effect of wax-printed micro-pillars in the microfluidics and evaluation of the analytical performance of the developed device for protein detection.

- Development of a novel strategy for enhancing the sensitivity of lateral flow assays through the use of AuNP modified secondary antibodies. Application of the developed device in the detection of Leishmania related DNA with interest for animal diagnostics.

Chapter 3

Alzheimer Disease biomarker detection through electrocatalytic water oxidation induced by iridium oxide nanoparticles

Related publication

Electroanalysis, 26 (2014), 1287–1294

Alzheimer Disease biomarker detection through electrocatalytic water oxidation induced by iridium oxide nanoparticles

Lourdes Rivas[1,2], Alfredo de la Escosura-Muñiz[1], Josefina Pons[2], and Arben Merkoçi[1,3]

[1]ICN2-Nanobioelectronics & Biosensors Group, Institut Català de Nanociència i Nanotecnologia, Campus UAB, 08193 Bellaterra (Barcelona), Spain

[2]Department of Chemistry, Universitat Autónoma de Barcelona, 08193, Bellaterra, Barcelona, Spain

[3]ICREA - Institució Catalana de Recerca i Estudis Avançats, 08010 Barcelona, Spain

Summary

In this Chapter, iridium oxide nanoparticles (IrO_2 NPs) synthetized following a previously reported chemical route are presented as novel tags for immunosensing taking advantage of their electrocatalytic activity towards water oxidation reaction (WOR). Cyclic voltammetry and chronoamperometry for the evaluation of the IrO_2 NPs electrocatalytic activity towards WOR at neutral pH are used. The chronoamperometric current recorded at a fixed potential of +1.3V constitutes the analytical signal allowing the quantification of IrO_2 NPs at nM levels. Modification of the surface of citrate-capped IrO_2 NPs with anti-Apolipoprotein E antibodies (α-ApoE) is successfully achieved and the as-prepared conjugates are used for the electrocatalytic detection of ApoE Alzheimer disease (AD) biomarker in a magnetosandwich immunoassay, reaching a detection limit of 68 ng/mL. Human plasma of a patient suffering AD is also evaluated, estimating an ApoE concentration of 20 μg/mL which is in concordance with the obtained in previously reported approaches. This novel IrO_2 NPs based electrocatalytic assay presents the advantage of the signal generation in the same medium where the immunoassay takes place (PBS, pH 7.4) avoiding the use of additional reagents which also opens the way to future integrated biosensing systems and platforms with interest for other proteins as well as DNA and cells analysis.

3.1. Introduction

Recent advances in materials science and, in particular, in the nanomaterials field have opened the way to great achievements in immunosensing technology. Outstanding optical and electrochemical properties of nanoparticle tags have been extensively studied and applied for immunosensing in the last years, offering excellent alternatives to existing conventional strategies/assays with interest in different fields, being the early diagnostics based on sensitive detection of protein biomarkers the most relevant one.[1–7] Of special interest is the possibility to electrochemically detect NP tags, due to the inherent advantages of the electrochemical techniques in terms of sensitivity, selectivity, low cost and ease of use mode, together with the possibility of miniaturization of the detection system. [8–10] NPs such as gold NPs (AuNPs) and quantum dots NPs (QDs) have been used as labels for protein biomarkers detection due to their excellent redox properties, electrocatalytic activity toward several substrates and easy preparation and bioconjugation capabilities.[11,12] However, these approaches often suffer the limitation related to the need of acidic solutions either for the total dissolution of the NP tag followed by stripping voltammetric detection[13–16] or as source of protons for further electrocatalytic detection based on the hydrogen evolution reaction (HER).[17–19] The use of such acidic solutions, in addition to inherent security risks, represents an additional step which not only increases the analysis time but also is a crucial limitation in case of really integrated sensing systems, such as those based on lab-on-a-chip or lateral-flow platforms. Hydrogen bubbles formed during hydrogen gas evolution is another inconvenience for the integration of HER based biosensing systems in microfluidics platforms. For these reasons, there is a demand for novel NP tags easy to be detected in the same medium of the immunoreaction, often saline buffers at neutral pH. In this context we consider that NPs able to catalyze water oxidation reaction (WOR) would be ideal candidates for this purpose.

Electrochemical water splitting is composed of two half-cells redox reactions which have been studied separately.[20] While the HER proceeds in two-electron process, the evolution of oxygen from water, WOR, is a more complex endothermic process (E^o= 1.23 eV at pH 0.0) that involves four electrons and formation of an oxygen-oxygen bond.

$$2H_2O \rightarrow O_2 + 4H^+ + 4e^- \qquad \text{Eq. 3.1}$$

In nature, the photosynthetic water oxidation is catalyzed by a Mn complex in a membrane protein complex located in photosynthetic organisms.[21,22] Due to its importance, many studies have been carried out so as to understand the mechanism of water splitting and oxygen formation driven naturally.[23] Molecular complexes based on Ru[24–26] , Mn[27,28] , Ir[29,30] ; bulk metal oxides of Co_3O_4[31,32] , RuO_2 and IrO_2[33] and moreover, their nanoparticulated metal oxides[34–38] have been studied in the pursuit of a synthetic catalyst capable to effectively oxidize water. In this context, IrO_2 is a very attractive material to be considered thanks to its catalytic activity, biocompatibility, low resistivity and outstanding chemical and thermal stability which has been used for applications in pH sensors[39,40] and neural stimulation.[41,42]

It is well known that nanomaterials exhibit a large surface area that leads to an increase in their reactivity, compared with the bulk material. Due to this property, the catalytic activity of iridium oxide nanoparticles (IrO_2 NPs, stabilized by citrate ions) towards water oxidation reaction, has been tested under photochemical conditions with strong oxidants showing a good catalytic performance.[34,35,43] Citrate capped IrO_2 NPs showed a remarkable catalytic activity toward the WOR when they were self-assembled on an indium tin oxide (ITO) forming an ester layer on the electrode.[36]

All these noteworthy features make IrO_2 NPs ideal candidates for using in biosensing field. However, to the best of our knowledge, neither the electrocatalytic activity of IrO_2 NPs in suspension nor their use as tags in biosensing have not been yet evaluated. Their easy to be measured electrocatalytic properties at neutral pH opens the way to their direct detection in the same medium where the immunoreaction takes place (*i.e.* PBS buffer, pH 7.4), overcoming the above mentioned limitations of other NP-based electrochemical immunosensing systems.

In this work we explore the excellent electrocatalytic property of IrO_2 NPs toward WOR and employ this as a new signaling route in protein diagnostics. Magnetic beads modified with antibodies are used as platforms of the immunoassay which is applied for the detection of Apolipoprotein E (ApoE), a well-established biomarker of Alzheimer disease (AD) [44,45] which is one of the most common cause of dementia.

3.2. Experimental section

3.2.1. Reagents and apparatus

Potassium hexachloroiridate (IV) (K_2IrCl_6), sodium hydrogen citrate sesquihydrate ($Na_2C_6H_6O_7 \cdot 1.5H_2O$), sodium hydroxide (NaOH); N-(3-Dimethylaminopropyl)-N′-ethylcarbodiimide hydrochloride (EDC), *N*-Hydroxysulfosuccinimide sodium salt (sulpho-NHS), phosphate buffer saline in tablet, 2-(*N*-morpholino)ethanesulfonic acid (MES buffer), Tween 20, bovine serum albumin (BSA), were purchased from Sigma Aldrich. Carboxyl-modified magnetic beads 2.8 μm sized (MBs) were purchased from Dynal Biotech. (Dynabeads® M-270, Invitrogen). Capture monoclonal antibody, biotinylated detection mAb, streptavidin-enzyme conjugate HRP and purified ApoE as a standard were purchased from Mabtech. mQ water, produced using a Milli-Q system (>18.2 $M\Omega cm^{-1}$) purchased from Millipore, was used for the preparation of all solutions. The stirrer used was a TS-100 Thermo shaker (BioSan). A thermostatic centrifuge (Sigma 2-16 PK, Fisher Bioblock Scientific) was used to purify the iridium oxide nanoparticles/antibody conjugates.

Human plasma samples of a patient suffering from Alzheimer disease were provided by the Institute of Neurology of Ulm University (Germany).

The electrochemical transducers used were homemade screen-printed carbon electrodes (SPCEs) in a semi-automatic screen-printing machine DEK248 (DEK International, Switzerland). The substrate and inks used for this process were: Autostat HT5 polyester sheet (McDermid Autotype, UK) and Electrodag 423SS carbon ink, Electrodag 6037SS silver/silver chloride ink and Minico 7000 Blue insulating ink (Acheson Industries, The Netherlands).

A microwave digester model MARSXpress (CEM Corporation, USA) and an inductively coupled plasma-optical emission spectrometry (ICP-OES) spectrometer model Optima 4300DV (Perkin-Elmer, USA) were used for iridium analysis.

X-ray photoelectron spectroscopy (XPS) experiments were performed in XPS spectroscope PHI 5500 Multitechnique System (Physical Electronics, USA).

Optical characterizations of IrO_2 NPs were conducted in a Field Emission Gun Transmission Electronic Microscope (TEM) model Tecnai^{TM} G2F20 (Fei, USA) and Gemini SpectraMax M2^{e} Multi-Mode Microplate Reader (Molecular Devices, USA).

Electrochemical measurements were performed using an Autolab 20 (Echo-chemie, The Netherlands) connected to a PC.

3.2.2. Methods

3.2.2.1. Fabrication of screen-printed carbon electrodes (SPCEs)

The electrochemical transducers used were homemade screen-printed carbon electrodes (SPCEs), consisting of three electrodes: working electrode, reference electrode and counter electrode in a single strip fabricated with a semi-automatic screen-printing machine DEK248. The full size of the sensor strip was 29 mm x 6.7 mm, and the WE diameter was 3mm. The fabrication of the SPCEs was carried out in three steps. First, a graphite layer was printed onto the polyester sheet, using the screen-printing machine with the stencil (where it is the electron pattern). After curing for 15 minutes at 95ºC, an Ag/AgCl layer was printed and cured for 15 minutes at 95ºC. Finally, the insulating ink was printed and cured at 95ºC for 20 minutes.

Figure 3.1 shows images of the screen-printing machine and the 45-sensor sheet obtained following the detailed experimental procedure.

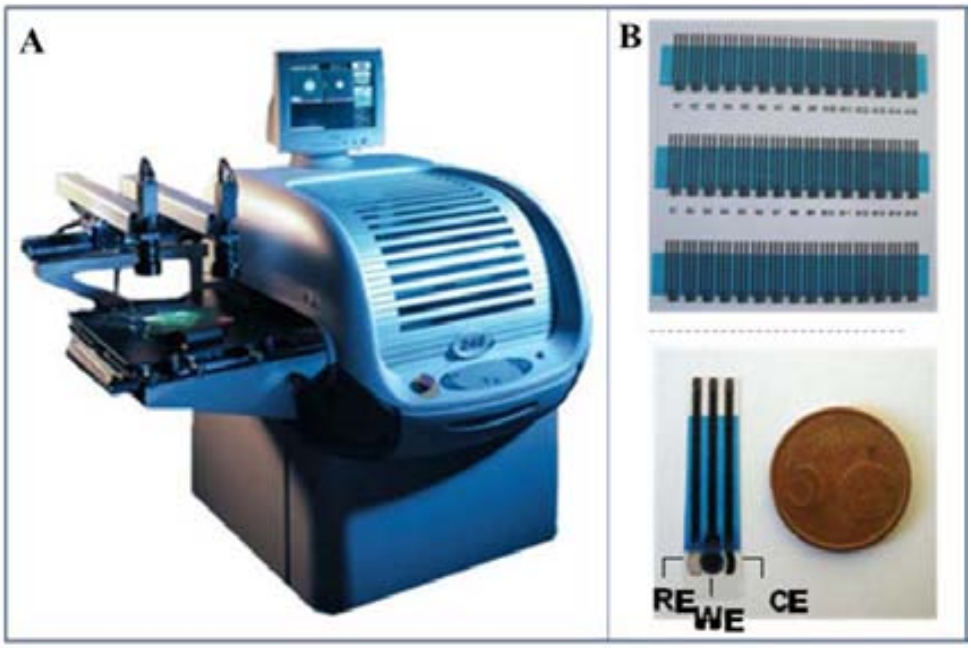

Figure 3.1. (**A**) Semi-automatic screen-printing machine DEK248. (B) Above: Images of the 45 SPCE sensors sheet obtained following the detailed experimental procedure. Bottom: Detail of one SPCE, containing the three electrodes in the working area: RE- Ag/AgCl reference electrode, WE- carbon working electrode and CE- carbon counter electrode.

3.2.2.2. Synthesis and characterization of iridium oxide nanoparticles (IrO_2 NPs)

The procedure for the synthesis of iridium oxide nanoparticles is based on Harriman work.[34] Briefly, 30 mg of K_2IrCl_6 were added to 50 mL aqueous solution of 3.8mM sodium hydrogen citrate. The resulting red-brown solution was adjusted to pH 7.5 using a 0.25 M NaOH solution and then refluxed with constant stirring for 30 min. After this, the solution changed its color to a light blue and it was cooled at room temperature and the pH of the solution was again adjusted to 7.5. Then, it was stirred and refluxed for 30 min. These steps were repeated until obtaining a constant value of pH 7.5. The solution was additionally refluxed for 2 h with oxygen bubbling through the solution to yield a deep blue suspension of IrO_2 NPs (Fig. 3.2). All the experiments were conducted with the as-prepared solution that was stored at 4ºC.

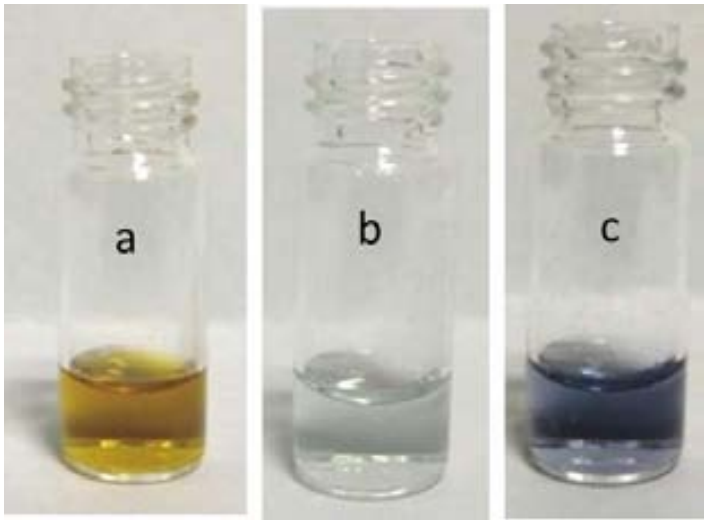

Figure 3.2. Pictures showing the changes in the solution color during the different steps of the synthesis of IrO_2 NPs. Iridium salt and citrate before refluxing (a), after first reflux (b) and final suspension of IrO_2 NPs (c).

The total amount of iridium in the NPs suspension was obtained by analysis with ICP-OES at the *Servei d'Anàlisi Química of the Universitat Autónoma de Barcelona*. Samples were diluted in *aqua regia* in a microwave digester and inserted in the ICP-OES spectrometer to obtain the total content of iridium, expressed in mg/L.

For UV-Vis characterization, 300 µL suspension of IrO_2 NPs were introduced in a well of a microplate and the optical density in the range between 400-800 nm was read with a microplate reader and analyzed using the SoftMax Pro 5.2 program.

For size and shape characterization of IrO_2 by TEM, 5µL of the as-prepared dispersion were dropped on a copper grid and let to be dried all the night.

XPS experiments were carried out in the *Centres Científics I Tecnològics of the Universitat de Barcelona* (CCiTUB) and were performed in a XPS spectroscope with a monochromatic X-ray source (Aluminium Kα line of 1486.6 eV energy and 350 W), placed perpendicularly to the analyzer axis and calibrated using the $3d_{5/2}$ line of Ag with a full width at half maximum (FWHM) of 0.8 eV. All measurements were made in an ultra-high vacuum (UHV) chamber pressure between $5x10^{-9}$ and $2x10^{-8}$ torr. Binding energies were calibrated respect to the C 1s electron peak at 284.8 eV.

3.2.2.3. Calculation of IrO_2 NPs concentration

In order to calculate the number of atoms of iridium per NP, for simplicity the shape of the agglomerated IrO_2 NP was considered as a perfect sphere and by taking the density (ρ) of IrO_2 as bulk 11.68 g/cm^3, the molecular weight (M) to be 224.22 g/mol and the Avogadro number (N_A) to be $6.02x10^{23}$, diameter of the particle (D) and the approximate number of Ir atoms per particle (N) is calculated to be $3.4x10^4$ using the following equation:[2,3]

$$N = \frac{\pi \rho D^3 N_A}{6M} \qquad \text{Eq. 3.2}$$

Thus, the concentration of iridium oxide stock solution was calculated to be about 35 nM using the concentration of Ir obtained by ICP-OES (0.227 mg/mL; 1.18 mM) divided by the number of atoms per particle (N).

3.2.2.4. Conjugation of IrO_2 NPs to αApoE antibodies

The αApoE antibodies immobilization on IrO_2 NPs was performed by direct random adsorption onto the NP surface. Briefly, 100µL of 100µg/mL αApoE monoclonal antibody (αApoE mAb) were added to 1.75mL of IrO_2 NPs suspension adjusted to pH 7. The resulting solution was incubated for 20 min at 650 rpm. Then, 150µL of 5% w/v BSA aqueous solution were added and the stirring was continued for other 20min at 650 rpm. Finally, the solution was centrifuged at 35000×g (4ºC) for 2 hours and 30 minutes.

The supernatant was removed and the pellet of iridium oxide NP/ αApoE mAb was re-suspended in 200 µL of milliQ water.

The same experimental procedure was previously followed for the conjugation of anti-human IgG-horseradish peroxidase (αHIgG-HRP) antibodies to IrO_2 NPs so as to check the antibody immobilization on the NPs surface. This study was performed by the addition of TMB solution (that acts as HRP substrate) to suspensions of IrO_2 NPs conjugates at different pH values (pH 7, 8 and 9). Typical change of color from colorless to blue was observed when the reaction between the TMB and the HRP labelling the antibodies took place, corresponding to the generation of a cation free-radical as oxidation product. The reaction was stopped by adding H_2SO_4, observing a stronger coloration for the conjugates prepared at pH 7 (Fig. 3.3), so these conditions were chosen for the preparation of the conjugate between IrO_2 NPs and the αApoE antibody.

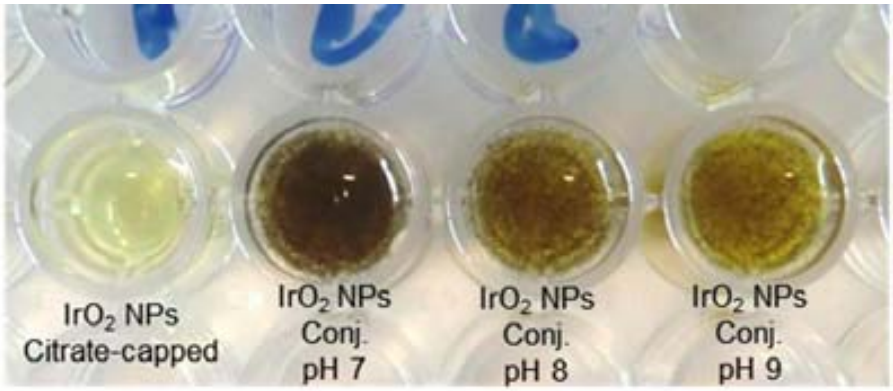

Figure 3.3. Qualitative assay for checking the conjugation between HIgG-HRP and IrO_2 NPs after the addition of TMB. An intense yellow coloration and precipitation was observed after the stopping the reaction enzymatic reaction with H_2SO_4.

3.2.2.5. Magnetosandwich immunoassay for ApoE capturing and labelling with IrO_2 NPs

Carboxylated magnetic microbeads were functionalized through the well-known EDC/sulfo-NHs chemistry. EDC was pre-activated by mixing 133 µL of EDC (10 mg/mL) with 25 µL of sulfo-NHS (100 mg/mL) for 10 min (both solutions in 100 mM MES, pH 5). After that, 842 µL of 10 mM MES pH 5 were added forming *solution 1*. 15 µL of carboxylated magnetic beads were placed in an Eppendorf tube, washed two times in MES buffer and reconstituted in 150 µL of the *solution 1*. The mixture was

incubated at 37 ºC for 30 min (700 rpm). Oriented antibody immobilization was performed by adapting a procedure previously optimized in our group.[46] Briefly, after washing two times in MES buffer, 30 µL of a 300 µg/mL monoclonal goat αApoE antibody solution and 120 µL of 10 mM MES, pH 5, were added to the microspheres and incubated at 37 ºC for 1 h (700 rpm). After washing two times in MES buffer, 150 µL of 5 % BSA (in MES buffer) were added to the microspheres and incubated first at 25 ºC for 20 min (700 rpm) and then at 4 ºC overnight.

After washing two times in PBS-Tween buffer and once in PBS buffer, 150 µL of recombinant ApoE standard in PBS buffer was added to the microspheres and incubated at 25 ºC for 20 min (700 rpm). After washing two times in PBS-Tween buffer and once in PBS buffer, 150 µL of the previously synthesized IrO_2 NPs/ αApoE antibody were added to the microspheres and incubated at 25 ºC for 20 min (700 rpm). The magnetic conjugate was washed four times in PBS-Tween 20 buffer, two times in PBS, once in water and reconstituted in 150 µL of 0.1 M PBS.

In the case of the analysis of human plasma samples, the same experimental procedure was followed, using serial diluted plasma samples in PBS buffer instead of the standard of ApoE.

3.2.2.6. Electrochemical measurements

Each electrochemical measurement was performed after dropping 50 µL of IrO_2 NPs suspension in 0.1M PBS pH 7.4 freshly prepared onto the SPCE. Blank signals were recorded following the same electrochemical procedure but using an aliquot of buffer. Cyclic voltammetry (CV) was carried out from -0.5 V to +1.3 V at 50 mV s^{-1} and chronoamperometry was performed at a fixed potential of +1.3V during 300 s.

The electrochemical detection of ApoE captured through the magnetosandwich immunoassay was evaluated through the water oxidation reaction. Briefly, 50 µL of the immunocomplex suspension were placed on the surface of the screen-printed carbon electrode (SPCE), where a magnet was previously attached to polyester on the reverse side of the working area. An oxidative potential of +1.3 V was applied during 300s. The water oxidation catalyzed by the IrO_2 NPs tags was chronoamperometrically followed measuring the current generated during the time. The absolute value of the current at

250 s was chosen as the analytical signal. For all the experiments, the measurements were made by triplicate at room temperature.

3.3. Results and discussion

3.3.1. Characterization of IrO_2 NPs

Characterization of IrO_2 NPs was conducted through different techniques as UV-visible spectrophotometry (UV-Vis), transmission electronic microscopy (TEM) and X-ray photoelectron spectroscopy (XPS). Hydrolysis of hexachloroiridate (IV) ion, $[IrCl_6]^{2-}$, in neutral aqueous solutions in the presence of citrate ions, results in formation of deep blue suspension of nanoparticles of $IrO_2 \cdot xH_2O$[34] (for simplicity, they will be denoted as IrO_2). TEM micrograph reveal the homogeneous distribution of IrO_2 NPs (Fig. 4) and is worthy to note the homogeneous size of observed agglomerates of 12.5±2.5 nm composed by smaller nanoparticles of 1.5±0.3 nm. This suggests that the initially formed small nanoparticles quickly form bigger agglomerates. This behavior is in agreement with previously reported studies.[35,47]

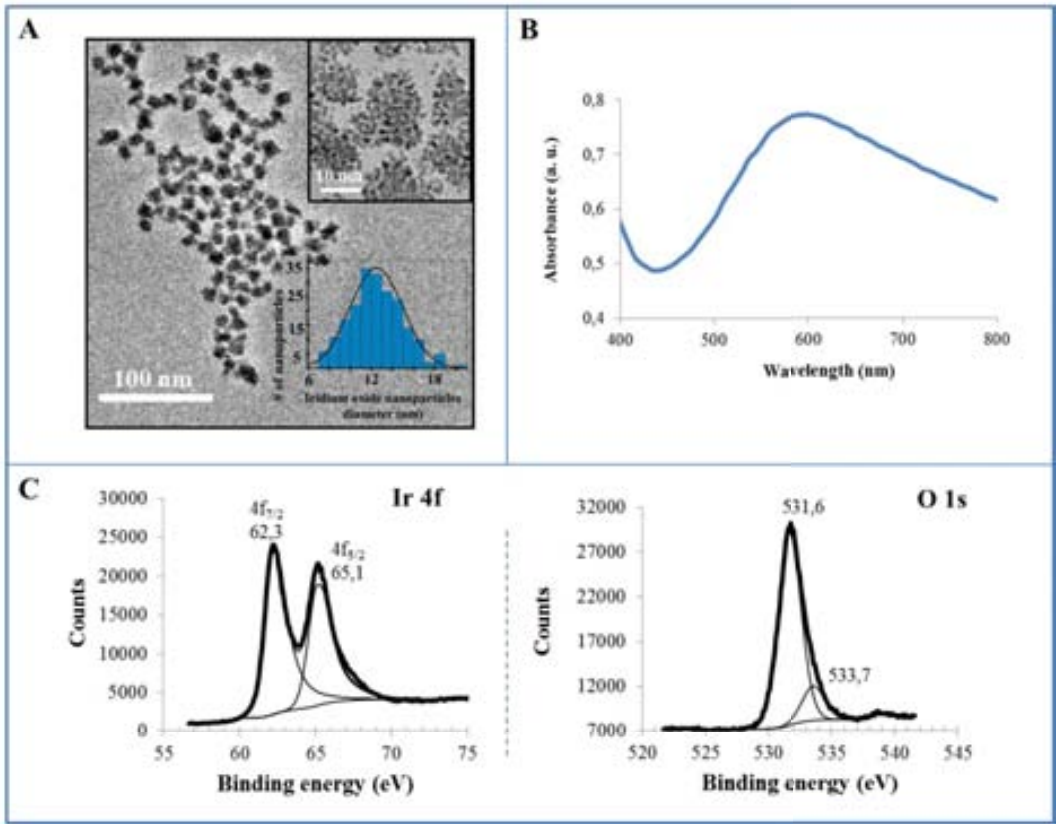

Figure 3.4. Characterization of IrO_2 NPs. (A) TEM micrographs, (B) UV-Vis spectrum, (C) XPS analysis: spectrum for Ir 4f line (left) and O 1s line (right).

UV-Vis spectrum of IrO_2 NPs is shown in Figure 3.4B, where a broad peak between 500-700nm with maximum at 590 nm, characteristic of Ir(IV) oxides and IrO_2 NPs is observed.[34]

XPS analyses were performed in order to confirm the chemical composition of the synthesized IrO_2 NPs (see Figure 3.4C, left). By deconvoluting the XPS spectra, two binding states for iridium are identified as $4f_{7/2}$ and $4f_{5/2}$ at 62.3 and 65.1 eV, respectively. These peaks are attributed to the 4+ oxidation state of iridium and they are similar to those of IrO_2 nanorods (62.0 and 65.0 eV) and similar to IrO_2 single crystal (which has values of 61.7 and 64.7 eV).[48] Regarding the oxygen 1s signal, a main peak at 531.6 and a small one at 533.7 eV were observed as shown in figure 3.4C (right). The former is similar to the value found for IrO_2 nanorods and IrO_2 single crystal, both at 530.5eV.[48] The broader feature at 533.7 eV might be attributed to the oxygen-containing citrate coating these nanoparticles.

According to the mentioned characterization, especially with the XPS analyses, it is possible to conclude that the deep-blue suspension synthetized corresponds to IrO_2 nanoparticles.

The concentration of iridium oxide stock solution was calculated to be around 35 nM using the concentration of Ir obtained by ICP-OES (0.227 mg/mL; 1.18 mM) divided by the number of atoms per particle (N) as stated in Experimental Section.

3.3.2. Electrocatalytic activity of IrO_2 NPs towards WOR

The electrocatalytic activity of IrO_2 NPs towards water oxidation reaction was first evaluated by cyclic voltammetry (CV) using SPCEs.

CV voltammograms were conducted in 0.1M PBS pH 7.4 and obtained by scanning from +0.1 to +1.3 V at 50mV/s scan rate. The as-performed voltammograms for different concentrations of IrO_2 NPs in 0.1 M PBS are shown in figure 3.5A. The background curve (a) shows that the oxidation of the medium's oxygen starts at approximately +1.10V. In the presence of the IrO_2 NPs (curves b-e) on the surface of the electrode, the potential for water oxidation shifts (by up to 300 mV, depending on the concentration of IrO_2 NPs) toward less positive potentials. Moreover, it can also be seen that, because of the catalytic effect of the IrO_2 NPs, a higher current is generated

(up to 70 μA higher, as evaluated for the potential value of +1.3 V, depending on the concentration of Ir O_2 NPs). A shift in the half-wave potential of the WOR to less positive potentials from 1.1V to up to 0.77 V (maximum shift of 332 m V) which is proportional to the quantity of Ir O_2 NPs due to their catalytic eff ect towards th is reaction can also be observed in the same figure.

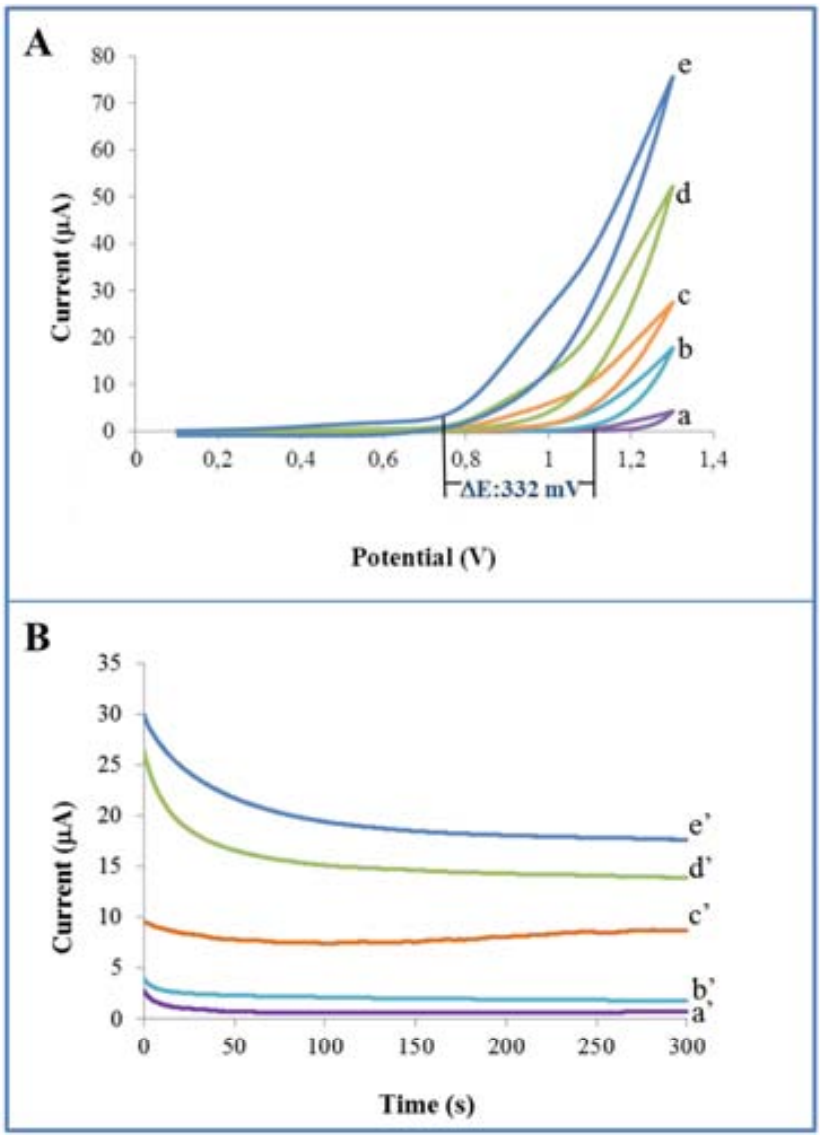

Figure 3.5. Electrocatalytic activity of IrO_2 NPs towards WOR. (A) Cyclic voltammograms recorded from +0.1 to +1.3 V at a scan rate of 50 mV/s for 0.1 M PBS (blank curve, a) and for increasing concentrations of IrO_2 NPs in 0.1 M PBS pH 7.4: (b) 0.7, (c) 1.8, (d) 7 and (e) 35 mM. (B) Chronoamperograms recorded at +1.3 V during 300 s using a 0.1 M PBS pH 7.4 (blank curve, a) and the same IrO_2 NPs concentrations as detailed above (b'-e') in 0.1M PBS.

The obtained results show that, for a fixed potential (*i.e.*, +1.3 V at which steady state currents values are achieved), the intensity of the current recorded in chronoamperometric mode during the stage of oxygen electro-oxidation (Figure 5B) can be related to the presence (curves b'-e') or absence (curve a') of IrO_2 NPs on the surface of the SPCE. A proportional increase of the catalytic current for increasing concentrations of IrO_2 NPs (from 0.7 to 35 nM) was observed.

Regarding the fixed interval of time selected for the current recording (analytical signal), it was observed that for intervals shorter than 250 s the current profiles were not reproducible. Looking at the behavior during the first 50 s, a rapid decrease in the anodic current was observed, probably due to an initial rapid oxidation of water on the surface of the IrO_2 NPs catalyzers followed by a current stabilization. This effect is more evident for higher IrO_2 NPs concentrations (curves d' and e'). The observed irreproducibility during the 50-250 s range could be attributed to the fact that IrO_2 NPs are still not accommodated onto the electrode surface being still under Brownian motions (stabilization time). The current value was stable in all cases after 250 s, so registering at this time interval was chosen as analytical signal.

A logarithmic relationship between the analytical signal and the concentration of IrO_2 NPs in the range of 0.7-35 nM adjusted to the following equation:

$$\text{Current } (\mu A) = 3.15 \ln[IrO_2 \text{ NPs}] + 8.13 \qquad \text{Eq. 3.3}$$

showing a good correlation (r=0.98) and a relative standard deviation of 5.6% for 7nM of IrO_2 NPs (n=3). The limit of detection was calculated as the concentration of IrO_2 NPs corresponding to three times the standard deviation of the estimated, giving a value of 0.13nM.

3.3.3. Electrocatalytic detection of ApoE Alzheimer disease biomarker in human plasma

Magnetic beads were used as platforms of the immunoassays for ApoE detection, taking advantage of their well-known characteristics for capturing/pre-concentrating the analyte and minimizing matrix effects. Carboxylated magnetic beads were modified with αApoE antibody using the EDC-sulpho-NHS coupling. First, EDC was used in order to activate the carboxylic groups located on the surface of magnetic beads. Then, addition of sulpho-NHS led to formation of a stable sulpho-ester, which reacts with the

amine groups located in the antibody, allowing forming of the αApoE modified magnetic beads (αApoE-MB). Blocking with BSA is performed in order to avoid unspecific absorptions onto the surface of the electrotransducer. When ApoE is present in the sample, it is recognized by the αApoE antibody forming the ApoE/αApoE-MB complex.

Once the washing step is performed, the conjugate of αApoE-IrO_2 NPs is able to recognize the ApoE, forming the magnetosandwich αApoE-IrO_2 NPs /ApoE/ αApoE-MB, being the amount of IrO_2 NPs proportional to the ApoE concentration in the sample.

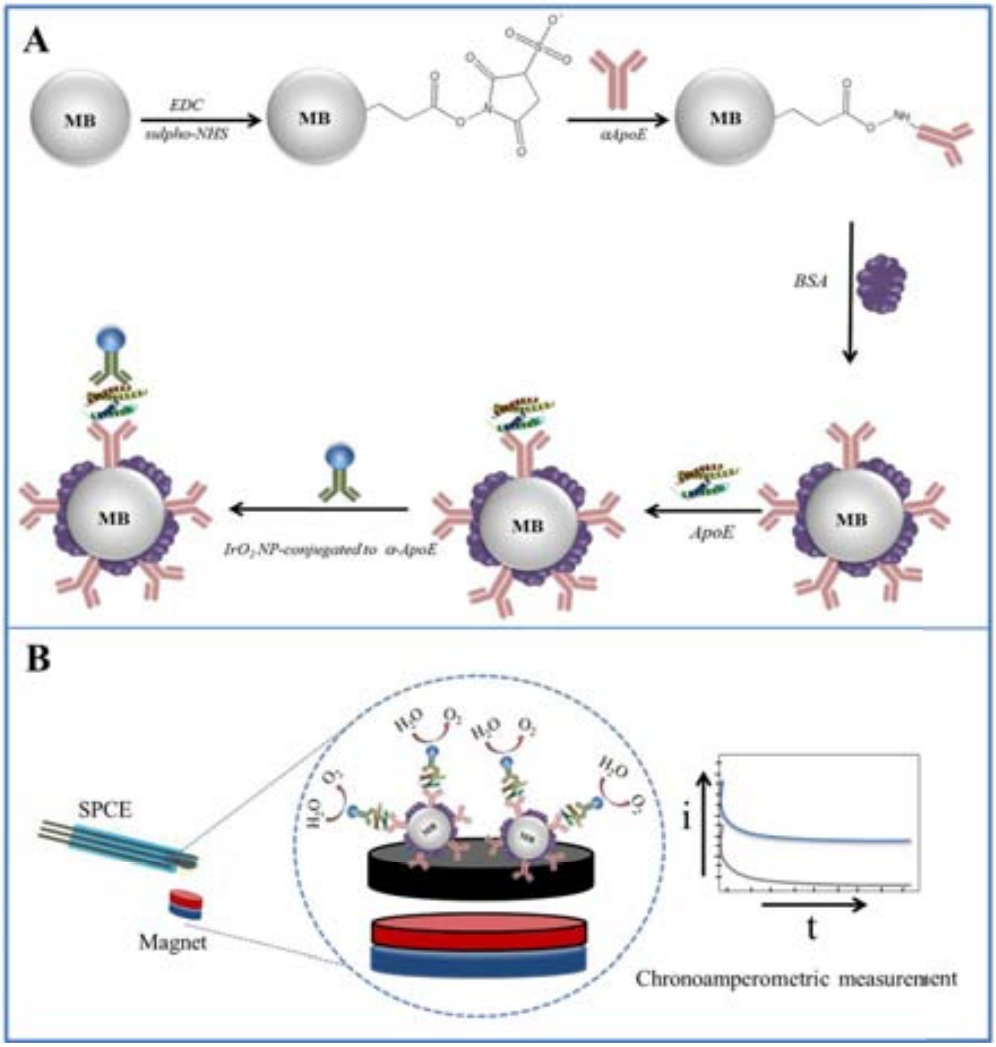

Figure 3.6. Schematics, not in scale, of: (A) experimental procedure of the magnetosandwich immunoassay using IrO_2 NPs tags and (B) electrochemical detection procedure based on the electrocatalytic water oxidation.

Electrochemical detection of ApoE was carried out using 50 µL of the immunocomplex suspension placed onto the surface of the SPCE and taking advantage of the electrocatalytic properties of IrO_2 NPs towards WOR. The catalytic behavior of the IrO_2 NPs generated by the oxidation of water is conducted by chronoamperometry and correlated to the amount of the ApoE in the sample. Figure 3.7A shows the chronoamperograms obtained for samples containing 0 (a), 100 (b), 200 (c), 500 (d) and 1000 (e) ng/mL of ApoE. As expected, the catalytic current increases when the concentration of ApoE increases. The relationship between the concentration of ApoE in the sample and the value of the analytical signal (current recorded at 250s) is adjusted to a logarithmic curve, as shown in Figure 3.7B. The curve exhibits a good correlation (r= 0.98) in the range of 100-1000 ng/mL, adjusted to the following equation:

$$\text{Current } (\mu A) = 2.64\ [\text{ApoE (ng/mL)}] - 10.94 \qquad \text{Eq. 3.4}$$

The limit of detection, calculated as stated before, gives a value of 68 ng/mL. The reproducibility of the responses (n=3) for 500 ng/mL of ApoE shows a relative standard deviation of 6%.

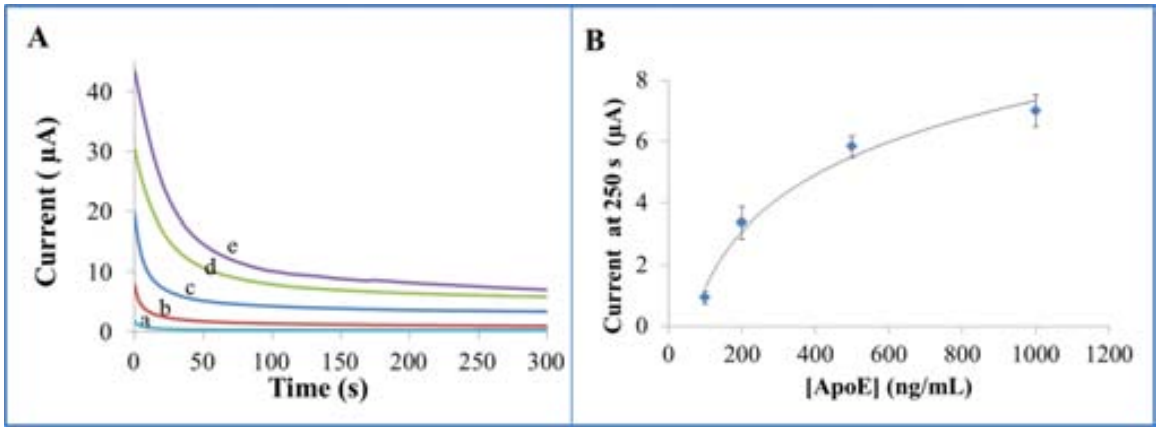

Figure 3.7. (A) Chronoamperograms recorded in PBS 0.1M pH 7.4 at a fixed potential of +1.3V, for a control sample (blank curve, a) and for samples containing 100, 200, 500 and 1000 ng/mL of ApoE. (B) Relationship between the ApoE concentration and the value of the analytical signal (catalytic current recorded at 250s). Samples correspond to the magnetosandwich prepared as detailed in the experimental section.

Finally, a human plasma sample with an unknown concentration of ApoE was electrocatalytically analyzed. As ApoE concentration in plasma typically ranges from 16 to 169 µg/mL,[49] very small volumes of plasma were diluted in PBS buffer before analysis. A dilution of the sample of 1:1000 was necessary to obtain a current within

the linear range of the method, obtaining a value of 3.08 ± 0.18 μA (*n*=3) for such a dilution. Extrapolating this value from Eq. 3.4, a concentration of ApoE of 20 ± 2 μg/mL was estimated in the sample. These results are in concordance with the above mentioned expected data and also with those previously obtained in our group using both microarray technology[50] and electrochemical detection[51] based on commercial Quantum Dot tags.

3.4. Conclusions

Iridium oxide nanoparticles (IrO_2 NPs) of 12 nm size were successfully synthesized, characterized and used as novel electrocatalytic tags for immunosensing. The stable NPs suspension exhibited a high catalytic effect towards the Water Oxidation Reaction (WOR), allowing their sensitive quantification at neutral pH in a simple chroroamperometric mode. This sensitive method was applied for the evaluation of ApoE in human plasma following an immunoassay format using IrO_2 NPs as advantageous tags, able to be detected in the same buffer where the immunoreaction takes place.

Both the IrO_2 NPs tags and electrocatalytic detection method present many advantages compared with previously reported ones based on quantum dots (QDs) or Hydrogen Evolution Reaction (HER) . On the one hand, the NP synthesis procedure is simpler and cheaper than *i.e.* the required for QDs preparation. Furthermore, the chronoamperometric detection based on the WOR is a simple, sensitive and quantitative methodology that can be performed in the same medium of the immunoreaction, avoiding the addition of acidic and hazardous solutions, (along with H_2 bubbles formation undesired in microfluidics), usually required for electrochemical detection of other NP tags (ex. AuNP using HER). These advantageous properties open the way to further applications in really integrated sensing systems, such as those based on lab-on-a-chip or lateral-flow platforms. Moreover, the UV-Vis absorption band observed at 590 nm (deep blue color) of the IrO_2 NPs suspension make these NPs excellent candidates for dual electrochemical/optical detection systems in future lateral flow biodetection platforms.

3.5. References

(1) De la Escosura-Muñiz, A.; Parolo, C.; Merkoçi, A. *Mater. Today* **2010**, *13*, 24–34.

(2) Dykman, L.; Khlebtsov, N. *Chem. Soc. Rev.* **2012**, *41*, 2256–2282.

(3) Dreaden, E. C.; Alkilany, A. M.; Huang, X.; Murphy, C. J.; El-Sayed, M. A. *Chem. Soc. Rev.* **2012**, *41*, 2740–2779.

(4) Walcarius, A.; Minteer, S. D.; Wang, J.; Lin, Y.; Merkoçi, A. *J. Mater. Chem. B* **2013**, *1*, 4878–4908.

(5) Ambrosi, A.; Castañeda, M. T.; de la Escosura-Muñiz, A.; Mekoçi, A. In *Biosensing using nanomaterials-Bionano*; Merkoçi, A., Ed.; Wiley-Interscience, 2009; pp. 177–197.

(6) Merkoci, A.; Ambrosi, A.; de la Escosura, A.; Pérez, B.; Guix, M.; Maltez, M.; Marin, S. In *Encyclopedia of Analytical Chemistry*; Meyers, R. A., Ed.; John Wiley: Chichester, 2010.

(7) Merkoci, A. *Biosensensors Bioelectron.* **2010**, *26*, 1164–1177.

(8) De la Escosura-Muñiz, A.; Ambrosi, A.; Merkoçi, A. *Trends Anal. Chem.* **2008**, *27*, 568–584.

(9) Merkoçi, A. *Electroanalysis* **2013**, *25*, 15–27.

(10) Merkoçi, A. *FEBS J.* **2007**, *274*, 310–316.

(11) De la Escosura-Muñiz, A.; Merkoçi, A. *Expert Opin. Med. Diagn.* **2010**, *4*, 21–37.

(12) Tang, D.; Cui, Y.; Chen, G. *Analyst* **2013**, *138*, 981–990.

(13) Dequaire, M.; Degrand, C.; Limoges, B. *Anal. Chem.* **2000**, *72*, 5521–5528.

(14) Zhu, N.; Zhang, A.; Wang, Q.; He, P.; Fang, Y. *Electroanalysis* **2004**, *16*, 577–582.

(15) Cui, R.; Pan, H. C.; Zhu, J. J.; Chen, H. Y. *Anal. Chem.* **2007**, *79*, 8494–8501.

(16) Wang, J.; Li, G.; Merkoçi, A. *J. Am. Chem. Soc.* **2003**, *125*, 3214–3215.

(17) Castañeda, M. T.; Alegret, S.; Merkoçi, A. *Electroanalysis* **2007**, *19*, 743–753.

(18) Ambrosi, A.; Castañeda, M. T.; Killard, A. J.; Smyth, M. R.; Alegret, S.; Merkoçi, A. *Anal. Chem.* **2007**, *79*, 5232–5240.

(19) De la Escosura-Muñiz, A.; Sánchez-Espinel, C.; Díaz-Freitas, B.; González-Fernández, A.; Maltez-Da Costa, M.; Merkoçi, A. *Anal. Chem.* **2009**, *81*, 10268–10274.

(20) Dau, H.; Limberg, C.; Reier, T.; Risch, M.; Roggan, S.; Strasser, P. *ChemCatChem* **2010**, *2*, 724–761.

(21) Meyer, T. J. *Nature* **2008**, *451*, 778–779.

(22) Umena, Y.; Kawakami, K.; Shen, J.-R.; Kamiya, N. *Nature* **2011**, *473*, 55–60.

(23) Joya, K. S.; Joya, Y. F.; Ocakoglu, K.; van de Krol, R. *Angew. Chemie, Int. Ed.* **2013**, *52*, 10426–10437.

(24) Sens, C.; Romero, I.; Rodríguez, M.; Llobet, A.; Parella, T.; Benet-Buchholz, J. *J. Am. Chem. Soc.* **2004**, *126*, 7798–7799.

(25) Romain, S.; Vigara, L.; Llobet, A. *Acc. Chem. Res.* **2009**, *42*, 1944–1953.

(26) Duan, L.; Bozoglian, F.; Mandal, S.; Stewart, B.; Privalov, T.; Llobet, A.; Sun, L. *Nat. Chem.* **2012**, *4*, 418–423.

(27) Kurz, P.; Berggren, G.; Anderlund, M. F.; Styring, S. *Dalt. Trans.* **2007**, 4258–4261.

(28) Karlsson, E. A.; Lee, B. L.; Akerman, T.; Jhonston, E.; Kärkäs, M.; Sun, J.; Hannson, Ö.; Bäckwall, J. E.; Akerman, B. *Angew. Chemie* **2011**, *123*, 11919–11922.

(29) McDaniel, N. D.; Coughlin, F. J.; Tinker, L. L.; Bernhard, S. *J. Am. Chem. Soc.* **2008**, *130*, 210–217.

(30) Junge, H.; Marquet, N.; Kammer, A.; Denurra, S.; Bauer, M.; Wohlrab, S.; Gärtner, F.; Pohl, M.-M.; Spannenberg, A.; Gladiali, S.; Beller, M. *Chemistry* **2012**, *18*, 12749–12758.

(31) Harriman, A.; Pickering, I. J.; Thomas, J. M.; Christensen, P. A. *J. Chem. Soc. Faraday Trans. I* **1988**, *84*, 2795–2806.

(32) Singh, R. N.; Mishra, D.; Anindita, A. S. K.; Singh, A. *Electrochem. commun.* **2007**, *9*, 1369–1373.

(33) Trasatti, S. *J. Electroanal. Chem. Interfacial Electrochem.* **1980**, *111*, 125–131.

(34) Harriman, A.; Thomas, J. M. *New J. Chem.* **1987**, *11*, 757–762.

(35) Hara, M.; Mallouk, T. E. *Chem. Commun.* **2000**, 1903–1904.

(36) Yagi, M.; Tomita, E.; Sakita, S.; Kuwabara, T.; Nagai, K. *J. Phys. Chem. B* **2005**, *109*, 21489–21491.

(37) Zhao, Y.; Hernandez-Pagan, E. A.; Vargas-Barbosa, N. M.; Dysart, J. L.; Mallouk, T. E. *J. Phys. Chem. Lett.* **2011**, 402–406.

(38) Lee, Y.; Suntivich, J.; May, K. J.; Perry, E. E.; Shao-horn, Y. *J. Phys. Chem. Lett.* **2012**, *3*, 399–404.

(39) O'Hare, D.; Parker, K. H.; Winlove, C. P. *Med. Eng. Phys.* **2006**, *28*, 982–988.

(40) Huang, W.-D.; Cao, H.; Deb, S.; Chiao, M.; Chiao, J. C. *Sensors Actuators A* **2011**, *169*, 1–11.

(41) Lu, Y.; Wang, T.; Cai, Z.; Cao, Y.; Yang, H.; Duan, Y. Y. *Sensors Actuators B Chem.* **2009**, *137*, 334–339.

(42) Göbbels, K.; Kuenzel, T.; van Ooyen, A.; Baumgartner, W.; Schnakenberg, U.; Bräunig, P. *Biomaterials* **2010**, *31*, 1055–1067.

(43) Hara, M.; Waraksa, C. C.; Lean, J. T.; Lewis, B. A.; Mallouk, T. E. *J. Phys. Chem. A* **2000**, *104*, 5275–5280.

(44) Kim, J.; Basak, J. M.; Holtzman, D. M. *Neuron* **2011**, *63*, 287–303.

(45) Reinvang, I.; Espeseth, T.; Westlye, L. T. *Neurosci. Biobehav. Rev.* **2013**, *37*, 1322–1335.

(46) Parolo, C.; de la Escosura-Muñiz, A.; Polo, E.; Grazu, V.; De La Fuente, J.; Merkoçi, A. *ACS Appl. Mater. Interfaces* **2013**, *5*, 10753−10759.

(47) Kwon, S. J.; Fan, F.-R. F.; Bard, A. J. *J. Am. Chem. Soc.* **2010**, *132*, 13165–13167.

(48) Chen, R. S.; Huang, Y. S.; Liang, Y. M.; Tsai, D. S.; Chi, Y.; Kai, J. J. *J. Mater. Chem.* **2003**, *13*, 2525.

(49) Vicent-Viry, M.; Schiele, F.; Gueguen, R.; Bohnet, K.; Visvikis, S. *Clin. Chem.* **1998**, *44*, 957–965.

(50) Morales-Narváez, E.; Montón, H.; Fomicheva, A.; Merkoçi, A. *Anal. Chem.* **2012**, *84*, 6821–6827.

(51) Medina-Sánchez, M.; Miserere, S.; Morales-Narváez, E.; Merkoçi, A. *Biosens. Bioelectron.* **2014**, *54*, 279–284.

Chapter 4

Label-free impedimetric aptasensor for ochratoxin-A detection using iridium oxide nanoparticles

Summary

In this Chapter, a novel aptasensor for ochratoxin A (OTA) detection based on screen-printed carbon electrode (SPCE) modified with polythionine (PTH) and iridium oxide nanoparticles (IrO_2 NPs) is presented. The electrotransducer surface is modified with an electropolymerized film of PTH followed by the assembly of IrO_2 NPs. Aminated aptamer selective to OTA is attached to the citrate ions surrounding IrO_2 NPs *via* electrostatic interactions. Electrochemical impedance spectroscopy (EIS) in the presence of $[Fe(CN)_6]^{-3/-4}$ redox probe is employed to characterize each step in the aptasensor assay and also for label-free detection of OTA in a range between 0.1-100 nM. This system shows high reproducibility, selectivity and to the best of our knowledge, the lowest limit of detection reported for OTA electrochemical detection (0.2 pM) reported so far.

4.1. Introduction

Ochratoxin A (OTA) is a mycotoxin generated by different fungi species such as *Aspergillus* and *Penicillium* during their growth. This toxin is an hazardous contaminant present in a great number of agricultural products such as cereals, coffee beans, dried fruits, cocoa, nuts, beer and wine, causing economic losses to agricultural trade.[1–4] Moreover, OTA has been reported in literature as nephrotoxic, teratogenic, immunotoxic agent[5,6] and it is also considered as possible human carcinogen (class 2B) by the International Agency for Research on Cancer.[7]

International organizations have established regulatory levels for OTA in food. In this context, the World Health Organization (WHO) has been set a tolerable weekly intake (TWI) of 100 ng/kg of body weight,[8] and the European Union (EU) through Commission Regulation (EC) 1881/2006 has established the TWI in 120 ng/kg of body weight, specifying the maximum permitted levels of OTA in different foodstuff such as: raw cereals (5 μg/kg), soluble coffee (10 μg/kg), wine (2 μg/kg) and baby food (0.5 μg/kg).[9]

Chromatographic methods are routinely used in laboratories for mycotoxins analysis because of their high sensitivity, but they require skilled personnel for operating and complex and expensive equipments.[10] Despite of the high analytical performances that offer these techniques, rapid and sensitive screening methods are needed for field setting purposes. Such is the case of enzyme-linked immunosorbent assay (ELISA) and lateral flow assays (LFA) which are immunological techniques able to semi-quantitatively detect mycotoxins in a less consuming-time process.[11,12] Although antibodies are typical examples of biorecognition elements in diagnostic applications, a new class of synthetic molecules has emerged in this field. These molecules, called aptamers, are short synthetic oligonucleotides that have several advantages compared to antibodies, such as their high affinity and specificity for a wide range of targets, their thermal and chemical stability, and their low-cost production.[13]

Nowadays, the interest for label-free based technologies is increasing since they are experimentally simpler and offer direct information about the interaction of the target with the sensing element by measuring changes on physical properties such as mass, refractive index or electrical resistivity, produced by this binding. In addition, it allows the real-time measurement of kinetics of biomolecular interactions.[14,15]

Impedimetric biosensors for label-free detection offer new opportunities to mycotoxin analysis due to their high sensitivity, easy use and possible miniaturization and portability, which are vital requirements for point-of-care (POC) applications. Moreover, several label-free impedimetric aptasensors for OTA detection using different electrotransducers *e.g.* gold electrodes,[16] indium-tin oxide (ITO) coated glass[17] and screen-printed carbon electrodes (SPCEs)[18,19] have been reported. Label-free impedimetric (bio)sensors require uniform and low resistive electrotransducer surfaces. Thus, electropolymerization is an alternative technique for improving the electrical conductivity on the surface of irregularly shaped electrodes.[20] Conductive dyes such as thionine can be electropolymerized producing stable redox-active coatings on the electrode surfaces and have been extensively used for biosensing applications thanks to their electrochemical properties.[21–24]

On the other hand, it is well known that nanomaterials represent a powerful tool for modifying electrode surfaces thanks to their high surface-to-volume ratio and good conductivity which make them useful for proposing novel electrochemical biosensors or greatly improving the existing ones.[25,26] Iridium oxide-based materials (in films and nanoparticle form), are attractive because of their catalytic activity, biocompatibility, low resistivity and outstanding chemical and thermal stability which have been used for applications in pH sensors[27] neural stimulation[28,29] and environmental biosensors.[30]

In this work, the development of an OTA aptasensor that takes advantage of electropolymerized thionine films onto SPCE and iridium oxide nanoparticles (IrO_2 NPs) is shown. Electrochemical impedance spectroscopy is used to monitor each step in the aptasensor development and also to detect OTA. The charge transfer resistance (*R*ct) increases proportionally to the concentration of OTA in a linear range of 0.1–100 nM. This system shows also good reproducibility, sensitivity and selectivity. To the best of our knowledge, this sensitive aptasensor exhibits the lowest limit of detection (LoD = 0.2 pM) reported so far for electrochemical detection of OTA.

4.2. Experimental section

4.2.1. Reagents, solutions and apparatus

HPSF (high purity salt free) purified 3'-aminated aptamer selective to OTA, previously reported by Cruz and Penner[31] (5'-GATCGGGTGTGGGTGGCGTAAAGGGAGCATCGGACAAAAAAAAAA-NH_2-3') was purchased from Isogen Life Science (Spain).

Ochratoxin A from *Aspergillus ochraceus* ($C_{20}H_{18}ClNO_6$), zearalenone fungal mycotoxin ($C_{18}H_{22}O_5$), potassium hexachloroiridate (IV) (K_2IrCl_6), sodium hydrogen citrate sesquihydrate ($Na_2C_6H_6O_7 \cdot 1.5H_2O$), sodium hydroxide (NaOH), sodium chloride (NaCl), sulphuric acid (H_2SO_4), ethanolamine (C_2H_7NO), thionine acetate salt ($C_{12}H_9N_3S.C_2H_4O_2$), potassium chloride (KCl), Trizma® hydrochloride ($NH_2C(CH_2OH)_3 \cdot HCl$, EDTA disodium salt ($C_{10}H_{14}N_2Na_2O_8 \cdot 2H_2O$) and $CaCl_2$ anhydrous were purchased from Sigma Aldrich (Spain). Potassium hexacyanoferrate (II)-($K_4[Fe(CN)_6] \cdot 3H_2O$) and potassium hexacyanoferrate (III)-$K_3[Fe(CN)_6]$ were purchased from Panreac (Spain).

The phosphate buffer saline solution (PBS) consisted of 0.1 M phosphate buffer, 1.37 M NaCl, 0.03 M KCl (pH 6.5). Tris-EDTA (TE) buffer pH 8.0 was used for dissolving the aptamer and consisted in 0.1 M Trizma® and 0.001 M EDTA. Binding buffer at pH 7.0-7.2 was used for OTA recognition consisted in 0.01 M Trizma®, 0.12 M NaCl, 0.005 M KCl and 0.02 M $CaCl_2$. Milli-Q water, produced using a Milli-Q system (>18.2 $M\Omega cm^{-1}$) from Millipore, was used for the preparation of all solutions.

The stirrer used was a TS-100 Thermo shaker (BioSan, Latvia). Veriti™ 96-well Thermal Cycler (Applied Biosystems, USA) was used PCR experiments. The electrochemical transducers used were homemade screen-printed carbon electrodes (SPCEs) and the impedance measurements were performed in an Autolab 302 potentiostat/galvanostat/ frequency-response analyzer PGST30, controlled by GPES/FRA Version 4.9 (Eco-chemie, The Neetherlands).

4.2.2. Morphological Characterization

The morphological characterization of IrO_2 NPs was conducted in a Field Emission Gun Transmission Electronic Microscope Fei, model Tecnai™ G2F20 (Fei, USA). Scanning electronic micrographs of working surface area of modified SPCEs were conducted in a Field Emission Gun Scanning Electronic Microscope Fei, model Quanta™ 650 (Fei,

USA). X-ray photoelectron spectroscopy (XPS) experiments were carried out in the *Centres Científics i Tecnològics of the Universitat de Barcelona* (CCiTUB) and were performed with a PHI 5500 Multitechnique System (Physical Electronics) with a monochromatic X-ray source (Aluminium Kα line of 1486.6 eV energy and 350 W), placed perpendicularly to the analyzer axis and calibrated using the $3d_{5/2}$ line of Ag with a full width at half maximum (FWHM) of 0.8 eV. All measurements were made in an ultra-high vacuum (UHV) chamber pressure between $5x10^{-9}$ and $2x10^{-8}$ torr. Binding energies were calibrated respect to the C 1s electron peak at 284.8 eV. Spectrophotometric measurements were performed using a Spectramax® M2E multi-mode microplate reader (Molecular Devices Inc, UK).

4.2.3. Methods

4.2.3.1. Screen-printed carbon electrodes (SPCEs) fabrication

The electrochemical transducers used were homemade screen-printed carbon electrodes (SPCEs) as stated in Experimental Section of **Chapter 3**.

4.2.3.2. Synthesis and morphological characterization of iridium oxide nanoparticles (IrO_2 NPs)

IrO_2 NPs 12 nm sized and stabilized by citrate, were prepared and characterized as previously described in Experimental Section of **Chapter 3**.

4.2.3.3. Aptasensor development

Firstly, SPCEs were activated after dropping 50µL of H_2SO_4 0.1M and applying a fixed current of 3 µA for 2 min. Then, they were washed with milliQ-water and PBS 0.1 M, pH 6.5.

For thionine film electrodeposition onto the working electrode (WE) of SPCE, 50 µL of thionine salt 0.5 mM (in PBS 0.1M, pH 6.5) were dropped and potential cycling with a triangular wave (20 cycles between 0.1 and -0.55V versus the Ag/AgCl reference electrode at a 50 mV/s scan rate) was used. After thionine film electrodeposition the electrodes were washed with milli-Q water and let to be dried completely. Then, 8 µL of IrO_2 NPs dispersion were deposited on the WE surface and allowed to be dried (around 30-45 min). For removing the excess of nanoparticles over the surface, the SPCEs were washed with water and dried at room temperature. After this, 8 µL of 3'-amino aptamer 5 µM in binding buffer, containing calcium for facilitating a proper recognition of OTA

by the aptamer,[16] were deposited onto the modified WE and then incubated overnight at 4ºC.

Before immobilization, aptamers were denatured by heating at 95ºC for 5 minutes and then ice-cooled for 5 minutes. After incubation, the SPCE was washed with water and 8 μL of aqueous solution of ethanolamine (EA) 10mM (used as blocking agent) were deposited onto working electrode surface and left for 90 minutes at room temperature. Unbounded EA was then removed by washing twice with binding buffer. Immediately, 8 μL of OTA at different concentrations in binding buffer were deposited onto the WE and incubated for 90 min. The washed electrodes with milli-Q water were ready for immediate impedimetric measurements.

4.2.3.4. Impedimetric measurements

Impedimetric measurements were performed using an Autolab 302 potentiostat/galvanostat/ frequency-response analyzer PGST30, controlled by GPES/FRA Version 4.9 (Eco-chemie, The Neetherlands). The measurements were done in a frequency range of 100 kHz-0.1 Hz, using a sinusoidal AC potential perturbation of 0.01 V (rms) and DC potential of 0.24 V was also applied. All measurements were performed in an aqueous solution of 1 mM $[Fe(CN)_6]^{-3/-4}$ with 0.1 M KCl.

4.3. Results and discussion

4.3.1. Electropolimerization of thionine

The electropolimerization of thionine is performed and monitored by cyclic voltammetry (See Figure 4.1).

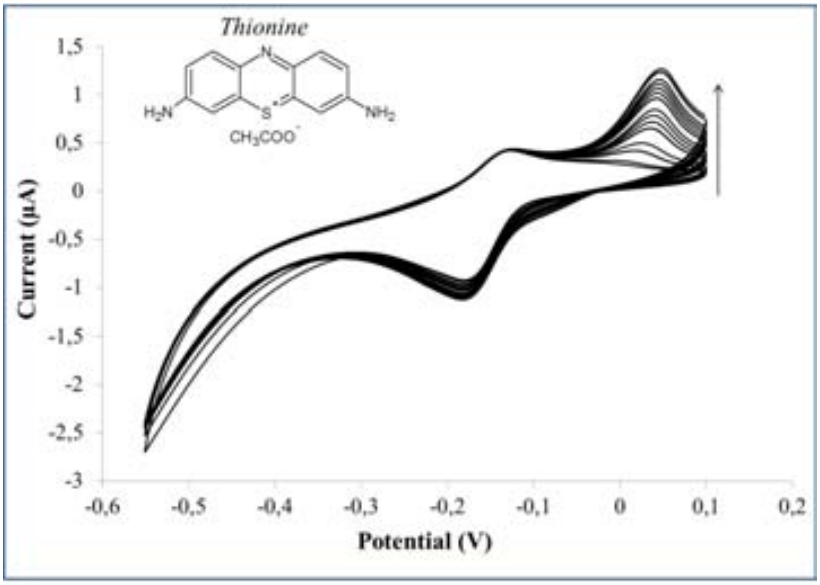

Figure 4.1. Thionine electropolymerization cycles (from inner to outer) by cyclic voltammetry in a 0.1 M PBS solution containing 0.5 mM thionine. Other experimental conditions as described in the text. Chemical structure of thionine is shown as inset.

Electrochemical behavior of thionine films is highly influenced by the electropolimerization conditions.[32] In this work, 20 scans were found to be suitable (current values reached saturation) to create a thionine film and to improve the electron transference. Cathodic (E_{pc}) and anodic (E_{pa}) potential peaks are observed in the range of -0.05 to -0.25 V. The E_{pc} slightly increased with increasing scan number, while E_{pa} remained stable through the process. However, a peak appeared at +0.05 V in the anodic process. This peak current gradually increased with the cycle number, observing also a shoulder peak at -0.1 V in the cathodic process during the thionine electropolimerization. This suggests the formation of the polymer film onto the WE of SPCE.

4.3.2. Impedimetric studies of the modified SPCE surface

The aptasensor for OTA detection is prepared modifying the WE surface of SPCEs by electropolymerization of thionine and adsorption of IrO_2 NPs *via* electrostatic interactions. Both modifications were conducted in order to improve the electron transfer in the SPCEs. After these steps, immobilization of aptamer selective to OTA and blocking steps are carried out before the impedimetric OTA detection (Figure 4.2).

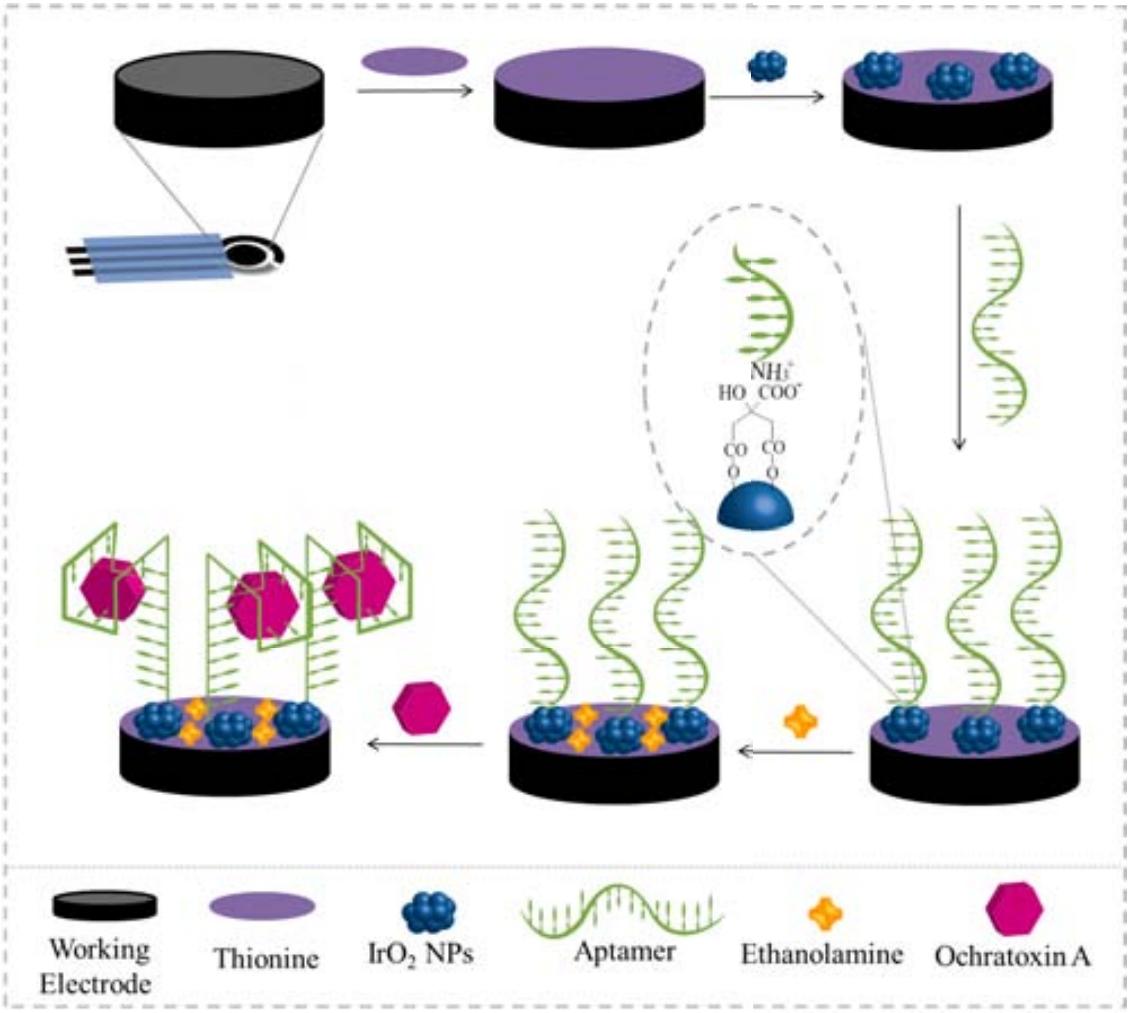

Figure 4.2. Schematic illu stration of the fabricatio n steps and working principle of the developed impedimetric aptasensor for ochratoxin-A (OTA) detection. Experimental conditions as described in the text.

The ele ctrochemical characterization of the sensor sur face at each fabrication step was conducted thr ough EIS using $[Fe(CN)_6]^{-3/-4}$ as redox probe. Im pedance spectra (Nyquist pl ots) for each surface functionalizat ion ste p are shown in Fig ure 4.3. The interface is modeled using Randle model modified with Warburg impedance (Zw) (see model in Figure 4.3). The Nyquist p lots sh ow a semicircle in w hich diameter corresponds to the cha rge-transfer resistance (*R*ct) and straight line co rresponds to the Warburg- impedance (Zw). Different *R*ct values are obtained for each fabrication step (see inset in Figure 4.3). It can be seen that the *R*ct value of the bar e SPCE (*a* curve) remarkably decr eases around one order of magnitude when conductive polyt hionine (PTH) fil ms are deposited (*b* curve). After IrO_2 NPs are adsorbed onto the SPCE/PTH, the *R*ct value increases (*c* curve) due to the negative charge fro m the cit rate groups

surrounding the IrO_2 NPs. This negatively charged layer acts as an electrostatic barrier between SPCE/PTH and the redox probe.

Once the aminated aptamer selective to OTA and ethanolamine (blocking agent) are attached onto the citrate groups of the IrO_2 NPs adsorbed onto the electrode (*d* curve), the *R*ct increases due to the additional negative charge from the phosphate backbone of aptamers.[16] Both, aminated aptamer and ethanolamine are attached to citrate groups onto the IrO_2 NPs through electrostatic interactions. In addition, in presence of 100 nM OTA the *R*ct significantly increases (*e* curve). This phenomena could be explained by the ionization of the phenolic and carboxylic moieties in OTA molecule at neutral pH[33] that increases the negative charge onto the electrode surface (see OTA molecular structure at Figure 4.2).

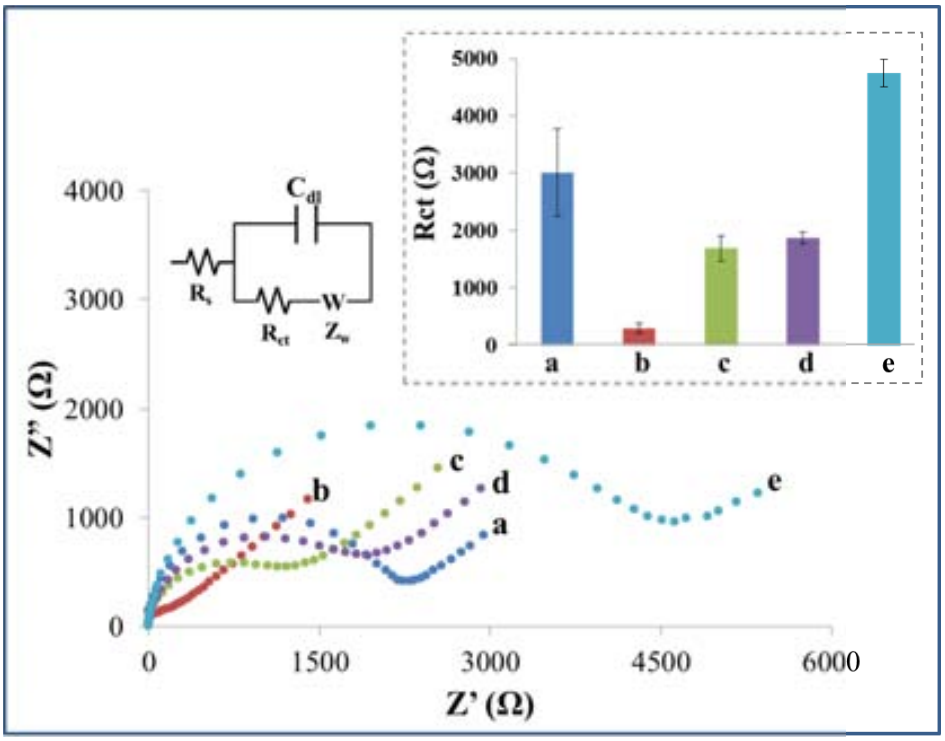

Figure 4.3. Nyquist plots for each aptasensor obtained after each fabrication step recorded in 1.0 mM $[Fe(CN)_6]^{-3/-4}$ in 0.1 M KCl solution by applying bias potential of 0.200 V vs. pseudo Ag/AgCl reference electrode and an AC amplitude of 10mV in a frequency range of 100 kHz to 0.1 Hz: (a) Bare SPCE; (b) SPCE/PTH; (c) SPCE/PTH after its modification with IrO_2 NPs; (d) the aptamer immobilization onto SPCE/PTH/IrO_2 NPs followed by blocking step by ethanolamine and (e) OTA interaction with the aptamer. Inset: *R*ct values corresponding to each fabrication step. Other experimental conditions as described in the text.

Prior to OTA detection, the optimization of blocking step is performed so as to avoid non-specific adsorptions and thus improving the sensitivity of the assay. Two types of blocking agents are tested, ovalbumin (OVA) and ethanolamine (EA). As shown in Figure 4.4, in presence of OVA, the *R*ct value considerably increases since this protein is negatively charged at neutral pH (its isoelectric point is around 4.8[34]). In consequence, if the pH is above or below the isoelectric point, the charge of the protein will be negative or positive, respectively. However, if a non-proteinaceous blocking agent such as EA is used, the electron transference is improved since no additional charge is added to the aptamer-modified electrode (see Figure 4.4). Additionally, EA helps to maintain straight the aptamers adsorbed on the electrode surface since the negative charge of the hydroxyl group of the EA repeals the negative charged phosphate backbone of the aptamers, while the amino group in the EA is attached to the remaining free carboxylic groups from the citrate-capped IrO_2 NPs.

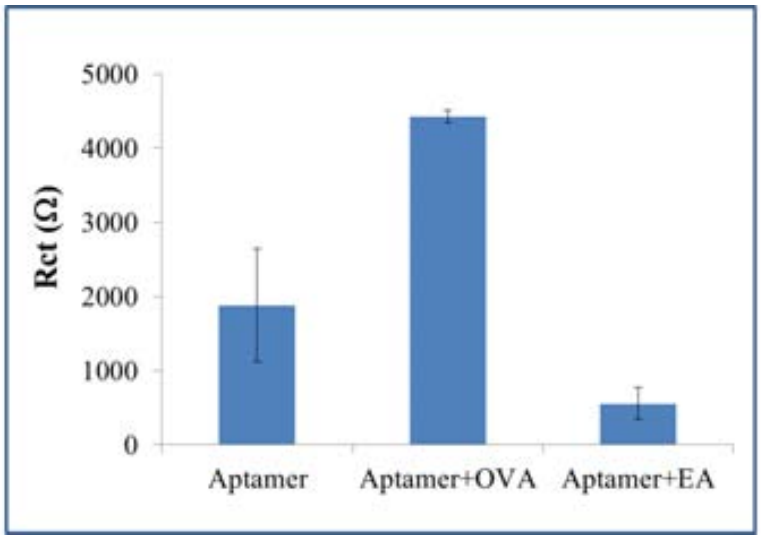

Figure 4.4. Evaluation of the effect of blocking agents such as ovalbumin (OVA) and ethanolamine (EA), for improving the impedimetric responses. Experimental conditions as described in the text.

The other parameter considered for improving the OTA detection was the effect produced by the presence of divalent cations in the binding buffer, especially with calcium ions (Ca^{+2}) which greatly enhance the binding between the OTA and the aptamer.[31] Possibly, OTA forms a complex with Mg^{+2} or Ca^{+2} with the aid of the

carboxyl and hydroxyl groups both present on the toxin, and this complex may enhance the binding to the aptamer.[31] This hypothesis is supported by previously reported works describing the influence of the concentration of [Ca^{2+}] in the binding buffer, which results optimum at 20 mM.[16]

In addition, the role of the IrO_2 NPs in the impedance response of this aptasensor is evaluated (see Figure 4.5A), following next equation:

$$\%\ \text{Relative Response} = \frac{(R_{\text{ct}}\ \text{aptamer} - R_{\text{ct}}\ \text{toxin})}{R_{ct}\ \text{aptamer}} \qquad \text{Eq. 4.1}$$

In the presense of IrO_2 NPs the impedance response is higher due to the fact that the aptamer has more afinity to the citrate groups surrounding IrO_2 NPs than to the PTH. SEM images of bare SPCE and SPCE/PTH/IrO_2NPs/OTA-aptamer are shown in Figures 4.5B and 4.5C, respectively. The presence of IrO_2 NPs adsorbed onto the electrode surface as bright dots (Fig. 4.5C inset) using backscatter electrons mode is observed, due to an enhancement of the contrast between heavy and light elements present onto the electrode surface.

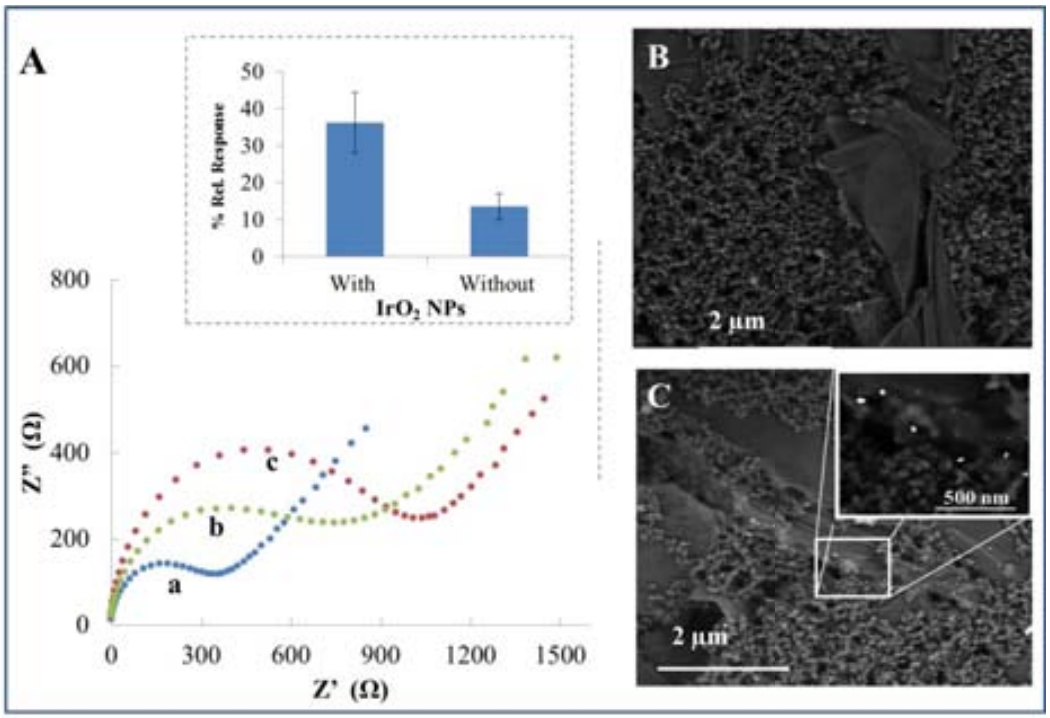

Figure 4.5. (A) Nyquist plots of aptasensor in presence of 0 (a) and 50 nM (b and c) of OTA, when aptasensor surface is modified (c) or not (b) with IrO_2 NPs. Inset: Effect of IrO_2 NPs in the response percentage of the aptasensor. SEM images of working electrode surface taken using backscattered electrons mode for: (B) bare SPCE and (C) SPCE/PTH/IrO_2NPs/OTA-aptamer modified electrode, including a magnified image as inset.

4.3.3. Impedimetric detection of OTA

Once the aptasensor is optimized, different OTA concentrations are incubated for 90 min. Experimental results show that *R*ct increases as the OTA concentration increases in the range of 0.1 to 100 nM (see Figure 4.6), due to the extra negative charge that is provided by OTA at neutral pH, as stated before. This behavior is in agreement with other reports.[16,18,33,35]

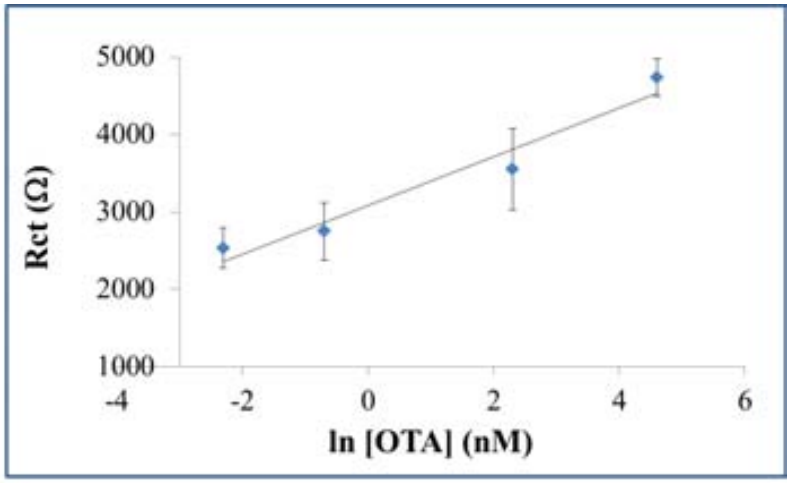

Figure 4.6. Calibration curve obtained by plotting the *R*ct values *vs*. Ln of OTA concentration in the range of 0.1 to 100 nM. Experimental conditions as described in the text.

The linear regression equation was adjusted to *R*ct (Ω) = 332.75*C (nM) + 3162 (r= 0.99) with an estimated LoD of 0.2 pM, calculated as the concentration of toxin corresponding to three times the standard deviation of the estimate. The relative standard deviation (RSD) of three measurements (*n*=3) is 10 % for 0.1 nM of OTA.

This aptasensor for OTA detection presents high analytical performance in terms of linear range, sensitivity and LoD (Table 4.1). Moreover, to the best of our knowledge the obtained LoD in this work is the lowest found in the literature for OTA electrochemical detection.

Table 4.1. Comparison of lineal range and limit of detection of different label-free impedimetric aptasensors for OTA

Transducer	Linear Range (nM)	LoD (nM)	Reference
Langmuir-Blodgett films of polyaniline (PANI)–stearic acid (SA) prepared on ITO coated glass plate.	0.25-24.8	0.25	17
Gold electrode surface	0.1-100	0.12-0.40	16
Electrografted binary films via click chemistry onto SPCE	0.003-1.24	0.006	18
Au electrode modified with AuNPs stabilized on hyper-branched polymer film	0.1-100	0.02	35
Au Electrode Modified with Ag Nanoparticles Decorated with Macrocyclic Ligand	0.3-30	0.05	36
SPCE modified with thionine and IrO_2NPs	0-100	0.0002	this work

4.3.4. Specificity of OTA aptasensor

The specificity of the developed aptasensor is evaluated by the incubation of 50 nM of *zearalenone* (ZEA) during 90 min. ZEA was selected since it is reported to simultaneously coexist with OTA in plants and foods, in despite of being structurally different.[37] As shown in Fig. 4.7, impedance responses corresponding to 0 (a), 50 nM of OTA (c) and 50 nM of ZEA (b) were evaluated. No significant difference in impedance response is observed before and after incubation of the aptasensors with ZEA (see inset of Figure 4.7). These results confirmed the specific OTA/aptamer complex formation.

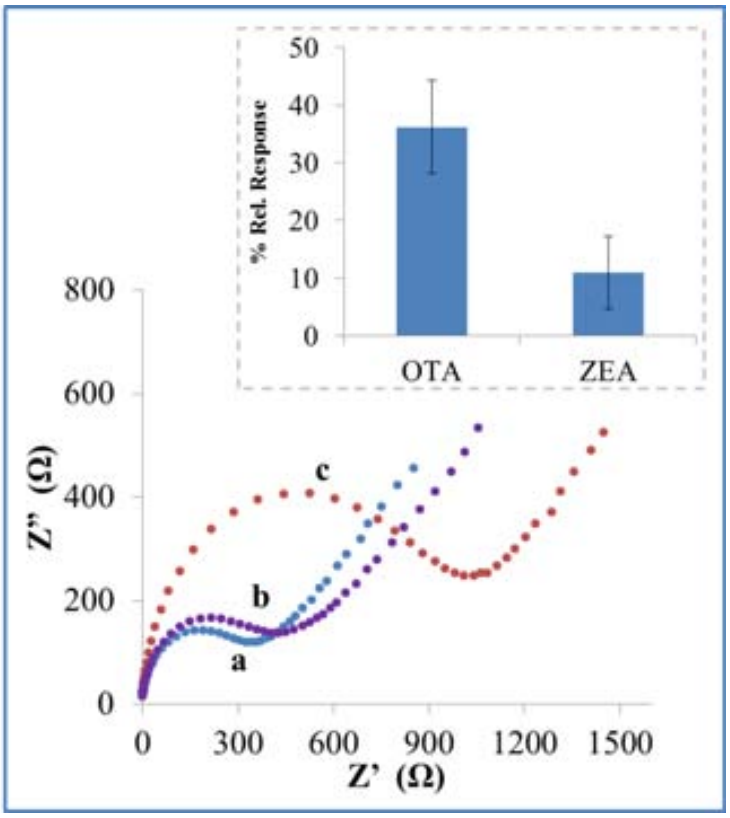

Figure 4.7. Nyquist plots ob tained for the control, ZEA and OTA. Inset: *R*ct values for the selectivity of the impedimetric OTA ap tasensor. Experimental conditions as de scribed in the text.

Studies related on applications of the developed aptasensor in real samples are still in process at our labor atories. Certainly, the response of this device may be of interest for various diagnostics applications that require very low limits of detection in addition to a highly robust and cost/efficient system, especially for those to be used directly in field.

4.4. Conclusions

A novel impedimetric aptasensor based on SPCE modified with conductive films of polythionine and citrate-capped IrO_2 NPs has been developed. Electrochemical impedance spectroscopy studies were conducted in order to characterize each fabrication step of the aptasensor and also, for OTA detection. In addition, these studies reveal that SPCE/PTH/IrO_2 NPs/aptamer sensor shows a linear range of 0.1 to 100 nM for OTA detection with a high reproducibility and selectivity. The developed aptasensor shows the lowest limit of detection (0.2 pM) found in the literature for OTA detection using electrochemical methods, which makes it useful for future applications in OTA analysis.

4.5. References

(1) FAO. *Manual on the application of the HACCP system in mycotoxin prevention and control*; Rome, 2001; p. 124.

(2) Meulenberg, E. P. *Toxins (Basel).* **2012**, *4*, 244–266.

(3) Anfossi, L.; D'Arco, G.; Baggiani, C.; Giovannoli, C.; Giraudi, G. *Food Control* **2011**, *22*, 1965–1970.

(4) Covarelli, L.; Beccari, G.; Marini, A.; Tosi, L. *Food Control* **2012**, *26*, 347–356.

(5) Benford, D.; Boyle, C.; Dekant, W.; Fuchs, R.; Gaylor, D. W.; Hard, G.; McGregor, D. B.; Pitt, J.; Plestina, R.; Shepard, G.; Solfrizzo, M.; Verger, P. J. P.; Walker, R. *JECFA (Joint FAO/WHO Expert Comm. Food Addit.* **2001**, *47*.

(6) Denli, M.; Pérez, J. F. *Toxins (Basel).* **2010**, *2*, 1065–1077.

(7) IARC. *International Agency for Food and Research on Cancer Monographs on the evaluation of carcinogenic risks to humans, some naturally occurring substances: Food items and constituents, heterocyclic aromatic amines and mycotoxins*; Lyon, 1993; Vol. 56, p. 609.

(8) *Evaluation of certain mycotoxins in food. Fifty-sixth report of the Joint FAO / WHO Expert Committee on Food Additives World Health Organization*; Geneva, 2002; p. 74.

(9) *Commission Regulation (EC) No 1881/2006 of 19 December 2006 setting maximum levels for certain contaminants in foodstuffs*; 2010; pp. 1–26.

(10) Gilbert, J.; Anklam, E. *TrAC Trends Anal. Chem.* **2002**, *21*, 468–486.

(11) Krska, R.; Welzig, E.; Berthiller, F.; Molinelli, A.; Mizaikoff, B. *Food Addit. Contam.* **2005**, *22*, 345–353.

(12) Shephard, G. S. *Chem. Soc. Rev.* **2008**, *37*, 2468–2477.

(13) *Aptamers in Bioanalysis*; Mascini, M., Ed.; Wiley-Interscience, 2009; p. 325.

(14) Skládal, P. *Electroanalysis* **1997**, *9*, 737–745.

(15) Cunningham, B. T. In *Label-free Biosensors: Techniques and Applications*; Cooper, M. A., Ed.; Cambridge University Press: NY, USA, 2009; p. 300.

(16) Castillo, G.; Lamberti, I.; Mosiello, L.; Hianik, T. *Electroanalysis* **2012**, *24*, 512–520.

(17) Prabhakar, N.; Matharu, Z.; Malhotra, B. D. *Biosens. Bioelectron.* **2011**, *26*, 4006–4011.

(18) Hayat, A.; Sassolas, A.; Marty, J.-L.; Radi, A.-E. *Talanta* **2013**, *103*, 14–19.

(19) Hayat, A.; Haider, W.; Rolland, M.; Marty, J.-L. *Analyst* **2013**, *138*, 2951–2957.

(20) Cosnier, S. *Anal. Bioanal. Chem.* **2003**, *377*, 507–520.

(21) Gao, Q.; Cui, X.; Yang, F.; Ma, Y.; Yang, X. *Biosens. Bioelectron.* **2003**, *19*, 277–282.

(22) Dempsey, E.; Diamond, D.; Collier, A. *Biosens. Bioelectron.* **2004**, *20*, 367–377.

(23) Yang, T.; Hu, Y.; Li, W.; Jiao, K. *Colloids Surf. B. Biointerfaces* **2011**, *83*, 179–182.

(24) Jiang, S.; Hua, E.; Liang, M.; Liu, B.; Xie, G. *Colloids Surf. B. Biointerfaces* **2013**, *101*, 481–486.

(25) *Biosensing using nanomaterials*; Merkoçi, A., Ed.; John Wiley & Sons: NJ, USA, 2009; p. 499.

(26) Liu, G.; Mao, X.; Gurung, A.; Baloda, M.; Lin, Y.; He, Y. In *Trace Analysis with Nanomaterials*; Pierce, D. T.; Zhao, J. X., Eds.; Wiley-VCH: USA, 2010; p. 418.

(27) Huang, W.-D.; Cao, H.; Deb, S.; Chiao, M.; Chiao, J. C. *Sensors Actuators A* **2011**, *169*, 1–11.

(28) Lu, Y.; Wang, T.; Cai, Z.; Cao, Y.; Yang, H.; Duan, Y. Y. *Sensors Actuators B Chem.* **2009**, *137*, 334–339.

(29) Göbbels, K.; Kuenzel, T.; van Ooyen, A.; Baumgartner, W.; Schnakenberg, U.; Bräunig, P. *Biomaterials* **2010**, *31*, 1055–1067.

(30) Mayorga Martinez, C.; Pino, F.; Kurbanoglu, S.; Rivas, L.; Ozkan, S.; Merkoçi, A. *J. Mater. Chem. B* **2014**, *2*, 2233–2239.

(31) Cruz-Aguado, J. A.; Penner, G. *J. Agric. Food Chem.* **2008**, *56*, 10456–10461.

(32) Farias, E. D.; Pfaffen, V.; Ortiz, P. I. *Electrochim. Acta* **2013**, *105*, 622–628.

(33) Radi, A.-E.; Muñoz-Berbel, X.; Lates, V.; Marty, J.-L. *Biosensensors Bioelectron.* **2009**, *24*, 1888–1892.

(34) Smith, E. R. B. *J. Biol. Chem.* **1935**, *108*, 187–194.

(35) Evtugyn, G.; Porfireva, A.; Stepanova, V.; Kutyreva, M.; Gataulina, A.; Ulakhovich, N.; Evtugyn, V.; Hianik, T. *Sensors* **2013**, *13*, 16129–16145.

(36) Evtugyn, G.; Porfireva, A.; Sitdikov, R.; Evtugyn, V.; Stoikov, I.; Antipin, I.; Hianik, T. *Electroanalysis* **2013**, *25*, 1847–1854.

(37) Li, Y.; Zhang, B.; He, X.; Cheng, W.-H.; Xu, W.; Luo, Y.; Liang, R.; Luo, H.; Huang, K. *Toxins (Basel)*. **2014**, *6*, 1177–1192.

Chapter 5

Improving sensitivity of gold nanoparticles-based lateral flow assays by using wax-printed pillars as delay barriers of microfluidics

Related publication

Lab on a chip, in press, DOI: 10.1039/C4LC00972J

Improving sensitivity of gold nanoparticles-based lateral flow assays by using wax-printed pillars as delay barriers of microfluidics

Lourdes Rivas[1,2], Mariana Medina-Sánchez[1], Alfredo de la Escosura-Muñiz[1] and Arben Merkoçi[1,3]

[1] ICN2-Nanobioelectronics & Biosensors Group,Institut Català de Nanociència i Nanotecnologia, Campus UAB, 08193 Bellaterra (Barcelona), Spain

[2]Department of Chemistry, Universitat Autónoma de Barcelona, 08193, Bellaterra, Barcelona, Spain

[3] ICREA - Institució Catalana de Recerca i Estudis Avançats, 08010 Barcelona, Spain

Summary

Although lateral flow assays (LFA) are currently being used in some point-of-care applications (POC) they cannot still be extended to a broader range of analytes for which higher sensitivities and lower detection limits are required. To overcome such drawbacks, a simple and facile alternative based on the use of delay hydrophobic barriers fabricated by wax-printing so as to improve the LFA sensitivity is presented in this Chapter. Several wax pillars patterns are printed onto nitrocellulose membrane in order to produce delays as well as pseudo turbulences into the microcapillary flow. The effect of the proposed wax pillar modified devices are also mathematically simulated corroborating the experimental results obtained for the different patterns tested afterwards for detection of HIgG as model protein in a gold nanoparticle-based LFA. The effect of the introduction of such wax-printed pillars represents a sensitivity improvement of almost 3-folds in comparison to a conventional free-barrier LFA.

5.1. Introduction

Constituted mainly by cellulose fibers, paper results very attractive for fabricating biosensors because of its low cost, flexibility and light weight making it useful for transport and storage. In addition, it has the capability to wick liquids via capillary action without use of external pumps and its biocompatibility makes it suitable for immobilizing biomolecules *e.g.* proteins.[1]

Paper has gained much interest in fabrication of diagnostic devices due to the necessity to use low cost materials for a single use, simplifying the fabrication process. Paper-based microfluidic is an emerging technology which uses the paper as substrate creating complex patterns of hydrophilic channels and hydrophobic barriers by using patterning techniques such as: photolithography,[2] wax patterning,[3,4] inkjet etching,[5] flexographic printing[6] and screen printing.[7]

The first paper-based sensor can be considered the paper chromatography developed by Martin and Synge at the beginning of 1940's.[8] Fifteen years later, the first semiquantitative paper-based biosensor for detection of glucose in urine,[9] became the commonest commercially available point-of-care (POC) lateral flow assay (LFA) device. Initially, the main application of LFAs was a pregnancy test[10] while nowadays their applications is extended to a wide variety of analytes that include cancer biomarkers,[11,12] DNA,[13,14] toxins[15,16] and metals.[17,18]

LFAs are characterized by their simple use, rapid result, low cost, good specificity and long shelf life. However, they suffer analytical performance limitations, mainly due to sensitivity and reproducibility issues. In this context, many efforts have been developed in order to improve the LFA sensitivity using different alternatives as immuno-gold silver staining,[19] dual gold nanoparticle (AuNP) conjugates[20] and AuNP loaded with enzymes[21]. Beside AuNPs other labels such as fluorescent Eu(III) nanoparticles[22] and quantum dots[23] have been also reported. Changes on the paper architecture were also proposed for improving the performance of LFA.[24]

The most important part of a LFA is the detection membrane which is made of cellulose nitrate or nitrocellulose (NC), a porous material where the capture reagents (*e.g.* antibodies) are immobilized due to a possible combination of electrostatic and hydrophobic forces.[25] In fact, NC has been widely used in blotting techniques thanks to its capacity of interact with proteins, DNA and RNA.[26] Wax printing is a simple and

low cost patterning technique based on the melting of solid wax printed onto porous substrate, which has been used for fabricating paper-based microfluidics in NC membrane and its application in protein pattern and dot immunoassay.[4] Recent reports have demonstrated the possibility to control the reagent transport by using novel and sensitive methods such as dissolvable barriers[27,28] and bridges made of sugars,[29] fluidic diodes and valves[30] and tunable-delay shunts.[31] Despite of their capability to improve the performance of paper-based devices which is related with their sensitivity, some of these methods are time consuming and require more reagents for fabricating of the devices.

We present here a new strategy for improving the sensitivity of gold nanoparticle-based lateral flow assays by using barriers (pillars) deposited onto the nitrocellulose membrane by wax printing technique. Different pillar designs were printed, in order to create hydrophobic barriers that can cause flow delay. To check the efficiency of such pillars, we used membranes with relatively fast flow so as to obtain higher sensitivity and low detection limits. The controlled delays in microfluidics increase the binding time between the immunocomplex and the detection antibody, in addition to the generation of pseudo turbulences in the pillars zone that improves mixing between the analyte and the labeled antibody. This microfluidics delay in certain zones (incubation areas) combined with the generation of the pseudo turbulences directly affects the analytical performance of the LFA being transduced to a better sensitivity and detection limit.

5.2. Experimental section

5.2.1. Reagents and apparatus

Hydrogen tetrachloroaurate (III) trihydrate ($HAuCl_4 \cdot 3H_2O$, 99.9%), trisodium citrate ($Na_3C_6H_5O_7 \cdot 2H_2O$), phosphate buffer saline tablet (P4417), human IgG from human serum (I2511), anti-human IgG (polyclonal antibody developed in goat; I1886) and anti-human IgG γ-chain specific-biotin (polyclonal antibody developed in goat; B1140) were purchased from Sigma-Aldrich (Spain). Anti-goat IgG (polyclonal antibody produced in chicken; ab86245) was purchased from Abcam (UK).

All the materials used for the production of the LFIA strips were purchased from Millipore (Billerica, USA): sample and absorbent pads (CFSP001700), conjugate pad (GFCP00080000), detection pads (Hi-Flow Plus 75, SHF0750425 and Hi-Flow Plus 75, SHF2400425) and the backing card (HF000MC100). mQ water, produced using a Milli-Q system (>18.2 MΩ cm^{-1}) purchased from Millipore was used for the preparation of all solutions. A thermostatic centrifuge (Sigma 2-16 PK, Fisher Bioblock Scientific, France) was used to purify the AuNP/antibody conjugates. A Xerox ColorQube 8570 wax printer (Xerox Corporation, USA) was used for printing different wax designs. A hot plate (VWR, USA) was used for heating and melting the wax ink. An IsoFlow reagent dispensing system (Imagene Technology, USA) was used to dispense the detection and control lines. A guillotine (Dahle 533, Germany) was used to cut the strips. The stirrer used was a TS-100 Thermo shaker (BioSan, Latvia). A strip reader (COZART — SpinReact, UK) was used for quantitative measurements. All the size measurements and shape observation of AuNPs were conducted in a Field Emission Gun Transmission Electronic Microscope Fei, model Tecnai™ G2F20 (Fei, USA). A spectrophotometer SpectraMax M2^e (Molecular Devices, UK) was used to record all UV-Vis spectra of AuNPs. Scanning electronic micrographs of nitrocellulose membrane were conducted in a Field Emission Gun Scanning Electronic Microscope Fei, model Quanta™ 650 (Fei, USA). A Leica DCM 3D dual core 3D measuring microscope (Leica Microsystems, Germany) was used for confocal images of nitrocellulose membrane. Image processing software, ImageJ (National Institute of Health, USA) was used for measuring the size of the wax pillars before and after melting step.

5.2.2. Methods

5.2.2.1. Preparation of gold nanoparticles (AuNPs)

Gold nanoparticles (AuNPs) 20 nm sized and stabilized by citrate, were prepared using the Turkevich's method.[32] Briefly, 50 mL aqueous solution of 0.1% $HAuCl_4$ was heated to boiling and vigorously stirred in a 250 mL round-bottom flask; 1.25 mL of sodium citrate 1% were added quickly to this solution. Boiling was continued for additional 10 min. The solution was cooled to room temperature with a continuous stirring. The colloids were stored in dark bottles at 4° C. All glassware used in this preparation was previously cleaned in *aqua regia* overnight and rinsed with double distilled H_2O and reflux was used for all the procedure.

5.2.2.2. AuNPs modification with antibodies

AuNPs were modified with antibodies following a previously optimized procedure.[33] First, the pH of the AuNPs suspension was adjusted to pH 9 with 0.1 M borate buffer. Then, 100 µL of a 100 µg mL^{-1} anti-human IgG γ-chain specific-biotin aqueous solution were added to 1.5 mL of the AuNPs suspension. The resulting solution was incubated for 20 min at 650 rpm. Then, 100 µL of 1 mg/mL BSA aqueous solution were added and the stirring was continued for other 20 min at 650 rpm. Finally, the solution was centrifuged at 14000 rpm and 4ºC for 20 min.

The supernatant was removed and the pellet of AuNP/anti-Human IgG was re-suspended in 500 µL of BB 2 mM pH 7.4, 10% sucrose.

5.2.2.3. Preparation of the strips

Once the pillar patterns have been designed with graphic design software (Corel Draw X4), the preparation of the modified detection pad consisted in three main steps: i) printing the pillars patterns onto the nitrocellulose (NC) membrane (Hi-Flow Plus 75, HF075) with a wax printer; ii) heating the NC membrane and melting the wax at 110ºC for 90 seconds by using the hot plate; and iii) dispensing antibodies onto the membrane. For this step, 1 mg/mL solution of anti-Human IgG (whole molecule) and anti-Goat IgG were spotted onto the detection pad at dispensing rate of 0.05 µL/mm using an IsoFlow reagent dispensing system so as to form the test and control line, respectively. Then, the detection pad was dried at 37ºC for 1 h.

The sample pad was prepared by dipping into 10 mM PBS, 5% BSA and 0.05% Tween®-20 and drying at 60ºC for 2h. The conjugate pad was prepared dipping it into the previously prepared anti-Human IgG γ-chain specific-biotin/AuNP conjugate and drying under vacuum for 1 h.

The different pads were sequentially laminated 2 mm with each other and pasted onto the adhesive backing card in the following order: detection, conjugation, sample and absorbent pads. Finally, the strips were cut 7 mm wide and used immediately.

5.2.2.4. Lateral-flow assay procedure

Sample solutions of 200 μL of different concentration Human IgG (HIgG) in PBS 10 mM, pH 7.4, ranging from 5 ng/mL to 500 ng/mL were dispensed onto the sample pad and keeping for 15 min until the flow is stopped. Then 200 μL of PBS was dispensed in order to wash away the excess of AuNPs/antibody. After drying the lateral flow strips at room temperature, they were read with the strip reader so as to obtain the calibration curve for HIgG. PBS without analyte was considered as blank. All the measurements were carried out by triplicate.

5.2.2.5. Mathematical simulations

Flow in porous media can be studied by the use of the Navier-Stokes equations, which describe the movement of fluid substances, which represent the effect of the diffusing viscosity and the pressure. These equations coupled with the Brinkman equations, can be useful for modeling of the flows through certain porous media. The initial conditions for the simulation such as porosity and permeability of the membranes (in this case, a different kind of membrane was used) were the same as in a previous work reported in our group.[24] These parameters were given by Millipore Corporation (porosity around 83%, and the permeability 4.3×10^{-6} m^2). On the other hand, the density and viscosity values at 25ºC (0.997 g/mL and 0.890 $N.s/m^2$) used were the ones of the water as an approximation. The boundary conditions for the simulation were the geometry (changing the pillars distribution). The velocity was calculated from the volume of the liquid introduced into the membrane (200 μL) and the cross section area of the absorbent pad and the time necessary to absorb the respective volume (1.47 m/s).

5.3. Results and discussion

5.3.1. Improvement of sensitivity of lateral flow assay by using wax delay barriers

Lateral flow assays must allow rapid responses with good sensitivity. For this purpose, manufacturers have developed different membranes which satisfy these requirements. Capillary flow rate is a common parameter to classify the membranes on basis of the required time for the liquid to travel and fill completely a 4-cm length of membrane. In this work, nitrocellulose membranes Hi-Flow Plus 75 (HF075) and Hi-Flow Plus 240 (HF240) provided by Millipore Corporation were used. The first one has a nominal flow rate of 75 s across 4 cm of membrane, and the last one has a higher nominal flow rate of 240 seconds across the same length.[32] Sensitivity in LFA is conditioned by various factors being crucial the performance of nitrocellulose membrane.

For a fast liquid velocity membrane (HF075), the sensitivity is low due to two main factors: i) the liquid takes less time to travel a defined length and ii) the formation of the immunocomplex between the analyte and AuNP-labeled antibody at the conjugate pad, as well at test and control lines, is less effective since the flow rate is faster. In the case of a slow velocity membrane (HF240) the sensitivity is higher since the flow rate is slower and there is enough time for an effective formation of immunocomplex at the beginning of the strip and at test and control line.

Based on that, we chose the faster membrane provided by Millipore (HF075) for its modification with wax pillars using the wax-printing technology so as to evaluate the effect (in terms of sensitivity and limit of detection) produced by these hydrophobic structures that can act as obstacles for delaying the sample flow on a AuNP-based LFA (see Fig. 5.1).

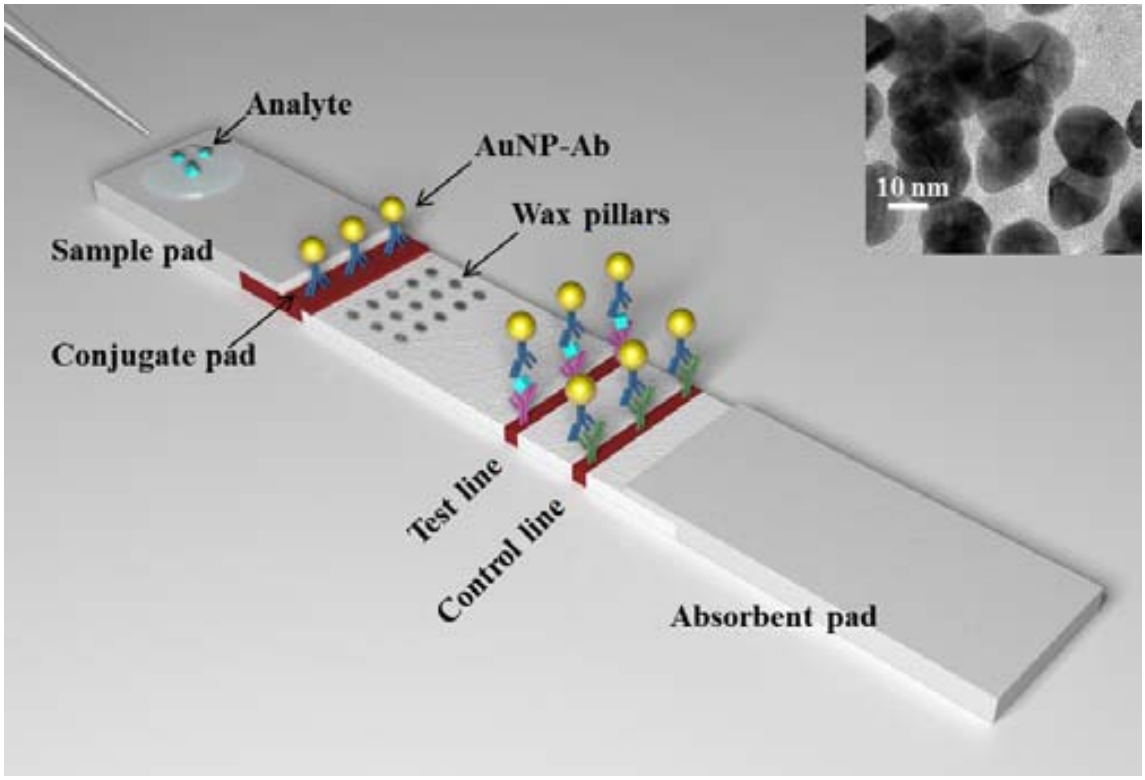

Figure 5.1. Schematic representation of a lateral flow strip modified with wax pillars for protein detection based on the use of AuNP. (Inset) TEM image of AuNPs used for the lateral flow assay (LFA) development.

Wax printing technology is used here to deposit wax on the surface of nitrocellulose, followed by a heating step for melting the wax pattern for its penetration through the pores of the membrane while maintaining the original design. The hydrophobic properties of the wax, make it suitable for the creation of barriers which can modulate the flow on membranes in a desirable way, *e.g.* for controlling the delivery time of reagents.[33]

In the wax printing process, the nitrocellulose membrane to be printed passes between the pressure roller and the print drum of the printer, suffering changes due to the pressure. To evaluate these alterations, empirical calculations of permeability and scanning electron micrographs for membranes characterizations were carried out.

In figure 5.2 transversal cuts of membranes with and without modifications produced just by applying heat and pressure are shown. When the membrane passes through the wax printer, a thickness reduction of around 30 μm is observed due to the compression

produced by the pressure roller and the drum of the printer (figure 5.2A-B). The results of the LFA performed for both approaches (figures 5.2C-2D) were compared so as to estimate the effect of mechanical compression of membrane in quantitative measurements (HIgG concentrations: 5, 50 and 500 ng/mL).

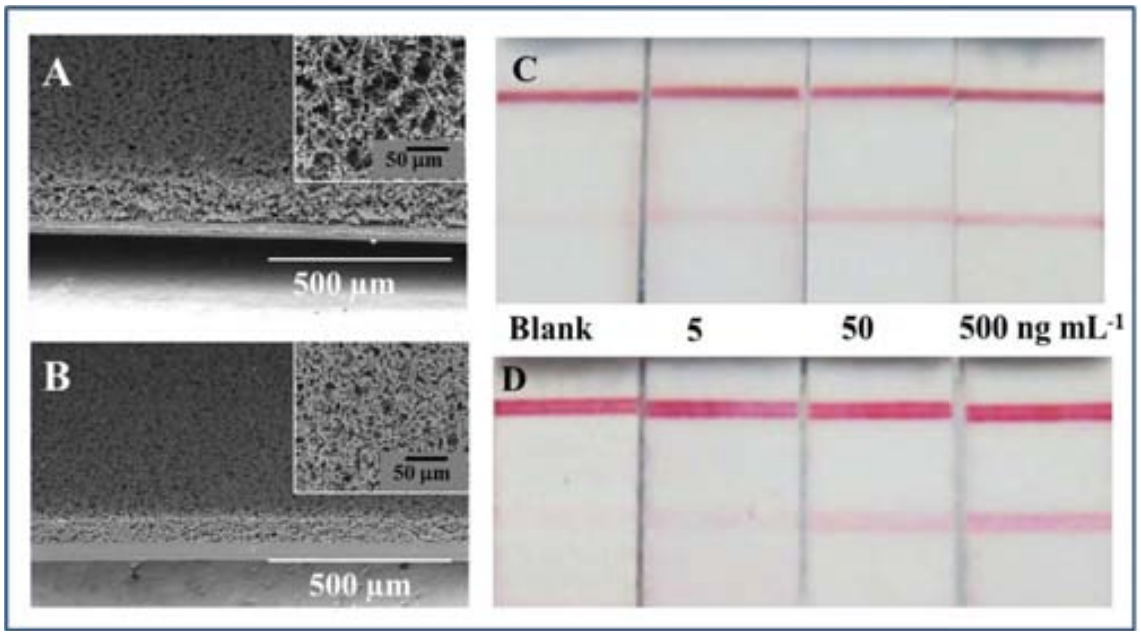

Figure 5.2. Left: Scanning electron micrographs (SEM) of transversal cuts: (A) unmodified and (B) modified membrane HF075. Right: LFA for HIgG detection using (C) unmodified and (D) heat and pressure-modified membrane for a blank assay and for assays performed with 5, 50 and 500 ng/mL of HIgG.

Indeed, when the membrane is flattened the sensitivity of LFA increases due to the fact that the modified membrane became thinner and this compression produces wider reagent lines making them easier to visualize a weak signal. This is related to the fact that due to the spreading of reagents, the fluid afterwards penetrates the whole thickness of the membrane laterally moving producing wider lines due to less depth to contain the same volume of reagent.[32] The limit of detection (LoD) using the strip reader (for all the LF formats described) was calculated as the concentration of HIgG corresponding to three times the standard deviation of the estimate, giving a value for the LF strips (with flattened membranes HF075) of 8.0 ng/mL of HIgG while by using membranes without any modification, this value is of 12 ng/mL. This suggests that only the compression of nitrocellulose membranes gives a 1.5-fold improvement in the sensitivity of the assay.

In traditional printing methods, the porosity plays an important role on the absorption of the ink by different paper substrates: high porosity papers absorb and spread more ink, while low porosity papers can prevent the penetration of the ink through their fibers. In the wax printing process used in this work, the wax penetrates only into superficial fibers of nitrocellulose. To ensure the presence of delay barriers along the whole thickness of the membrane, a melting process was conducted. Two nominal wax pillars of 0.4 and 1.0 mm diameters were measured before and after melting process, and results showed that wax pillar diameters increased up to 20% regarding to the original printing size after melting step (see Fig. 5.3)

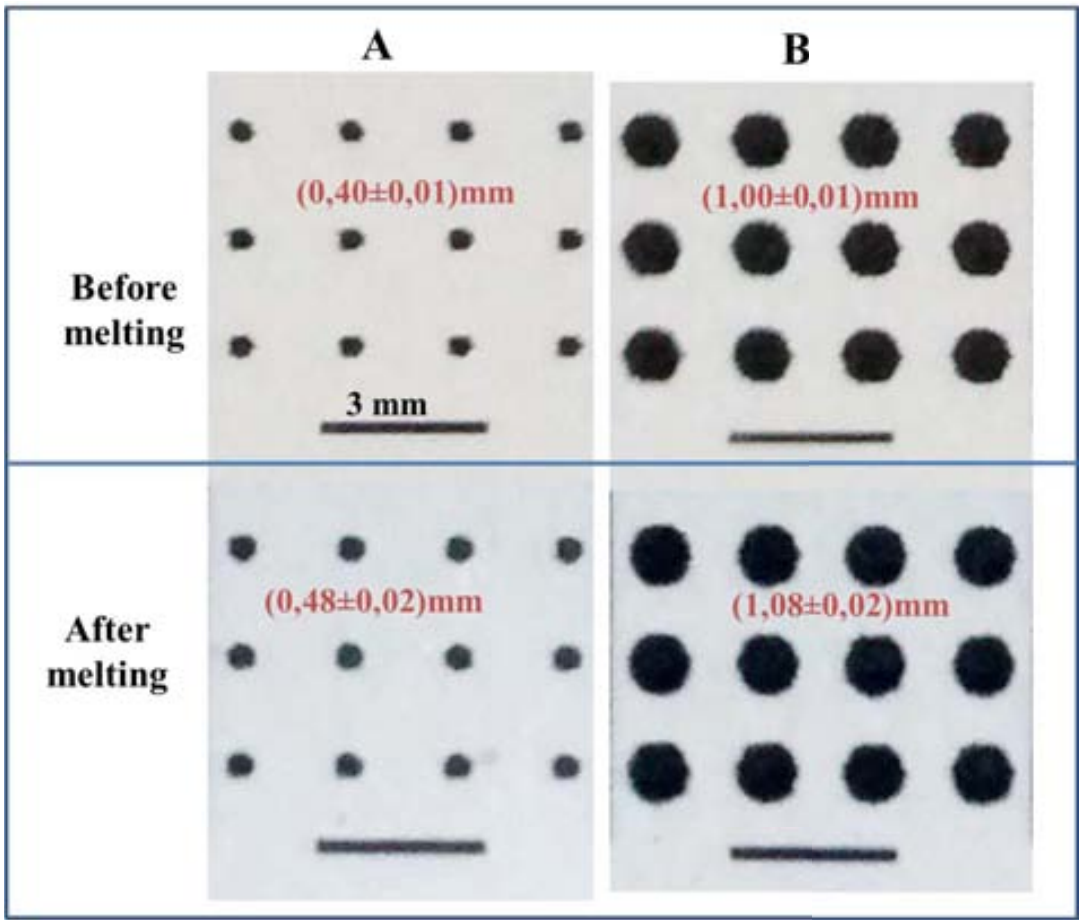

Figure 5.3. Wax printed pillars of (A) 0.4 and (B) 1.0 mm, before and after melting process.

Once the melted wax enters through the fibers of membrane a lateral spreading occurs and decreases the resolution of the printed pattern, which is affected by the porosity and thickness of membrane.[3] Although just one type of NC membrane was employed for

printing purposes (approximate pore size 12-17 μm), if a membrane with smaller pores is used, the increment after melting could be lower due to the higher packaging of nitrocellulose fibers that reduces the possibility of air passages and avoids the spread of the ink. The effect on the sensitivity caused by changing the wax pillar diameter was tested in quantitative measurements of HIgG. Results showed that the presence of wax pillars with small diameters (0.4 mm) reduced considerably the unspecific signals, showing strips with clear backgrounds and a better differentiation of intensities of test lines observed through the concentration range if compared with the modified membrane (see Fig. 5.4 A-B). Regarding to the sensitivity, the presence of small diameter wax pillars produces a slight increment of 1.2-fold respect to the modified membrane, which corresponds to a LoD of 6.6 ng/mL. This result indicates that wax pillars are acting as delay barriers of the fluid due to their hydrophobic nature allowing in this way, a suitable recognition between the analyte and the capture AuNP labeled antibody before arriving to test line. However, this size (0.4 mm) was not enough to increase even more the sensitivity of the assay. On the other hand, wax pillar of a bigger diameter (1.0 mm) was tested and experimental results showed that sensitivity was affected. This occurred because the pillars delayed the regular flow in such way that the time of the assay was substantially long making it useless for practical purposes; a considerable amount of AuNPs which could not reach properly to test and control lines remained along the membrane, showing a pink background; thus a high LoD of 15.6 ng/mL was obtained (see Fig. 5.4C). It is worthy to note that the wax pillar size is an important parameter that affects the sensitivity in different ways and the proper choice for wax pillar size must be a compromise between the sensitivity and the time of the assay.

For the remaining experiments, the wax pillars diameter chosen was 0.5 mm and the effect produced by different wax pillars arrangements on the microfluidic was tested. Four different patterns (“P1”, “P2”, “P3” and “P4”) as well as strips with and without modifications were tested for HIgG detection. Experimental results clearly showed the effect on the sensitivity of the assay produced by the wax pillars geometries (see Fig. 5.5).

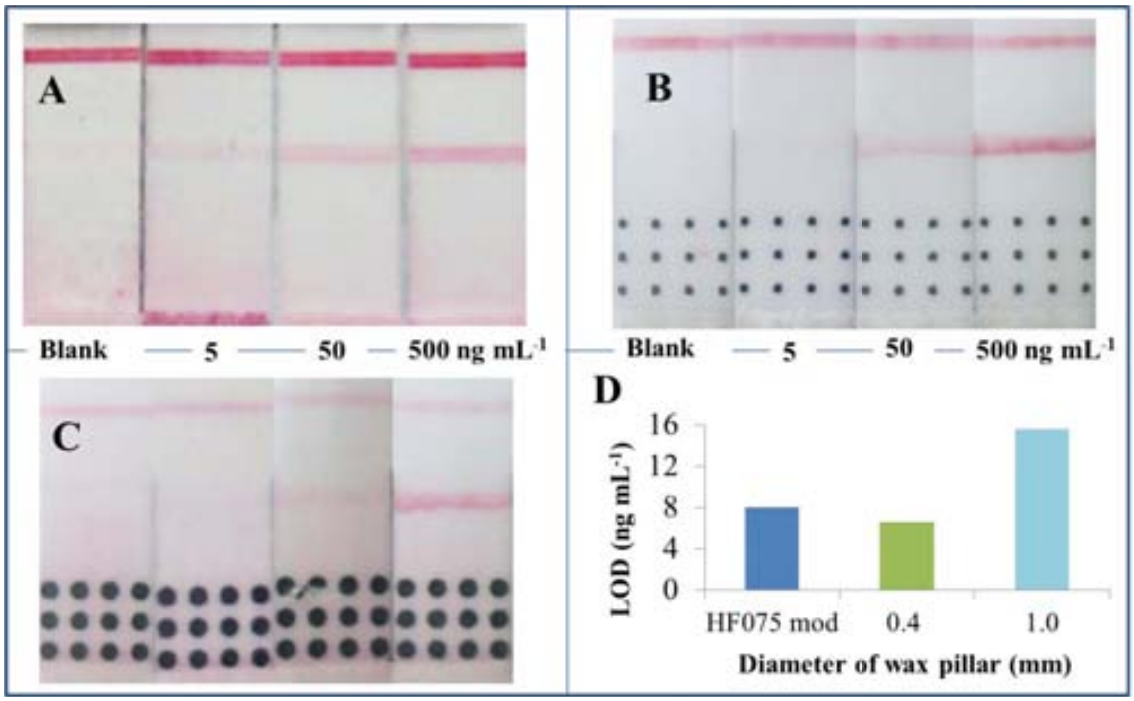

Figure 5.4. LF strips with heat and pressure modifications, HF075 mod (A); LF strips modified with different wax pillars diameters: 0.4 mm (B) and 1.0 mm (C). Effects on sensitivity of wax pillars diameters in LF quantitative measurement of HIgG (D).

As stated before, an improvement of sensitivity is produced by: i) mechanical compression of membrane and ii) the presence of wax pillars of proper size. Slightly increasing the diameter of the wax pillar up to 0.5 mm, it was possible to improve the sensitivity, especially for "P1" and "P2" patterns up to 1.7- and 2.6-fold respect to modified and unmodified membrane, respectively. These results showed that sensitivity in LFA can be affected by presence of wax pillars, their diameters and also the spatial arrangements. Moreover, mathematical simulations were performed to study these phenomena. For each pattern, the flow speed, vorticity and force around the pillars, were calculated at the end of the pillars zone and control line. All these data are summarized in Table 5.1.

Three different flow parameters were mathematically considered to correlate them with the experimental results. Mathematical simulations for HF075 were achieved as blank in order to compare the differences observed in the mentioned parameters in the presence of several wax pillars patterns. According to the data in Table 5.1, the highest flow velocities at the end of wax pillars zone corresponds to patterns "P1" and "P2" which are compensated by the vorticity range (a physical magnitude that describes the

rotation of a fluid near to some point). While bigger is this range, higher is the rotation of the fluid. In addition, the pressures are higher for these two patterns. These results are consistent with the most sensitive modified LFA which are “P1” and “P2” patterns.

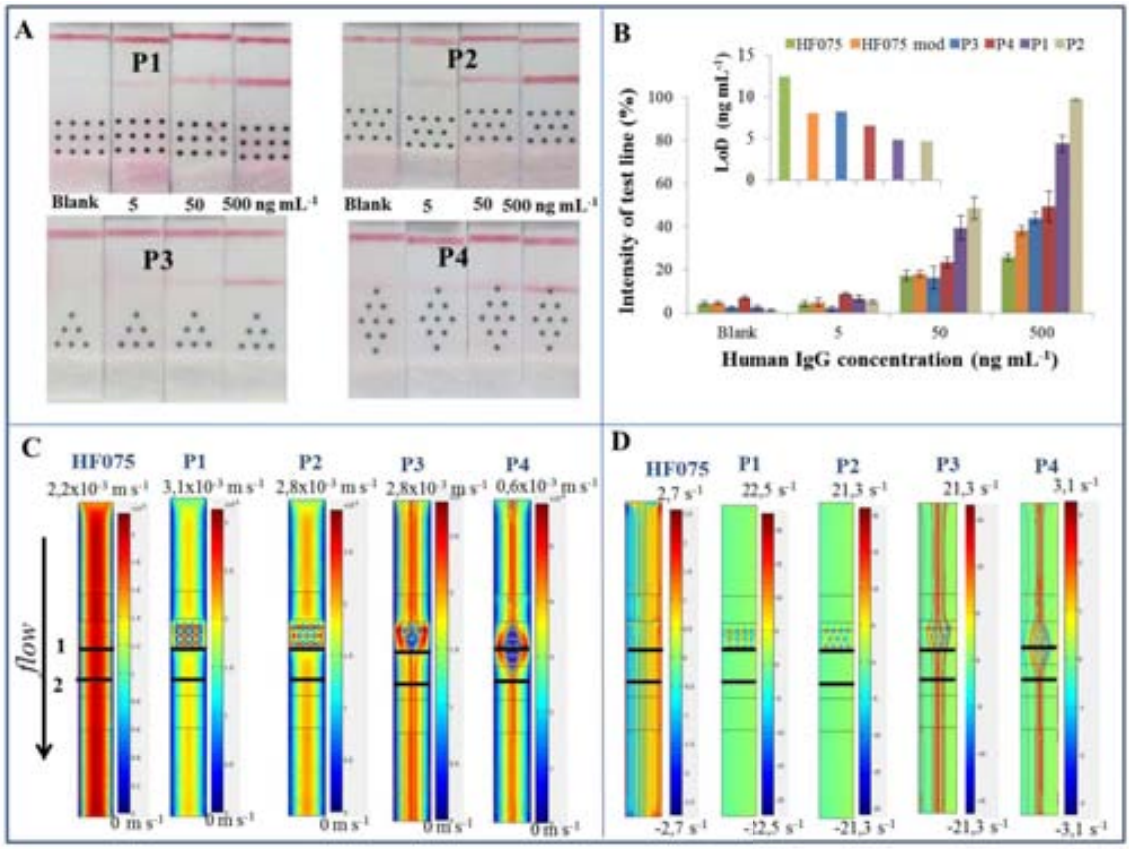

Figure 5.5. (A) LF strips modified with different pattern of wax pillars. (B) Effect of the wax pillars in LF quantitative measurement for different concentrations of HIgG and the corresponding LoDs (inset). (C) Flow speed simulations for modified and unmodified LF. (D) Simulated results of vorticity for modified and unmodified LF.

Table 5.1. Parameters measured with mathematical simulations for LFAs modified with wax pillars

Pattern	Average Velocity ($x10^{-3}$ m/s)	Vorticity (1/s)	Average Pressure Force per unit of area (Pa)
HF075	V_1= 1.03 V_2= 1.03	$Vort_1$= (-1.4 to 1.4) $Vort_2$= (-1.4 to 1.4)	F_1= 0 F_2= 0
P1	V_1= 1.60 V_2= 1.03	$Vort_1$= (-4.7 to 4.7) $Vort_2$= (-1.4 to 1.4)	F_1= 2.5e-5 F_2= 0
P2	V_1= 1.40 V_2= 1.03	$Vort_1$= (-4.5 to 4.5) $Vort_2$= (-1.4 to 1.4)	F_1= 2e-5 F_2= 0
P3	V_1= 1.03 V_2= 1.03	$Vort_1$= (-2.4 to 2.4) $Vort_2$= (-1.4 to 1.4)	F_1= 3e-8 F_2= 0
P4	V_1= 0.18 V_2= 0.18	$Vort_1$= (-0.47 to 0.47) $Vort_2$= (-0.25 to 0.25)	F_1= 3.6e-8 F_2= 0

Making the same considerations for the remaining patterns, the "P3" resulted with higher flow velocities and vorticity values and low pressure compared with "P4". However, the experimental results showed that LoD for "P4" (6.5 ng/mL) is better than the obtained for "P3" (8.2 ng/mL).

With the purpose to confirm if the wax truly acts as a barrier across membrane, characterizations by using scanning electron and confocal microscopes were performed. A transversal cut of wax dots area in order to verify if the melted wax penetrates through the entire thickness of membrane was made as it is shown in figure 5.6A. Due to the density of the wax and membrane itself, it was difficult to characterize by SEM if the area of barriers was only covered with wax. Therefore it was necessary to characterize the area of barriers by using confocal technology. Figure 5.6B shows a surface roughness profile on the wax dots area and it is possible to observe different surface roughness values. This means that the melted wax (darker points) has filled the pores of the membrane creating a tridimensional structure (like a pillar) capable of obstructing the normal flow of the sample across the whole membrane thickness (Fig. 5.6C).

Based on the previous experimental results and mathematical simulations, "P3" and "P4" wax patterns were discarded due to the fact that they showed a lower sensitivity compared to "P1" and "P2" and an accurate calibration curve was carried out (see Figure 5.5). In this experiment, unmodified and modified membranes (HF075 and HF240), where used to compare the effect produced by mechanical compression and also, the presence of the wax pillars on LFA. As expected, unmodified HF075 membrane presents less sensitivity as its capillary flow time is lower if compared with unmodified HF240 membrane. This means that sample flow needs shorter time interval to travel a defined distance on the membrane, thus there is not enough time for formation of the immunocomplex and its sensitivity is affected.

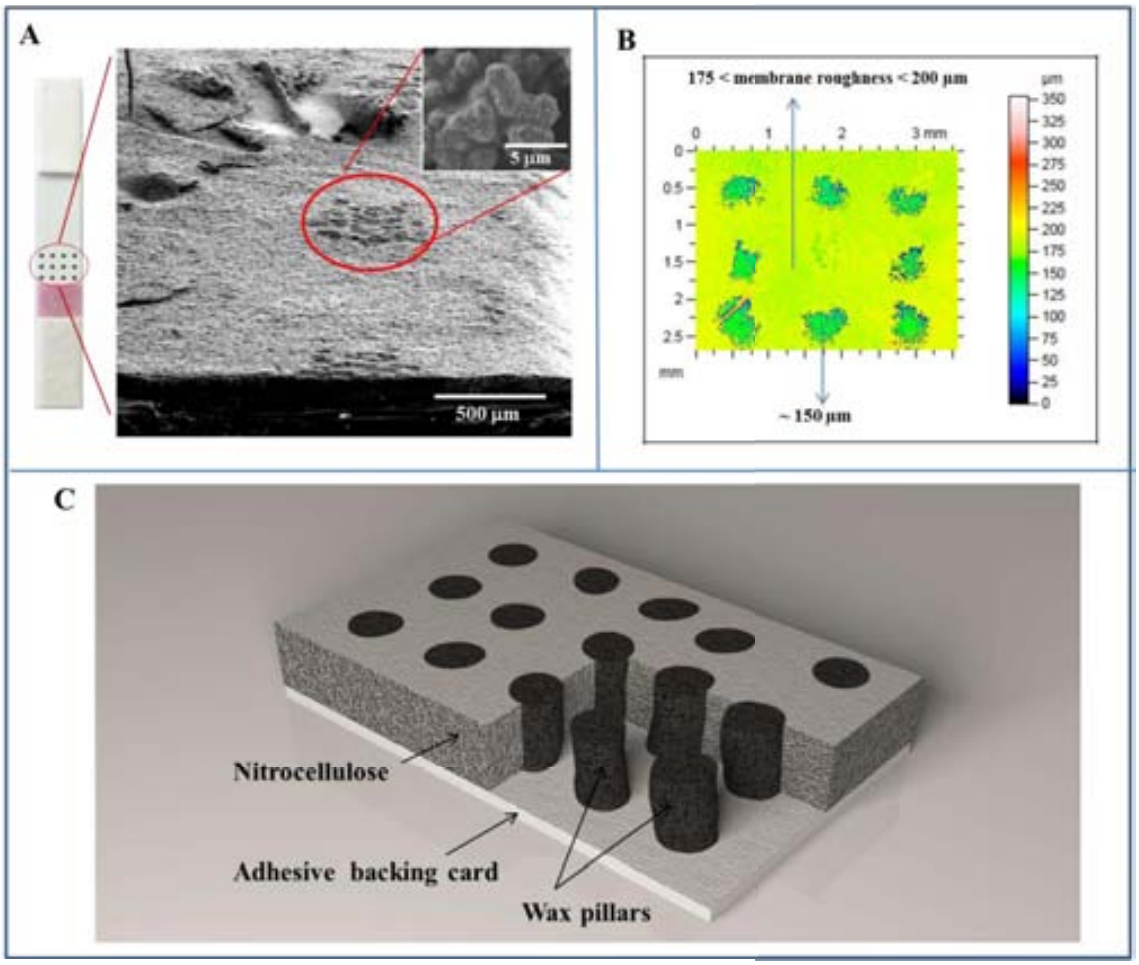

Figure 5.6. (A) SEM image for transversal cut of wax pillars area on a lateral flow strip. Inset corresponds to a membrane covered with melted wax. (B) Surface profile roughness of LFA modified with wax pillars. (C) Schematic of a transversal cut of pillars zone on nitrocellulose membrane.

When the HF075 membrane suffered the mechanical compression by the roller and the print drum, detection lines became wider and its sensitivity increased as stated before.

LoD for modified HF075 membrane is comparable to the value obtained for the most sensitive unmodified membrane HF240. In addition, the selected patterns showed lower LoD regarding to the value obtained for the most sensitive membrane, HF240, produced by Millipore. The reproducibility of the responses (n=3) for a 100 ng/mL HIgG concentration was also studied, and relative standard deviation (RSD) and limits of detection for different patterns and membranes can be found in the table 5.2.

Table 5.2. Limit of detection and relative standard deviation using unmodified and modified LFA with wax pillars

Lateral Flow Assays	**Limit of detection (ng/mL)**	**Relative Standard Deviation (RSD) for 100 ng/mL**
Unmodified HF075	12.4	7.5
Modified HF075	7.6	4.0
Unmodified HF240	8.0	6.8
P1	5.6	2.3
P2a	4.5	2.2
P2b	4.7	3.3

Lateral flow assays with printed wax pillars resulted to be more sensitive and showed lower limits of detection than lateral flow assays without modifications. Moreover, all blank measurements gave a lower background signal compared with LFA without modifications.

In order to verify which is the role of the location of wax pillars patterns in the sensitivity of LFA, two "P2" patterns have been studied: one near to the conjugate pad (P2a) and other one near to the test line (P2b). Results showed that there is not any significant difference on the value of the limit of detection if the wax pattern is located near or far away from the conjugate pad. This is attributable to the fact that the capillary flow rate is considerably faster at the beginning of the detection membrane and decreases exponentially as the liquid moves along it, until reaching a steady flow rate when the bed volume of membrane is saturated.[32] Therefore, when the wax pillars area is located at the beginning of the membrane this is enough to improve the sensitivity of

LFA. In addition this contributes significantly to delay the flow rate leading to better limits of detection.

Wax printing was used as patterning technique, in order to create delay barriers on LF devices that lead to increase on sensitivity of the assays. Despite of the sensitivity improvements obtained by the developed devices, these are fast, easy to use, low-cost and their fabrication just includes an extra step of printing that takes few minutes, compared with other controlling fluid methods previously reported, which are more sensitive but the fabrication are laborious and require additional reagents.

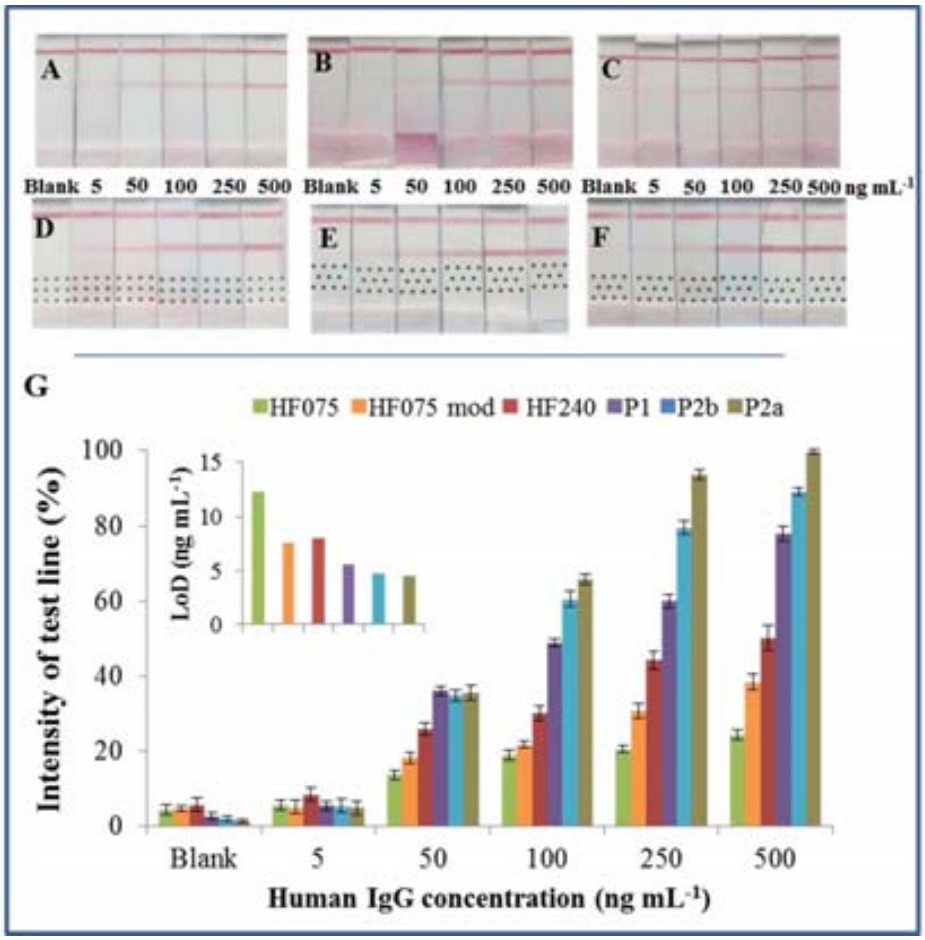

Figure 5.7. Results of LFA assays for HIgG detection performed with (A) unmodified HF075; (B) modified HF075 and (C) unmodified HF240 membranes. (D), (E), (F) correspond to the same membranes modified with P1, P2b, and P2a patterns, respectively. (G) Quantitative evaluation of the performance of the assays performed with the different membranes.

In this context, our approach constitutes an important strategy for the sensitivity improvement on lateral flow assays using paper-based microfluidic techniques, that can be improved by other techniques such as inkjet technology, which allows to print directly on the surface of nitrocellulose membrane by using a hydrophobic solution or ink capable to create well defined patterns without have direct contact with it.[34]

5.4. Conclusions

We have presented a new and easy strategy for improving the sensitivity of a gold nanoparticle-based LFA by the deposition of hydrophobic barriers of wax printed at the detection pad of a LFA. These barriers act as obstacles delaying the regular flow on the strip by increasing the binding time between the analyte and the labeled antibody and therefore allowing an effective formation of immunocomplex. Different designs were evaluated and the optimized ones allowed improving of almost 3-folds the limit of detection compared with the non-modified membranes. Mathematical simulations corroborate the experimental results obtained for the different patterns. This approach is simpler than other previously reported strategies since is not time-consuming, is low-cost, does not require the use of additional reagents for signal amplification or even changes on the configuration of LF strip. In consequence, the proposed strategy can be easily extended to any type of LFA design and could expand the landscape to the use of LF designs with patterning techniques facilitating its use in point-of-care applications.

5.5. References

(1) Parolo, C.; Merkoçi, A. *Chem. Soc. Rev.* **2013**, *42*, 450–457.

(2) Martinez, A. W.; Phillips, S. T.; Butte, M. J.; Whitesides, G. M. *Angew. Chem. Int. Ed. Engl.* **2007**, *46*, 1318–1320.

(3) Carrilho, E.; Martinez, A. W.; Whitesides, G. M. *Anal. Chem.* **2009**, *81*, 7091–7095.

(4) Lu, Y.; Shi, W.; Qin, J.; Lin, B. *Anal. Chem.* **2010**, *82*, 329–335.

(5) Abe, K.; Suzuki, K.; Citterio, D. *Anal. Chem.* **2008**, *80*, 6928–6834.

(6) Olkkonen, J.; Lehtinen, K.; Erho, T. *Anal. Chem.* **2010**, *82*, 10246–10250.

(7) Dungchai, W.; Chailapakul, O.; Henry, C. S. *Analyst* **2011**, *136*, 77–82.

(8) Martin, A. J. P.; Synge, R. L. M. *Biochem. J.* **1941**, *35*, 1358–1368.

(9) Comer, J. *Anal. Chem.* **1956**, *28*, 1748–1750.

(10) Brucker, M. C.; MacMullen, N. J. *J. Obstet. Gynecol. neonatal Nurs.* **1985**, *14*, 353–359.

(11) Fernández-Sánchez, C.; McNeil, C. J.; Rawson, K.; Nilsson, O. *Anal. Chem.* **2004**, *76*, 5649–5656.

(12) Fernández-Sánchez, C.; McNeil, C. J.; Rawson, K.; Nilsson, O.; Leung, H. Y.; Gnanapragasam, V. *J. Immunol. Methods* **2005**, *307*, 1–12.

(13) Aveyard, J.; Mehrabi, M.; Cossins, A.; Braven, H.; Wilson, R. *Chem. Commun.* **2007**, 4251–4253.

(14) Lie, P.; Liu, J.; Fang, Z.; Dun, B.; Zeng, L. *Chem. Commun.* **2012**, *48*, 236–238.

(15) Lattanzio, V. M. T.; Nivarlet, N.; Lippolis, V.; Della Gatta, S.; Huet, A. C.; Delahaut, P.; Granier, B.; Visconti, A. *Anal. Chim. Acta* **2012**, *718*, 99–108.

(16) Anfossi, L.; Baggiani, C.; Giovannoli, C.; D'Arco, G.; Giraudi, G. *Anal. Bioanal. Chem.* **2013**, *405*, 467–480.

(17) Liu, J.; Mazumdar, D.; Lu, Y. *Angew. Chemie* **2006**, *118*, 8123–8127.

(18) López Marzo, A. M.; Pons, J.; Blake, D. A.; Merkoçi, A. *Anal. Chem.* **2013**, *85*, 3532–3528.

(19) Cho, I. H.; Seo, S. M.; Paek, E. H.; Paek, S. H. *J. Chromatogr. B Anal. Technol. Biomed. Life Sci.* **2010**, *878*, 271–277.

(20) Choi, D. H.; Lee, S. K.; Oh, Y. K.; Bae, B. W.; Lee, S. D.; Kim, S.; Shin, Y.-B.; Kim, M.-G. *Biosens. Bioelectron.* **2010**, *25*, 1999–2002.

(21) Parolo, C.; de la Escosura-Muñiz, A.; Merkoçi, A. *Biosens. Bioelectron.* **2013**, *40*, 412–416.

(22) Juntunen, E.; Myyryläinen, T.; Salminen, T.; Soukka, T.; Pettersson, K. *Anal. Biochem.* **2012**, *428*, 31–38.

(23) Lin, Y.-Y.; Wang, J.; Liu, G.; Wu, H.; Wai, C. M.; Lin, Y. *Biosens. Bioelectron.* **2008**, *23*, 1659–1665.

(24) Parolo, C.; Medina-Sánchez, M.; de la Escosura-Muñiz, A.; Merkoçi, A. *Lab Chip* **2013**, *13*, 386–390.

(25) Wong, R. C. *Lateral Flow Immunoassay*; Wong, R.; Tse, H., Eds.; Humana Press: Totowa, NJ, 2009; p. 236.

(26) Tonkinson, J. L.; Stillman, B. A. *Front. Biosci.* **2002**, *7*, C1–12.

(27) Fu, E.; Lutz, B.; Kauffman, P.; Yager, P. *Lab Chip* **2010**, *10*, 918–920.

(28) Lutz, B.; Liang, T.; Fu, E.; Ramachandran, S.; Kauffman, P.; Yager, P. *Lab Chip* **2013**, *13*, 2840–2847.

(29) Houghtaling, J.; Liang, T.; Thiessen, G.; Fu, E. *Anal. Chem.* **2013**, *85*, 11201–11204.

(30) Chen, H.; Cogswell, J.; Anagnostopoulos, C.; Faghri, M. *Lab Chip* **2012**, *12*, 2909–2913.

(31) Toley, B. J.; Mckenzie, B.; Liang, T.; Buser, J. R.; Yager, P.; Fu, E. *Anal. Chem.* **2013**, *85*, 11545–11552.

(32) Millipore Corporation. *Rapid Lateral Flow Test Strips. Considerations for product development*; 2002; p. 39.

(33) Noh, H.; Phillips, S. T. *Anal. Chem.* **2010**, *82*, 8071–8078.

(34) Apilux, A.; Ukita, Y.; Chikae, M.; Chailapakul, O.; Takamura, Y. *Lab Chip* **2013**, *13*, 126–135.

Chapter 6

Enhanced lateral-flow assay using secondary antibodies: sensitive detection of isothermal amplified Leishmania DNA

Related publication

Submitted

Triple lines gold nanoparticle-based lateral flow for enhanced and simultaneous Leishmania DNA detection and endogenous control of isothermal amplified blood samples

Lourdes Rivas[1,2], Alfredo de la Escosura-Muñiz[1], Lorena Serrano[3], Laura Altet[3], Olga Francino[3], Armand Sánchez[3], and Arben Merkoçi[1,4]

[1]ICN2-Nanobioelectronics & Biosensors Group, Institut Català de Nanociència i Nanotecnologia, Campus UAB, 08193 Bellaterra (Barcelona), Spain

[2]Department of Chemistry, Universitat Autónoma de Barcelona, 08193, Bellaterra, Barcelona, Spain

[3]Vetgenomics S.L., Bellaterra (Barcelona), Spain

[4]ICREA - Institució Catalana de Recerca i Estudis Avançats, 08010 Barcelona, Spain

Summary

In this Chapter, a novel triple-lines lateral-flow design with enhanced sensitivity for the sensitive detection of isothermal amplified Leishmania DNA is presented. DNA primers labeled with biotin and FITC for the isothermal amplification reaction are used. The enhanced methodology takes advantage of the use of gold nanoparticle tags (AuNPs) connected with polyclonal secondary antibodies which recognize anti-FITC antibodies. The polyclonal nature of the secondary antibodies allows their multiple connections with primary ones, giving rise to the enhancement of the AuNP signal. Furthermore, an endogenous control consisting in the amplification of the 18S rRNA gene is introduced so as to avoid false negatives. Using this strategy, up to 30 parasites/mL are detected being the detection limit comparable to other isothermal amplification techniques but with the advantage of being a simpler alternative with interest to be extended to several other DNA detection scenarios.

6.1. Introduction

Leishmaniasis is a vector-borne and poverty-related disease potentially fatal in humans and dogs which represents an important public health problem[1–3]. Two main Leishmania species are associated to several clinical signs: cutaneous leishmaniasis which can be cured but leaves skin damages[4] and visceral leishmaniasis which is mortal if is untreated[5]. According to the World Health Organization, an estimated of 12 million of persons are infected around the world and every year appears 1-2millons new cases.[6] More than 500.000 cases correspond to visceral leishmaniasis and the mortality estimated is 50.000 deaths per year.[5,6] Canine Leishmaniasis (CanL) caused by Leishmania Infantum is transmitted by the bite of an insect vector, phlebotomine sand fly, which transmits the flagellated infective promastigote. The intracellular amastigote form is then developed and replicated in the mammal.[7]

Different methods for the detection and diagnosis of CanL including parasitological[8–10], serolological[11,12] and molecular techniques[13–18] have been reported. Polymerase chain reaction (PCR) method for the amplified detection of parasite DNA constitutes the main approach for CanL detection allowing a high sensitivity and specificity. However, the well-known limitations of the PCR related to the thermocycling make necessary the development of novel alternative methods for an early detection in order to apply a successful medical treatment. Isothermal amplification is an alternative approach to the traditional PCR which overcomes many of the complications related to the thermocycling since it is performed at a constant temperature thanks to the use of specific enzymes. Various isothermal amplification methods that depend on the enzymes and the temperature used have been developed. The variation called Recombinase Polymerase Amplification (RPA) commercialized by Twist (TwistDx's®)[19] employs recombinase enzymes which are capable of pairing oligonucleotide primers with homologous sequence in duplex DNA. Through this method, DNA synthesis is directed to defined points in a sample DNA. If the target sequence is indeed present, DNA amplification reaction is initiated; no other sample manipulation such as thermal or chemical melting is required. The reaction progresses rapidly and results in specific DNA amplification from just a few target copies to detectable levels typically within 5 - 10 minutes. Using labeled primers, the amplified product is double-labeled, opening the way to different detection methodologies. RPA technique has been used for amplifying DNA from bacteria[20–22] and viruses[23,24]

followed in most cases by fluorescent detection[20,21] which has the well-known limitations related to the use of fluorescent tags.

In this context, lateral flow assays (LFA) appear as an invaluable tool which fulfills the requirements of an ASSURED biosensing system: affordable, sensitive, specific, user-friendly, rapid and robust, equipment free and deliverable to end-users.[25] Double-labeled primers have been used for the final detection of RPA amplified HIV-virus using commercially available LFA strips.[23] In the case of Leishmania, strips for specific CanL antigen (kR39) are commercially available (InBiosInc®, CTK Biotec®, DiaMet IT®) for detection of visceral leishmaniasis[14,26–29] but there are not examples of detection of RPA amplified CanL DNA using LFA, which can enhance in a high extent the sensitivity of the antigen based detection.

Due to the importance of LFA for field analysis, many efforts have been achieved in order to enhance their sensitivity, being of special interest those which take advantage of the tools offered by the nanotechnology. Recent reports showed the increase of sensitivity in LFA using dual gold nanoparticle conjugates[30], gold nanoparticles loaded with enzymes[31] and even simple changes on the paper architecture.[32]

Given the importance of Leishmania DNA detection we offer a novel LFA design with enhanced sensitivity able to detect very low quantities of isothermal RPA amplified analyte. DNA primers labeled with biotin and FITC for the isothermal amplification reaction were used. The enhanced methodology takes advantage of the use of gold nanoparticle tags (AuNPs) connected with polyclonal secondary antibodies which recognize anti-FITC antibodies. The polyclonal nature of the secondary antibodies allowed their multiple connections with primary ones, giving rise to the enhancement of the AuNP signal. Furthermore, an endogenous control consisting in a third line in the LFA that corresponds to the amplification of the 18S rRNA gene was introduced so as to avoid false negatives.

6.2. Experimental section

6.2.1. Reagents and apparatus

A kit for isothermal amplification of DNA based on RPA method was purchased from TwistDx's®. The suitable labeled primers for the amplification of Leishmania infantum kinetoplast DNA were purchased from Sigma Aldrich (Spain).

Hydrogen tetrachloroaurate (III) trihydrate ($HAuCl_4 \bullet 3H_2O$, 99.9%), trisodium citrate ($Na_3C_6H_5O_7 \bullet 2H_2O$) and Streptavidin from Streptomyces avidinii were purchased from Sigma-Aldrich (Spain). Anti-goat IgG (polyclonal antibody produced in chicken; ab86245) and anti-FITC IgG (polyclonal antibody produced in goat; ab19224) were purchased from Abcam (UK). All the reagents used for the preparation of the different buffers were supplied by Sigma Aldrich (Spain):

Boric acid (H_3BO_3, 99%) and sodium tetraborate decahydrate ($B_4NaO_7.H_2O$, 99%) for the preparation of Borate buffer (BB); Sodium phosphate monobasic monohydrate ($NaH_2PO_4.H_2O$, 99%) and sodium phosphate dibasic (Na_2HPO_4, 99%) for the preparation of phosphate buffer (PB); Trizma® HCl ($C_4H_{11}NO_3$, 99%) and sodium chloride (NaCl, 99.5%) for the preparation of tris buffer saline-tween (TBST); Tween®-20 ($C_{58}H_{114}O_{26}$), sucrose ($C_{12}H_{22}O_{11}$, 99.5%), bovine serum albumin (BSA, 96%) and sodium dodecyl sulphate ($C_{12}H_{25}NaO_4S$, 98.5%) for the preparation of blocking buffers; Phosphate buffer saline tablet for the preparation of PBS buffer.

All the materials used for the production of the LFIA strips were purchased from Millipore (Billerica, MA 08128, USA): sample and absorbent pads (CFSP001700), conjugate pad (GFCP00080000), detection pad (SHF1800425) and the backing card (HF000MC100). A guillotine Dahle 533 (Germany) was used to cut the strips. An IsoFlow reagent dispensing system (Imagene Technology, USA) was used to dispense the detection and control lines. A strip reader (COZART — SpinReact, UK) was used for quantitative measurements. mQ water, produced using a Milli-Q system (>18.2 MΩ/cm) purchased from Millipore (Sweden), was used for the preparation of all solutions. The stirrer used was a TS-100 Thermo shaker (BioSan, Latvia). A thermostatic centrifuge (Sigma 2-16 PK, Fisher Bioblock Scientific, France) was used to purify the AuNP/antibody conjugates. All the size measurements and shape observation of AuNPs were conducted in a Field Emission Gun Transmission Electronic Microscope, model Tecnai^{TM} G2F20 (Fei, USA).

6.2.2. Methods

6.2.2.1. Designs for RPA amplification of Leishmania infantum kinetoplast DNA

Leishmania parasite was spiked on DNA samples extracted from dog blood. After that, Leishmania infantum kinetoplast DNAwas isothermal amplified using primers labeled with biotin and FITC ("positive" samples). Samples from dogs without spiked parasite ("blank" samples) were also amplified so as to evaluate the specificity of the method. For endogen control assays, an additional pair of primers that amplify the 18S rRNA gene (always present in both "positive" and "blank" samples), labeled in this case with FITC and digoxigenin was also used.

6.2.2.2. Preparation of gold nanoparticles

Gold nanoparticles (AuNP) 20 nm sized and stabilized by citrate, were prepared using the Turkevich's method[33] as previously described in **Chapter 5**.

6.2.2.3. AuNPs modification with antibodies: preparation of the double antibody solution

The conjugation of AuNPs with antibodies was performed according to the following procedure, previously optimized by our group.[31] First of all, the pH of the AuNPs suspension was corrected to pH 9 with 0.1M borate buffer. Then, 100 µL of a 100 µg/mL anti-goat IgG aqueous solution were added to 1.5 mL of the AuNPs suspension. The resulting solution was incubated for 20 min at 650 rpm. Then, 100 µL of 1 mg/mL BSA aqueous solution were added and the stirring was continued for other 20min at 650 rpm. Finally, the solution was centrifuged at 14000 rpm and 4ºC.

The supernatant was removed and the pellet of AuNP/anti-goat IgG was re-suspended in 300 µL of 3 µg/mL anti-FITC IgG solution in BB 2 mM pH 7.4, 10% sucrose. In this way, a suspension containing both anti-FITC IgG and AuNPs/anti-goat IgG was obtained, being immediately used for conjugate pad preparation.

6.2.2.4. Preparation of the strips

1 mg/mL solution of anti-goat IgG and streptavidin in PB 10 mM, pH 7.4 were spotted onto the detection pad at dispensing rate of 0.05 μL/mm using an IsoFlow reagent dispensing system so as to form the control and test line, respectively. For the detection of the endogen control, an additional line with 1 mg/mL of anti-digoxigenin was also spotted. Then, the detection pad was dried at 37ºC for 1h. After that, the membrane was blocked using a 2% BSA aqueous solution for 5 minutes. Finally, the membrane was washed for 15 minutes using PB (5mM pH 7.4), 0.05% SDS and dried at 37ºC for 2h.

The sample pad was prepared by dipping into 10mM PBS, 5% BSA and 0.05% Tween®-20 and drying at 60ºC for 2h. The conjugate pad was prepared dipping it into the previously prepared double antibody solution (anti-FITC IgG and AuNP/anti-goat IgG) and drying under vacuum for 1 h.

The different pads were sequentially laminated 2 mm with each other and pasted onto the adhesive backing card in the following order: detection, conjugation, sample and absorbent pads. Finally, the strips were cut 7 mm wide and stored in dry conditions at 4ºC until their use up to a week.

6.2.2.5. Lateral-flow assay procedure

Isothermal amplified Leishmania DNA sample solutions labeled with FITC and biotin were first diluted in Tris buffer saline 10mM Trizma®-HCl pH 7.6 and 0.05% Tween®-20 (TBST) at different dilution factors. Typical assay consisted in mixing 10 μL of the diluted sample (different dilution factors in TBST were assayed: 1:100, 1:250: 1:500 and 1:1250) with 200 μL of TBST, immersing the strip into this solution and keeping for 10 min until the flow is stopped. Then 200 μL of TBST were dispensed in order to wash away the excess of the double antibody solution. Three replicates of each sample were done and intensities of lines were read with the strip reader so as to obtain the corresponding calibration curve.

6.3. Results and discussion

6.3.1. Principle of the enhanced detection

The principle of the signal enhancement is based on an indirect ELISA. In a typical assay, after the analyte recognition by a capture antibody, the sandwich is completed with a label-free primary antibody. After that, an AuNP labeled polyclonal secondary antibody is used for the recognition of the primary one. The polyclonal nature of the secondary antibody makes possible the connection of a high number of labeled antibodies to each primary one, giving rise to an increase in the number of AuNP labels and consequently an enhancement in the analytical signal.[33]

In our approach, the novel and simple strategy for the signal amplification is based on the immobilization on the conjugation pad of primary antibodies specific to the analyte and secondary antibodies labeled with AuNPs which recognize the primary ones. The secondary antibodies (chicken anti-goat IgG) were labeled with AuNPs which can recognize a primary one that acts as detection antibody (goat anti-FITC) forming a complex which was dispensed onto the conjugation pad. Two reagents were deposited on the nitrocellulose membrane: streptavidin and anti-goat IgG, forming the test line and the control line respectively. When the sample starts to flow though the strip, the primary antibody/secondary antibody complex is released, producing the capture of the isothermal amplified DNA through the tails labeled with FITC. While the sample keeps migrating though the membrane, the test line becomes visible due to the binding of streptavidin with the biotin present in the isothermal amplified DNA. The control line turns visible when the anti-species antibodies capture any excess of antibody labeled with gold nanoparticles (see Figure 6.1).

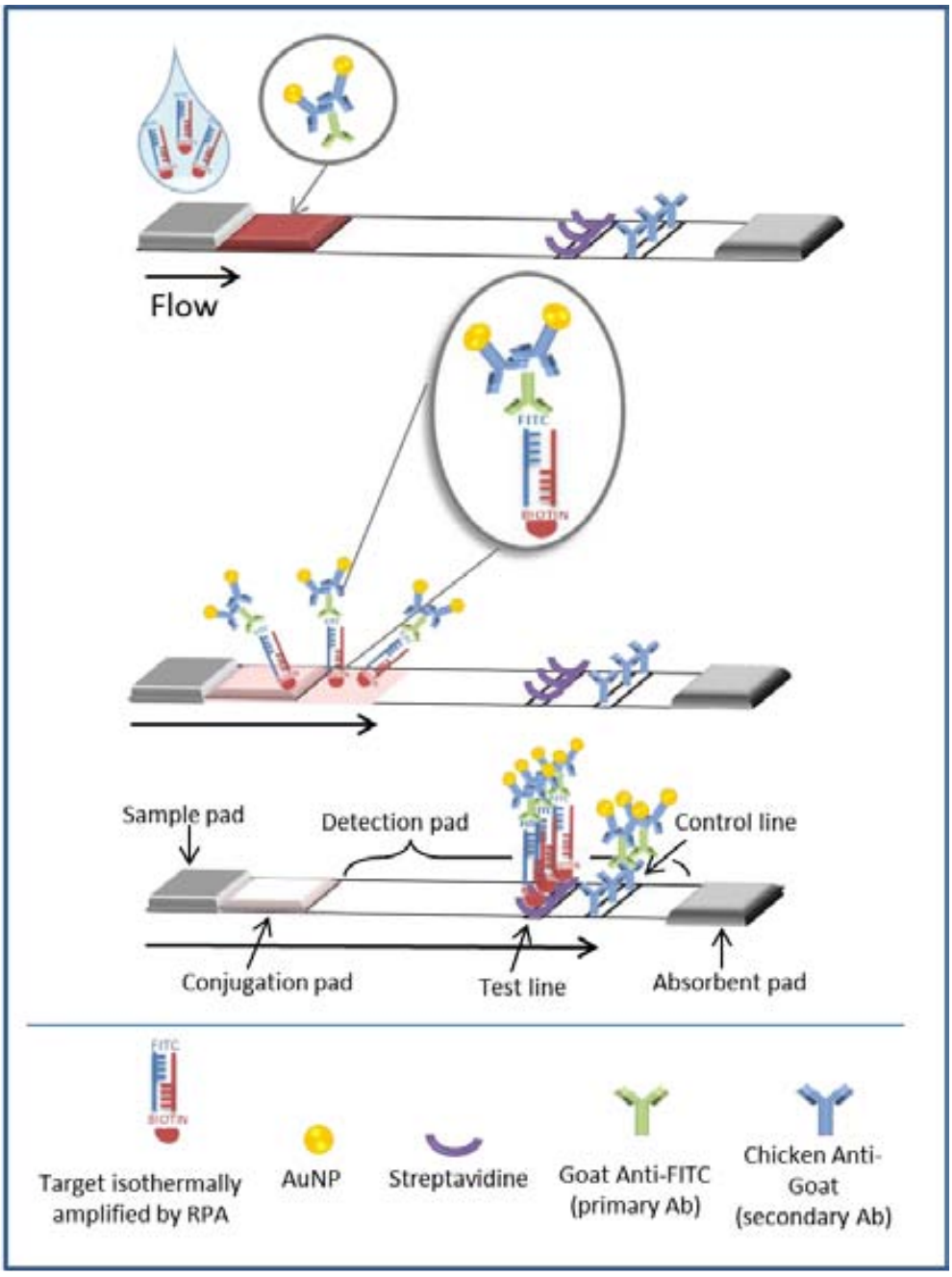

Figure 6.1. Scheme, not in scale, of the enhanced LFA based on the use of secondary antibodies for the detection of double labeled (FITC/biotin) isothermal amplified DNA.

6.3.2. Optimization of the enhanced lateral flow assay

Different parameters affecting the analytical signal, including blocking steps, concentration of antibodies in the double antibody complex and running buffer were optimized.

6.3.2.1. Blocking agent

Nitrocellulose membranes have been traditionally blocked with different agents (e.g. proteins, surfactants or polymers) not only to avoid non-specific bindings of nanoparticles over the membrane[34,35] but also to control the flow rate and stabilize test and control line.[36] The best conditions for blocking the membrane for each specific approach must be thoroughly optimized. In our case, a solution containing 2% BSA for preventing the non-specific adsorptions after dispensing the antibodies over the nitrocellulose membrane was found as suitable as blocking agent (Fig. 6.2).

6.3.2.2. Running buffer

The formation of antigen-antibody complex can be affected by matrix parameters such as pH, temperature and ionic strength.[37] Tris buffer is well known for its capability of solubilize DNA so as to avoid its degradation, so three running buffers with different Tris concentrations and additives were tested, for positive and blank samples (Fig. 6.2). Results showed that when the ionic strength of running buffer increased, the test line became more intense, the sensitivity was improved and no unspecific signal in the test line for the blank sample was observed. Although when the ionic strength between buffers B and C was not significantly different, the presence of surfactant (Tween-20®) allowed a better flow of nanoparticles through the membrane avoiding non desirable adsorptions. Thus, the most suitable running buffer for this assay was found to be TrisHCl 50 mM, 150mM NaCl and 0.05% Tween-20®. These observations are in agreement with previously reported studies showing that ionic strength of running buffer together with the presence of surfactant have an important influence of the background signal decreasing the non-specific bindings over the membrane.[36,38,39]

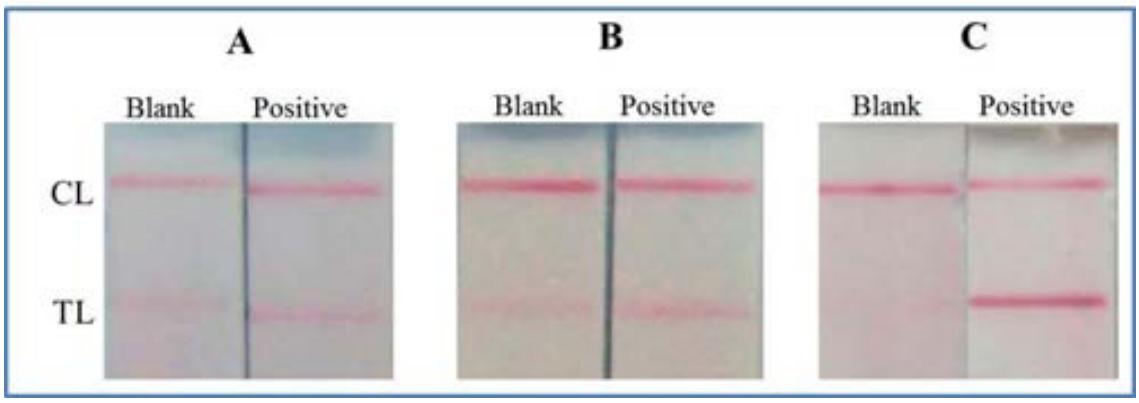

Figure 6.2. Optimization of running buffer for an isothermally amplified product diluted at 1:50. Buffers are: (A) 25 mM Tris, 150 mM NaCl, pH 7.6, (C) 50 mM Tris, 138mM NaCl, 0.27mM KCl, 1% BSA and (D) 50mM Tris, 150 mM NaCl, 0.05% Tween-20. All the membranes were previously blocked with 2% BSA.

6.3.2.3. Concentration of primary antibody

Different concentrations of primary antibody for a fixed quantity of the conjugate of the secondary antibody/AuNPs were evaluated. As it is shown in Figure 6.3, it was found that the most suitable concentration of goat anti-FITC in the double antibody solution was 3 µg/mL. This can be probably due to the fact that for higher concentrations of primary antibody, the primary Ab / secondary Ab ratio is close to 1:1 and consequently the AuNPs concentration in the test line is lower, as also schematized in Figure 6.3.

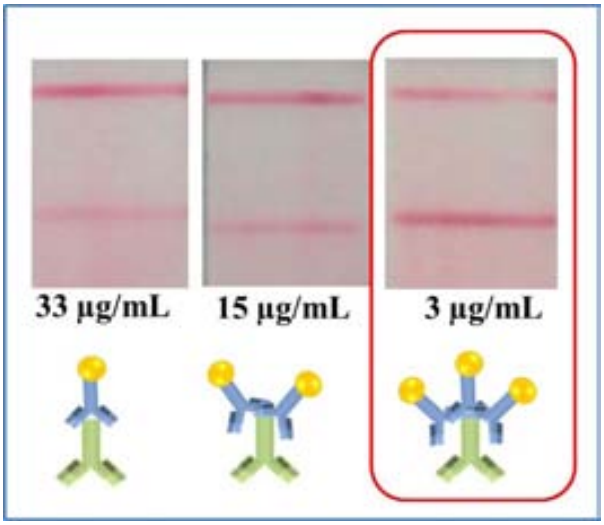

Figure 6.3. Optimization of primary antibody concentration in double antibody-AuNP conjugate. Assays performed for an isothermal amplified product diluted at 1:50. Other conditions as detailed at the experimental section.

6.3.3. Semiquantitative assays: evaluation of the enhancement

Preliminary tests were performed under the optimized conditions, for isothermal amplified DNA using the enhanced LFA strategy. The results were compared with those obtained using a direct LFA without using secondary antibodies and summarized in figure 6.4. In both cases, the concentrated amplified DNA was serially diluted so as to evaluate the ability of the sensing system to detect lower quantities of labeled product.

A clear improvement in the sensitivity thanks to the use of secondary antibodies was noticed even with the naked eye. The obtained enhancement allows visual detection of isothermal amplified products diluted at a 1:500 factor, whereas with the direct assay only products diluted up to 1:250 are visualized.

The advantages of the enhanced strategy are even more evident with the measurements of optical density performed with the scanner (Fig. 6.4B). It is important to point out that with this novel strategy not only the sensitivity is improved but also the lines are better defined, which is crucial for an adequate and reproducible reading by the scanner. Thanks to the optical density measurements, isothermal amplified products diluted up to a 1:1250 ratio can be detected.

Finally, the enhanced strategy was used for the evaluation of isothermal amplified products prepared from samples containing different quantities of parasite. Values of intensity of test line were plotted vs. the logarithm of parasite concentrations (Fig. 6.5), resulting in a linear relationship in the range of 0.035 to 16 parasites per µL. A limit of detection of 32 parasites/mL (0.032 parasites/µL) was estimated as the analyte concentration giving a signal equal to the blank signal plus three times its standard deviation. The reproducibility of responses (n=3) for 1.6 parasites/µL was also studied, obtaining a relative standard deviation (RSD) of 4%.

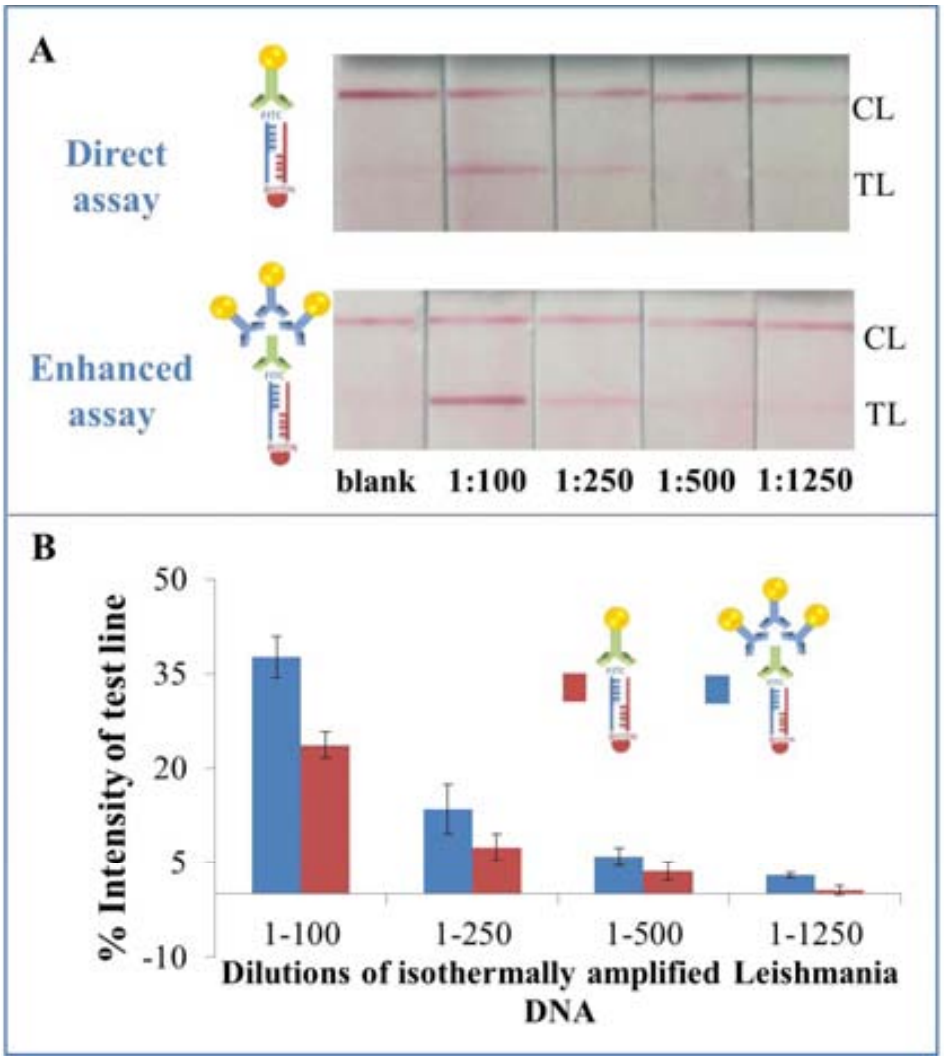

Figure 6.4. (A) Pictu res of LFA strips after the assay perfo rmed for isot hermal amplified Leishmania DNA at different dilution ratios, using the enhanced and the direct strategy. (B) The corresponding intensity values obtained with the strip reader for both assays.

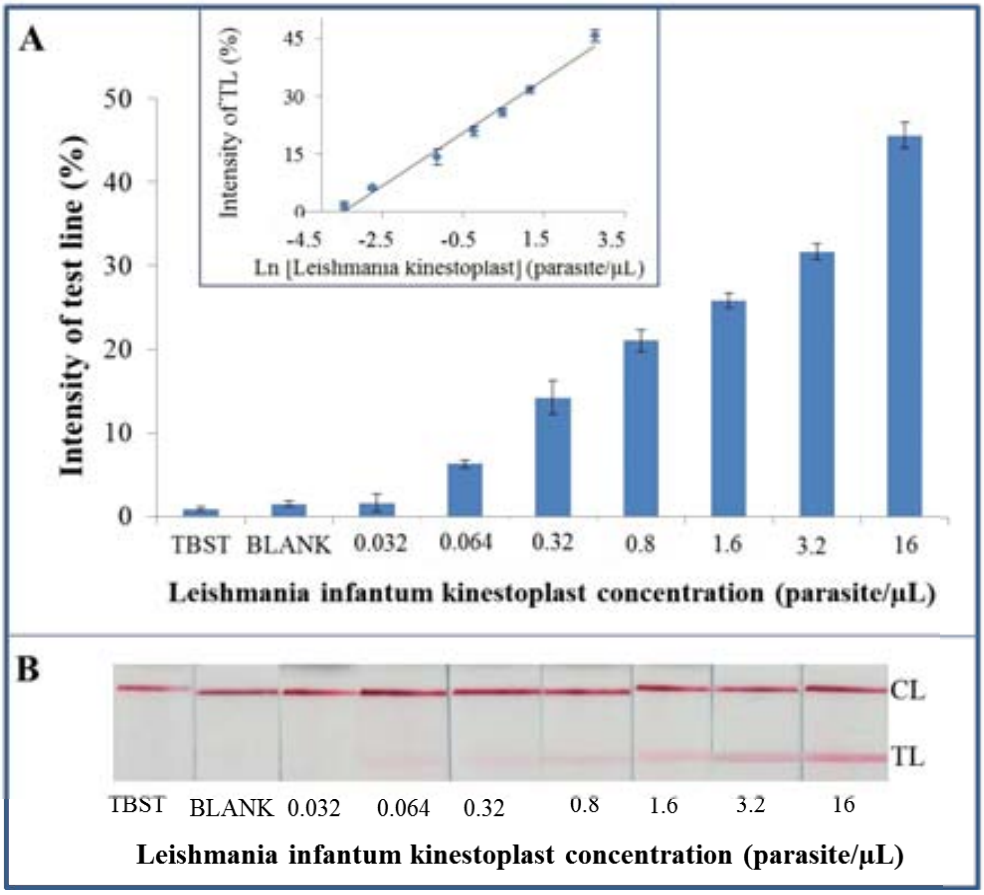

Figure 6.5. (A) Bar in tensity graphic for enhanced lateral flow assay. The lo garithmic relationship between the parasite concentration and the % of intensity in the test line is shown in the inset graphic. (B) Corresponding pictures of the LFA strips.

Most of LFA for Leishmania detection are offered for qualitative tests only being few of them able to achieve semi-quantitative analytical res ponse.[15,27,40–42] Our AuNP based amplification approach results are quite similar to those obtained by se mi-quantitative test using nucleic acid sequence based amplification (NASBA) and coupled to oligochromatography (OC) for Leishmania detecti on which rea ch detection lim its o f 0.01 parasites/µL.[42] However, our technique provides a valuable proof of concept due to the enhancement approach which is a universal methodology that can be applied for any LFA design.

6.3.4. Second test line for endogenous control

Using the standard LFA design, a negative response (no signal in the detection line) can be due not only to the absence of the Leishmania in the sample but also to errors in the isothermal amplification procedure. In order to solve this, an endogenous control was also performed and introduced in the LFA design. It consists in introducing an additional pair of primers that amplify the 18S rRNA gene (always present in the sample), so this amplified product must be always present, for both positive and blank samples. These primers were labeled with FITC and digoxigenin as schematized in figure 6.6A. As result, in the positive samples both products (biotin-FITC and digoxigenin-FITC labeled) will be present while only the digoxigenin-FITC pair will be found in the blank samples.

In order to detect both products, the LFA strip was slightly modified, adding an additional line in the detection pad, where anti-digoxigenin antibodies were immobilized. This line must be always visualized, even for blank samples, evidencing that the amplification procedure worked properly, as illustrated in figure 6.6B.

The performance of the enhanced strategy for the assay containing the endogenous control was evaluated for amplified DNA serially diluted. As it is shown in figure 6.7 (lower part), the additional test line is clearly visualized. Furthermore, the intensity of color in the control line remains constant while the corresponding ones to the two test lines decrease when the dilution factor is increased, demonstrating that the amplification procedure worked properly.

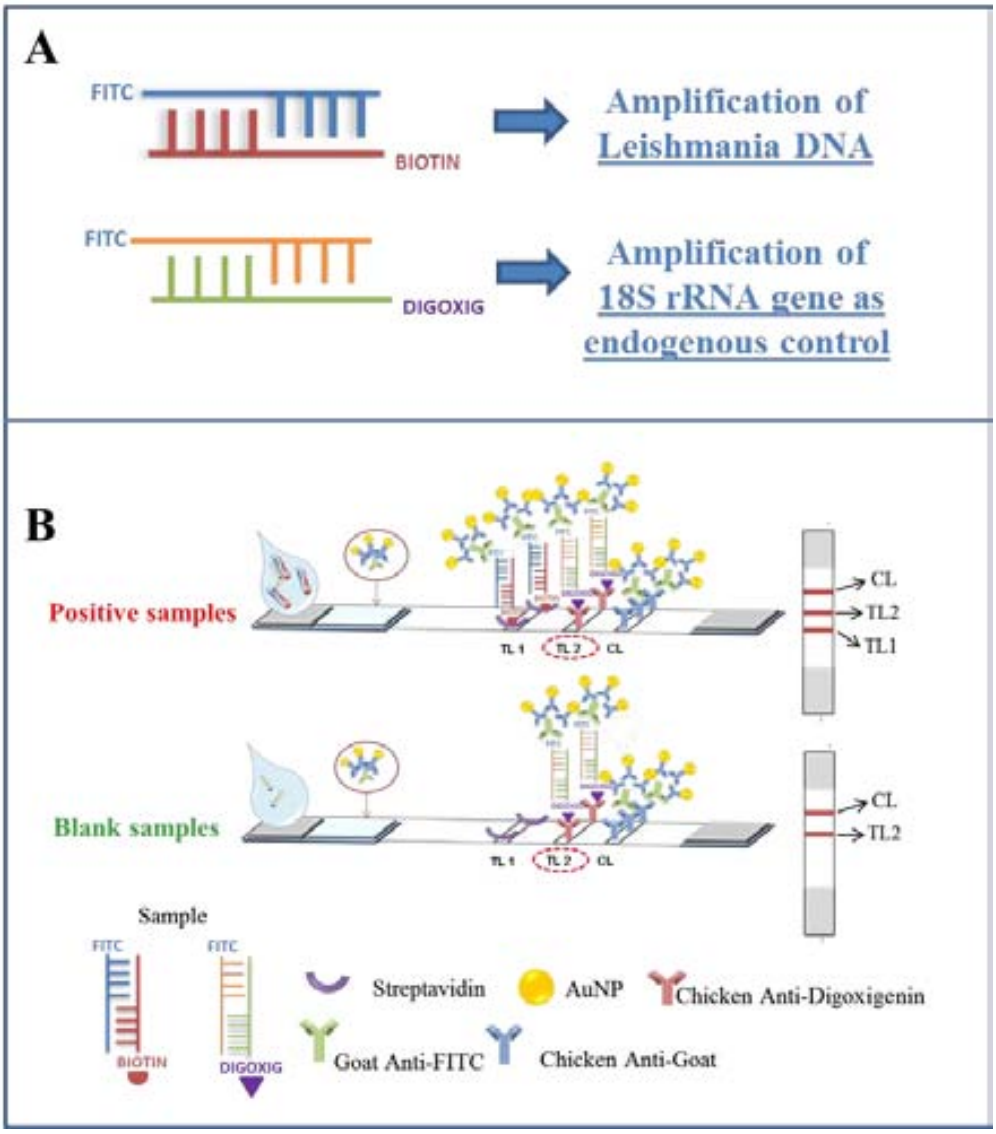

Figure 6.6. (A) Sche me of th e design of primers for th e simultaneous amplification of Leishmania DNA and 18S rNA gene (endogenous control). (B) Design of the LFA strips with the additional test line (TL2) for the endogenous control detection.

The results were also compared with the obtained using the direct assay (without secondary antibodies; figure 6.7-upper part) observing again the advantageous effect of the enhanced strategy, ensuring now that false negatives are avoided.

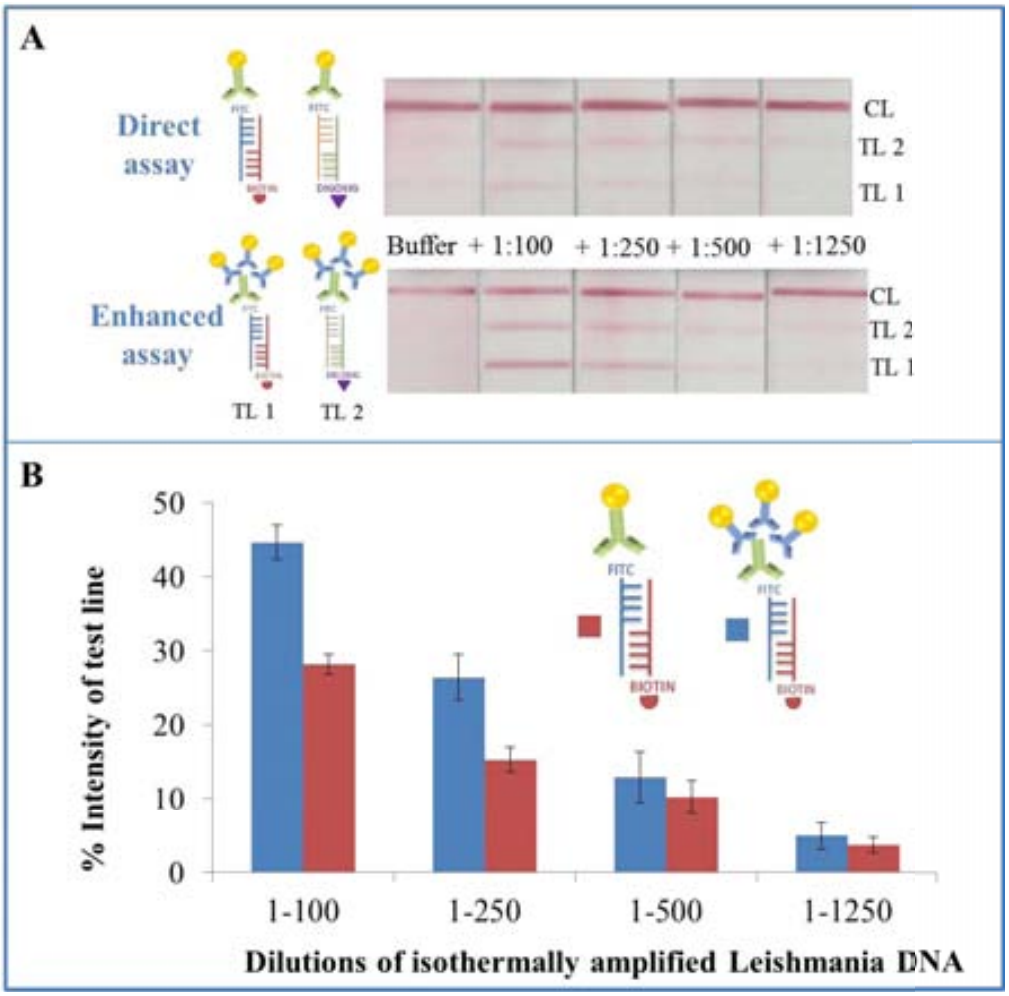

Figure 6.7. Pictures of LFA strips after the assay performed for isothermal amplified Leishmania DNA at different dilution factors, containing the endogenous control. The direct and the enhanced assays are also compared. TL1 corresponds to the test line while TL2 stands for the endogenous control.

Finally, the enhanced strategy in combination with the endogenous control was applied for the evaluation of isothermal amplified products prepared from samples containing different quantities of parasite. A linear relationship between the parasite concentration and the intensity of the test line was obtained in the range 0.032 to 16 parasites/μL. A limit of detection of 30 parasites/mL (0.030 parasite/μL) was estimated, calculated as explained above (Fig. 6.8). This value is almost the same as the one obtained with only

one test line for Leishmania parasite detection, demonstrating that the addition of a second test line provides in the same lateral flow strip a control for checking the isothermal amplification and also a tool for Leishmania parasite detection with out affecting the sensitivity of the enhanced LFA.

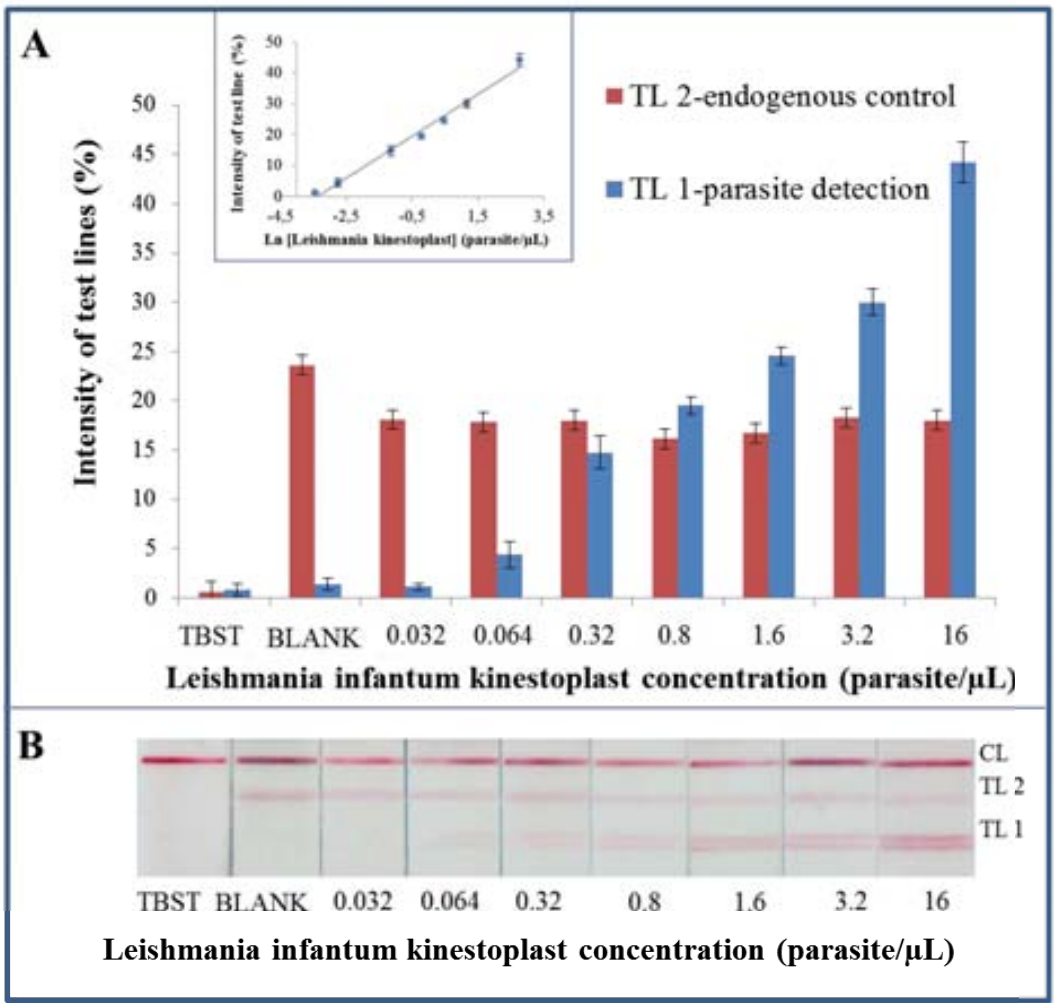

Figure 6.8. (A) Bar intensity graphic for enhanced lateral flow assay containing the endogenous control. The logarithmic relationship between the parasite concentration and the % of intensity in the test line is shown in the inset graphic. (B) Corresponding pictures of the LFA strips. TL1 corresponds to the test line while TL2 stands for the endogenous control.

6.4. Conclusions

A novel design of Lateral Flow Assay (LFA) based on the use of secondary antibodies in the conjugation pad was successfully accomplished and applied for the detection of isothermal amplified Leishmania infantum kinetoplast DNA extracted from dog blood. This isothermal amplification approach overcomes many of the complications related to the thermocycling since it is performed at a constant temperature. The use of labeled primers allows to obtain double labeled (biotin/FITC) products that can be detected using a lateral Flow Assay (LFA). Thanks to the use of secondary antibodies, the intensity of the signal in the test line and consequently the sensitivity of the assay is highly increased, allowing to detect up to 30 parasites/mL.

Furthermore, an additional control, the so- called endogen control, was included so as to avoid false negatives. It was simply performed by adding an additional pair of primers that amplify the 18S rRNA gene (always present in the sample) labeled with FITC and digoxigenin and introducing an additional test line in the LFA strip, containing anti-digoxigenin antibodies. This approach was successfully implemented, without losing the efficiency of the signal enhancement. The enhancement strategy proposed is a versatile and universal methodology that can be applied for any LFA design. It has also the advantage of the fact that the specific antibody against the analyte does not need to be directly labeled and it represents clear advantages in terms of technology cost.

6.5. References

(1) Alvar, J.; Yactayo, S.; Bern, C. *Trends Parasitol.* **2006**, *22*, 552–557.

(2) Maia, C.; Campino, L. *Vet. Parasitol.* **2008**, *158*, 274–287.

(3) Dantas-Torres, F.; Solano-Gallego, L.; Baneth, G.; Ribeiro, V. M.; de Paiva-Cavalcanti, M.; Otranto, D. *Trends Parasitol.* **2012**, *28*, 531–538.

(4) Ciaramella, P.; Oliva, G.; Luna, R. De; Gradoni, L.; Ambrosio, R.; Cortese, L.; Scalone, A.; Persechino, A. *Vet. Rec.* **1997**, *141*, 539–543.

(5) Chappuis, F.; Sundar, S.; Hailu, A.; Ghalib, H.; Rijal, S.; Peeling, R. W.; Alvar, J.; Boelaert, M. *Nat. Rev. Microbiol.* **2007**, *5*, 873–882.

(6) *World Heal. Organ. WHO, Tech. Rep. Ser. 949* **2010**, 1–186.

(7) Solano-Gallego, L.; Miró, G.; Koutinas, A.; Cardoso, L.; Pennisi, M. G.; Ferrer, L.; Bourdeau, P.; Oliva, G.; Baneth, G. *Parasit. Vectors* **2011**, *4*, 1–16.

(8) Solano-Gallego, L.; Fernández-Bellon, H.; Morell, P.; Fondevila, D.; Alberola, J.; Ramis, a.; Ferrer, L. *J. Comp. Pathol.* **2004**, *130*, 7–12.

(9) De Fátima Madeira, M.; de O Schubach, A.; Schubach, T. M. P.; Pereira, S. a; Figueiredo, F. B.; Baptista, C.; Leal, C. a; Melo, C. X.; Confort, E. M.; Marzochi, M. C. a. *Vet. Parasitol.* **2006**, *138*, 366–370.

(10) Xavier, S. C.; de Andrade, H. M.; Monte, S. J. H.; Chiarelli, I. M.; Lima, W. G.; Michalick, M. S. M.; Tafuri, W. L.; Tafuri, W. L. *BMC Vet. Res.* **2006**, *2*, 17.

(11) Figueiredo, F. B.; Madeira, M. F.; Menezes, R. C.; Pacheco, R. S.; Pires, M. Q.; Furtado, M. C.; Pinto, a G.; Schubach, T. M. P. *Vet. J.* **2010**, *186*, 123–124.

(12) Marcondes, M.; Biondo, a W.; Gomes, a a D.; Silva, a R. S.; Vieira, R. F. C.; Camacho, a a; Quinn, J.; Chandrashekar, R. *Vet. Parasitol.* **2011**, *175*, 15–19.

(13) Reithinger, R.; Dujardin, J.-C. *J. Clin. Microbiol.* **2007**, *45*, 21–25.

(14) Srividya, G.; Kulshrestha, A.; Singh, R.; Salotra, P. *Parasitol. Res.* **2012**, *110*, 1065–1078.

(15) Deborggraeve, S.; Laurent, T.; Espinosa, D.; Van der Auwera, G.; Mbuchi, M.; Wasunna, M.; El-Safi, S.; Al-Basheer, A. A.; Arévalo, J.; Miranda-Verástegui, C.; Leclipteux, T.; Mertens, P.; Dujardin, J.-C.; Herdewijn, P.; Büscher, P. *J. Infect. Dis.* **2008**, *198*, 1565–1572.

(16) Lombardo, G.; Pennisi, M. G.; Lupo, T.; Migliazzo, A.; Caprì, A.; Solano-Gallego, L. *Vet. Parasitol.* **2012**, *184*, 10–17.

(17) Naranjo, C.; Fondevila, D.; Altet, L.; Francino, O.; Ríos, J.; Roura, X.; Peña, T. *Vet. J.* **2012**, *193*, 168–173.

(18) Van der Meide, W.; Guerra, J.; Schoone, G.; Farenhorst, M.; Coelho, L.; Faber, W.; Peekel, I.; Schallig, H. *J. Clin. Microbiol.* **2008**, *46*, 73–78.

(19) www.twistdx.co.uk.

(20) Lutz, S.; Weber, P.; Focke, M.; Faltin, B.; Hoffmann, J.; Müller, C.; Mark, D.; Roth, G.; Munday, P.; Armes, N.; Piepenburg, O.; Zengerle, R.; von Stetten, F. *Lab Chip* **2010**, *10*, 887–893.

(21) Shen, F.; Davydova, E. K.; Du, W.; Kreutz, J. E.; Piepenburg, O.; Ismagilov, R. F. *Anal. Chem.* **2011**, *83*, 3533–3540.

(22) Euler, M.; Wang, Y.; Otto, P.; Tomaso, H.; Escudero, R.; Anda, P.; Hufert, F. T.; Weidmann, M. *J. Clin. Microbiol.* **2012**, *50*, 2234–2238.

(23) Rohrman, B. a; Richards-Kortum, R. R. *Lab Chip* **2012**, *12*, 3082–3088.

(24) Euler, M.; Wang, Y.; Nentwich, O.; Piepenburg, O.; Hufert, F. T.; Weidmann, M. *J. Clin. Virol.* **2012**, *54*, 308–312.

(25) Peeling, R. W.; Holmes, K. K.; Mabey, D.; Ronald, a. *Sex. Transm. Infect.* **2006**, *82 Suppl 5*, v1–6.

(26) Salotra, P.; Sreenivas, G.; Ramesh, V.; Sundar, S. *Br. J. Dermatol.* **2001**, *145*, 630–632.

(27) Chappuis, F.; Mueller, Y.; Nguimfack, A.; Rwakimari, J. B.; Couffignal, S.; Boelaert, M.; Cavailler, P.; Loutan, L.; Piola, P. *J. Clin. Microbiol.* **2005**, *43*, 5973–5977.

(28) Sundar, S.; Maurya, R.; Singh, R. K.; Bharti, K.; Chakravarty, J.; Parekh, A.; Rai, M.; Kumar, K.; Murray, H. W. *J. Clin. Microbiol.* **2006**, *44*, 251–253.

(29) Welch, R. J.; Anderson, B. L.; Litwin, C. M. *Clin. vaccine Immunol.* **2008**, *15*, 1483–1484.

(30) Choi, D. H.; Lee, S. K.; Oh, Y. K.; Bae, B. W.; Lee, S. D.; Kim, S.; Shin, Y.-B.; Kim, M.-G. *Biosens. Bioelectron.* **2010**, *25*, 1999–2002.

(31) Parolo, C.; de la Escosura-Muñiz, A.; Merkoçi, A. *Biosens. Bioelectron.* **2013**, *40*, 412–416.

(32) Parolo, C.; Medina-Sánchez, M.; de la Escosura-Muñiz, A.; Merkoçi, A. *Lab Chip* **2013**, *13*, 386–390.

(33) Crowther, J. R. *The ELISA guidebook*; Humana Press: New Jersey, 2001; p. 421.

(34) Wong, R. C. *Lateral Flow Immunoassay*; Wong, R.; Tse, H., Eds.; Humana Press: Totowa, NJ, 2009; p. 236.

(35) Millipore Corporation. *Rapid Lateral Flow Test Strips. Considerations for product development*; 2002; p. 39.

(36) Molinelli, A.; Grossalber, K.; Führer, M.; Baumgartner, S.; Sulyok, M.; Krska, R. *J. Agric. Food Chem.* **2008**, *56*, 2589–2594.

(37) Farhat Basir, S. *Textbook of immunology*; PHI Learning: New Delhi, 2009; p. 256.

(38) Liu, J.; Mazumdar, D.; Lu, Y. *Angew. Chem. Int. Ed. Engl.* **2006**, *45*, 7955–7959.

(39) Hua, X.; Yang, J.; Wang, L.; Fang, Q.; Zhang, G.; Liu, F. *PLoS One* **2012**, *7*, e53099.

(40) Mettler, M.; Grimm, F.; Capelli, G.; Camp, H.; Deplazes, P. *J. Clin. Microbiol.* **2005**, *43*, 5515–5519.

(41) Carson, C.; Quinnell, R. J.; Holden, J.; Garcez, L. M.; Deborggraeve, S.; Courtenay, O. *J. Clin. Microbiol.* **2010**, *48*, 3325–3330.

(42) Mugasa, C. M.; Laurent, T.; Schoone, G. J.; Basiye, F. L.; Saad, A. a; El Safi, S.; Kager, P. a; Schallig, H. D. *Parasit. Vectors* **2010**, *3*, 13.

Chapter 7

Conclusions and future perspectives

7.1. Conclusions

Novel and improved biosensing systems taking advantage of the optical, electrical and electrocatalytic properties of gold nanoparticles (AuNPs) and iridium oxide nanoparticles (IrO_2 NPs) have been developed. These biosensing approaches have been developed on both plastic and paper-based platforms, showing an excellent performance in the point-of-care detection of protein biomarkers, DNA and toxins.

Considering the detailed objectives described in **Chapter 2** and the obtained results in **Chapters 3**, **4**, **5** and **6**, the conclusions are detailed as follows:

Development of an iridium oxide-based electrochemical biosensor. 12 nm-sized IrO_2 NPs were successfully synthesized, characterized and used as novel electrocatalytic tags for immunosensing. The stable NPs suspension exhibited a high catalytic effect towards the Water Oxidation Reaction (WOR), allowing their sensitive quantification at neutral pH in a simple chronoamperometric mode. This sensitive method was applied for the evaluation of Apolipoprotein (ApoE) Alzheimer disease biomarker in human plasma, following an immunoassay format using IrO_2 NPs as advantageous tags. These tags are detected on screen-printed carbon electrodes (SPCEs) in the same buffer where the immunoreaction takes place, avoiding the addition of acidic and hazardous solutions (along with H_2 bubbles formation, undesired in microfluidics) usually required for electrochemical detection.

Label-free aptasensor based on iridium oxide-modified electrodes. A novel and highly sensitive aptamer-based sensing platform for ochratoxin A detection using a disposable and single-use SPCE was developed. Deposition of a redox dye, thionine, was successfully achieved on the working electrode surface of SPCE by electropolimerization, followed by the adsorption of IrO_2 NPs. Then, aminated-aptamer selective to OTA was efficiently immobilized onto the citrate-capped IrO_2 NPs adsorbed onto the electrode surface. Electrochemical impedance spectroscopy in the presence of ferri/ferrocyanide as redox probe, was used to characterize each step in the aptasensor development and for quantifying OTA. The increase in charge transfer resistance (*R*ct) values due to the specific aptamer–OTA interaction was proportional to

the concentration of OTA in a range of 0.1–100 nM showing also a good reproducibility and selectivity. This sensitive aptasensor exhibited a very low limit of detection (0.2 pM OTA) which can be with interest for its future application in real samples analysis.

Enhanced gold nanoparticles-based lateral-flow device for protein detection using wax-printed micropillars. A new and easy strategy for improving the sensitivity of a gold nanoparticle (AuNP)-based lateral flow assay (LFA) by the deposition of hydrophobic wax microbarriers printed at the detection pad was developed. These barriers act as obstacles delaying the regular flow on the strip by increasing the binding time between the analyte and the labeled antibody and therefore allowing an effective formation of immunocomplex. Different wax-printed pillars designs were evaluated and the optimized ones allowed to improve up to 3-folds the limit of detection compared with the non-modified membranes. Mathematical simulations corroborate the experimental results obtained for the different patterns. Although the limit of detection obtained was similar with other strategies reported in literature, this work offers a low-cost and simple strategy which could be improved and easily extended to any type of LFA desing.

DNA detection using an enhanced gold nanoparticles/secondary antibody-based lateral flow. A novel LFA improvement based on the use of secondary antibodies in the conjugate pad was successfully accomplished and applied for the detection of isothermal amplified Leishmania infantum kinetoplast DNA extracted from dog blood. The use of labeled primers allows to obtain double labeled (biotin/FITC) products that can be detected using a LFA. Thanks to the use of secondary antibodies, the intensity of the signal in the test line and consequently the sensitivity of the assay was highly increased, allowing to detect up to 30 parasites/mL. Furthermore, an additional control, the so- called endogen control, was included so as to avoid false negatives. This approach was successfully implemented, without losing the efficiency of the signal enhancement. The enhancement strategy proposed is a versatile and universal methodology that can be applied for any LFA design. It has also the advantage of the fact that the specific antibody against the analyte does not need to be directly labeled and it represents clear advantages in terms of technology cost.

7.2. Future perspectives

Nanotechnology has expanded the scope for the development of (bio)sensors thanks to the use of nanoparticles which exhibits unique properties, as well the integration of new nanomaterials and nanoelectronics for the development of simple, low cost and high throughput devices.

The application of electrocatalytic nanoparticles which can be detected by electrochemical systems in the same medium of the immunoreaction or without the use of additional and hazardous reagents may open the way to further applications in really integrated sensing systems, such as those based on lab-on-a-chip or lateral-flow platforms. In this regard, development of screen-printed paper-based electrodes has been recently reported as suitable alternative to other detection platforms[1,2] . A full integration of simple and qualitative assessment offered by paper-based biosensors (*e.g.* lateral flow devices) with the sensitive detection of electrochemical devices can be expected in a near future. Particularly, IrO_2 NPs are promising dual labels for their application in electrochemical/optical detection systems in future lateral flow biodetection platforms, due to their strong UV-Vis absorption and electrocatalytic properties. Moreover, thanks to their conductivity and biocompatibility, IrO_2 NPs can be easily applied as excellent platforms for immobilization of biomolecules onto electrotransducing surfaces for developing of sensitive electrochemical biosensors.

On the other hand, in despite the fact that LFAs are excellent tools which fulfill the requirements for point-of-care testing, this sensing technology has disadvantages regarding to sensitivity issues. In this context, two novel and universal approaches were presented in order to overcome such drawbacks. Although the enhancement obtained by the LF strips modified with wax pillars was not remarkable compared with other reports strategies, clearly constitutes a simple, low cost and fast approach for improving the sensitivity of the assays. In addition, could be further improved by using other printing techniques such as inkjet printing technology that is a non-contact and provides a high resolution printing, suitable for sensing devices. The second enhancement strategy based on the use of secondary antibodies can be applied to any other analyte and labels offering in this way new improvements opportunities for various applications

Finally, the current work in progress in our laboratories focused on electrochemical evaluation of gold nanospheres and gold concave nanocubes (see **Annex 1**), may extend their application in electrochemical biosensing systems that employ NP catalytic properties while being used as labels for DNA, protein and cells sensing.

7.3. References

(1) Parolo, C.; Medina-Sánchez, M.; Montón, H.; de la Escosura-Muñiz, A.; Merkoçi, A. *Part. Part. Syst. Charact.* **2013**, *30*, 662–666.

(2) Metters, J. P.; Houssein, S. M.; Kampouris, D. K.; Banks, C. E. *Anal. Methods* **2013**, *5*, 103–110.

Annex A

Electrochemical studies of spherical gold nanoparticles and gold concave nanocubes

Summary

The shape-controlled nanoparticle synthesis has gained importance during last years due to the wide range of fields where the anisotropic nanoparticles can be used, such as optical, (bio)sensing, catalysis and biomedical areas. Typical shape-controlled synthesis involves a two-step process, where small seeds are synthetized and then, larger structures with well-defined morphologies grown over these seeds. In this Annex, we study for the first time the size- and shape-effect on the electrohemical response of gold nanoparticles (AuNPS) using differential pulse voltammetry (DPV) on screen-printed carbon electrodes (SPCEs). Gold Nanospheres (AuNS) and concave nanocubes (AuNC) with sizes ranging from 20 to 50 nm are evaluated. It is found that the high number of unsaturated atoms in the vertices and edges of the AuNC make them more electrocative than the AuNS, allowing to detect lower quantities of nanoparticles. These achievements are very interesting for further applications of the studied concave nanocubes as advantageous novel tags in electrochemical biosensing systems.

A.1. Introduction

Design and shape-control of noble metal nanoparticles have grown during the last years because of their unique size and shape-dependent properties at nanometric scale, such as localized surface plasmon resonance (LSPR) and surface-enhanced Raman scattering (SERS).[1] In the particular case of gold nanoparticles (AuNPs), they are attractive not just for their outstanding properties as nanomaterial but also their biocompatibility, which make them useful in a wide range of biomedical applications.[2–5]

AuNPs can be synthetized in different ways, but the most common method is by chemical or electrochemical reduction of Au (III) precursor. Chemical reduction can be achieved by: a) "*in-situ*" methods were the nucleation and growth occur in the same process, resulting mainly in spherical nanoparticles and b) the "seed-mediated growth" method in which the nucleation and growth occur in separated processes, resulting in shape-controlled nanoparticles.[6,7] Briefly, the "seed-mediated growth" consists in formation of small seed particles as first step followed by the seeds addition to the "growth" solution which contains more gold ions together with stabilizing and reducing agents. In this step, newly reduced Au (0) grows onto the seed surface forming larger nanoparticles with a well-defined shape.[6] However, in order to produce high-quality and reproducibility of anisotropic nanoparticles, experimental conditions must be carefully chosen for seeds and growth solutions. Employing this method, AuNPs in a wide variety of morphologies such as: nanorods[8], octahedra[9], cubes,[9,10] rhombic dodecahedra,[9,11] obtuse triangular bypiramids,[11] nanoprisms[12] and concave cubes[13] have been synthetized.

Gold nanospheres (AuNS) have been extensively used as tags in electrochemical biosensing systems, thanks to their outstanding electroactive properties which allow their detection without previous nanoparticle dissolution in highly oxidative media.[14–19] However, these properties have not been yet evaluated for different shaped AuNPs.

In this context, Mirkin's group[13] described the synthesis and morphology study of gold concave cubes (AuNC), enclosed by 24 high-index facets {720} employing the seed-mediated growth method. The authors reported the influence of the counter ion in the surfactant which produces a different morphology of the nanostructure, obtaining concave cubes by using cetyltrimethylammonium chloride (CTAC). Moreover, they showed a preliminary study about the catalytic performance of these nanostructures in a cyclic voltammetry indicating that concave cubes with {720} facets are more catalytic compared

with the octahedral nanostructure with tightly {111} packed facets because of their lower oxidation peak. However, the direct voltammetric detection of AuNC, their size-effect and comparison with standard gold nanospheres (AuNS) have not been yet evaluated.

In this work, we present for the first time a complete study about the above mentioned electrochemical evaluation of AuNC *vs* AuNS, showing promising results for further application in electrochemical biosensing systems.

A.2. Experimental section

A.2.1. Reagents and apparatus

All the reagents used for preparation of concave gold nanocubes (AuNC) were purchased from Sigma-Aldrich (Spain): hydrogen tetrachloroaurate (III) trihydrate ($HAuCl_4.3H_2O$, 99.9%), silver nitrate ($AgNO_3$, 99.9%), hydrochloric acid (HCl, 37%), L-ascorbic acid ($C_6H_8O_6$, 98%) and cetyltrimethylammonium chloride solution (CTAC, 25%). Spherical gold nanoparticles of 20 and 50 nm were purchased from British Biocell (United Kingdom). Carbon (Electrodag 423SS), silver/silver chloride (Electrodag 6037SS) and blue insulating (Minico 7000) inks were used for fabricating screen-printed carbon electrodes (SPCEs) and purchased from Acheson Industries (The Netherlands). Autostat HT5 polyester sheet for using as electrode platform was purchased from McDermid Autotype (United Kingdom). All the size measurements and shape observation of AuNC were conducted in a Field Emission Gun Transmission Electronic Microscope Fei (TEM, model Tecnai^{TM} G2F20, USA) and in a Field Emission Gun Scanning Electronic Microscope Fei (SEM, model Quanta^{TM} 650, USA). A spectrophotometer SpectraMax M2^e (Molecular Devices, USA) was used to record the UV-Vis spectra of concave cubic and gold nanoparticles. A semi-automatic screen-printing machine DEK248 (DEK International, Switzerland) was used for fabricating the electrodes. A PGSTAT100 (Echo Chemie, The Netherlands) potentiostat/galvanostat was used for electrochemical measurements. The total amount of gold in the AuNC suspension was obtained by inductively coupled plasma-optical emission spectrometry (ICP-OES) analysis at the *Servei d'Anàlisi Química of the Universitat Autónoma de Barcelona* (Spain). Samples were diluted in aqua regia in a microwave digester (CEM Corporation, model MARSXpress, USA) and inserted in the ICP-OES spectrometer (Perkin-Elmer, model Optima 4300DV, USA) to obtain the total content of gold, expressed in mg/L.

A.2.2. Methods

A.2.2.1. Screen-printed carbon electrodes (SPCE) fabrication

The electrochemical transducers used were homemade screen-printed carbon electrodes (SPCEs), consisting of three electrodes: working electrode (WE), reference electrode (RE) and counter electrode (CE). Briefly, a graphite layer was printed onto the polyester sheet, using the screen-printing machine with the stencil. After curing for 15 minutes at 95ºC, an Ag/AgCl layer was printed and cured for 15 minutes at 95ºC. Finally, the insulating ink was printed and cured at 95ºC for 20 minutes. The full size of the sensor strip was 29 mm x 6.7 mm, and the WE diameter was 3 mm.

A.2.2.2. Synthesis of gold concave nanocubes (AuNC)

Gold concave nanocubes (AuNC) were prepared following a procedure previously reported by Mirkin's group.[13] The method consisted in a two-step seed-mediated growth process. First, seed solution was prepared adding 0.60 mL of cold and freshly prepared 0.01 M $NaBH_4$, to a solution that contained 0.25 mL of 0.01M $HAuCl_4$, and 10 mL of 0.1 M CTAC. It was stirred for 1 minute and left undisturbed for two hours. The second step consisted in the growth solution which was prepared by the sequential addition of the following solutions: 0.50 mL of 0.01 M $HAuCl_4$, 0.10 mL of 0.01 M $AgNO_3$, 0.20 mL of 1 M HCl and 0.10 mL of 0.1 M ascorbic acid into 10 mL of 0.1 M CTAC.

Preparation of 20 and 50 nm AuNC consisted in addition of 25 and 1 μL of seeds to the growth solution, respectively. The solutions were stirred for 1 minute and undisturbed overnight.

A.2.2.3. Electrochemical measurements

Each electrochemical measurement was performed dropping 50 μL of nanoparticles (AuNS or AuNC) suspension in 0.1 M HCl solution and leaving it adsorbing for 2 minutes onto the working electrode area.

Electrochemical detection was conducted following a previously optimized procedure.[16] Briefly, it consisted in applying a fix potential of +1.25 V (*vs.* Ag/AgCl) for 2 minutes in order to oxidize the surface of AuNPs from gold (0) to gold (III) and immediately after this step, differential pulse voltammetry (DPV) was performed scanning from +1.25 to 0.00 V (step potential 10 mV/s and modulation amplitude 50 mV). The cathodic peak of

currents recorded at 0.37 V -corresponding to the reduction of gold (III) to gold (0)- was chosen as analytical signal.

Background signals were recorded following the same electrochemical procedure but using an aliquot of 50 μL of 0.1 M HCl.

A.3. Results and discussion

A.3.1 Characterization of concave gold nanocubes (AuNC)

TEM and SEM characterization were conducted in order to measure the size of AuNC and visualize their morphology. An extensive characterization of these nanocubes was reported by Mirkin and co-workers.[13] The sizes of AuNC were determined by the length of their edges. Thus, it was possible to obtain AuNC of 20 ± 3 nm, 24 ± 3 nm, 32 ± 4 nm, 46 ± 8 nm and 51 ± 7 nm. It was also observed that the bigger AuNC exhibited more defined edges and controlled morphology than the smaller ones (see Fig. 1). For AuNS, the sizes obtained for AuNS were 21 ± 3 and 48 ± 5 nm.

It is well known that different factors such as the size, shape and surrounding medium properties have a strong effect on the maximum and bandwidth of surface plasmon band (SPB) which is theoretically described by Mie's theory.[20] In this context, characterization by UV-Vis for 20 and 50 nm AuNCs showed maximum of absorbance at different wavelengths for each particle. While smaller AuNC showed a maximum wavelength at 552 nm, bigger ones exhibited a red-shift up to 648 nm. This behavior is also observed for spherical gold nanoparticles.[20]

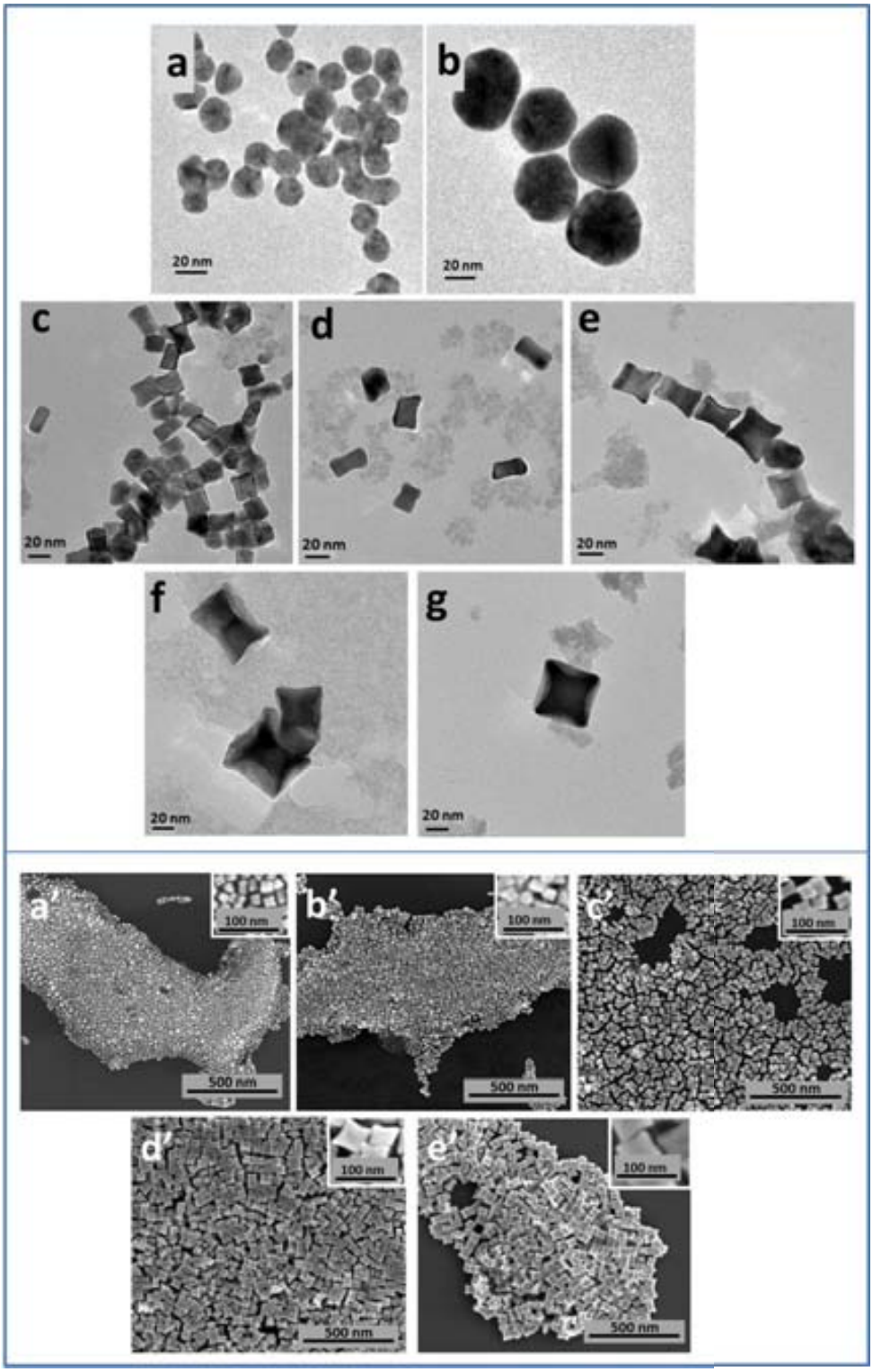

Figure A.1. TEM micrographs corresponding to AuNS of 20 and 50nm (a-b) and to AuNC of 20 (c), 24 (d), 32 (e), 46 (e) and 50 nm (f). Micrographs from c' to e' correspond to SEM analysis of AuNCs in the same range of sizes.

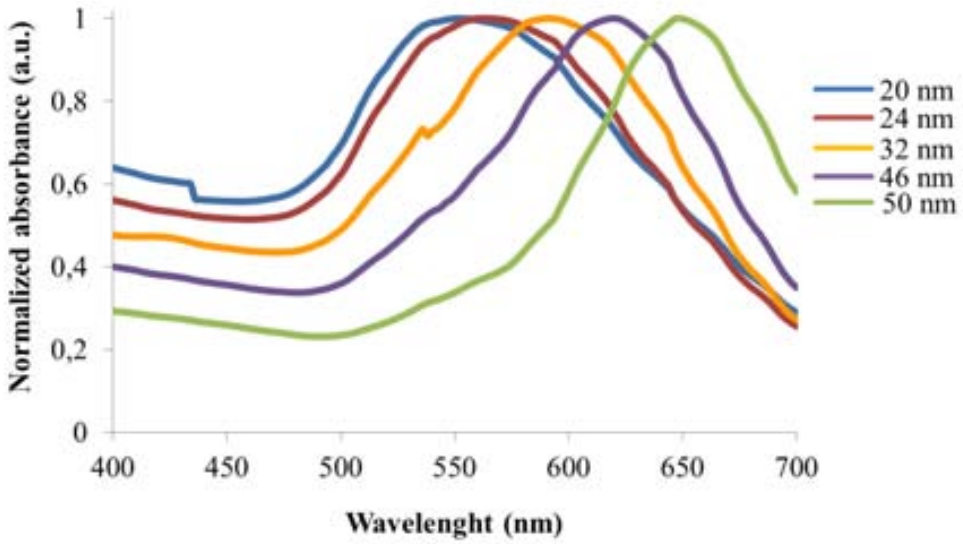

Figure A.2. UV-Vis spectrum for AuNC ranging from 20 to 50 nm.

A.3.2 Electrochemical studies of AuNC: size-effect evaluation

Due to the non-commercial availability of AuNS in the wide range of sizes of the obtained AuNC, 20nm and 50 nm sized nanoparticles were chosen for the comparative study of the size effect on the voltammetric signal. In addition, for electrochemical experiments, it was necessary to normalize the total amount of gold atoms in all gold nanoparticles (AuNS and AuNC) which was calculated by ICP-OES.

Direct electrochemical detection has been reported by our group on graphite-epoxy composite electrodes[21–23] and more recently, on screen-printed carbon electrodes.[24] This electrochemical detection consists mainly in two steps: 1) electrochemical oxidation step in which the outer superficial atoms on gold nanoparticles are oxidized releasing gold (III) ions and 2) electrochemical reduction of gold (III) to gold (0), recording the analytical signal corresponding to the cathodic peak of current associated.

The size-effect on the voltammetric response for the same amount of gold atoms was evaluated for different sized AuNC suspensions in the range between 20-50 nm (see Fig. 3). As expected, the current was lower as the size of AuNC increases since smaller nanocubes have more surface area, so more gold (III) is released on the oxidation step and consequently a higher peak current is observed when the electrochemical reduction step is performed. The same behavior was reported by our group[24] for AuNS for 20-80 nm range.

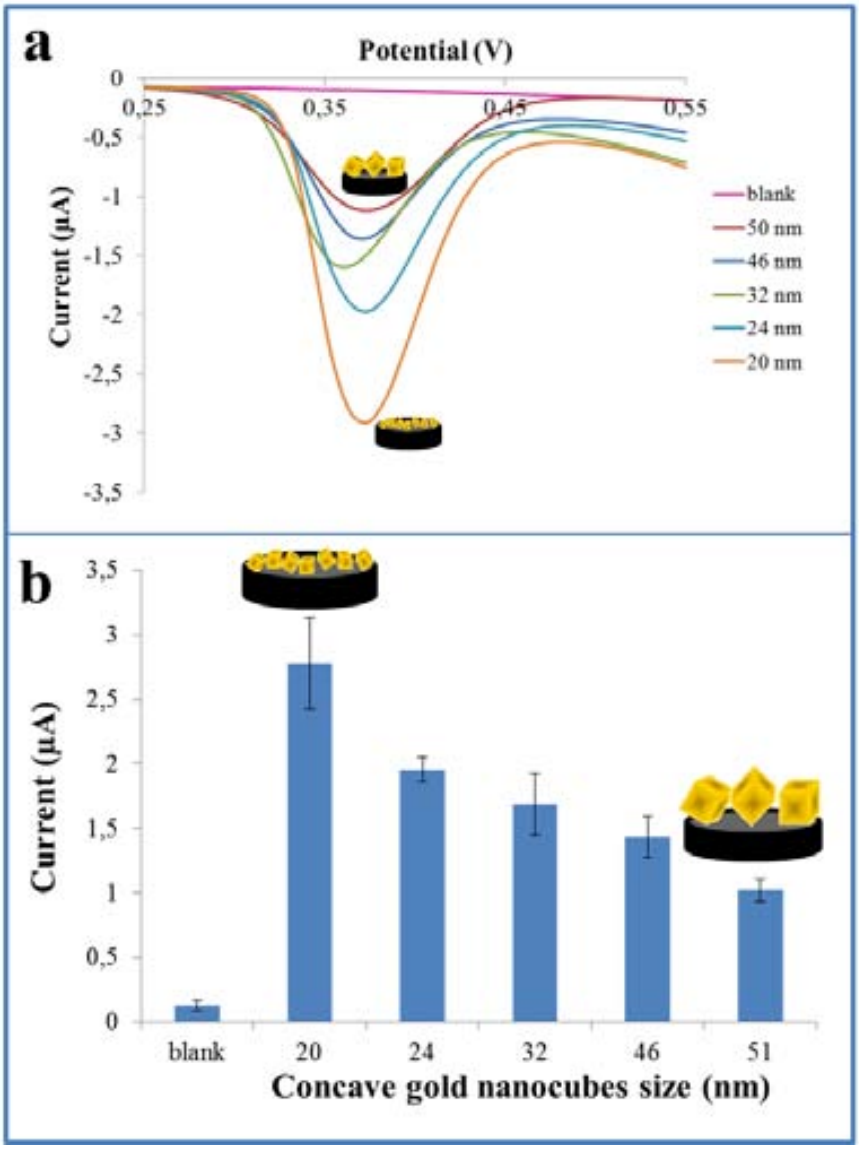

Figure A.3. A) Differential pulse voltammograms for AuNC suspensions of different sizes containing $3.71x10^{16}$ Au atoms/mL. (B) Summary of the relationship between the analytical signal (absolute value of the cathodic peak current) and the AuNC size.

A.3.4 Shape effect evaluation: nanocubes vs nanospheres

A comparative study between AuNC and AuNS is shown in figure 4. The decrease in the voltammetric signal when increasing the nanoparticle size is dramatic in the case of AuNC, as explained in the previous section. However, this decrease is not observed for the AuNS, where in fact a slight increase in the signal is noticed. This contradictory behavior observed for the AuNS could be attributed to the Brownian motions which avoid a better response for smaller particles. In the case of the AuNC, the presence of much higher reactive surface atoms seems to counteract the adverse effect of such motions.

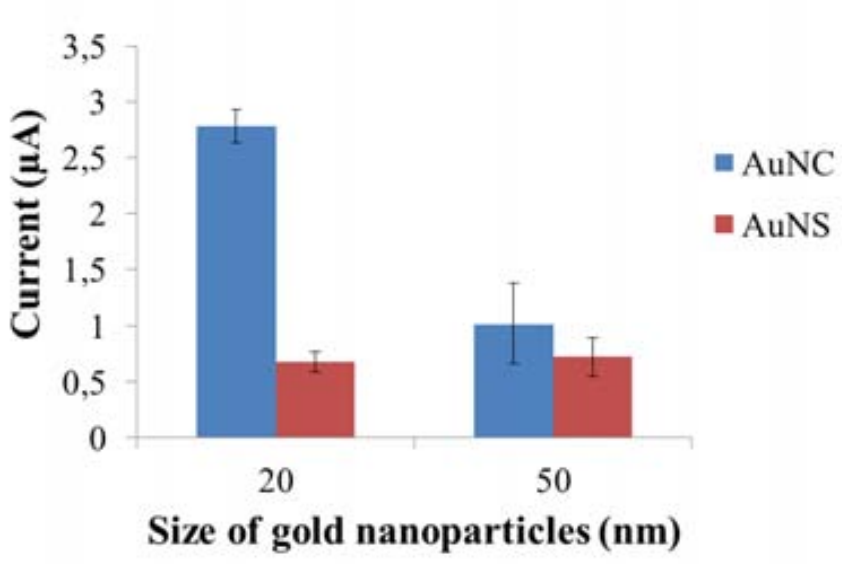

Figure A.4. Comparative study of AuNC and AuNS of 20 and 50nm.

Direct electrochemical detection of AuNPs requires an efficient adsorption on the surface of electrode in order to ensure an appropriate analytical signal. Due to the morphology of the AuNC, with high-index {720} facets, the surface atoms on the edges of nanocubes are easy to be oxidized because of their open atomic arrangement and their low coordinated atoms which act as the catalytically active sites in the structure.[13,25] In consequence, these atoms are able to produce more gold (III) ions during the oxidation step and as a result, a higher current peak is observed than for the similar sized AuNS which have {111} facets.

A.4. Conclusions and perspectives

Narrow sized concave gold nanocubes (AuNC) with sizes of 20 ± 3 nm, 24 ± 3 nm, 32 ± 4 nm, 46 ± 8 nm and 51 ± 7 nm have been successfully prepared and characterized by UV-Vis, TEM and SEM analysis. Electrochemical studies revealed that the high number of unsaturated atoms in the vertices and edges of the AuNC make them more electroactive than gold nanospheres (AuNS). This effect is so strong that counteract the Brownian motions which avoid a better response for small AuNS.

Current work is focused on complementary studies related to High Resolution TEM analysis (HRTEM) and theoretical calculations that could provide additional information about the active surface atoms of AuNC and AuNS. The synthesis and evaluation of nanocubes with flat faces (in contrast with the concave ones) will be proposed.

Due to the optical properties of noble metal nanoparticles, such as gold, coupled with their biocompatible properties, recent efforts have been addressed to combine the synthesis of new plasmonic nanostructures and their possible applications in biosensing field, specifically in point-of-care devices. Despite of the development of LSPR- and SERS-based biosensors in recent years and their incipient commercialization, there is still work to be done, especially because current applications are mainly focused in the properties of these nanomaterials and they are not built around a specific clinical application.

A.5. References

(1) Anker, J. N.; Hall, W. P.; Lyandres, O.; Shah, N. C.; Zhao, J.; Van Duyne, R. P. *Nat. Mater.* **2008**, *7*, 442–453.

(2) Giljohann, D. A.; Seferos, D. S.; Daniel, W. L.; Massich, M. D.; Patel, P. C.; Mirkin, C. A. *Angew. Chem. Int. Ed. Engl.* **2010**, *49*, 3280–3294.

(3) Thakor, A. S.; Jokerst, J.; Zavaleta, C.; Massoud, T. F.; Gambhir, S. S. *Nano Lett.* **2011**, *11*, 4029–4036.

(4) Dykman, L.; Khlebtsov, N. *Chem. Soc. Rev.* **2012**, *41*, 2256–2282.

(5) Dreaden, E. C.; Alkilany, A. M.; Huang, X.; Murphy, C. J.; El-Sayed, M. A. *Chem. Soc. Rev.* **2012**, *41*, 2740–2779.

(6) Grzelczak, M.; Pérez-Juste, J.; Mulvaney, P.; Liz-Marzán, L. M. *Chem. Soc. Rev.* **2008**, *37*, 1783–1791.

(7) Zhao, P.; Li, N.; Astruc, D. *Coord. Chem. Rev.* **2013**, *257*, 638–665.

(8) Nikoobakht, B.; El-Sayed, M. A. *Chem. Mater.* **2003**, *15*, 1957–1962.

(9) Niu, W.; Zheng, S.; Wang, D.; Liu, X.; Li, H.; Han, S.; Chen, J.; Tang, Z.; Xu, G. *J. Am. Chem. Soc.* **2009**, *131*, 697–703.

(10) Sau, T. K.; Murphy, C. J. *J. Am. Chem. Soc.* **2004**, *126*, 8648–8649.

(11) Personick, M. L.; Langille, M. R.; Zhang, J.; Harris, N.; Schatz, G. C.; Mirkin, C. a. *J. Am. Chem. Soc.* **2011**, *133*, 6170–6173.

(12) Millstone, J. E.; Park, S.; Shuford, K. L.; Qin, L.; Schatz, G. C.; Mirkin, C. a. *J. Am. Chem. Soc.* **2005**, *127*, 5312–5313.

(13) Zhang, J.; Langille, M. R.; Personick, M. L.; Zhang, K.; Li, S.; Mirkin, C. A. *J. Am. Chem. Soc.* **2010**, *132*, 14012–14014.

(14) Merkoçi, A. *Biosensensors Bioelectron.* **2010**, *26*, 1164–1177.

(15) Merkoçi, A. *Electroanalysis* **2013**, *25*, 15–27.

(16) Ambrosi, A.; Castañeda, M.; Killard, A.; Smyth, M.; Alegret, S.; Merkoçi, A. *Anal. Chem.* **2007**, *79*, 5232–5240.

(17) De la Escosura-Muñiz, A.; Ambrosi, A.; Merkoçi, A. *Trends Anal. Chem.* **2008**, *27*, 568–584.

(18) De la Escosura-Muñiz, A.; Parolo, C.; Maran, F.; Merkoçi, A. *Nanoscale* **2011**, *3*, 3350–3356.

(19) Maltez-Da Costa, M.; de la Escosura-Muñiz, A.; Nogués, C.; Barrios, L.; Ibáñez, E.; Merkoçi, A. *Nano Lett.* **2012**, *12*, 4164−4171.

(20) Link, S.; El-Sayed, M. A. *J. Phys. Chem. B* **1999**, *103*, 8410–8426.

(21) Pumera, M.; Aldavert, M.; Mills, C.; Merkoçi, A.; Alegret, S. *Electrochim. Acta* **2005**, *50*, 3702–3707.

(22) Pumera, M.; Castañeda, M. T.; Pividori, M. I.; Eritja, R.; Merkoçi, A.; Alegret, S. *Langmuir* **2005**, *21*, 9625–9629.

(23) Ambrosi, A.; Castañeda, M. T.; Killard, A. J.; Smyth, M. R.; Alegret, S.; Merkoçi, A. *Anal. Chem.* **2007**, *79*, 5232–5240.

(24) De la Escosura-Muñiz, A.; Parolo, C.; Maran, F.; Mekoçi, A. *Nanoscale* **2011**, *3*, 3350–3356.

(25) Quan, Z.; Wang, Y.; Fang, J. *Acc. Chem. Res.* **2013**, *46*, 191–202.

Full Paper

Wiley Online Library

ELECTROANALYSIS

Special Issue DIAGNOSTICS

DOI: 10.1002/elan.201400027

Alzheimer Disease Biomarker Detection Through Electrocatalytic Water Oxidation Induced by Iridium Oxide Nanoparticles

Lourdes Rivas,[a, b] Alfredo de la Escosura-Muñiz,[a] Josefina Pons,[b] and Arben Merkoçi*[a, c]

Abstract: Iridium oxide nanoparticles (IrO_2 NPs) synthesized following a previously reported chemical route are presented as novel tags for immunosensing taking advantage of their electrocatalytic activity towards water oxidation reaction (WOR). Cyclic voltammetry and chronoamperometry for the evaluation of the IrO_2 NPs electrocatalytic activity towards WOR at neutral pH were used. The chronoamperometric current recorded at a fixed potential of +1.3 V constituted the analytical signal allowing the quantification of IrO_2 NPs at nM levels. Modification of the surface of citrate-capped IrO_2 NPs with anti-Apolipoprotein E antibodies (αApoE) was successfully achieved and the as-prepared conjugates were used for the electrocatalytic detection of ApoE Alzheimer disease (AD) biomarker in a magnetosandwich immunoassay, reaching a detection limit of 68 ng/mL. Human plasma of a patient suffering AD was also evaluated, estimating an ApoE concentration of 20 μg/mL which is in concordance with the obtained in previously reported approaches. This novel IrO_2 NPs based electrocatalytic assay presents the advantage of the signal generation in the same medium where the immunoassay takes place (PBS, pH 7.4) avoiding the use of additional reagents which also opens the way to future integrated biosensing systems and platforms with interest for other proteins as well as DNA and cells analysis.

Keywords: Iridium oxide nanoparticles · Electrocatalytic activity · Water oxidation reaction (WOR) · Diagnostics · ApoE, Alzheimer

1 Introduction

Recent advances in materials science and, in particular, in the nanomaterials field have opened the way to great achievements in immunosensing technology. Outstanding optical and electrochemical properties of nanoparticle tags have been extensively studied and applied for immunosensing in the last years, offering excellent alternatives to existing conventional strategies/assays with interest in different fields, being the early diagnostics based on sensitive detection of protein biomarkers the most relevant one [1–7]. Of special interest is the possibility to electrochemically detect NP tags, due to the inherent advantages of the electrochemical techniques in terms of sensitivity, selectivity, low cost and ease of use mode, together with the possibility of miniaturization of the detection system [8–10]. NPs such as gold NPs (AuNPs) and quantum dots NPs (QDs) have been used as labels for protein biomarkers detection due to their excellent redox properties, electrocatalytic activity toward several substrates and easy preparation and bioconjugation capabilities [11,12]. However, these approaches often suffer the limitation related to the need of acidic solutions either for the total dissolution of the NP tag followed by stripping voltammetric detection [13–18] or as source of protons for further electrocatalytic detection based on the hydrogen evolution reaction (HER) [19]. The use of such acidic solutions, in addition to inherent security risks, represents an additional step which not only increases the analysis time but also is a crucial limitation in case of really integrated sensing systems, such as those based on lab-on-a-chip or lateral-flow platforms. Hydrogen bubbles formed during hydrogen gas evolution is another inconvenience for the integration of HER based biosensing systems in microfluidics platforms. For these reasons, there is a demand for novel NP tags easy to be detected in the same medium of the immunoreaction, often saline buffers at neutral pH. In this context we consider that NPs able to catalyze water oxidation reaction (WOR) would be ideal candidates for this purpose.

Electrochemical water splitting is composed of two half-cells redox reactions which have been studied separately [20]. While the HER proceeds in two-electron process, the evolution of oxygen from water, WOR, is a more complex endothermic process ($E^\circ = 1.23$ eV at

[a] L. Rivas, A. de la Escosura-Muñiz, A. Merkoçi
ICN2 – Institut Catala de Nanociencia i Nanotecnologia
Campus UAB, 08193 Bellaterra (Barcelona), Spain
tel: +34937374604
*e-mail: arben.merkoci@icn.cat

[b] L. Rivas, J. Pons
Department de Química, Universitat Autónoma de Barcelona
08193, Bellaterra (Barcelona), Spain

[c] A. Merkoçi
ICREA – Institucio Catalana de Recerca i Estudis Avançats
08010 Barcelona, Spain

Supporting Information for this article is available on the WWW under http://dx.doi.org/10.1002/elan.201400027.

pH 0.0) that involves four electrons and formation of an oxygen-oxygen bond.

$$2H_2O \rightarrow O_{2+}4H^+ + 4e^- \quad (1)$$

In nature, the photosynthetic water oxidation is catalyzed by a Mn complex in a membrane protein complex located in photosynthetic organisms [21,22]. Due to its importance, many studies have been carried out so as to understand the mechanism of water splitting and oxygen formation driven naturally [23]. Molecular complexes based on Ru [24–26], Mn [27,28], Ir [29,30]; bulk metal oxides of Co_3O_4 [31,32], RuO_2 and IrO_2[33] and moreover, their nanoparticulated metal oxides [34–38] have been studied in the pursuit of a synthetic catalyst capable to effectively oxidize water. In this context, IrO_2 is a very attractive material to be considered thanks to its catalytic activity, biocompatibility, low resistivity and outstanding chemical and thermal stability which has been used for applications in pH sensors [39,40] and neural stimulation [41,42].

It is well known that nanomaterials exhibit a large surface area that leads to an increase in their reactivity, compared with the bulk material. Due to this property, the catalytic activity of iridium oxide nanoparticles (IrO_2 NPs, stabilized by citrate ions) towards water oxidation reaction, has been tested under photochemical conditions with strong oxidants showing a good catalytic performance [34,35,43]. Citrate capped IrO_2 NPs showed a remarkable catalytic activity toward the WOR when they were self-assembled on an indium tin oxide (ITO) forming an ester layer on the electrode [36].

All these noteworthy features make IrO_2 NPs ideal candidates for using in biosensing field. However, to the best of our knowledge, neither the electrocatalytic activity of IrO_2 NPs in suspension nor their use as tags in biosensing have not been yet evaluated. Their easy to be measured electrocatalytic properties at neutral pH opens the way to their direct detection in the same medium where the immunoreaction takes place (i.e. PBS buffer, pH 7.4), overcoming the above mentioned limitations of other NP-based electrochemical immunosensing systems.

In this work we explore the excellent electrocatalytic activity of IrO_2 NPs toward WOR and employ this as a new signaling route in protein diagnostics. Magnetic beads modified with antibodies are used as platforms of the immunoassay which is applied for the detection of Apolipoprotein E (ApoE), a well-established biomarker of Alzheimer disease (AD) [44,45] which is one of the most common cause of dementia. The use of this novel label is expected to allow a simpler and user-friendlier methodology for biomarkers detection and also to open the way to future integrated biosensing systems and platforms.

2 Experimental

2.1 Materials and Apparatus

Potassium hexachloroiridate (IV) (K_2IrCl_6), sodium hydrogen citrate sesquihydrate ($Na_2C_6H_6O_7 \cdot 1.5H_2O$), sodium hydroxide (NaOH); *N*-(3-dimethylaminopropyl)-*N*′-ethylcarbodiimide hydrochloride (EDC), *N*-hydroxysulfosuccinimide sodium salt (sulfo-NHS), phosphate buffer saline in tablet, 2-(*N*-morpholino)ethanesulfonic acid (MES buffer), Tween 2, bovine serum albumin (BSA), TMB and anti-human IgG-horseradish peroxidase antibodies were purchased from Sigma Aldrich. Carboxyl-modified magnetic beads 2.8 μm sized (MBs) were purchased from Dynal Biotech (Dynabeads M-270, Invitrogen). Capture and detection of monoclonal antibodies anti-ApoE and purified standard ApoE solution were purchased from Mabtech. mQ water, produced using a Milli-Q system ($>18.2\,M\Omega\,cm^{-1}$) purchased from Millipore, was used for the preparation of all solutions. The stirrer used was a TS-100 Thermo shaker (BioSan). A thermostatic centrifuge (Sigma 2-16 PK, Fisher Bioblock Scientific) was used to purify the iridium oxide nanoparticles/antibody conjugates.

Human plasma samples of a patient suffering from Alzheimer disease were provided by the Institute of Neurology of Ulm University (Germany).

The electrochemical transducers used were homemade screen-printed carbon electrodes (SPCEs) and the measurements were performed using a home-made methacrylate cell connected to an Autolab 20 (Eco-Chemie). See the detailed SPCE fabrication procedure at the Supporting Information.

2.2 Synthesis and Characterization of Iridium Oxide Nanoparticles (IrO_2 NPs)

The procedure for the synthesis of iridium oxide nanoparticles is based on Harriman work [34]. Briefly, 30 mg of K_2IrCl_6 were added to 50 mL aqueous solution of 3.8 mM sodium hydrogen citrate. The resulting red-brown solution was adjusted to pH 7.5 using a 0.25 M NaOH and then refluxed with constant stirring for 30 min. After this, the solution changed its color to a light blue, it was cooled at room temperature and the pH of the solution was again adjusted to 7.5. Then, it was stirred and refluxed for 30 min. These steps were repeated until obtaining a constant value of pH 7.5. The solution was additionally refluxed for 2 h with oxygen bubbling through the solution to yield a deep blue suspension of IrO_2 NPs (see Figure S2 at the Supporting Information). All the experiments were conducted with the as-prepared solution that was stored at 4 °C.

The total amount of iridium in the NPs suspension was obtained by analysis with inductively coupled plasma-optical emission spectrometry (ICP-OES) at the *Servei d'Anàlisi Química of the Universitat Autónoma de Barcelona*. Samples were diluted in aqua regia in a microwave di-

gester (CEM Corporation, model MARSXpress) and inserted in the ICP-OES spectrometer (Perkin-Elmer, model Optima 4300DV) to obtain the total content of iridium, expressed in mg/L.

All the sizing measurements and shape characterization of IrO_2 NPs were conducted in a Field Emission Gun Transmission Electronic Microscope (Fei, model Tecnai G2F20). For the sample preparation, 5 μL of the as-prepared IrO_2 NPs dispersion were dropped on a copper grid and let to be dried all the night.

X-ray photoelectron spectroscopy (XPS) experiments were carried out in the *Centres Científics I Tecnològics of the Universitat de Barcelona* (CCiTUB) and were performed with a PHI 5500 Multitechnique System (Physical Electronics) with a monochromatic X-ray source (Aluminium Kα line of 1486.6 eV energy and 350 W), placed perpendicularly to the analyzer axis and calibrated using the $3d_{5/2}$ line of Ag with a full width at half maximum (FWHM) of 0.8 eV. All measurements were made in an ultra-high vacuum (UHV) chamber pressure between 5×10^{-9} and 2×10^{-8} Torr. Binding energies were calibrated respect to the C 1s electron peak at 284.8 eV.

2.3 Conjugation of IrO_2 NPs to αApoE Antibodies

The αApoE antibodies immobilization on IrO_2 NPs was performed by direct random adsorption onto the NP surface. Briefly, 100 μL of 100 μg/mL αApoE monoclonal antibody (αApoE mAb) were added to 1.75 mL of IrO_2 NPs suspension adjusted to pH 7. The resulting solution was incubated for 20 min at 650 rpm. Then, 150 μL of 5% w/v BSA aqueous solution were added and the stirring was continued for other 20 min at 650 rpm. Finally, the solution was centrifuged at 35000×g (4 °C) for 2 hours and 30 minutes. The supernatant was removed and the pellet of IrO_2 NP/αApoE mAb was re-suspended in 200 μL of milliQ water.

The same experimental procedure was previously followed for the conjugation of anti-human IgG-horseradish peroxidase (αHIgG-HRP) antibodies to IrO_2 NPs so as to check the antibody immobilization on the NPs surface. This study was performed by the addition of TMB solution (that acts as HRP substrate) to suspensions of IrO_2 NPs conjugates at different pH values (pH 7, 8 and 9). Typical change of color from colorless to blue was observed when the reaction between the TMB and the HRP labelling the antibodies took place, corresponding to the generation of a cation free-radical as oxidation product. The reaction was stopped by adding H_2SO_4, observing a stronger coloration for the conjugates prepared at pH 7 (see Figure S3 in the Supporting Information), so these conditions were chosen for the preparation of the conjugate between IrO_2 NPs and the αApoE antibody.

2.4 Magnetosandwich Immunoassay for ApoE Capturing and Labeling with IrO_2 NPs

Carboxylated magnetic microbeads were functionalized through the well-known EDC/sulfo-NHs chemistry. EDC was pre-activated by mixing 133 μL of EDC (10 mg/mL) with 25 μL of sulfo-NHS (100 mg/mL) for 10 min (both solutions in 100 mM MES, pH 5). After that, 842 μL of 10 mM MES pH 5 were added forming *Solution 1*. 15 μL of carboxylated magnetic beads were placed in an Eppendorf tube, washed two times in MES buffer and reconstituted in 150 μL of the *Solution 1*. The mixture was incubated at 37 °C for 30 min (700 rpm). Oriented antibody immobilization was performed by adapting a procedure previously optimized in our group [46]. Briefly, after washing two times in MES buffer, 30 μL of a 300 μg/mL monoclonal goat αApoE antibody solution and 120 μL of 10 mM MES, pH 5, were added to the microspheres and incubated at 37 °C for 1 h (700 rpm). After washing two times in MES buffer, 150 μL of 5% BSA (in MES buffer) were added to the microspheres and incubated first at 25 °C for 20 min (700 rpm) and then at 4 °C overnight.

After washing two times in PBS-Tween buffer and once in PBS buffer, 150 μL of recombinant ApoE standard in PBS buffer was added to the microspheres and incubated at 25 °C for 20 min (700 rpm). After washing two times in PBS-Tween buffer and once in PBS buffer, 150 μL of the previously synthesized IrO_2 NPs/ αApoE antibody were added to the microspheres and incubated at 25 °C for 20 min (700 rpm). The magnetic conjugate was washed four times in PBS-Tween 20 buffer, two times in PBS, once in water and reconstituted in 150 μL of 0.1 M PBS.

In the case of the analysis of human plasma samples, the same experimental procedure was followed, using serial diluted plasma samples in PBS buffer instead of the standard of ApoE.

2.5 Electrochemical Measurements

Each electrochemical measurement was performed after dropping 50 μL of IrO_2 NPs suspension in 0.1 M PBS pH 7.4 freshly prepared onto the SPCE. Blank signals were recorded following the same electrochemical procedure but using an aliquot of buffer. Cyclic voltammetry (CV) was carried out from −0.5 V to +1.3 V at 50 mV s^{-1} and chronoamperometry was performed at a fixed potential of +1.3 V during 300 s.

The electrochemical detection of ApoE captured through the magnetosandwich immunoassay was evaluated through the water oxidation reaction. Briefly, 50 μL of the immunocomplex suspension were placed on the surface of the screen-printed carbon electrode (SPCE), where a magnet was previously attached to polyester on the reverse side of the working area. An oxidative potential of +1.3 V was applied during 300 s. The water oxidation catalyzed by the IrO_2 NPs tags was chronoamperometrically followed measuring the current generated

during the time. The absolute value of the current at 250 s was chosen as the analytical signal. For all the experiments, the measurements were made by triplicate at room temperature.

3 Results and Discussion

3.1 Characterization of IrO_2 NPs

Characterization of IrO_2 NPs was conducted through different techniques such as UV-visible spectrophotometry (UV-Vis), transmission electronic microscopy (TEM) and X-ray photoelectron spectroscopy (XPS). Hydrolysis of hexachloroiridate (IV) ion, $[IrCl_6]^{2-}$, in neutral aqueous solutions in the presence of citrate ions, results in formation of deep blue suspension of nanoparticles of $IrO_2.xH_2O$[34] (for simplicity, they will be denoted as IrO_2). TEM micrographs reveal the homogeneous distribution of IrO_2 NPs (see Figure 1) and is worthy to note the homogeneous size of observed agglomerates of 12.5 ± 2.5 nm composed by smaller nanoparticles of 1.5 ± 0.3 nm. This suggests that the initially formed small nanoparticles quickly form bigger agglomerates. This behavior is in agreement with previously reported studies [35,47].

UV-Vis spectrum of IrO_2 NPs is shown in Figure 1B, where a broad peak between 500–700 nm with maximum at 590 nm, characteristic of Ir(IV) oxides and IrO_2 NPs is observed.[34]

XPS analyses were performed in order to confirm the chemical composition of the synthesized IrO_2 NPs (see Figure 1C, left). By deconvoluting the XPS spectra, two binding states for iridium are identified as $4f_{7/2}$ and $4f_{5/2}$ at 62.3 and 65.1 eV, respectively. These peaks are attributed to the 4+ oxidation state of iridium and they are similar to those of IrO_2 nanorods (62.0 and 65.0 eV) and similar to IrO_2 single crystal (which has values of 61.7 and 64.7 eV) [48]. Regarding the oxygen 1s signal, a main peak at 531.6 and a small one at 533.7 eV were observed as shown in Figure 1C (right). The former is similar to the value found for IrO_2 nanorods and IrO_2 single crystal,

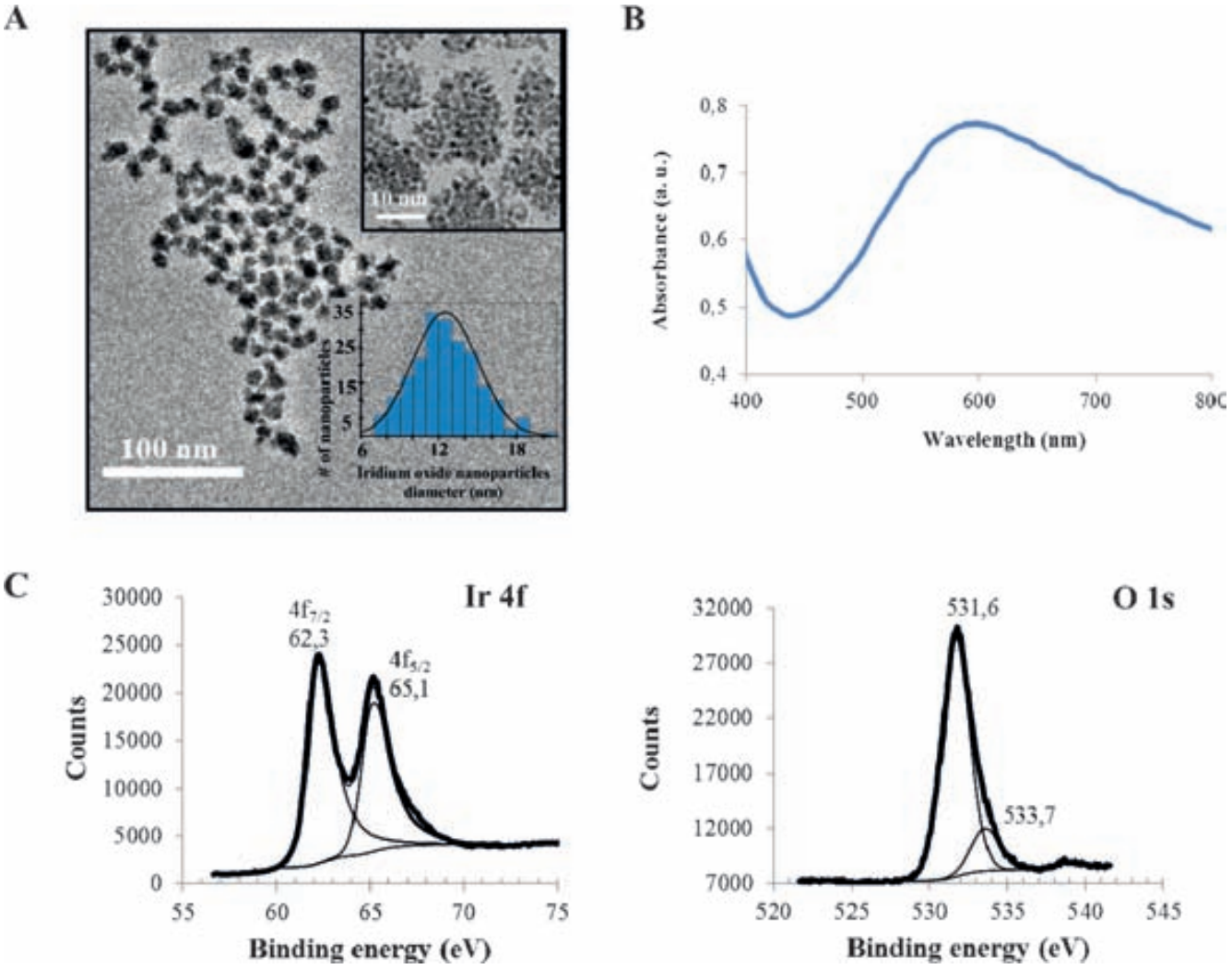

Fig. 1. Characterization of IrO_2 NPs. (A) TEM micrographs, (B) UV-Vis spectrum, (C) XPS analysis: spectrum for Ir 4f line (left) and O 1s line (right).

both at 530.5 eV [48]. The broader feature at 533.7 eV might be attributed to the oxygen-containing citrate coating these nanoparticles.

According to the mentioned characterization, especially with the XPS analyses, it is possible to conclude that the deep-blue suspension synthesized corresponds to IrO_2 nanoparticles.

The concentration of iridium oxide stock solution was calculated to be around 35 nM using the concentration of Ir obtained by ICP-OES (0.227 mg/mL; 1.18 mM) divided by the number of atoms per particle (N) as stated in Supporting Information.

3.2 Electrocatalytic Activity of IrO_2 NPs Towards WOR

The electrocatalytic activity of IrO_2 NPs towards water oxidation reaction was first evaluated by cyclic voltammetry (CV) using screen-printed carbon electrodes (SPCE).

CV voltammograms were conducted in 0.1 M PBS pH 7.4 and obtained by scanning from +0.1 to +1.3 V at 50 mV/s scan rate. The as-performed voltammograms for different concentrations of IrO_2 NPs in 0.1 M PBS are shown in Figure 2A. The background curve (a) shows that the oxidation of the medium's oxygen starts at approximately +1.10 V. In the presence of the IrO_2 NPs (curves b–e) on the surface of the electrode, the potential for water oxidation shifts (by up to 300 mV, depending on the concentration of IrO_2 NPs) toward less positive potentials. Moreover, it can also be seen that, because of the catalytic effect of the IrO_2 NPs, a higher current is generated (up to 70 μA higher, as evaluated for the potential value of +1.3 V, depending on the concentration of IrO_2 NPs). A shift in the half-wave potential of the WOR to less positive potentials from 1.1 V to up to 0.77 V (maximum shift of 332 mV) which is proportional to the quantity of IrO_2 NPs due to their catalytic effect towards this reaction can also be observed in the same figure.

The obtained results show that, for a fixed potential (i.e., +1.3 V at which steady state currents values are achieved), the intensity of the current recorded in chronoamperometric mode during the stage of oxygen electro-oxidation (Figure 2B) can be related to the presence (curves b′–e′) or absence (curve a′) of IrO_2 NPs on the surface of the SPCE. A proportional increase of the catalytic current for increasing concentrations of IrO_2 NPs (from 0.7 to 35 nM) was observed.

Regarding the fixed interval of time selected for the current recording (analytical signal), it was observed that for intervals shorter than 250 s the current profiles were not reproducible. Looking at the behavior during the first 50 s, a rapid decrease in the anodic current was observed, probably due to an initial rapid oxidation of water on the surface of the IrO_2 NPs catalyzers followed by a current stabilization. This effect is more evident for higher IrO_2 NPs concentrations (curves d′ and e′). The observed irreproducibility during the 50–250 s range could be attributed to the fact that IrO_2 NPs are still not accommodated

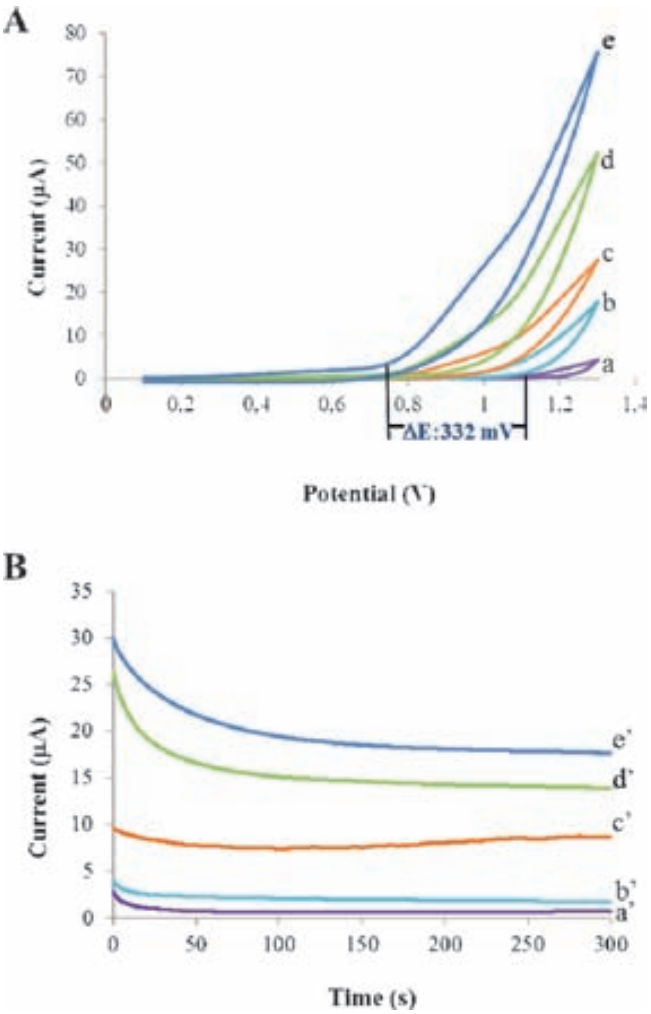

Fig. 2. Electrocatalytic activity of IrO_2 NPs towards WOR. (A) Cyclic voltammograms recorded from +0.1 to +1.3 V at a scan rate of 50 mV/s for 0.1 M PBS (blank curve, a) and for increasing concentrations of IrO_2 NPs in 0.1 M PBS pH 7.4: (b) 0.7, (c) 1.8, (d) 7 and (e) 35 nM. (B) Chronoamperograms recorded at +1.3 V during 300 s using a 0.1 M PBS pH 7.4 (blank curve, a) and the same IrO_2 NPs concentrations as detailed above (b′–e′) in 0.1 M PBS.

onto the electrode surface being still under Brownian motions (stabilization time). The current value was stable in all cases after 250 s, so registering at this time interval was chosen as analytical signal.

A logarithmic relationship between the analytical signal and the concentration of IrO_2 NPs in the range of 0.7–35 nM adjusted to the following equation:

$$\text{Current } (\mu A) = 3.15 \ln[IrO_2 \text{ NPs } (nM)] + 8.13 \quad (2)$$

showing a good correlation ($r = 0.98$) and a relative standard deviation of 5.6 % for 7 nM of IrO_2 NPs ($n = 3$). The limit of detection was calculated as the concentration of IrO_2 NPs corresponding to three times the standard deviation of the estimated, giving a value of 0.13 nM.

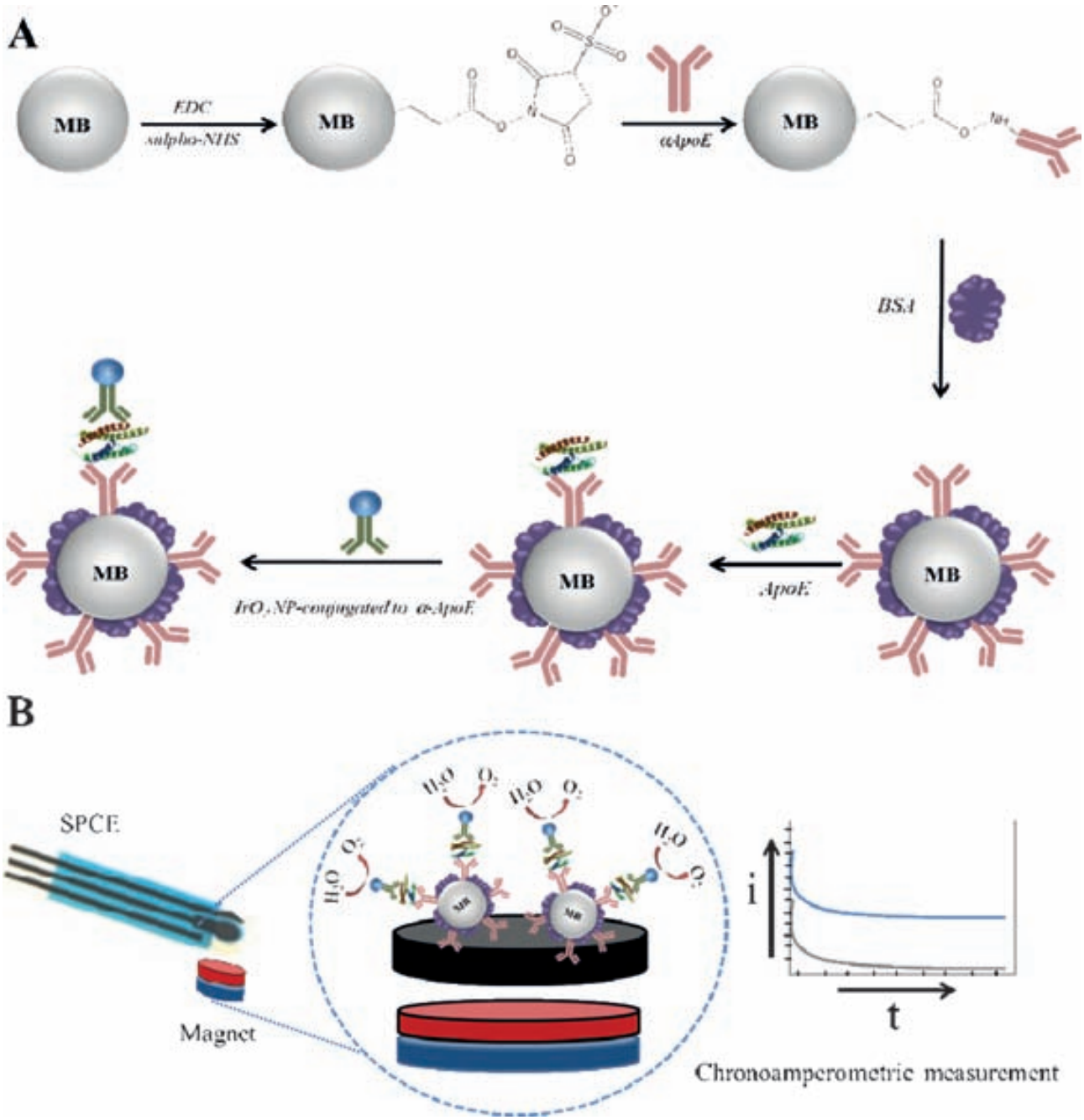

Fig. 3. Schematics, not in scale, of: (A) experimental procedure of the magnetosandwich immunoassay using IrO_2 NPs tags and (B) electrochemical detection procedure based on the electrocatalytic water oxidation.

3.3 Electrocatalytic Detection of ApoE Alzheimer Disease Biomarker in Human Plasma

Magnetic beads were used as platforms of the immunoassays for ApoE detection, taking advantage of their well-known characteristics for capturing/pre-concentrating the analyte and minimizing matrix effects. Carboxylated magnetic beads were modified with αApoE antibody using the EDC-sulfo-NHS coupling. First, EDC was used in order to activate the carboxylic groups located on the surface of magnetic beads. Then, addition of sulfo-NHS led to formation of a stable sulfo-ester, which reacts with the amine groups located in the antibody, allowing forming of the αApoE modified magnetic beads (αApoE-MB). Blocking with BSA is performed in order to avoid unspecific absorptions onto the surface of the electrotransducer. When ApoE is present in the sample, it is recognized by the αApoE antibody forming the ApoE/αApoE-MB complex.

Once the washing step is performed, the conjugate of αApoE-IrO_2 NPs is able to recognize the ApoE , forming the magnetosandwich αApoE-IrO_2 NPs/ApoE/αApoE-MB, being the amount of IrO_2 NPs proportional to the ApoE concentration in the sample.

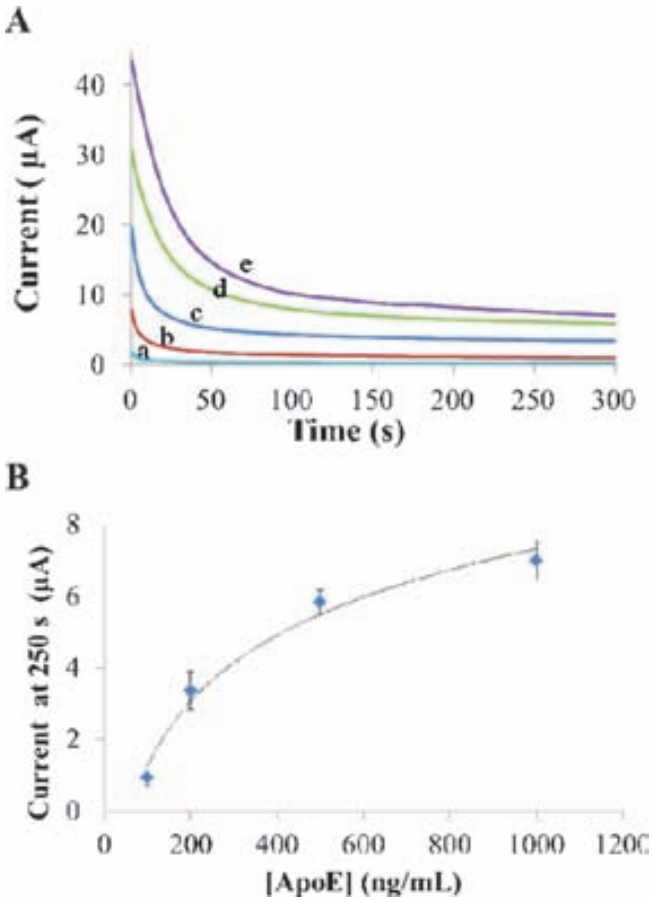

Fig. 4. (A) Chronoamperograms recorded in PBS 0.1 M pH 7.4 at a fixed potential of +1.3 V, for a control sample (blank curve, a) and for samples containing 100 (b), 200 (c), 500 (d) and 1000 (e) ng/mL of ApoE. (B) Relationship between the ApoE concentration and the value of the analytical signal (catalytic current recorded at 250 s). Samples correspond to the magnetosandwich prepared as detailed in Experimental.

Electrochemical detection of ApoE was carried out using 50 μL of the immunocomplex suspension placed onto the surface of the SPCE and taking advantage of the electrocatalytic properties of IrO_2 NPs towards WOR. The catalytic behavior of the IrO_2 NPs towards the oxidation of water is conducted by chronoamperometry and correlated to the amount of the ApoE in the sample. Figure 4A shows the chronoamperograms obtained for samples containing 0 (a) , 100 (b), 200 (c), 500 (d) and 1000 (e) ng/mL of ApoE. As expected, the catalytic current increases when the concentration of ApoE increases. The relationship between the concentration of ApoE in the sample and the value of the analytical signal (current recorded at 250 s) is adjusted to a logarithmic curve, as shown in Figure 4B. The curve exhibits a good correlation ($r=0.98$) in the range of 100–1000 ng/mL, adjusted to the following equation:

$$\text{Current } (\mu A) = 2.64\ [\text{ApoE } (ng/mL)] - 10.94 \quad (3)$$

The limit of detection, calculated as stated before, gives a value of 68 ng/mL. The reproducibility of the responses ($n=3$) for 500 ng/mL of ApoE shows a relative standard deviation of 6%.

Finally, a human plasma sample with an unknown concentration of ApoE was electrocatalytically analyzed. As ApoE concentration in plasma typically ranges from 16 to 169 μg/mL [49], very small volumes of plasma were diluted in PBS buffer before analysis. A dilution of the sample of 1:1000 was necessary to obtain a current within the linear range of the method, obtaining a value of 3.08 ± 0.18 μA ($n=3$) for such a dilution. Extrapolating this value from Equation 3, a concentration of ApoE of 20 ± 2 μg/mL was estimated in the sample. Matrix effects are not relevant in our assay due to two main factors. First of all, possible interfering substances are highly diluted in the analyzed sample (1:1000). Furthermore, and more importantly, the use of magnetic bead platforms modified with an specific antibody allow us to capture the ApoE protein and then separate the magnetic bead/ApoE complex from the matrix of the sample, thanks to the use of a magnetic field. Magnetic beads are conveniently blocked before with BSA so as to avoid unspecific absorptions. The final measurements are performed in PBS buffer, so not background contributions are neither found at the +1.3 V voltage applied.

The obtained results are in concordance with the above mentioned expected data and also with those previously obtained in our group using both microarray technology [50] and electrochemical detection [51] based on commercial Quantum Dot tags.

4 Conclusions

Iridium oxide nanoparticles (IrO_2 NPs) of 12 nm size were successfully synthesized, characterized and used as novel electrocatalytic tags for immunosensing. The stable NPs suspension exhibited a high catalytic effect towards the Water Oxidation Reaction (WOR), allowing their sensitive quantification at neutral pH in a simple chroroamperometric mode. This sensitive method was applied for the evaluation of ApoE in human plasma following an immunoassay format using IrO_2 NPs as advantageous tags, able to be detected in the same buffer where the immunoreaction takes place.

Both the IrO_2 NPs tags and electrocatalytic detection method present many advantages compared with previously reported ones based on quantum dots (QDs) or Hydrogen Evolution Reaction (HER) . On the one hand, the NP synthesis procedure is simpler and cheaper than *i.e.* the required for QDs preparation. Furthermore, the chronoamperometric detection based on the WOR is a simple, sensitive and quantitative methodology that can be performed in the same medium of the immunoreaction, avoiding the addition of acidic and hazardous solutions, (along with H_2 bubbles formation undesired in microfluidics), usually required for electrochemical detection of other NP tags (ex. AuNP using HER). These advantageous properties open the way to further applications in really integrated sensing systems, such as those

based on lab-on-a-chip or lateral flow platforms. Moreover, the UV-Vis absorption band observed at 590 nm (deep blue color) of the IrO_2 NPs suspension make these NPs excellent candidates for dual electrochemical/optical detection systems in future lateral flow biodetection platforms.

This novel methodology can be extended for the detection of other AD biomarkers (i.e. β-amyloid) representing a simple, rapid and sensitive alternative for AD diagnostics. Furthermore, it opens the way to future integrated biosensing systems and platforms with interest for other proteins as well as DNA and cells analysis.

Acknowledgements

We acknowledge the support from *MINECO* (Spain) under Project MAT2011–25870 and the *E.U.* under FP7 Contract No. 246513 "NADINE". Prof. Dr. *Markus Otto* from the Institute of Neurology of Ulm University (Germany) is also acknowledged for kindly providing the human serum samples of a patient suffering from Alzheimer disease.

References

[1] A. de la Escosura-Muñiz, C. Parolo, A. Merkoçi, *Mater. Today* **2010**, *13*, 24.
[2] L. Dykman, N. Khlebtsov, *Chem. Soc. Rev.* **2012**, *41*, 2256.
[3] E. C. Dreaden, A. M. Alkilany, X. Huang, C. J. Murphy, M. A. El-Sayed, *Chem. Soc. Rev.* **2012**, *41*, 2740.
[4] A. Walcarius, S. D. Minteer, J. Wang, Y. Lin, A. Merkoçi, *J. Mater. Chem. B* **2013**, *1*, 4878.
[5] A. Ambrosi, M. T. Castañeda, A. de la Escosura-Muñiz, A. Merkoçi, in *Biosensing using nanomaterials-Bionano* (Ed: A. Merkoçi), Wiley-Interscience, New York **2009**, pp. 177–197.
[6] A. Merkoci, A. Ambrosi, A. de la Escosura, B. Pérez, M. Guix, M. Maltez, S. Marin, in *Encyclopedia of Analytical Chemistry* (Ed: R. A. Meyers), Wiley, Chichester **2010**, pp. 1–26
[7] A. Merkoci, *Biosensens. Bioelectron.* **2010**, *26*, 1164.
[8] A. de la Escosura-Muñiz, A. Ambrosi, A. Merkoçi, *Trends Anal. Chem.* **2008**, *27*, 568.
[9] A. Merkoçi, *Electroanalysis* **2013**, *25*, 15.
[10] A. Merkoçi, *FEBS J.* **2007**, *274*, 310.
[11] A. de la Escosura-Muñiz, A. Merkoçi, *Expert Opin. Med. Diagn.* **2010**, *4*, 21.
[12] D. Tang, Y. Cui, G. Chen, *Analyst* **2013**, *138*, 981.
[13] M. Dequaire, C. Degrand, B. Limoges, *Anal. Chem.* **2000**, *72*, 5521.
[14] N. Zhu, A. Zhang, Q. Wang, P. He, Y. Fang, *Electroanalysis* **2004**, *16*, 577.
[15] R. Cui, H. C. Pan, J. J. Zhu, H. Y. Chen, *Anal. Chem.* **2007**, *79*, 8494.
[16] J. Wang, G. Li, A. Merkoçi, *J. Am. Chem. Soc.* **2003**, *125*, 3214.
[17] M. T. Castañeda, S. Alegret, A. Merkoçi, *Electroanalysis* **2007**, *19*, 743.
[18] A. Ambrosi, M. T. Castañeda, A. J. Killard, M. R. Smyth, S. Alegret, A. Merkoçi, *Anal. Chem.* **2007**, *79*, 5232.
[19] A. de la Escosura-Muñiz, C. Sánchez-Espinel, B. Díaz-Freitas, A. González-Fernández, M. Maltez-Da Costa, A. Merkoçi, *Anal. Chem.* **2009**, *81*, 10268.
[20] H. Dau, C. Limberg, T. Reier, M. Risch, S. Roggan, P. Strasser, *ChemCatChem* **2010**, *2*, 724.
[21] T. J. Meyer, *Nature* **2008**, *451*, 778.
[22] Y. Umena, K. Kawakami, J. R. Shen, N. Kamiya, *Nature* **2011**, *473*, 55.
[23] K. S. Joya, Y. F. Joya, K. Ocakoglu, R. van de Krol, *Angew. Chemie, Int. Ed.* **2013**, *52*, 10426.
[24] C. Sens, I. Romero, M. Rodríguez, A. Llobet, T. Parella, J. Benet-Buchholz, *J. Am. Chem. Soc.* **2004**, *126*, 7798.
[25] S. Romain, L. Vigara, A. Llobet, *Acc. Chem. Res.* **2009**, *42*, 1944.
[26] L. Duan, F. Bozoglian, S. Mandal, B. Stewart, T. Privalov, A. Llobet, L. Sun, *Nat. Chem.* **2012**, *4*, 418.
[27] P. Kurz, G. Berggren, M. F. Anderlund, S. Styring, *Dalt. Trans.* **2007**, 4258.
[28] E. A. Karlsson, B. L. Lee, T. Akerman, E. Jhonston, M. Kärkäs, J. Sun, Ö. Hannson, J. E. Bäckwall, B. Akerman, *Angew. Chemie* **2011**, *123*, 11919.
[29] N. D. McDaniel, F. J. Coughlin, L. L. Tinker, S. Bernhard, *J. Am. Chem. Soc.* **2008**, *130*, 210.
[30] H. Junge, N. Marquet, A. Kammer, S. Denurra, M. Bauer, S. Wohlrab, F. Gärtner, M. Pohl, A. Spannenberg, S. Gladiali, M. Beller, *Chemistry* **2012**, *18*, 12749.
[31] A. Harriman, I. J. Pickering, J. M. Thomas, P. A. Christensen, *J. Chem. Soc. Faraday Trans. I* **1988**, *84*, 2795.
[32] R. N. Singh, D. Mishra, A. S. K. Anindita, A. Singh, *Electrochem. commun.* **2007**, *9*, 1369.
[33] S. Trasatti, *J. Electroanal. Chem. Interfacial Electrochem.* **1980**, *111*, 125.
[34] A. Harriman, J. M. Thomas, *New J. Chem.* **1987**, *11*, 757.
[35] M. Hara, T. E. Mallouk, *Chem. Commun.* **2000**, 1903.
[36] M. Yagi, E. Tomita, S. Sakita, T. Kuwabara, K. Nagai, *J. Phys. Chem. B* **2005**, *109*, 21489.
[37] Y. Zhao, E. A. Hernandez-Pagan, N. M. Vargas-Barbosa, J. L. Dysart, T. E. Mallouk, *J. Phys. Chem. Lett.* **2011**, 402.
[38] Y. Lee, J. Suntivich, K. J. May, E. E. Perry, Y. Shao-horn, *J. Phys. Chem. Lett.* **2012**, *3*, 399.
[39] D. O'Hare, K. H. Parker, C. P. Winlove, *Med. Eng. Phys.* **2006**, *28*, 982.
[40] W. D. Huang, H. Cao, S. Deb, M. Chiao, J. C. Chiao, *Sens. Actuators A* **2011**, *169*, 1.
[41] Y. Lu, T. Wang, Z. Cai, Y. Cao, H. Yang, Y. Y. Duan, *Sens. Actuators B Chem.* **2009**, *137*, 334.
[42] K. Göbbels, T. Kuenzel, A. van Ooyen, W. Baumgartner, U. Schnakenberg, P. Bräunig, *Biomaterials* **2010**, *31*, 1055.
[43] M. Hara, C. C. Waraksa, J. T. Lean, B. A. Lewis, T. E. Mallouk, *J. Phys. Chem. A* **2000**, *104*, 5275.
[44] J. Kim, J. M. Basak, D. M. Holtzman, *Neuron* **2011**, *63*, 287.
[45] I. Reinvang, T. Espeseth, L. T. Westlye, *Neurosci. Biobehav. Rev.* **2013**, *37*, 1322.
[46] C. Parolo, A. de la Escosura-Muñiz, E. Polo, V. Grazu, J. De La Fuente, A. Merkoçi, *ACS Appl. Mater. Interfaces* **2013**, *5*, 10753.
[47] S. J. Kwon, F. R. Fan, A. J. Bard, *J. Am. Chem. Soc.* **2010**, *132*, 13165.
[48] R. S. Chen, Y. Huang, Y. M. Liang, D. S. Tsai, Y. Chi, J. J. Kai, *J. Mater. Chem.* **2003**, *13*, 2525.
[49] M. Vicent-Viry, F. Schiele, R. Gueguen, K. Bohnet, S. Visvikis, *Clin. Chem.* **1998**, *44*, 957.
[50] E. Morales-Narváez, H. Montón, A. Fomicheva, A. Merkoçi, *Anal. Chem.* **2012**, *84*, 6821.
[51] M. Medina-Sánchez, S. Miserere, E. Morales-Narváez, A. Merkoçi, *Biosens. Bioelectron.* **2014**, *54*, 279.

Received: January 20, 2014
Accepted: February 11, 2014
Published online: April 3, 2014

Lab on a Chip

PAPER

View Article Online
View Journal

Cite this: DOI: 10.1039/c4lc00972j

Improving sensitivity of gold nanoparticle-based lateral flow assays by using wax-printed pillars as delay barriers of microfluidics†

Lourdes Rivas,[ab] Mariana Medina-Sánchez,[a] Alfredo de la Escosura-Muñiz[a] and Arben Merkoçi*[ac]

Received 20th August 2014,
Accepted 5th September 2014

DOI: 10.1039/c4lc00972j

www.rsc.org/loc

Although lateral flow assays (LFAs) are currently being used in some point-of-care applications (POC), they cannot still be extended to a broader range of analytes for which higher sensitivities and lower detection limits are required. To overcome such drawbacks, we propose here a simple and facile alternative based on the use of delay hydrophobic barriers fabricated by wax printing so as to improve LFA sensitivity. Several wax pillar patterns were printed onto the nitrocellulose membrane in order to produce delays as well as pseudoturbulence in the microcapillary flow. The effect of the proposed wax pillar-modified devices was also mathematically simulated, corroborating the experimental results obtained for the different patterns tested afterwards for detection of HIgG as model protein in a gold nanoparticle-based LFA. The effect of the introduction of such wax-printed pillars was a sensitivity improvement of almost 3-fold compared to the sensitivity of a conventional free-barrier LFA.

Introduction

Constituted mainly of cellulose fibers, paper is very attractive for fabricating biosensors because of its low cost, flexibility and light weight, which make it useful for transport and storage. In addition, it has the capability to wick liquids *via* capillary action without the use of external pumps and its biocompatibility makes it suitable for immobilizing biomolecules, *e.g.* proteins.[1]

The use of paper for fabrication of diagnostic devices has gained much interest due to the necessity to use low-cost materials for single use, simplifying the fabrication process. Paper-based microfluidics is an emerging technology which uses paper as the substrate, creating complex patterns of hydrophilic channels and hydrophobic barriers by using patterning techniques such as photolithography,[2] wax patterning,[3,4] inkjet etching,[5] flexographic printing[6] and screen printing.[7]

The first paper-based sensor considered was the paper chromatography developed by Martin and Synge at the beginning of 1940s.[8] Fifteen years later, the first semi-quantitative paper-based biosensor for detection of glucose in urine[9] became the most common commercially available point-of-care (POC) lateral flow assay (LFA) device. Initially, the main application of LFAs was as a pregnancy test,[10] while nowadays their applications is extended to a wide variety of analytes that include cancer biomarkers,[11,12] DNA,[13,14] toxins[15,16] and metals.[17,18]

LFAs are characterized by their simple use, rapid result, low cost, good specificity and long shelf life. However, they suffer from analytical performance limitations mainly due to sensitivity and reproducibility issues. In this context, many efforts have been made in order to improve LFA sensitivity by using different alternatives such as immunogold silver staining,[19] dual gold nanoparticle (AuNP) conjugates[20] and AuNP loaded with enzymes.[21] Besides AuNPs, other labels such as fluorescent Eu(III) nanoparticles[22] and quantum dots[23] have been also reported. Changes in the paper architecture have also been proposed for improving the performance of LFAs.[24]

The most important part of a LFA is the detection membrane, which is made of cellulose nitrate or nitrocellulose (NC), a porous material where the capture reagents (*e.g.* antibodies) are immobilized due to a possible combination of electrostatic and hydrophobic forces.[25] In fact, NC has been widely used in blotting techniques due to its capacity to interact with proteins, DNA and RNA.[26] Wax printing is a simple and low-cost patterning technique based on the melting of solid wax printed onto the porous substrate, which

[a] *ICN2 – Nanobioelectronics & Biosensors Group, Institut Catala de Nanociencia i Nanotecnologia, Campus UAB, 08193 Bellaterra, Barcelona, Spain. E-mail: arben.merkoci@icn.cat; Tel: +34937374604*

[b] *Departament de Química, Universitat Autònoma de Barcelona, 08193, Bellaterra, Barcelona, Spain*

[c] *ICREA – Institucio Catalana de Recerca i Estudis Avançats, 08010 Barcelona, Spain*

† Electronic supplementary information (ESI) available. See DOI: 10.1039/c4lc00972j

has been used for fabricating paper-based microfluidics in the NC membrane and applied in protein patterning and dot immunoassay.[4] Recent reports have demonstrated the possibility of controlling the reagent transport by using novel and sensitive methods such as dissolvable barriers[27,28] and bridges made of sugars,[29] fluidic diodes and valves[30] and tunable delay shunts.[31] Despite their capability to improve the performance of paper-based devices, which is related to their sensitivity, some of these methods are time consuming and require more reagents for fabricating the devices.

We present here a new strategy for improving the sensitivity of gold nanoparticle-based lateral flow assays by using barriers (pillars) deposited onto the nitrocellulose membrane by a wax printing technique. Different pillar designs were printed in order to create hydrophobic barriers that can cause flow delay. To check the efficiency of such pillars, we used membranes with relatively fast flow so as to obtain higher sensitivity and low detection limits. The controlled delays in microfluidics increase the binding time between the immunocomplex and the detection antibody, in addition to the generation of pseudoturbulence in the pillar zone which improves mixing between the analyte and the labeled antibody. This microfluidic delay in certain zones (incubation areas) combined with the generation of pseudoturbulence directly affects the analytical performance of the LFA, resulting in a better sensitivity and detection limit.

Materials and methods

Chemicals and equipment

Hydrogen tetrachloroaurate(III) trihydrate ($HAuCl_4 \cdot 3H_2O$, 99.9%), trisodium citrate ($Na_3C_6H_5O_7 \cdot 2H_2O$), phosphate buffered saline tablet (P4417), human IgG from human serum (I2511), anti-human IgG (polyclonal antibody developed in goat; I1886) and anti-human IgG (γ-chain specific)-biotin (polyclonal antibody developed in goat; B1140) were purchased from Sigma-Aldrich (Spain). Anti-goat IgG (polyclonal antibody produced in chicken; ab86245) was purchased from Abcam (UK).

All of the materials used for the production of the LFA strips were purchased from Millipore (Billerica, USA): sample and absorbent pads (CFSP001700), the conjugate pad (GFCP00080000), detection pads (Hi-Flow Plus 75, SHF0750425 and Hi-Flow Plus 75, SHF2400425) and the backing card (HF000MC100). Milli-Q water, produced using a Milli-Q system (>18.2 MΩ cm^{-1}) purchased from Millipore, was used for the preparation of all solutions. A thermostatic centrifuge (Sigma 2-16PK, Fisher Bioblock Scientific, France) was used to purify the AuNP/antibody conjugates. A Xerox ColorQube 8570 wax printer (Xerox Corporation, USA) was used for printing different wax designs. A hot plate (VWR, USA) was used for heating and melting the wax ink. An IsoFlow reagent dispensing system (Imagene Technology, USA) was used to dispense the detection and control lines. A guillotine (Dahle 533, Germany) was used to cut the strips. The stirrer used was a TS-100 Thermo-Shaker (Biosan, Latvia). A strip reader (Cozart, SpinReact, UK) was used for quantitative measurements. All of the size measurements and shape observation of AuNPs were conducted using a FEI Tecnai™ G2F20 field emission gun transmission electron microscope (FEI, USA). A SpectraMax M2^e spectrophotometer (Molecular Devices, UK) was used to record all UV-Vis spectra of AuNPs. Scanning electron micrographs of the nitrocellulose membrane were obtained using a FEI Quanta™ 650 field emission gun scanning electron microscope (FEI, USA). A Leica DCM 3D dual core 3D measuring microscope (Leica Microsystems, Germany) was used to obtain confocal images of the nitrocellulose membrane. An image processing software program, ImageJ (National Institutes of Health, USA), was used for measuring the size of the wax pillars before and after the melting step.

Preparation of gold nanoparticles (AuNPs)

Gold nanoparticles (AuNPs), 20 nm in size and stabilized by citrate, were prepared using the Turkevich method.[32] Briefly, 50 mL of aqueous solution of 0.1% $HAuCl_4$ was heated to boiling and vigorously stirred in a 250 mL round-bottom flask; 1.25 mL of 1% sodium citrate was added quickly to this solution. Boiling was continued for additional 10 min. The solution was cooled to room temperature under continuous stirring. The colloids were stored in dark bottles at 4° C. All glassware used in this preparation was previously cleaned with *aqua regia* overnight and rinsed with double distilled H_2O; reflux was used for all of the procedure.

AuNP modification with antibodies

AuNPs were modified with antibodies following a previously optimized procedure.[33] First, the pH of the AuNP suspension was adjusted to pH 9 with 0.1 M borate buffer. Then, 100 μL of 100 μg mL^{-1} anti-human IgG (γ-chain specific)-biotin aqueous solution was added to 1.5 mL of the AuNP suspension. The resulting solution was incubated for 20 min at 650 rpm. Then, 100 μL of 1 mg mL^{-1} BSA aqueous solution was added and stirring was continued for another 20 min at 650 rpm. Finally, the solution was centrifuged at 14 000 rpm and 4 °C for 20 min.

The supernatant was removed and the pellet of AuNP/anti-human IgG was resuspended in 500 μL of BB (2 mM, pH 7.4, 10% sucrose).

Preparation of the strips

Once the pillar patterns have been designed with graphic design software (CorelDraw X4), the preparation of the modified detection pad consisted of three main steps: i) printing the pillar patterns onto the nitrocellulose (NC) membrane (Hi-Flow Plus 75, HF075) with a wax printer; ii) heating the NC membrane and melting the wax at 110 °C for 90 seconds by using a hot plate; and iii) dispensing antibodies onto the membrane. For this step, 1 mg mL^{-1} solution of anti-human IgG (whole molecule) and anti-goat IgG was spotted onto the detection pad at a dispensing rate

of 0.05 μL mm^{-1} using an IsoFlow reagent dispensing system so as to form the test and control lines, respectively. Then, the detection pad was dried at 37 °C for 1 h.

The sample pad was prepared by dipping into 10 mM PBS, 5% BSA and 0.05% Tween®-20 and drying at 60 °C for 2 h. The conjugate pad was prepared by dipping it into the previously prepared anti-human IgG (γ-chain specific)-biotin/AuNP conjugate and drying under vacuum for 1 h.

The different pads were sequentially laminated 2 mm from each other and pasted onto the adhesive backing card in the following order: detection, conjugation, sample and absorbent pads. Finally, the strips were cut 7 mm wide and used immediately.

Lateral flow assay procedure

Sample solutions of 200 μL of different human IgG (HIgG) concentrations in PBS (10 mM, pH 7.4), ranging from 5 ng mL^{-1} to 500 ng mL^{-1}, were dispensed onto the sample pad and kept for 15 min until the flow was stopped. Then, 200 μL of PBS was dispensed in order to wash away the excess AuNP/antibody. After drying the lateral flow strips at room temperature, they were read with a strip reader so as to obtain the calibration curve for HIgG. PBS without analyte was considered as blank. All of the measurements were performed in triplicate.

Mathematical simulations

Flow in porous media can be studied by the use of the Navier–Stokes equations, which describe the movement of fluid substances, which represent the effect of the diffusion viscosity and the pressure. These equations coupled with the Brinkman equations can be useful for modeling the flows in certain porous media. The initial conditions for the simulation such as porosity and permeability of the membranes (in this case, a different kind of membrane was used) were the same as in a previous study reported by our group.[24] These parameters were given by Millipore Corporation (porosity around 83% and the permeability 4.3×10^{-6} m^2). On the other hand, the density and viscosity values used at 25 °C (0.997 g mL^{-1} and 0.890 N s m^{-2}, respectively) as an approximation were those of water. The boundary conditions for the simulation were the geometry (changing the pillar distribution). The velocity was calculated from the volume of the liquid introduced into the membrane (200 μL), the cross-section area of the absorbent pad and the time necessary to absorb the respective volume (1.47 m s^{-1}).

Results and discussion

Improvement in sensitivity of the lateral flow assay by using wax delay barriers

Lateral flow assays must allow rapid responses with good sensitivity. For this purpose, manufacturers have developed different membranes which satisfy these requirements. The capillary flow rate is a common parameter to classify the membranes on the basis of the time required for the liquid to travel and fill completely a 4 cm long membrane. In this work, nitrocellulose membranes Hi-Flow Plus 75 (HF075) and Hi-Flow Plus 240 (HF240), provided by Millipore Corporation, were used. The former has a nominal flow rate of 75 s across the 4 cm long membrane, and the latter has a higher nominal flow rate of 240 seconds across the same length.[34] Sensitivity of the LFA is conditioned by various factors which are crucial to the performance of the nitrocellulose membrane.

For the fast liquid velocity membrane (HF075), the sensitivity is low due to two main factors: i) the liquid takes less time to travel across a defined length and ii) the formation of the immunocomplex between the analyte and the AuNP-labeled antibody at the conjugate pad, as well as at the test and control lines, is less effective since the flow rate is faster. In the case of the slow velocity membrane (HF240), the sensitivity is higher since the flow rate is slower and there is enough time for an effective formation of the immunocomplex at the beginning of the strip and at the test and control lines.

Based on this, we chose to modify the faster membrane provided by Millipore (HF075) with wax pillars using the wax printing technology so as to evaluate the effect (in terms of sensitivity and limit of detection) produced by these hydrophobic structures that can act as obstacles delaying the sample flow in a AuNP-based LFA (see Fig. 1).

Wax printing technology is used here to deposit wax on the surface of nitrocellulose, followed by a heating step to melt the wax pattern in order for it to penetrate through the pores of the membrane while maintaining the original design. The hydrophobic properties of the wax make it suitable for the creation of barriers which can modulate the flow on membranes in a desirable way, *e.g.* for controlling the delivery time of reagents.[35]

In the wax printing process, the nitrocellulose membrane to be printed passes between the pressure roller and the print drum of the printer, suffering from changes due to the pressure. To evaluate these alterations, empirical calculations

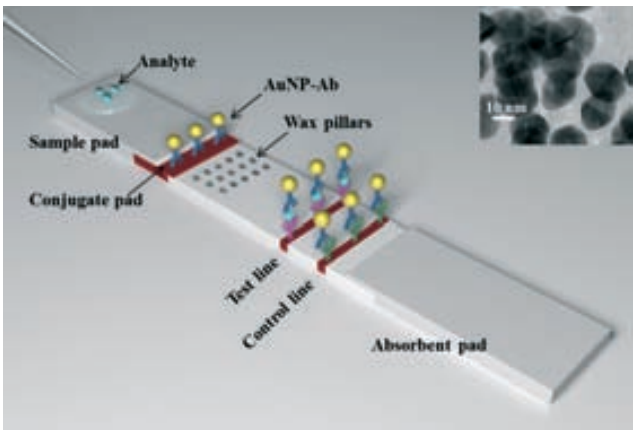

Fig. 1 Schematic representation of a lateral flow strip modified with wax pillars for protein detection based on the use of AuNPs. (Inset) TEM image of AuNPs used for lateral flow assay (LFA) development.

of permeability and scanning electron micrographs for membrane characterization were performed.

In Fig. 2, transversal cuts of membranes with and without modifications produced just by applying heat and pressure are shown. When the membrane passes through the wax printer, a thickness reduction of around 30 μm is observed due to the compression produced by the pressure roller and the drum of the printer (Fig. 2A and B). The results of the LFA performed for both approaches (Fig. 2C and D) were compared so as to estimate the effect of mechanical compression of the membrane on quantitative measurements (HIgG concentrations: 5, 50 and 500 ng mL^{-1}). Indeed, when the membrane is flattened the sensitivity of the LFA increases due to the fact that the modified membrane became thinner and this compression produces wider reagent lines, making it easier to visualize a weak signal. This is related to the fact that due to the spreading of reagents, the fluid moving laterally penetrates the whole thickness of the membrane, producing wider lines due to less depth to contain the same volume of the reagent.[34] The limit of detection (LoD), determined using the strip reader (for all of the LF formats described), was calculated as the concentration of HIgG corresponding to three times the standard deviation of the estimate, giving a value of 8.0 ng mL^{-1} of HIgG for the LF strips (with flattened membranes HF075), while by using membranes without any modification, this value is 12 ng mL^{-1}. This suggests that only the compression of nitrocellulose membranes gives a 1.5-fold improvement in the sensitivity of the assay.

In traditional printing methods, porosity plays an important role in the absorption of the ink by different paper substrates: high-porosity papers absorb and spread more ink, while low-porosity papers can prevent the penetration of the ink through their fibers. In the wax printing process used in this work, the wax penetrates only into the superficial fibers of nitrocellulose. To ensure the presence of delay barriers along the whole thickness of the membrane, a melting process was conducted. Two nominal wax pillars of 0.4 and 1.0 mm diameters were measured before and after the melting process, and results showed that wax pillar diameters increased up to 20% from the original printing size after the melting step (see Fig. S1†). Once the melted wax enters through the fibers of the membrane, lateral spreading occurs and decreases the resolution of the printed pattern, which is affected by the porosity and thickness of the membrane.[3] Although just one type of NC membrane was employed for printing purposes (approximate pore size 12–17 μm), if a membrane with smaller pores is used, the increment after melting could be lower due to the higher packing of nitrocellulose fibers that reduces the possibility of air passages and avoids the spread of ink. The effect of changing the wax pillar diameter on the sensitivity was tested by quantitative measurements of HIgG. Results showed that the presence of wax pillars with small diameters (0.4 mm) reduced considerably the unspecific signals, showing strips with clear backgrounds, and a better differentiation of intensities of test lines was observed over the concentration range when compared with the modified membrane (see Fig. S2A–B†). In regard to the sensitivity, the presence of small diameter wax pillars produces a slight increment of 1.2-fold with respect to the modified membrane, which corresponds to a LoD of 6.6 ng mL^{-1}. This result indicates that wax pillars act as delay barriers of the fluid due to their hydrophobic nature allowing, in this way, a suitable recognition between the analyte and the captured AuNP-labeled antibody before arriving at the test line. However, this size (0.4 mm) was not

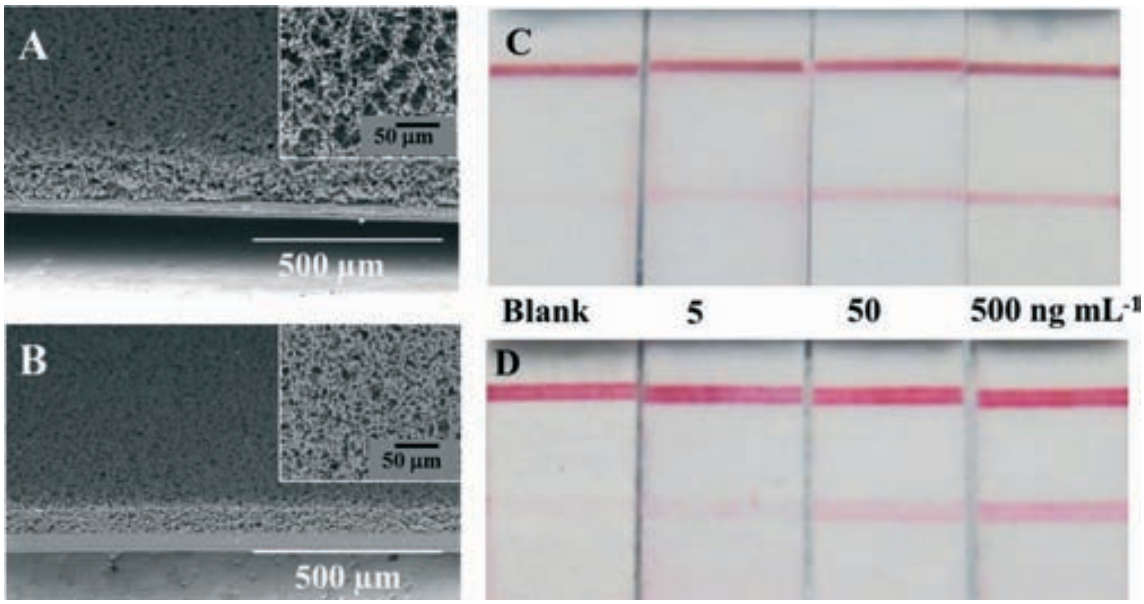

Fig. 2 Left: scanning electron micrographs (SEM) of transversal cuts: (A) unmodified and (B) modified HF075 membrane. Right: LFA for HIgG detection using (C) unmodified and (D) heat and pressure-modified membrane for a blank assay and for assays performed with 5, 50 and 500 ng mL^{-1} HIgG.

enough to increase even more the sensitivity of the assay. On the other hand, a wax pillar of a larger diameter (1.0 mm) was tested and experimental results showed that sensitivity was affected. This occurred because the pillars delayed the regular flow in such a way that the time of the assay was substantially long, making it useless for practical purposes; a considerable amount of AuNPs which could not reach properly the test and control lines remained along the membrane, showing a pink background; thus a high LoD of 15.6 ng mL^{-1} was obtained (see Fig. S2C†). It is worth noting that the wax pillar size is an important parameter that affects the sensitivity in different ways and the proper choice of wax pillar size must be a compromise between the sensitivity and the time of the assay.

For the remaining experiments, the wax pillar diameter chosen was 0.5 mm and the effect produced by different wax pillar arrangements in the microfluidic device was tested. Four different patterns ("P1", "P2", "P3" and "P4") as well as strips with and without modifications were tested for HIgG detection. Experimental results clearly showed the effect of the wax pillar geometries on the sensitivity of the assay (see Fig. 3). As stated before, an improvement in sensitivity is produced by: i) mechanical compression of the membrane and ii) the presence of wax pillars of proper size. By slightly increasing the diameter of the wax pillar up to 0.5 mm, it was possible to improve the sensitivity, especially for "P1" and "P2" patterns up to 1.7- and 2.6-fold with respect to modified and unmodified membrane, respectively. These results showed that sensitivity of the LFA can be affected by the presence of wax pillars, their diameters and also their spatial arrangements. Moreover, mathematical simulations were performed to study these phenomena. For each pattern, the flow speed, vorticity and force around the pillars were calculated at the end of the pillar's zone and control lines. All of these data are summarized in Table 1.

Three different flow parameters were mathematically considered to correlate them with the experimental results. Mathematical simulations for HF075 were performed and chosen as blank in order to compare the differences observed in the mentioned parameters in the presence of several wax pillar patterns. According to the data in Table 1, the highest flow velocities at the end of the wax pillar zone corresponds

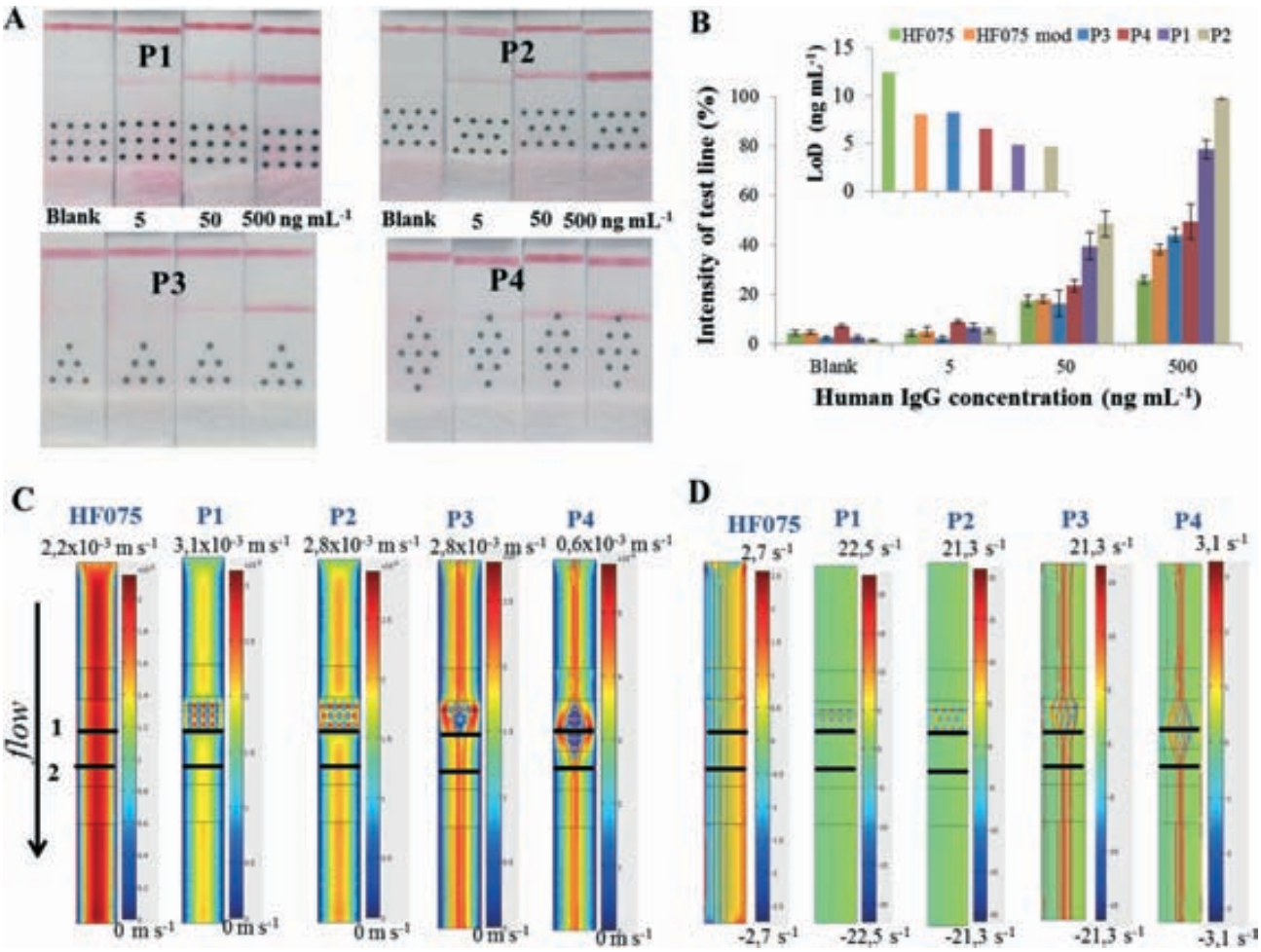

Fig. 3 (A) LF strips modified with different patterns of wax pillars. (B) Effect of the wax pillars on the quantitative measurement of LF for different concentrations of HIgG and the corresponding LoD (inset). (C) Flow speed simulations for modified and unmodified LFs. (D) Simulated results of vorticity for modified and unmodified LFs.

Table 1 Parameters measured with mathematical simulations for LFAs modified with wax pillars

Pattern	Average velocity ($\times 10^{-3}$ m s^{-1})	Vorticity (s^{-1})	Average pressure force per unit of area (Pa)
HF075	V_1 = 1.03	$Vort_1$ = (−1.4 to 1.4)	F_1 = 0
	V_2 = 1.03	$Vort_2$ = (−1.4 to 1.4)	F_2 = 0
P1	V_1 = 1.60	$Vort_1$ = (−4.7 to 4.7)	$F_1 = 2.5 \times 10^{-5}$
	V_2 = 1.03	$Vort_2$ = (−1.4 to 1.4)	F_2 = 0
P2	V_1 = 1.40	$Vort_1$ = (−4.5 to 4.5)	$F_1 = 2 \times 10^{-5}$
	V_2 = 1.03	$Vort_2$ = (−1.4 to 1.4)	F_2 = 0
P3	V_1 = 1.03	$Vort_1$ = (−2.4 to 2.4)	$F_1 = 3 \times 10^{-8}$
	V_2 = 1.03	$Vort_2$ = (−1.4 to 1.4)	F_2 = 0
P4	V_1 = 0.18	$Vort_1$ = (−0.47 to 0.47)	$F_1 = 3.6 \times 10^{-8}$
	V_2 = 0.18	$Vort_2$ = (−0.25 to 0.25)	F_2 = 0

to patterns "P1" and "P2", which are compensated for by the vorticity range (a physical magnitude that describes the rotation of a fluid near some point). When this range is wider, the rotation of the fluid becomes faster. In addition, the pressures are higher for these two patterns. These results are consistent with the most sensitive modified LFA, which are "P1" and "P2" patterns. Making the same considerations for the remaining patterns, "P3" exhibited higher flow velocities and vorticity values and lower pressure than "P4". However, the experimental results showed that the LoD for "P4" (6.5 ng mL^{-1}) is better than that for "P3" (8.2 ng mL^{-1}).

With the purpose of confirming if the wax truly acts as a barrier across the membrane, characterization by using scanning electron and confocal microscopes was performed. A transversal cut of a wax-dotted area was made in order to verify if the melted wax penetrates through the entire thickness of the membrane, as shown in Fig. 4A. Due to the density of the wax and the membrane itself, it was difficult to

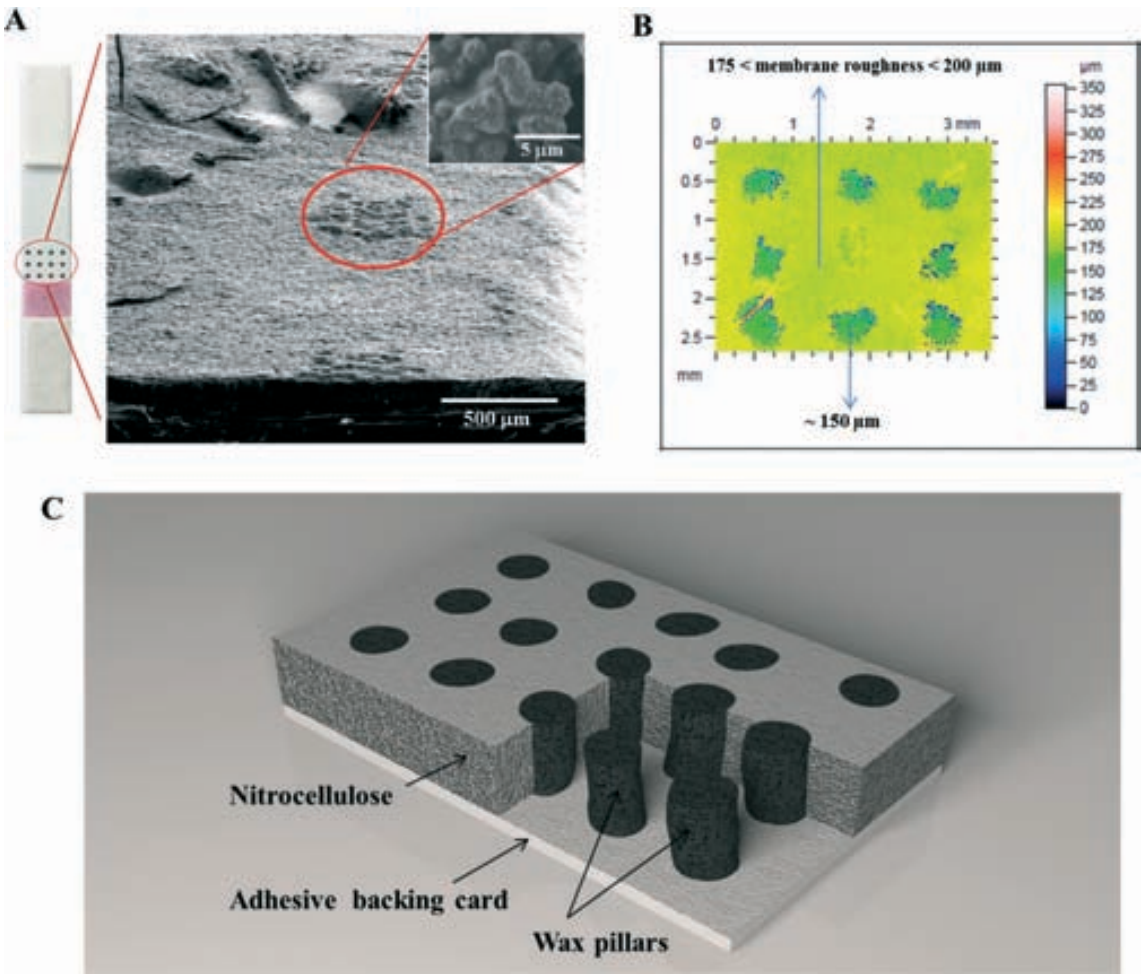

Fig. 4 (A) SEM image for transversal cut of the wax pillar area on a lateral flow strip. The inset corresponds to a membrane covered with melted wax. (B) Surface profile roughness of LFA modified with wax pillars. (C) Schematic of a transversal cut of the pillar zone on the nitrocellulose membrane.

characterize by SEM if the area of barriers was only covered with wax. Therefore, it was necessary to characterize the area of barriers by using confocal technology. Fig. 4B shows the surface roughness profile of the wax-dotted area and it is possible to observe different surface roughness values. This means that the melted wax (darker points) has filled the pores of the membrane, creating a tridimensional structure (like a pillar) capable of obstructing the normal flow of the sample across the whole membrane thickness (Fig. 4C).

Based on the previous experimental results and mathematical simulations, "P3" and "P4" wax patterns were discarded due to the fact that they showed lower sensitivity than "P1" and "P2" and an accurate calibration curve was done (see Fig. 5). In this experiment, unmodified and modified membranes (HF075 and HF240) were used to compare the effect produced by mechanical compression and also the presence of the wax pillars in the LFA. As expected, the unmodified HF075 membrane presents less sensitivity as its capillary flow time is lower when compared with that of the unmodified HF240 membrane. This means that sample flow requires a shorter time interval to travel a defined distance across the membrane, thus there is not enough time for formation of the immunocomplex and its sensitivity is affected.

When the HF075 membrane experienced the mechanical compression caused by the roller and the print drum, detection lines became wider and its sensitivity increased as stated before. The LoD for the modified HF075 membrane is

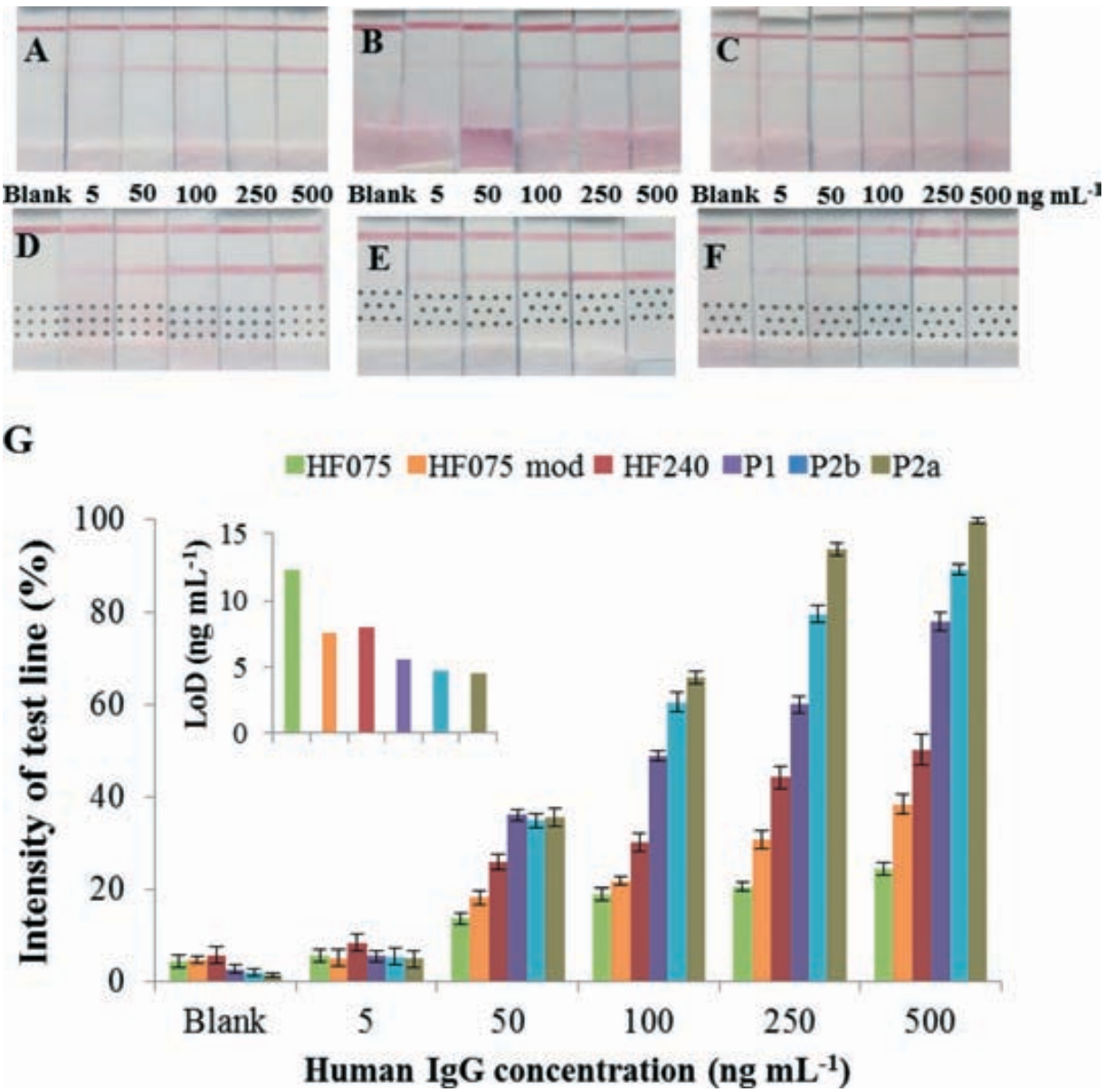

Fig. 5 Results of LFA for HIgG detection performed with (A) unmodified HF075, (B) modified HF075 and (C) unmodified HF240 membranes. (D), (E), and (F) correspond to the same membranes modified with P1, P2b, and P2a patterns, respectively. (G) Quantitative evaluation of the assays performed with the different membranes and the corresponding LoD (inset).

comparable to the value obtained for the most sensitive unmodified membrane HF240. In addition, the selected patterns showed a lower LoD with respect to the value obtained for the most sensitive membrane, HF240, produced by Millipore. The reproducibility of the responses (n = 3) for a 100 ng mL^{-1} HIgG concentration was also studied, and the relative standard deviation (RSD) and limits of detection for different patterns and membranes can be found in the ESI.†

Lateral flow assays with wax printed pillars were found to be more sensitive and showed lower limits of detection than lateral flow assays without modifications. Moreover, all blank measurements gave a lower background signal compared with those of LFA without modifications.

In order to verify the role of the location of wax pillar patterns in the sensitivity of LFA, two "P2" patterns have been studied: a pattern near to the conjugate pad (P2a) and another pattern near to the test line (P2b). Results showed that there is no significant difference in the value of the limit of detection whether the wax pattern is located near or far away from the conjugate pad. This is attributable to the fact that the capillary flow rate is considerably faster at the beginning of the detection membrane and decreases exponentially as the liquid moves along it, until reaching a steady flow rate when the bed volume of the membrane is saturated.[34] Therefore, placing the wax pillar area at the beginning of the membrane is enough to improve the sensitivity of the LFA. In addition, this contributes significantly to the delay of the flow rate, leading to better limits of detection.

Wax printing was used as a patterning technique in order to create delay barriers on LF devices that lead to increase in sensitivity of the assays. Besides the sensitivity improvements obtained in the developed devices, they are also fast, easy to use, and low-cost and their fabrication just includes an extra step of printing that takes a few minutes compared with other controlling fluid methods previously reported, which are more sensitive but the fabrication processes are laborious and require additional reagents.

In this context, our approach constitutes an important strategy for sensitivity improvement in lateral flow assays using paper-based microfluidic techniques that can be improved by other techniques such as inkjet technology, which allows to print directly on the surface of the nitrocellulose membrane by using a hydrophobic solution or an ink capable of creating well-defined patterns without having direct contact with it.[36]

Conclusion

We have presented a new and easy strategy for improving the sensitivity of a gold nanoparticle-based LFA by the deposition of hydrophobic barriers of wax printed at the detection pad of a LFA. These barriers act as obstacles delaying the regular flow on the strip by increasing the binding time between the analyte and the labeled antibody and therefore allowing an effective formation of the immunocomplex. Different designs were evaluated and the optimized designs exhibited an improvement of almost 3-fold in the limit of detection compared with the non-modified membranes. Mathematical simulations corroborate the experimental results obtained for the different patterns. This approach is simpler than other previously reported strategies since it is not time-consuming, is low-cost and does not require the use of additional reagents for signal amplification or even changes in the configuration of the LF strip. As a result, the proposed strategy can be easily extended to any type of LFA design and could expand the scope for the use of LF designs with patterning techniques, facilitating its use in point-of-care applications.

Acknowledgements

We acknowledge MINECO (Madrid) for the project MAT2011-25870. L. R. also acknowledges Universitat Autònoma de Barcelona for her pre-doctoral grant.

References

1 C. Parolo and A. Merkoçi, *Chem. Soc. Rev.*, 2013, **42**, 450–457.
2 A. W. Martinez, S. T. Phillips, M. J. Butte and G. M. Whitesides, *Angew. Chem., Int. Ed.*, 2007, **46**, 1318–1320.
3 E. Carrilho, A. W. Martinez and G. M. Whitesides, *Anal. Chem.*, 2009, **81**, 7091–7095.
4 Y. Lu, W. Shi, J. Qin and B. Lin, *Anal. Chem.*, 2010, **82**, 329–335.
5 K. Abe, K. Suzuki and D. Citterio, *Anal. Chem.*, 2008, **80**, 6928–6934.
6 J. Olkkonen, K. Lehtinen and T. Erho, *Anal. Chem.*, 2010, **82**, 10246–10250.
7 W. Dungchai, O. Chailapakul and C. S. Henry, *Analyst*, 2011, **136**, 77–82.
8 A. J. P. Martin and R. L. M. Synge, *Biochem. J.*, 1941, **35**, 1358–1368.
9 J. Comer, *Anal. Chem.*, 1956, **28**, 1748–1750.
10 M. C. Brucker and N. J. MacMullen, *J. Obstet. Gynecol. Neonatal Nurs.*, 1985, **14**, 353–359.
11 C. Fernández-Sánchez, C. J. McNeil, K. Rawson and O. Nilsson, *Anal. Chem.*, 2004, **76**, 5649–5656.
12 C. Fernández-Sánchez, C. J. McNeil, K. Rawson, O. Nilsson, H. Y. Leung, V. Gnanapragasam and J. Immunol, *Methods*, 2005, **307**, 1–12.
13 J. Aveyard, M. Mehrabi, A. Cossins, H. Braven and R. Wilson, *Chem. Commun.*, 2007, 4251–4253.
14 P. Lie, J. Liu, Z. Fang, B. Dun and L. Zeng, *Chem. Commun.*, 2012, **48**, 236–238.
15 V. M. T. Lattanzio, N. Nivarlet, V. Lippolis, S. Della Gatta, A. C. Huet, P. Delahaut, B. Granier and A. Visconti, *Anal. Chim. Acta*, 2012, **718**, 99–108.
16 L. Anfossi, C. Baggiani, C. Giovannoli, G. D'Arco and G. Giraudi, *Anal. Bioanal. Chem.*, 2013, **405**, 467–480.
17 J. Liu, D. Mazumdar and Y. Lu, *Angew. Chem.*, 2006, **118**, 8123–8127.

18 A. M. López Marzo, J. Pons, D. A. Blake and A. Merkoçi, *Anal. Chem.*, 2013, **85**, 3532–3538.
19 I. H. Cho, S. M. Seo, E. H. Paek and S. H. Paek, *J. Chromatogr. B: Anal. Technol. Biomed. Life Sci.*, 2010, **878**, 271–277.
20 D. H. Choi, S. K. Lee, Y. K. Oh, B. W. Bae, S. D. Lee, S. Kim, Y.-B. Shin and M.-G. Kim, *Biosens. Bioelectron.*, 2010, **25**, 1999–2002.
21 C. Parolo, A. de la Escosura-Muñiz and A. Merkoçi, *Biosens. Bioelectron.*, 2013, **40**, 412–416.
22 E. Juntunen, T. Myyryläinen, T. Salminen, T. Soukka and K. Pettersson, *Anal. Biochem.*, 2012, **428**, 31–38.
23 Y.-Y. Lin, J. Wang, G. Liu, H. Wu, C. M. Wai and Y. Lin, *Biosens. Bioelectron.*, 2008, **23**, 1659–1665.
24 C. Parolo, M. Medina-Sánchez, A. de la Escosura-Muñiz and A. Merkoçi, *Lab Chip*, 2013, **13**, 386–390.
25 R. C. Wong, *Lateral Flow Immunoassay*, Humana Press, Totowa, NJ, 2009.
26 J. L. Tonkinson and B. A. Stillman, *Front. Biosci., Landmark Ed.*, 2002, **7**, C1–C12.
27 E. Fu, B. Lutz, P. Kauffman and P. Yager, *Lab Chip*, 2010, **10**, 918–920.
28 B. Lutz, T. Liang, E. Fu, S. Ramachandran, P. Kauffman and P. Yager, *Lab Chip*, 2013, **13**, 2840–2847.
29 J. Houghtaling, T. Liang, G. Thiessen and E. Fu, *Anal. Chem.*, 2013, **85**, 11201–11204.
30 H. Chen, J. Cogswell, C. Anagnostopoulos and M. Faghri, *Lab Chip*, 2012, **12**, 2909–2913.
31 B. J. Toley, B. Mckenzie, T. Liang, J. R. Buser, P. Yager and E. Fu, *Anal. Chem.*, 2013, **85**, 11545–11552.
32 J. Turkevich, P. C. Stevenson and J. Hillie, *Discuss. Faraday Soc.*, 1951, 55–75.
33 A. Ambrosi, M. T. Castañeda, A. J. Killard, M. R. Smyth, S. Alegret and A. Merkoçi, *Anal. Chem.*, 2007, **79**, 5232–5240.
34 Millipore Corporation, *Rapid Lateral Flow Test Strips. Considerations for product development*, 2002.
35 H. Noh and S. T. Phillips, *Anal. Chem.*, 2010, **82**, 8071–8078.
36 A. Apilux, Y. Ukita, M. Chikae, O. Chailapakul and Y. Takamura, *Lab Chip*, 2013, **13**, 126–135.